Master's thesis

NTNU
Norwegian University of Science and Technology
Faculty of Engineering
Department of Civil and Environmental Engineering

Fahad Pervaiz

Evaluation of Ice loads on Beitstadsundet bridge by deterministic and probabilistic approaches

Master's thesis in Coastal and Marine Engineering and Management (CoMEM)
Supervisor: Prof. Knut Vilhelm Høyland
July 2019

NTNU
Norwegian University of Science and Technology

ERASMUS +: ERASMUS MUNDUS MOBILITY PROGRAMME

Master of Science in

COASTAL AND MARINE ENGINEERING AND MANAGEMENT

CoMEM

Evaluation of Ice loads on Beitstadsundet bridge by deterministic and probabilistic approaches.

Norwegian University of Science and Technology
8 July 2019

Fahad Pervaiz

The Erasmus+: Erasmus Mundus MSc in Coastal and Marine Engineering and Management is an integrated programme including mobility organized by five European partner institutions, coordinated by Norwegian University of Science and Technology (NTNU).

The joint study programme of 120 ECTS credits (two years full-time) has been obtained at two or three of the five CoMEM partner institutions:

- Norges Teknisk- Naturvitenskapelige Universitet (NTNU) Trondheim, Norway
- Technische Universiteit (TU) Delft, The Netherlands
- Universitat Politècnica de Catalunya (UPC). BarcelonaTech. Barcelona, Spain
- University of Southampton, Southampton, Great Britain
- City University London, London, Great Britain

During the first three semesters of the programme, students study at two or three different universities depending on their track of study. In the fourth and final semester an MSc project and thesis has to be completed. The two-year CoMEM programme leads to a multiple set of officially recognized MSc diploma certificates. These will be issued by the universities that have been attended by the student. The transcripts issued with the MSc Diploma Certificate of each university include grades/marks and credits for each subject.

Information regarding the CoMEM programme can be obtained from the programme coordinator:

Øivind A. Arntsen, Dr.ing.
Associate professor in Marine Civil Engineering
Department of Civil and Environmental Engineering
NTNU Norway
Mob.: +4792650455 Fax: + 4773597021
Email: oivind.arntsen@ntnu.no

CoMEM URL: https://www.ntnu.edu/studies/mscomem

CoMEM Thesis

This thesis was completed by:
Fahad Pervaiz

Under supervision of:
Knut Vilhelm Høyland
Professor
Department of Civil and Environmental Engineering Norwegian University of Science and Technology

As a requirement to attend the degree of
Erasmus+: Erasmus Mundus Master in Coastal and Marine Engineering and Management (CoMEM)

Taught at the following educational institutions:

Norges Teknisk- Naturvitenskapelige Universitet (NTNU)
Trondheim, Norway

Technische Universiteit (TU) Delft
Delft, The Netherlands

At which the student has studied from August 2017 to July 2019.

NORWEGIAN UNIVERSITY OF SCIENCE AND TECHNOLOGY
DEPARTMENT OF CIVIL AND ENVIRONMENTAL ENGINEERING

Report Title:	Date: 08 July 2019			
Evaluation of Ice loads on Beitstadsundet bridge by deterministic and probabilistic approaches.	Number of pages (incl. appendices): 170			
	Master Thesis	X	Project Work	
Name: Fahad Pervaiz				
Professor in charge/supervisor: Knut Vilhelm Høyland, Professor, Department of Civil and Environmental Engineering, NTNU				
Other external professional contacts/supervisors: Dr.Jeroen Hoving (TU Delft), Dr.Torodd Nord (NTNU), Dr.Erik de Goede (Deltares)				

Abstract:

Ice loads on the bridge piers can be one of the major components for the Extreme Limit State (ELS) combinations, specified in the Euro Code. In arctic and sub-arctic regions, the ice action on infrastructures such as platforms, light houses, sub-sea pipelines, or wind turbines may exceed the total forces of wind, waves and currents and may, therefore, determine the design. For example, in regions such as Beitstad in Norway, ice loads can be the predominant lateral force in the design of bridge sub-structures. Therefore, accurate estimation of ice forces that can act on bridge piers in northern climates is critical in both cases – the design of new bridges and the structural evaluation of existing bridges. Different design codes provide empirical formulae to calculate the design ice forces, based on the effective ice strength, thickness and other important empirical environmental or climatic coefficients. Ice forces must be considered in the design of the coastal and hydraulic structures. Both the ice conditions and the environmental factors are combined in a formula to calculate the magnitude of ice forces that a structure is expected to withstand in the future and over its lifetime. The existing standards for estimation of the ice loads on vertical and sloping structures adopt different analysis methods, and to determine the global ice loads on these structures, the ice-structure interaction scenarios must be identified.

In this study, most of the focus will be on fjord and lake ice conditions and their loadings on a bridge pier will be assessed and compared by using different shapes of structure and standards of different countries, followed by the deterministic extreme value analysis , probabilistic assessment and uncertainty analysis of the ice loading during the design lifetime of the bridge sub-structure.

Keywords:

1. Ice actions
2. Beitstadsundet bridge
3. Determinstic extreme value anylasis
4. Probablistic Assessment

Abstract

Ice loads on the bridge piers can be one of the major components for the Extreme Limit State (ELS) combinations, specified in the Euro Code. In arctic and sub-arctic regions, the ice action on infrastructures such as oil platforms, lighthouses, sub-sea pipelines, or wind turbines may exceed the total forces of wind, waves, and currents and may, therefore, determine the design. For example, in regions such as Beitstad in Norway, ice loads can be the predominant lateral force in the design of bridge piers. Therefore, accurate estimation of ice forces that can act on bridge piers in northern climates is critical in both cases – the design of new bridges and the structural evaluation of existing bridges. Different design codes provide empirical formulae to calculate the design ice forces, based on the effective ice strength, thickness and other important empirical environmental or climatic coefficients. Ice forces must be considered in the design of the coastal and hydraulic structures. To predict the Ice forces, expected ice conditions, like ice thickness, strength, morphology, etc., must be determined appropriately along with the environmental driving forces, i.e. wind, current, and thermal expansion. Both the ice conditions and the environmental factors are combined in a formula to calculate the magnitude of ice forces that a structure is expected to withstand in the future and over its lifetime. The existing standards for estimation of the ice loads on vertical and sloping structures adopt different analysis methods, and to determine the global ice loads on these structures, the ice-structure interaction scenarios must be identified.

The ice load applied to a structure depends on the nature of the failure mechanism induced through the ice feature, which depends on the shape of the structure. Generally, structures that are vertical, or close to vertical, causing the ice to fail in crushing while sloping structures cause the ice to fail in bending. Secondly, most of the standards used in the field are related to offshore structures, while few standards are focusing on fjord and lake structures. In both cases, the ice conditions and environmental conditions will be different. Therefore, this imposes a dire need to dig in by doing more research in the ice, existing on fjords and lakes. In this thesis, most of the focus will be on fjord and lake ice conditions and their loadings on a bridge pier will be assessed and compared by using different shapes of structures and standards of different countries, followed by the deterministic extreme value analysis and probabilistic assessment and uncertainty analysis of the ice loading during the design lifetime of the bridge sub-structure.

Acknowledgments

Studying for a master's degree at TU Delft-Netherlands and NTNU-Norway has been an exciting period of my life. First, I would like to sincerely appreciate and thank to my supervisors Professor Knut Vilhelm Høyland (NTNU), Dr.Jeroen Hoving (TU Delft), Dr.Torodd Nord (NTNU) and Dr.Erik de Goede (Deltares) for their enthusiastic support and supervision. Their comments and advises during my thesis have made my knowledge stronger and deeper. Sincere gratitude to Sonja Marie Ekrann Hammer and Dr. Øivind Arntsen, Dr. Raed Lubbad and everyone else involved in the CoMEM program.

Special thanks to my seniors; Einar for taking me to the field measurements; Akhshan ul Islam, Ankit Aggarwal, Saud Afzal for guiding me throughout my Masters; Chana sinsabvarodom and Erik de Goede for giving the advice that was helpful during the Monte-Carlo simulation and modelling in Delft3D-FLOW (Ice module) carried out in this thesis. At last, I would like to thank my classmates for great support throughout my study in the Delft and Trondheim.

Table of Contents

List of Figures

List of Tables

Nomenclature

Abbreviations

ISO= International organization of standardization

AASHTO= American association of state highway and transportation officials

NRC= National research council, Canada

SLR= Sea level rise

HAT= Highest astronomical tide

LAT= Lowest astronomical tide

CD= Chart datum

CFDD= Cumulative freezing degree days

MCS= Montecarlo simulation

DHI= Danish Hydraulic Institute

MSL= mean sea level

PDF= probability density function

CDF= Cumulative distribution function

FORM= First order reliability method

Symbols

k_i	Thermal conductivity of ice
S	Ice salinity
h_i	Ice thickness
$T(fr)$	Freezing temperature
P	Sea-level pressure
V_{brine}	Brine volume
T	Ice temperature
η	Ice porosity

V_{air}	Air volume
$\rho_{sea\ ice}$	Seawater density
$\rho_{pure\ ice}$	Pure water density
ε	The strain rate of ice
σ_C^V	Vertical compressive strength
σ_C^H	Horizontal compressive strength
$\Delta\ Amp_{tidal}$	Changes in the amplitude and phase of a tidal constituent
H	The water depth
ρ	Water density
r	Friction
mx	Mixing
Qr	River discharge
$\Psi\omega$	Frequency-dependent tidal response to astronomical tidal forcing
h_0	Initial ice thickness
C_{FDD}	Cumulated freezing degree days
T_s	The temperature at the ice surface
l	Latent heat of diffusion
ρ_{ice}	Density of ice
A	Empirical freezing degree day factor
d	First-order decay process
$C(x, y, \sigma, t)$	Ice concentration
$H(x, y)$	Total water depth
$D(h, v)$	Horizontal diffusion
t	Time
Q_{snow}	Snowfall
λ_d	Water elevation
f	Coriolis force
M	Ice mass
g	Acceleration due to gravity
F	Internal stresses

τ_a	Air stresses
τ_w	Water stresses
ρ_a	Air density of water
C_d	Wind drag coefficient
U_{10}	Wind speed in at 10 m above the ice
p^* and C	Empirical constants
u_w	Current at the uppermost grid layer near the surface
I_0	Net incident solar radiation (short wave)
Q_{ai}	Net incident atmospheric radiation (long wave)
Q_{br}	Back radiation (long wave)
Q_{ei}	Evaporative heat flux (latent heat)
Q_{si}	Convective heat flux (sensible heat)
T_a	Air temperature
r	Reflection coefficient
ε	Emissivity factor of ice
u_*	Friction velocity
P_{rt}	A turbulent Prandtl number
z	Vertical coordinate corresponding to the temperature
z_0	Roughness length
k	Von Karman constant
B_T	Molecular sub-layer correction
P_t	Molecular Prandtl number
v	The kinematic viscosity of water
P_G	The global average crushing pressure
A	Nominal contact area
P_G	Effective ice pressure
w	Structure width under ice action
h^*	Reference thickness
m	Experimental constant
n	Experimental constant

C_R	Ice reference strength for subarctic climate
H_B	Load required to break the ice blocks against the slope
H_R	Load required to push the ice blocks up the slope
H_T	Load required to turn the ice block at the top of the slope
H_P	Load required to push the sheet ice through the rubble
H_L	Load required to lift the ice rubble with the unbroken ice floe
ξ	The ratio of horizontal and vertical forces
σ_f	Ice flexural strength
E	Elastic modulus of the ice
l_c	Length of circumferential bending crack
μ_i/μ	ice-ice coefficient of friction / Ice structure friction coefficient
F_c	Horizontal force in which ice floes fail by crushing over the full width of a bridge pier
C_a	Constant to account for the aspect ratio effect found in small-scale indentation tests
D	Pier diameter
σ	compressive strength of ice sheet
$\alpha 1$	The angle between the sloping surface and the horizontal
l	The characteristic length of the floating ice sheet
ν	Poisson's ratio of ice
$\rho_i g$	The specific weight of ice
P_5	Load on pie in a direction along its major axis resulting from a collision with a drifting ice floe
j	Coefficient depends on the obstacle ice floe encounter
v_i	The calculated velocity of a drifting ice floe
w	Wind velocity calculated based on metrological data
P_T	Static load per unit of length of contact between the ice and a structure resulting from thermal expansion of the ice cover
R_0	The elastic limit of the ice
$\alpha 2$	Coefficient of linear expansion of ice

ϑ	Rate of increase in air temperature
P_O	Static load on a pier when an ice-free area is maintained in the spans between them
l	Width of span
b	Width of support
R_p	Crushing strength of ice
P_{2H}	The horizontal component of the ice load acting on a pier in the direction of its axis
R_i	Failure strength of ice in bending
β	The angle between the cutting edge of the pier and the horizontal
P_{2V}	The vertical component of the ice load
F_r	Froude number
P_1	The force caused by current drag on the lower surface of the ice field per unit area
P_2	The force of hydrodynamic pressure on the edge of the ice field caused by flow, per unit edge surface area
P_3	The horizontal component of the force of gravity on the ice field where there is a slope of the free flow surface, per unit surface area of the ice field
P_4	The force resulting from the air drag against the upper surface of the ice field, per unit surface area
L_z	The length of the ice jam from which pressure is transmitted against the structure
L	Mean length of the ice field in the direction of the flow
i	Water surface slope
$\mathrm{F_G}$	The global average pressure, for crushing
$\mathrm{k_s}$	Interference and sheltering factor
$\mathrm{k_n}$	The factor for the effect of non-simultaneous failure
$\mathrm{k_j}$	Ice jamming factor
Pr	Probability of exceedance for life of the structure

p	Probability of exceedance for a single year
d	Ice floe diameter
$\bar{L}$	Mean ice floe diameter
$\bar{V}$	Mean drifting velocity of an ice floe
$C_{d,a}$	Drag coefficient of air
$C_{d,w}$	Drag coefficient of water
D_{floe}	Diameter of ice floe
V_c	Current velocity
V_w	Wind velocity
ρ_a	Density of air
ρ_w	Density of water

Chapter 1

Introduction

1.1 Background

Ice impacts people in many ways that we only started to understand in the latest decades. In Arctic and sub-arctic regions, ice is characterized as a natural danger that can imperil human lives and interfere with human activities, for instance, structures and industrial production. Moreover, ice can interfere with flood control projects, sediments and scouring, navigation and water supply and power plant. Therefore, coastal and riverine structures in these regions shall withstand the significant forces exerted by the ice, driven by wind or current. Furthermore, ice has also impact on the global climatic change (Ashton, 1986).

Ice loads on a bridge structure can be one of the major components for the Extreme Limit State (ELS) combinations, specified in the Euro Code. In arctic and sub-arctic regions, the ice action on infrastructures such as platforms, lighthouses, sub-sea pipelines, or wind turbines may exceed the total forces of waves and currents and may, therefore, determine the design. For example, in regions such as Beitstad in Norway, ice loads can be the predominant lateral force in the design of bridge sub-structures. Therefore, accurate estimation of ice forces that can act on bridge piers in northern climates is critical in both cases – the design of new bridges and the evaluation of existing bridges. Different design codes provide empirical formulae to calculate the design ice forces, based on the effective ice strength, thickness and other important empirical environmental or climatic coefficients. Even with accurate values for the ice strength and the ice thickness, ice loads, calculated based on empirical formulae, may be inaccurate because of the boundary conditions and the ice breaking conditions that may not be as assured as in the formula. Therefore, these calculated ice forces may result in over-designed with cost overruns, or under-designed that may endanger public safety (Ahrenstorff, 2017). The mechanism of ice formation in sea, fjords, rivers, and lakes and ice loads on bridge sub-structures had been studied for the last many decades, as a commonly encountered phenomenon in cold regions. Accurate prediction of extreme lateral ice forces on

supporting structures at the water surface is of special interest to researchers due to its implications on the structural design (Frederiking et al., 2014). Varied methods were employed to estimate the ice loads, including modeling of the ice-structure interaction, using nonlinear finite element models (e.g., Ahmed 1994, Yuan 2009), scale-model test in a laboratory (Timco 1995, Lever 2001), and full-scale structures in the field (Frederking 1992, Brown 2010). According to these studies, there is a variety of factors that can have a significant influence on ice loads, such as the shape of the sub-structure, ice conditions, and the ice failure mode.

Ice forces must be considered in the design of the coastal and hydraulic structures. To predict Ice forces, the ice conditions, like thickness, strength, morphology, etc., must be understood appropriately (Frederking 1992, Brown 2010). Also, the environmental driving forces, i.e. wind, current, and temperature, must be understood appropriately. Both the ice conditions and the environmental factors are combined in a formula to calculate the magnitude of ice forces that a structure is expected to withstand in the future and over its lifetime. The existing standards for estimation of the ice loads on vertical and sloping structures adopt different analysis methods, and to determine the global ice loads on these structures, the ice-structure interaction must be identified. Therefore, the analysis methods of the ice loads are much influenced by the local ice conditions over the area of concern (Gudmestad et al., 2006).

The ice load applied to a structure depends on the nature of the failure mechanism induced through the ice feature, which depends on the shape of the structure. Generally, structures that are vertical, or close to vertical, causing the ice to fail in crushing while sloping structures cause the ice to fail in bending. Secondly, most of the standards used in the field are related to offshore structures, while few standards are focusing on riverine and lake structures. In both cases, the ice conditions and environmental conditions will be different. Therefore, this imposes a dire need to dig in by doing more research in the ice, existing on fjords and lakes. In this study, most of the focus will be on fjord and lake ice conditions and their loadings on a bridge pier will be assessed and compared by using different shapes of structures and standards of different countries, followed by the deterministic extreme value analysis and probabilistic assessment of the ice loading during the design lifetime of the structure.

1.2 Research objective

The main objective of this study is to predict the ice actions on the bridge over the Beitstadsundet for the whole design lifetime of the bridge by using different standards adopted in different countries – Norway (ISO), America (AASHTO), and Canada (NRC). In order to elaborate more on the objective of the study, the following tasks were planned:

- Estimation of the ice conditions from the hydrological data and field measurements, and the development of a relationship between the driving forces and the meteorological conditions.
- Effect of river discharges (falling in the fjord) on the tidal discharge and current.
- Comparison of ice thickness and growth model predicted with Delft3D-FLOW (Ice module) and the conventional deterministic approaches i.e. (Stefan's law, Lebedev & Zubov's model) in order to validate this module on this small scale.
- Comparison of the different standards – ISO, AASHTO, and the NRC-Canada Standard to predict the ice loads, and determination of mechanisms that might induce the maximum ice load on the bridge pier.
- A deterministic extreme value analysis of the global ice actions to compute the design ice forces over the lifetime of the bridge – by considering different scenarios.
- Probabilistic assessment and uncertainty analysis (associated with the global ice action due to ice structure interaction) by using Monte-Carlo simulation.

1.3 Research motivation

As interest and investment in hydraulic and coastal structure projects have been increasing worldwide, some structures will be built in locations where the ice of significant thickness forms and grows on the water surface. Then, ice moves under the driving forces of wind, current and thermal effects, and may result in substantial forces on bottom-fixed support structures. Design of the support structures for such projects requires an integrated tool that can calculate the cumulative effects of forces due to their operations, wind, waves and floating ice. In addition, the dynamic nature of ice forces requires that these forces must be included in the design simulations.

The aspiration is to determine the correct ice loads on the bridge piers and to estimate and to reduce the risk to the riverine and coastal infrastructures. Ice can interact with structures in regions with at least seasonal ice coverage. Therefore, the prediction of ice loads on offshore and hydraulic structures is required by many standards or classification rules and guidelines. In order to do so, empirical formulae are often prescribed. These formulae are based on assumptions in combination with model- or full-scale tests. Yet there are very few publications where the results of the formulae are compared with each other. A case study is made for ice loads on the Beitstadsundet bridge in Norway.

First, the ice thickness and growth model, predicted by the empirical formulae, is compared to the process-based mode i.e. Delft3D-FLOW (Ice module). Secondly, current empirical formulae, given by standard bodies or classification societies, are reviewed with focus on applicability and recommendations regarding the processes of ice-structure interactions in both cases of sloping and vertical structures, and highlighted the differences between them and whichever parameters, involved in the mathematical expressions that will influence the ice load on the bridge piers, may lead to give a reasonable ice load over the design lifetime of the structure. These formulae could prove to be very useful in determining the accuracy of the originally calculated loads at the site and the methods which could be used to calculate the ice loads in the future.

The interaction between ice and the bridge can result in damage or destruction of the bridge sub-structures and can alter ice movement such that ice impacts the banks of the fjord. Therefore, it is important to understand the factors governing the interaction between the bridge and ice in order to appropriately design bridges on fjords and lakes with seasonal ice covers.

1.4 Research structure

This study is organized into different tasks and milestones to be followed in a row to do the proposed thesis. These milestones are as given as under:

1) Literature review of previous similar relevant works.
2) Observation and collection of hydrological and meteorological data to calculate the ice parameters which are critical to finding the ice actions against the bridge pier.

3) Detailed site overview with respect to water levels, currents, wind velocity, and direction and discharge.
4) Prediction of 100-year design values for the ice load by fitting different distributions on the important ice force input parameters.
5) Review of the existing ice growth and load calculation models and standards to choose the most suitable option for the study under consideration.
6) Preparation of charts and graphs to facilitate analysis and comparison.
7) Results and outcomes.
8) Drawing conclusions and making recommendations for further improvements.

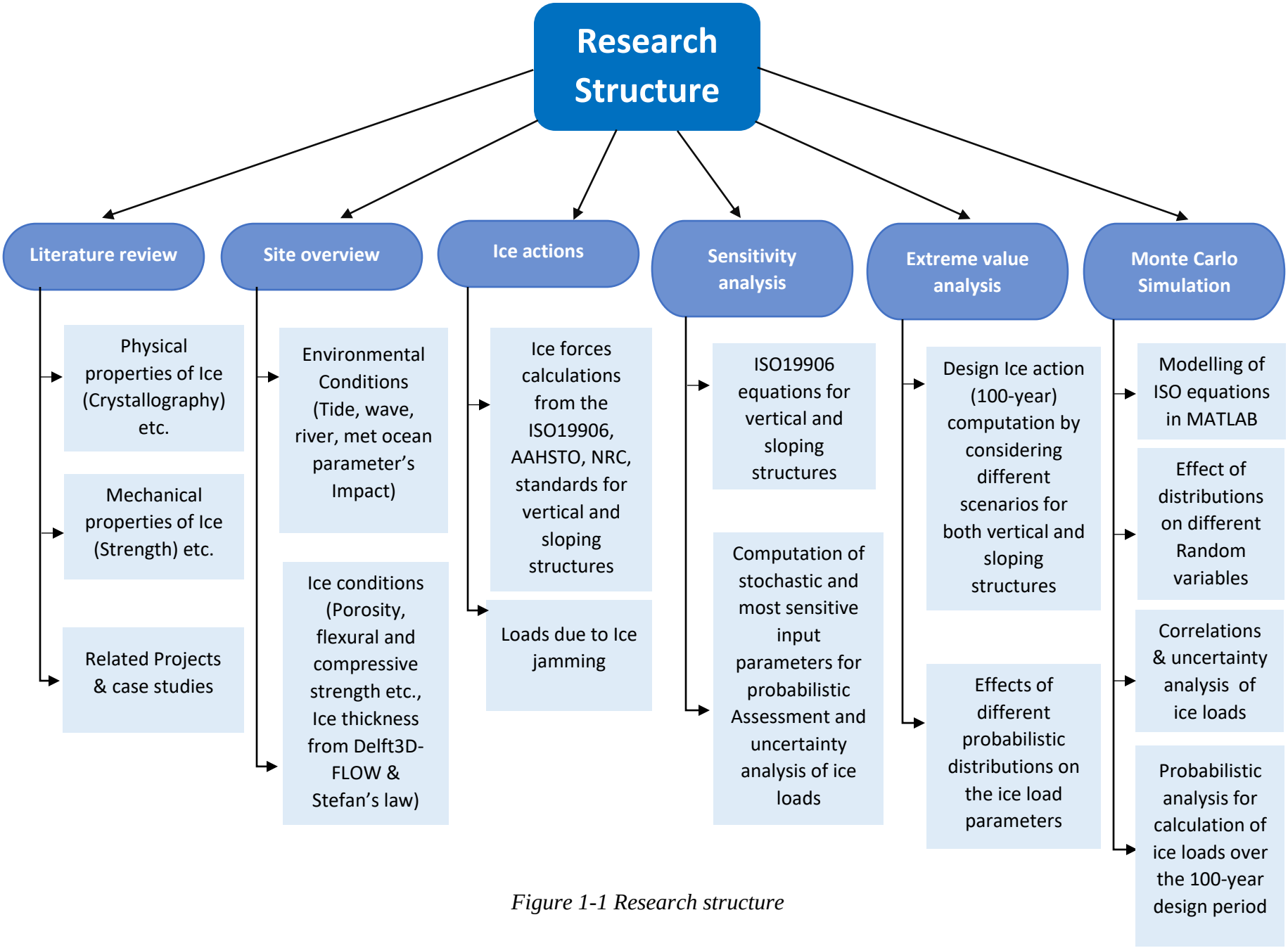

Figure 1-1 Research structure

1.5 Research limitations

The empirical model for the ice growth used in the current study was not comprehensive, and It is prone to site-specific issues, and can be used for a very specific type of project, along with this there was a lot of uncertainty in the met-ocean data used in the analysis and made a lot of assumptions regarding ice properties and probabilistic analysis of the ice loads. Other than these limitations, the following phenomena are not included in the model:

- Uncertainty in the bathymetric and water depth data at the bridge upstream.
- The tidal current along with wind speed is only considered to drag the ice against the structure.
- Ice floe of uniform thickness is considered for the computation of ice actions.
- A lot of site-specific empirical coefficients in different standards were defined according to their own sites and were involved to calculate the ice loads on bridge piers, and those were assumed according to the best fit at the proposed location of the project.
- For modeling in Delft3D-FLOW (Ice module) a record of met-ocean data for the past 50 years was required, but among them, the values of relative humidity and cloudiness and snow thickness were extrapolated based on the available data.
- For the deterministic extreme value analysis number of ice floe hittings per year (hitting rate) against the bridge pier were assumed as there was no data available regarding ice concentration and encounter probability.
- In Monte-Carlo simulation, a sample size of 10,000 was assumed.
- In the correlation analysis of the most sensitive observed input parameters and to generate the uncertainty in the calculation of ice loads, Gaussian copula (Nataf Model) is used to create the desired correlation between the most important parameter

Chapter 2

Literature review of ice properties and similar case studies

2.1 Review of ice processes and properties

2.1.1 Introduction into the ice processes and properties

In order to determine the ice actions on hydraulic and coastal structures, it is inevitable to understand the ice processes and properties. Each year, ice grows on and disappears from fjords and lakes in tune with the cycles in nature. Unless the ice causes problems, for instance, flooding, blocking and damage to the hydraulic structures, few people pay more than cursory attention. Ice processes on lakes and fjords are different from those on rivers – the size of the water body affects which processes take place for both lakes and rivers. Ice owes its existence to the thermal process of heat transfer, but its evolution is greatly influenced by the physical and mechanical processes, as per Article 2-1 in AASHTO. Therefore, this chapter introduces the phases of ice formation and evolution, the failure mechanisms and identifies the principal physical and mechanical properties that govern the ice processes, which are important to determine the forces, exerted by the ice on bridge piers.

2.1.2 Physical properties of ice

Some physical properties of the ice on fjords and lakes are related to the physical aspects of the ice, such as density, salinity, structure, grain sizes, thickness, porosity, etc. (Sultabayev, 2015). To determine the ice actions, as per different standards there is no need for a detailed description of the microstructure and the crystallography of the ice. Therefore, this section only focuses on a minimal required explanation of the molecular structure of the ice and the physical properties that determine engineering decisions, such as design ice load.

2.1.2.1 Crystal structure of ice

Several forms of ice are existing under different conditions of temperatures and pressures, but only one form, called ice Ih, takes place in nature. The crystal structure of ice Ih builds on a crystallographic arrangement of molecules of water, which have a repeating tetrahedral geometry with hexagonal symmetry (see Figure 2-1). Along with this, the ice structure has a series of parallel planes, called basal plane, and a major axis of symmetry, called c-axis, that is normal to the basal plane as shown in Figure 2-1. Furthermore, three a-axes at 120° to each other are perpendicular to the c-direction (Sultabayev, 2015).

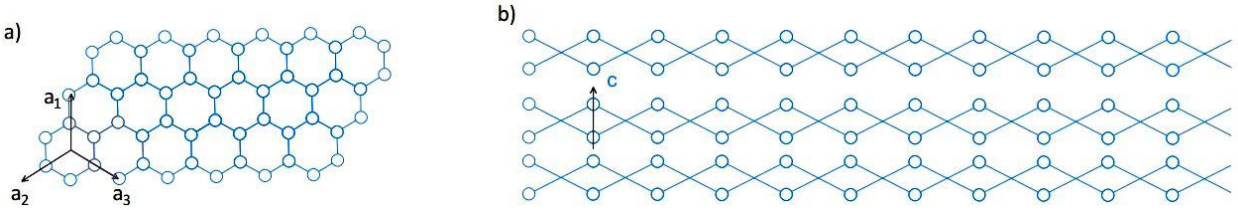

Figure 2-1 Idealized arrangement of atoms in Ih ice wherein oxygen atoms are presented in white circles and view of crystal lattice looking a) along the c-axis and b) along with basal-plane layers (Palmer and Croasdale, 2012; modified)

The Ice structure effects the ice formation process. It is very easy to add atoms to an existing basal plane, that is perpendicular to the c-axis (see Figure 2-2), so that's why crystal's growth is in the a-directions. Furthermore, differences in the mechanical behavior of ice under different directional loadings can also be explained in terms of the structure of ice. So, an ice crystal has three hydrogen bonds, 9 in the basal plane and only one hydrogen bond along the c-axis. Therefore, fracture along the basal plane requires rupturing two hydrogen bonds in the unit cell, while fracture of the unit cell along planes normal to the basal plane requires rupturing at least 4 hydrogen bonds. Additionally, ice properties, such as thermal conductivity, atomic diffusivity, and elastic stiffness, are also isotopically perpendicular to this c-axis (Løset S., 2014b).

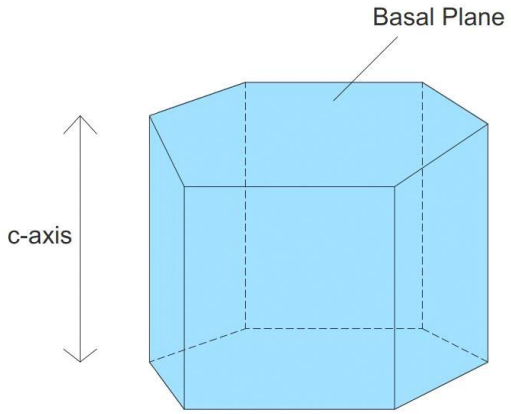

Figure 2-2 Basal plane perpendicular to the c-axis of ice crystal

However, ice crystals may significantly vary in size. A group of ice crystals, forming sea ice, may have the c-axis randomly oriented. As illustrated in Figure 2-3, ice is mainly an orthotropic material (i.e., columnar ice) with randomly orientated c-axes, covered by the layer of granular ice. It should be noted that the salinity and the temperature of ice are not constant and change through the ice sheet (Løset et al. 1998).

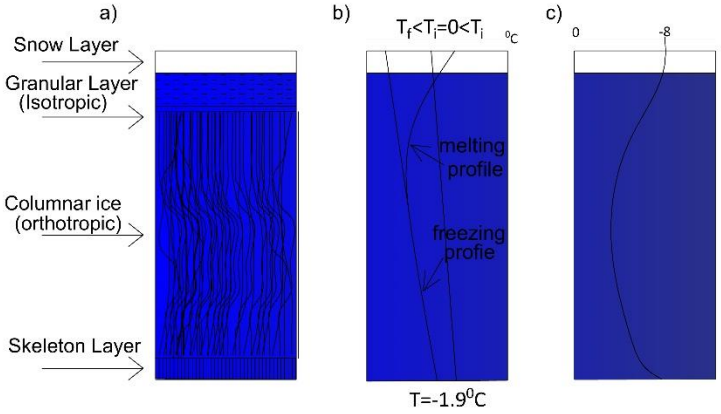

Figure 2-3 Ice morphology, temperature and salinity profiles across an ice sheet – a) typical morphology of sheet ice layer; b) typical temperature profile during freezing and melting where $T_{freezing}$ is the freezing temperature of ice and T_i is the designated ice temperature; and c) typical salinity profile through ice sheet (Gürtner, 2009; modified).

2.1.2.2 Density

The density of freshwater ice is 916.8 kg/m^3 at 0°C. Like other materials, ice becomes denser as the temperature is decreasing the density of ice at –30°C is about 920.6 kg/m^3. Along with the

temperature, the density of ice is also affected by the presence of impurities within the structure of ice. The two common impurities are air bubbles and unfrozen water. The presence of air bubbles reduces the density of ice, while the presence of unfrozen water increases the density of ice. For ice found on natural water bodies, it is very difficult to determine these impurities. Therefore, the approximation of 910–917 kg/m^3 for the ice density is probably adequate for the ice loads calculations, as per Article 2-2 in AASHTO.

2.1.2.3 Thermal conductivity

The thermal conductivity of ice defines the ability of ice to transmit heat under a unit temperature gradient and it is a very important parameter to determine the ice cover thickness which is used to calculate the ice loads. The temperature dependence of thermal conductivity is described by the following expression:

$$k_i = 2.21 - 0.011\,T$$

Where:

T = temperature in degree F, in the English unit system, degree C: $k_i = 1.27 - 0.0061(T - 32)$, and

k_i = thermal conductivity in watts per meter per degree Celsius ($W/m\,°C$), thermal conductivity in British unit system, feet per hour per square foot per degree Fahrenheit: $Btu\ ft/hr\ ft^2\,°F$.

Ice is not a great insulator, but also it does not conduct much of the heat. The thermal conductivity of ice is notably affected by air bubbles and the inclusion of unfrozen water that's why for determining the density of ice, the amount of both impurities in ice on natural water bodies is usually not known, and, thus, their influence is usually neglected, as per Article 2-2 in AASHTO.

2.1.2.4 Latent heat of fusion

Pure water freezes at 0 °C under standard atmospheric pressure of 101325 Pa. When water freezes, 333.4 J/g (143.3 Btu/lb) heat is released which is called of latent heat. Table 2-1 shows the amount of heat required to melt ice per unit mass and volume, as per Article 2-2 in AASHTO.

Table 2-1 Amount of heat required to melt ice per unit mass and volume

Unit	Amount
gram	333.4 J/g
kilogram	3.33 × 105 J/kg
pound	143.3 Btu/lb
cubic meter	3.06 × 108 J/m^3
cubic foot	8196.8 Btu/ft

2.1.2.5 Salinity

For the first-year level ice, the salinity is usually expressed as the mass of the salts contained in a unit mass (i.e., parts per thousand or ppt). The salinity varies over the depth of an ice sheet. This depth dependence decreases throughout the lifetime of the ice sheet because the salt within the ice migrates downward through the ice. Salinity, together with temperature, determines the brine volume which is a very important parameter to calculate the flexural strength of ice which is an important parameter to calculate the ice loads in sloping structures. Any increase of salinity yields a larger brine volume, and thus a higher porosity, making the ice weaker. Although there may be significant salinity changes within a small sample of ice, the average salinity of a growing first-year level ice sheet is related to the ice thickness. This is found empirically and given as in ISO19906 as under:

$$S = \begin{cases} 13.4 - 17.4\ h_i & h_i \leq 0.34m \\ 8.0 - 1.62\ h_i & h_i > 0.34m \end{cases}$$

Where:

S = ice salinity, and

h_i = ice thickness.

2.1.2.6 Temperature

The freezing point of seawater depends on the salinity and the pressure. According to the UNESCO handbook (1983), named as 'Algorithms for the computation of fundamental properties of seawater, the freezing point of seawater can be found using the following expression:

$$T(fr) = \left(-57.5S + 1.71S\sqrt{S} - 0.2155S^2 - 7.53P\right)10^{-3}$$

Where:

T = freezing temperature, and

P = sea-level pressure.

At average sea-level pressure, the relation between the freezing point and the salinity of seawater may be considered linear. Therefore, one can state that for every 1 ppt increase in salinity, the freezing point approximately decreases with 0.055 °C and thus the equation above reduces to:

$$T(fr) = -0.55S$$

The freezing temperature is a very important parameter to calculate the freezing degree days which is very important to calculate the ice thickness.

2.1.2.7 Porosity

The porosity of sea ice is often expressed in terms of the brine volume, existing in the ice. Therefore, the brine volume is defined as the amount of liquid brine in the ice matrix. Brine volume is influenced by both temperature and the salinity. The brine volume is calculated as given in ISO19906 as under:

$$V_{brine} = S\left(\frac{49.18}{|T|} + 0.53\right) \qquad -22.9℃ < T < -0.5℃$$

Where:

V_{brine} = brine volume, and

T = ice temperature.

Next, to brine, the air is always present in the ice. As brine drainage occurs, the air volume may be significant. Therefore, the expression for the total porosity will be as given in ISO19906 as under:

$$\eta = V_{brine} + V_{air}$$

$$V_{air} \approx 1 - \frac{\rho_{sea\ ice}}{\rho_{pure\ ice}}$$

Where:

η = ice porosity,

V_{air} = air volume,

$\rho_{sea\ ice}$ = seawater density, and

$\rho_{pure\ ice}$ = pure water density.

2.1.3 Mechanical properties of ice

The mechanical properties of ice have a significant effect on the forces required to fail an ice sheet against a structure. Therefore, the mechanical properties of the ice are briefly reviewed in the following sections before going over the methodologies adopted to estimate the ice forces on a bridge pier. Ice can creep with little applied stress, or it can fracture catastrophically under high strain rate. There are two ways to classify the ice. One way is based on the melt from which ice grows (i.e., freshwater or seawater), and the second way is depending on the size of the ice floes (i.e., large ice floes or accumulations of broken ice in random ice rubble). Thus, the conditions under which ice forms determine the grain structure of the ice, with common forms, such as frazil ice, columnar ice, discontinuous columnar ice, and granular ice. Porosity and the grain structure both, noticeably influence the mechanical properties of the ice (Sultabayev, 2015).

Sea ice is an inhomogeneous, anisotropic and nonlinear viscous material (Sand, 2008). The mechanical properties of ice, including tensile, compressive, flexural and shear strengths, along with Young's modulus, Poisson ratio and friction coefficients, are functions of the physical properties (i.e., the structure of ice, brine volume and porosity), temperature, the confinement of the ice sample, strain rate, etc. These ice properties could be derived from the relationship

developed from physical modeling and field observations (Sultabayev, 2015). Hence, the mechanical properties, required in the calculation of the ice forces on the bridge pier, are described in the following section.

2.1.3.1 Compressive strength

The compressive strength of ice is the maximum principal stress corresponding to failure begging under the ice compression (Løset et al., 2006). Mostly, ice fails in the compression which takes place when thick ice interacts with offshore structures (Timco and Weeks, 2010). Thus, the ice is presented by two kinds of inelastic behaviors under compression (see Figure 2-4). Based on the shape of the stress-strain curve, three zones can be distinguished: (i) brittle regime, (ii) ductile regime and (iii) transition zone. Ice shows the ductile behavior when the stress-strain curve has a plateau and, on the other hand, the strain rate is lower than $\dot{\varepsilon}_{D/B}$. The peak stress (or ductile compressive strength) increases with (i) increasing strain rate; (ii) decreasing temperature and (iii) decreasing salinity and porosity of the ice. The grain size does not significantly influence on the peak stress (Sand B., 2008).

Another important zone is the transition point, where the compressive strength reaches its maximum. Hence, the ice loads on a structure will be maximum as well. The decreasing of the compressive strength after the transition might be explained by the begging of the crack propagation (see Figure 2-5) – at strain rates lower than $\dot{\varepsilon}_{D/B}$ (i.e. ductile ice behavior), cracks form without propagation, while at strain rates above $\dot{\varepsilon}_{D/B}$ (i.e. brittle ice behavior), wing cracks propagate from the cracks formed before. The transition rate $\dot{\varepsilon}_{D/B}$ belongs to the range from 10^{-4} to $10^{-3}\ s^{-1}$ at temperatures from -40 °to -5 °C (Sultabayev, 2015).

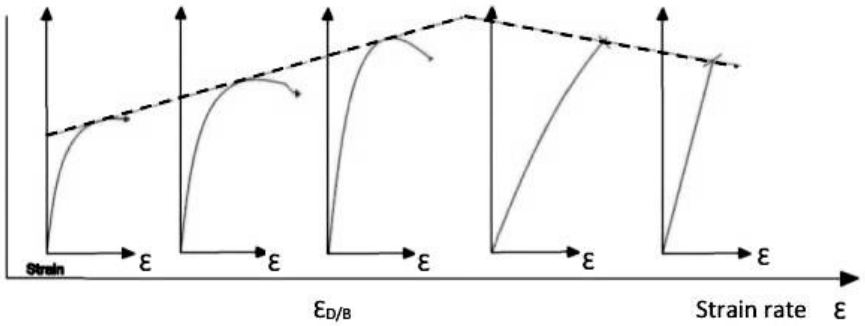

Figure 2-4 Schematic sketch showing the effect of strain rate on the compressive stress-strain behavior of ice (Sand, 2008; modified)

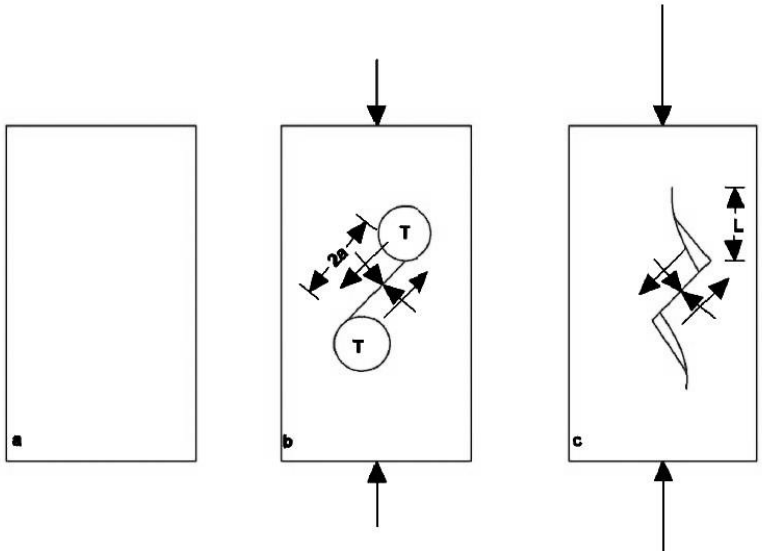

Figure 2-5 Development of the wing crack mechanism: a) Zero load. No cracks. b) Cracks nucleate at critical compressive stress. Normal stress acts to close cracks and shear stress acts to cause sliding. T denotes tensile zone. c) wings of length L nucleate in the tensile zone at higher stress (after Sand, 2008; modified)

The uniaxial compressive strength of sea ice in horizontal and vertical directions (also see Figure 2-6) are respectively found from tests as given in the equations as under (Timco & Frederking, 1990):

$$\sigma_C^H = 37\varepsilon^{0.22}\left(1 - \sqrt{\frac{\eta}{0.27}}\right)$$

$$\sigma_C^V = 160\varepsilon^{0.22}\left(1 - \sqrt{\frac{\eta}{0.2}}\right)$$

Where:

η = ice porosity,

ε = strain rate of ice,

σ_C^V = vertical compressive strength $[MPa]$ and,

σ_C^H = horizontal compressive strength $[MPa]$,

Typical values from 0.14 to 6-8 Mpa.

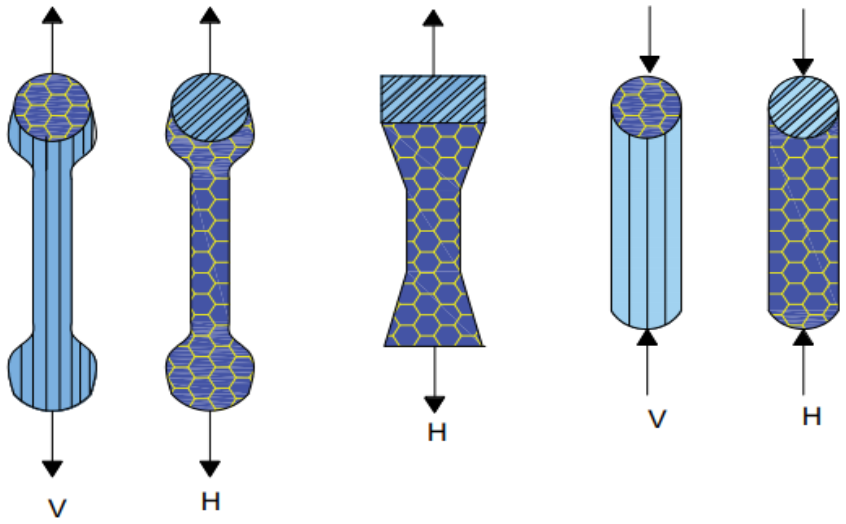

Figure 2-6 V= Tension or Compression along the vertical axis of an ice sheet & H= Tension or Compression along the horizontal axis of an ice sheet

The typical ranges for the compressive strength in both the directions are given as follows;

$$\sigma_C^H \approx 2 - 5\ MPa$$

$$\sigma_C^V \approx 5 - 15\ MPa$$

$$\frac{\sigma_C^V}{\sigma_C^H} \approx 3$$

2.1.3.2 Flexural strength

The flexural strength of ice is also referred to as the bending strength of ice. It is the maximum stress that an ice sheet or ice floe can withstand when it is subjected to a vertical load at the edge of the ice sheet, e.g., interacting with an inclined bridge pier. The flexural strength of ice has been

measured in several studies (Frankenstein 1968, Lavrov 1969, Gow 1977). Based on these studies, the expected bending strength of columnar freshwater ice ranges from low 0.5 to 1.2 Mpa The range of values reflects that this variety in the obtained results depends on whether the tests were conducted with the top of the ice specimen under tension or the bottom of the ice specimen under tension, and the corresponding variation in crystal ice (as per article 2-3 in AASHTO). Based on many small-scale tests, the flexural strength is found using the following equation:

$$\sigma_f = 1.76e^{-5.88\sqrt{V_b}}$$

Where:

σ_f = flexural strength $[MPa]$.

V_b = Brine volume $[fraction]$.

2.1.3.3 Friction

Friction forces are very important in problems associated with interactions between ice and coastal structures. Due to static and dynamic ice-structure interactions, static and kinetic friction coefficients are distinguished. The friction depends on the ice temperature, the roughness of interacting surfaces and relative velocity. The effect of the temperature of the ice on the friction coefficients is not that much high but the friction coefficient decreases as the relative velocity is increasing. The static and kinetic components of the friction do not depend on the contact area, as per AASHTO. The friction coefficients for the ice interaction with concrete, ice and ground are presented in Table 2-2.

Table 2-2 Friction coefficients for the ice interaction with concrete, ice, and ground

Construction material	Influence of sliding velocity					
	$v_s \leq 0.01$ m/s		$v_s = 0.1$ m/s		$v_s = 0.5$ m/s	
	Mean	St. Dev	Mean	St. Dev	Mean	St. Dev
Smooth steel	0.1	0.02	0.05	0.01	0.05	0.01
Smooth concrete	0.12	0.02	0.05	0.015	0.05	0.01
Corroded steel	0.15	0.03	0.1	0.03	0.1	0.03
Rough concrete	0.22	0.05	0.1	0.03	0.1	0.03

2.1.3.4 Modulus of elasticity

The elastic modulus (E) defines the relationship between the stress and the strain. In the case of ice, the elastic modulus depends on the ice temperature, crystal structure, and the rate of stress loading. Like other mechanical properties of ice, the measured values of the elastic modulus also depend on the technique of measurement. The values measured in the field for the elastic modulus of intact freshwater ice have ranged from about 0.4 to 9.8 GPa (55 to 1350 kpsi). On the other hand, the elastic modulus of ice grown in laboratory tanks ranges from about 4.3 to 8.3 GPa (600 to 1150 kpsi), the elastic modulus of small laboratory specimens is higher. Furthermore, the values for widely cracked ice may be much lower (as per article 2-3 in AASHTO).

2.1.3.5 Poisson's ratio

Poisson's ratio is defined as the ratio of the lateral strain to the longitudinal strain in a homogeneous material for a uniaxial loading condition (Timco and Weeks, 2010). Poisson's ratio is an important engineering property of a material in terms of viscoelasticity effects in sea ice. Poisson's ratio used for in the formulas that are used to calculate the ice actions on sloping structures. (as per AASHTO).

2.1.4 Ice features

Different ice features have different size and thermo-mechanical properties. Hence, the ice action exerted by an ice ridge is different than that exerted by level ice. Therefore, it is worthy to differentiate ice by its own feature type. Also, it is important to estimate how often different ice features may interact or affect the structure. Ice features are usually undeformed ice or deformed ice. Undeformed ice is ice that has not been deformed mechanically, whereas deformed ice is ice that has been deformed mechanically, typically by waves, currents, wind, thermal expansion, etc. Undeformed ice can be distinguished into three categories of ice. These are rafted ice which is formed by two or more pieces of level ice overriding each other, ice ridges which result from compaction of broken pieces of ice partly frozen together, and broken ice may be added as a separate feature. It consists of individual floes with water in between. In other words, the ocean surface is not completely covered by sea ice (Høyland, 2017). In this study, ice floes of different sizes (Uniform distribution) were taken to determine the Ice loads against the bridge pier.

2.1.5 Ice floe: failure types

Many studies in the past looked at ice formation and break-up processes in waterways. Other studies focused more on the effects of ice loads on bridge structures, and how to take it into consideration when designing. These studies have added to the knowledge related to the dynamic ice forces on bridge piers and their effects. Furthermore, ice formation varies across the globe, and ice will have different properties based on the process. Along with the ice growth and properties, another important topic is the ice floe failure types. Montgomery et al. (1984) described five types of failure that are commonly seen when a moving ice floe strikes a bridge pier. The type of failure is influenced by the strength of the ice, the geometry of the pier, and the size of the ice floe. The types of ice failure are; crushing, bending, splitting, impact and buckling. Crushing takes place when ice fails by local crushing across the width of the pier, and crushed ice is continually cleared from a zone around the pier as the ice floe moves past, while bending happens floe for bridge piers with inclined noses when a vertical reaction component acts on the impinging ice, and this reaction causes the floe to raise the pier nose and fail as flexural cracks form. Splitting occurs when a comparatively small floe strikes a pier, and therefore stress cracks split the ice floe into smaller parts, whereas impact takes place if the ice floe is small, and it is brought to a halt when impinging on the nose of the pier by bending or splitting. Finally, buckling occurs for very wide piers, where a large floe cannot clear the pier as it fails, therefore compressive forces cause the ice floe to fail by buckling in front of the pier nose. Figure 2-7 shows ice floe failure modes for vertical structures. However, only crushing and bending failure modes have been considered in this case study. Moreover, Figure 2-8 shows ice floe failure against vertical and sloping structures.

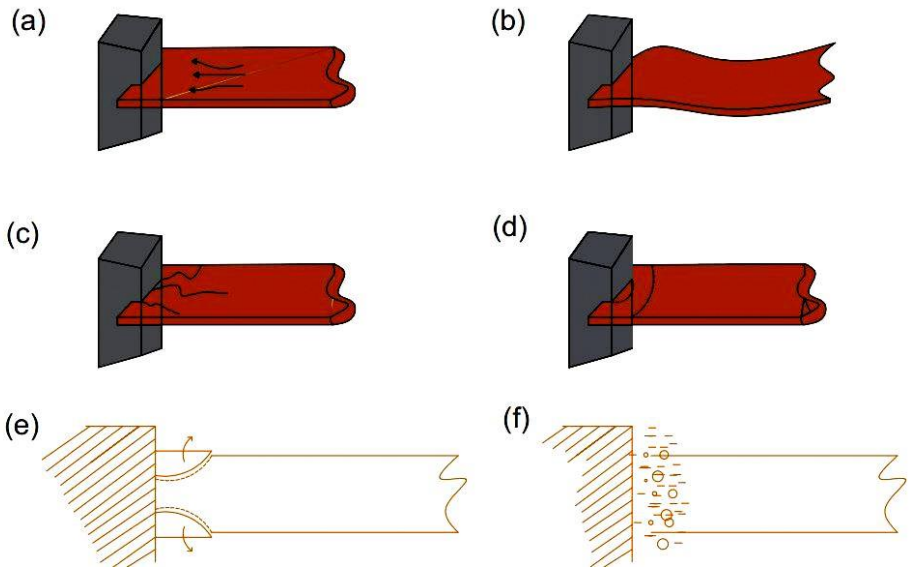

Figure 2-7 Ice failure modes for vertical structures – a) creep; b) buckling; c) radial cracking; d) circumrenal cracking; e) spalling and f) crushing (Sanderson, 1988; modified)

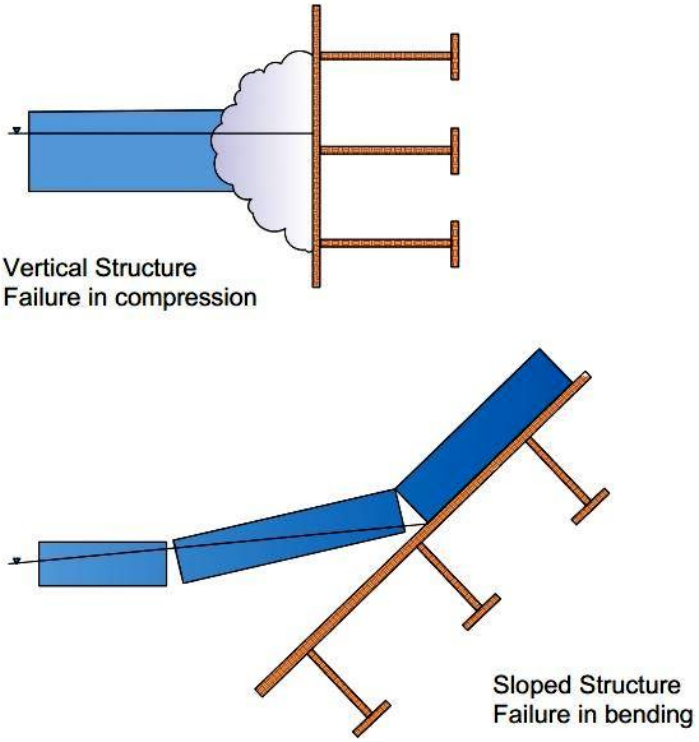

Figure 2-8 Ice failure against vertical and sloping structures

Montgomery et al. (1984) also stated that the controlling design dynamic ice forces on typical bridge piers on larger bodies of water will be caused by crushing and bending ice failures. However, impact failures could be the controlling force for bridges on smaller streams not capable of carrying large ice floes. Due to the high uncertainty in ice formation and characteristics, criteria

based on actual field measurements (Haynes et al. 1991) must be developed for the design of bridges under ice loads. These measurements are made at existing bridges to refine the design loads for future designs. To date, there has been only a handful of papers wrote about direct measurements studies (Haynes et al. 1991; Brown et al. 2009). With most of these studies conducted for bridges over straits and ocean water, there is a lack of studies on inland rivers and streams. Also, there was no study completed previously at Beitstadsundet regarding this.

2.2 Review of ice-bridge interactions and relevant projects

2.2.1 Ice-bridge interactions

In accordance with the International Standardization Organization (ISO19906), it is adapted to use the words: actions and action effects. These refer to:

1) Loads exerted on a structure due to ice.
2) Loads applied on a structure externally; i.e. the structure does not move and does not deform or there is no damage due to the applied ice loads. Therefore, the structure is assumed to be rigid.
3) Loads due to imposed deformations and/or accelerations; i.e. the structure endures additional loads due to the ice-induced motion of the structure or dynamics structural damage, such as vibrations.

The three limiting mechanisms and the corresponding types of ice-structure interaction that are identified given as following:

- Limit Energy - Ice impact
- Limit Force - Driving forces
- Limit Stress – Ice failure

Initially, as the ice floe collides with the structure the action is always determined by limit energy, until the relative velocity between ice and structure becomes zero and/or another mechanism takes over. Ice forces on structures are determined either by the environmental driving forces (Limit force) or by the force required to fail the ice sheet and move the ice around the structure (Limit stress); whichever is the least. Several state-of-the-art techniques are there to predict these forces on fixed rigid structures. A rigid structure is where the ice interaction process is not influenced by

the deformation of the structure itself. Hence, structures are considered in three broad categories; structures with sloping sides, structures with vertical sides, and such wide structures as artificial islands. Forces exerted on structures as a result of thermal expansion of ice or water level fluctuations are static loads, whereas the impact and pressure forces exerted, e.g., by drifting ice are dynamic loads. Therefore, when designing individual construction elements that may be affected by ice formation, it is necessary to consider their reliability performance under these conditions. (Carstensen, 2008).

2.2.2 Ice-loading projects in the past

Over the last three decades, several bridge piers have been instrumented in Canada and US for ice load measurements. Hondo bridge in the Athabasca River was instrumented during the construction stage in 1966 and gave the first ice force measurements in the spring of the year 1967. Two bridges over smaller streams in Alberta, Kneehills Creek, and the Pembina River, were later constructed and instrumented to record the ice forces.

However, the Kneehills Creek instrumentation was dismantled due to insignificant ice runs. During two winters in the late 1960s, Schwarz (1970) instrumented a test pile on the Eider Estuary. More recently, the National Research Council of Canada (NRC) has instrumented a bridge pier in the Rideau River in Eastern Ontario and did the extreme value analysis of the ice loads on the confederation bridge during its designed lifetime. Also, the US Army Corps of Engineers Cold Regions Research and Engineering Laboratory (CRREL) have instrumented several piers in different rivers, including St. Regis, Ottauquechee and White Rivers, and South Dakota river. These bridge piers were selected to be examined in detail based on the availability and quality of the information about the time-load records and the ice conditions that caused those loads to occur. Along with the site measurements, ice loads were also computed using the empirical relations, and then a reasonable comparison was made between the measured loads at the site and the load calculated from the empirical relations (Timco et al., 1999).

Chapter 3

Methodology

3.1 General approach to finding the ice action

To find out the ice action on Beitstadsundet bridge piers, the first step taken was the assessment of likely ice conditions from the metrological data for the past 50 years, i.e., ice thickness, strength, features, etc. Ice conditions and properties can vary from year to year. Hence, critical design ice conditions that could occur during the lifetime of the structure have been defined. To act upon this, climatic data for air temperatures, snowfall, wind speed, cloudiness, relative humidity, and tidal water level were collected from the hydrological or oceanographic administration websites to develop the relationship between the ice conditions and metrological parameters. Ice cover thickness was calculated by applying Stefan's formula and then compared with the results from Delft3D-FLOW (Ice module). For the estimation of other ice properties, e.g., salinity, porosity, flexural and compressive strength, etc., formulae from ISO19906 and AASHTO have been employed.

Ice in its simplest form is unbroken level ice of uniform thickness which has been considered in this case study. However, it might be broken, and ice floes override each other to form the ice ridges, or it might be broken into individual floes of different sizes and thicknesses, floating at different speeds, being dragged by the wind and current and subject to thermal changes. Therefore, to compute ice actions on the bridge pier at Beitstadsundet, important parameters of ice conditions and critical condition that is likely to be encountered over the lifetime of the structure was determined by assuming some simplifications. Hence, the general approach to finding the governing ice actions according to ISO19906 is shown in Figure 3-1 below.

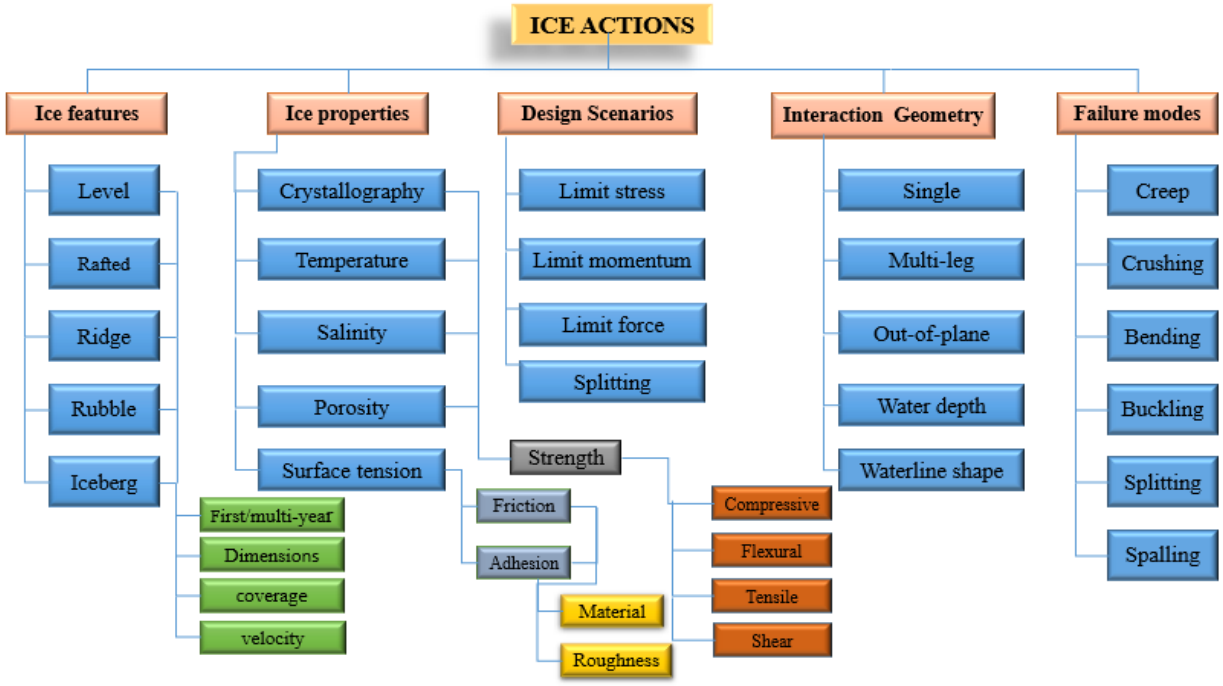

Figure 3-1 General approach to finding ice actions on structures (Løset et al., 2006; modified)

After the calculation of ice properties and conditions at Beitstadsundet, the equations given in different standards were applied to calculate the governing ice actions by considering the interaction of the proposed structure with a large ice floe. Initially, as the ice floe collides with the proposed structure, the action is always determined by the limit energy, until the relative velocity between ice and the proposed structure becomes zero and another mechanism takes place. After this, ice actions were determined in two limits: The limit force and the limit stress. The limit force is calculated as the driving forces due to wind and current in addition to the loads due to thermal expansion. Also, the limit stress is calculated as the ice action required for ice to fail upon interaction with the proposed structure. This was done according to three different standards: International, American and Canadian standards. Therefore, the governing ice action is always the lowest value of the limit force and the limit stress, as shown in Figure 3-2. Hence, the design ice action reflects the relevant ice interaction scenario, the limiting mechanism and ice failure mode for the geographical location of the proposed structure and the structural configuration.

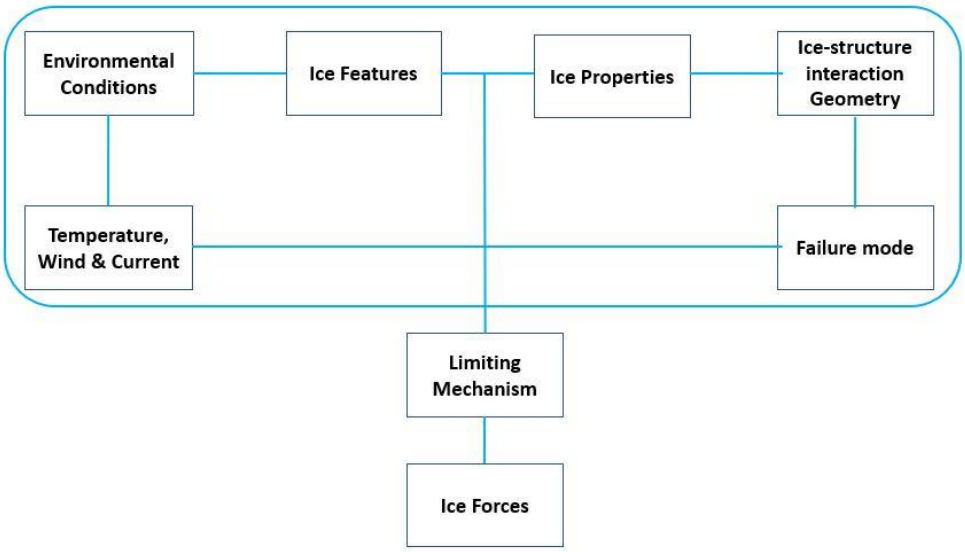

Figure 3-2 Procedure for determination of the limiting ice mechanism and the governing force

3.2 Approach to find the design ice action for the life of the structure

For the computation of the design ice loads, the results from the ISO19906 equations have been used because ISO19906 equations are more detailed in nature and contain many variables. Firstly, the sensitivity analysis of ISO19906 equations was carried out to check which input parameters can be the most sensitive in the computation of the governing ice actions. Sensitivity analysis of the ice load parameters gives information about the parameters that should be considered as stochastic variables and which parameters should be taken as deterministic values. Secondly, the correlation analysis between the most sensitive observed or measured parameters was done which can be very critical to find out the design ice actions since it can increase the probability of exceedance and governing ice actions. Then, the deterministic extreme value analysis for the computation of the design ice load is done, where different scenarios are considered to find the governing ice action. Finally, Monte-Carlo simulations were performed for the probabilistic analysis and uncertainty quantification of the governing ice loads.

Chapter 4

Site overview and characteristics

4.1 Location

Beitstadsundet is in the north-eastern end of Trondheim fjord in Norway, with direction almost east-west. The road starts in Østvik and ends in the east in Hjellbotn, which is the inner part of the Trondheim fjord. Statens vegvesen (Norwegian Public Roads Administration) wants to construct a new bridge for Fv-17, crosses Beitstadsundet with a small angle.

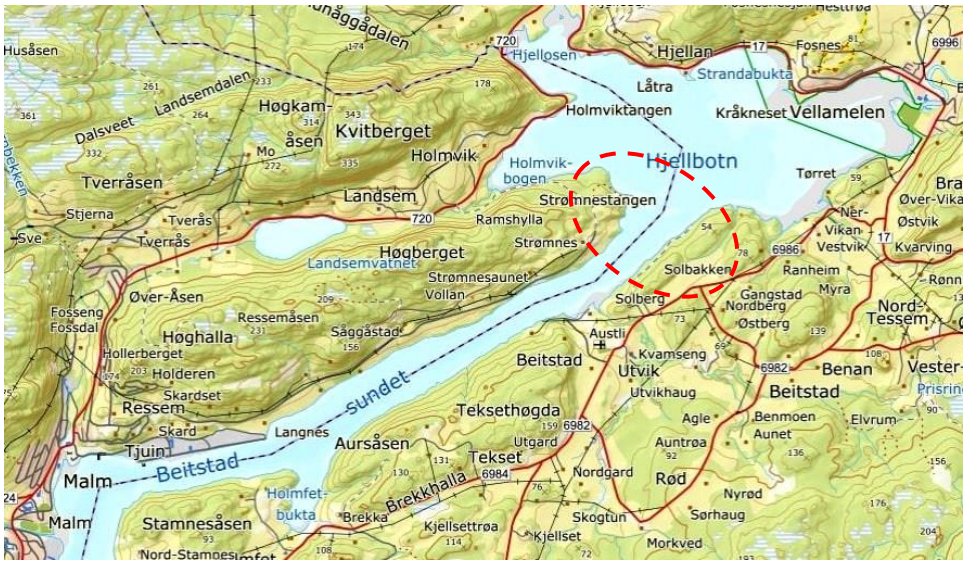

Figure 4-1 Location of the bridge (Reference: www.iskart.no*)*

Beitstadsundet bridge is a part of the project county roads 17 and 720 Dyrstad-Sprova-Malm. Along with this, the entire project involves the construction of a new county road 17 on the south side of Hjellbotn (i.e., 8.8 km new road), and the construction of a new county road 720 from a new junction at Strømnestangen along Beitstadsundet to the center of Malm (i.e., 5.8 km new road) (Nor consult, 2018).

4.2 Bridge characteristics

The bridge has been designed with the following characteristics and dimensions:

- Design life = 100 years
- Length = 580 m
- Number of Spans = 6
- Steel box bridge with cooperating concrete deck, and grounded with rammed steel piles
- Width = 11 m
- The diameter of pier = 4.5 m

Figure 4-2 shows the alignment for the bridge along with the dimensions of the structural elements of the bridge, whereas Figure 4-3 Digital elevation model layover on google earth to check the exact location of the fjord.

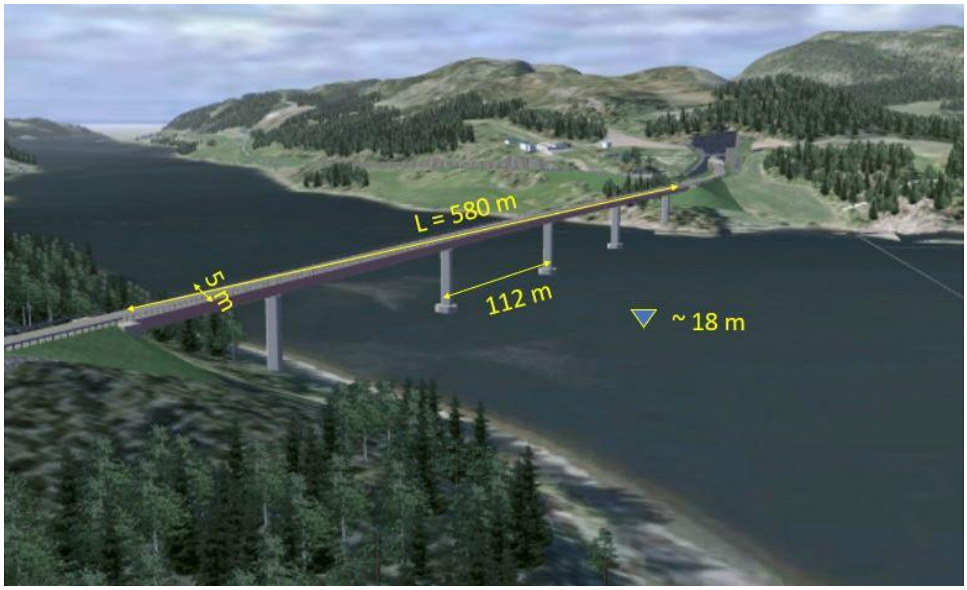

Figure 4-2 Alignment and dimensions of the bridge (Reference: www.vegvesen.no)

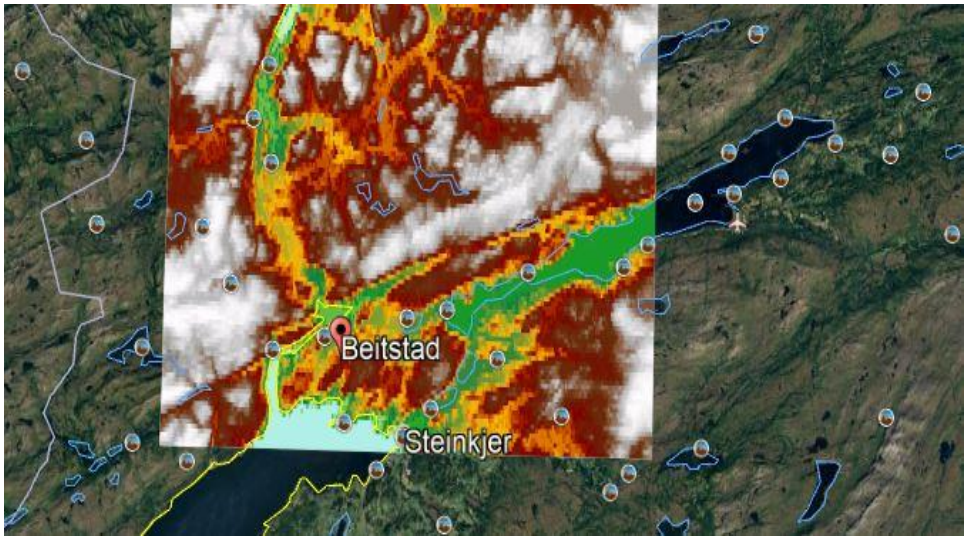

Figure 4-3 Digital elevation model layover on google earth to check the exact location of the fjord

To compute the cross-sectional dimensions and alignment of the fjord along with upstream and downstream cross-sections, Arc-GIS was used as shown in Figure 4-4. Bridge cross-section with the water depth is shown in Figure 4-5 and Figure 4-6 shows the alignment of the bridge from the feasibility study report of this bridge by Norconsult.

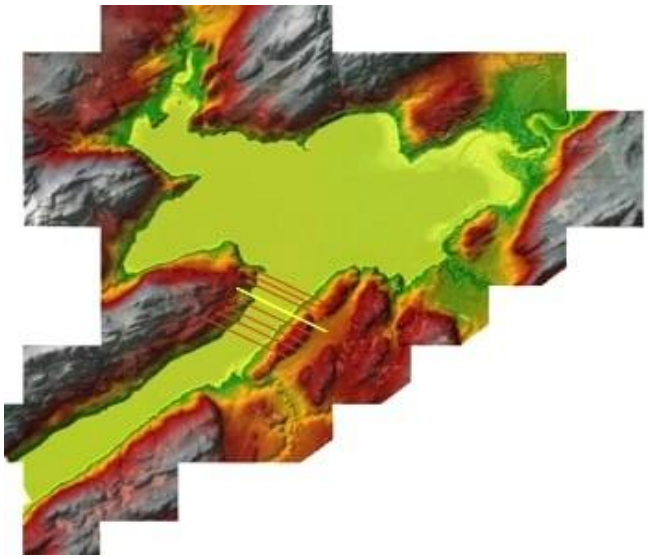

Figure 4-4 Cross sections from the digital elevation model. The yellow line shows the bridge location and the brown lines shows the upstream and downstream cross sections (Reference: www.nve.no)

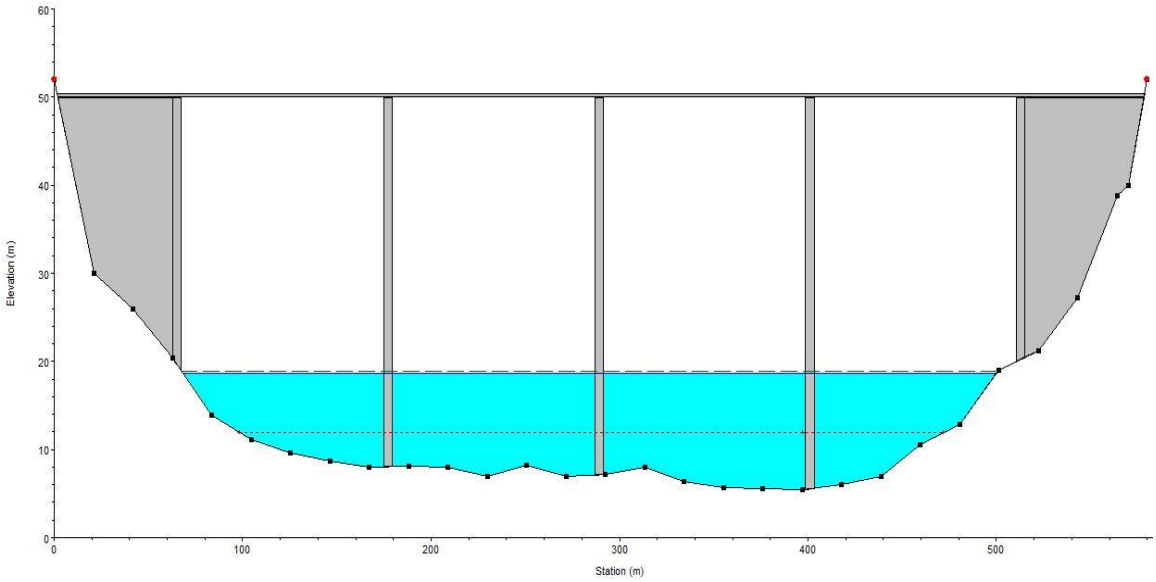

Figure 4-5 Bridge cross section from the digital elevation model

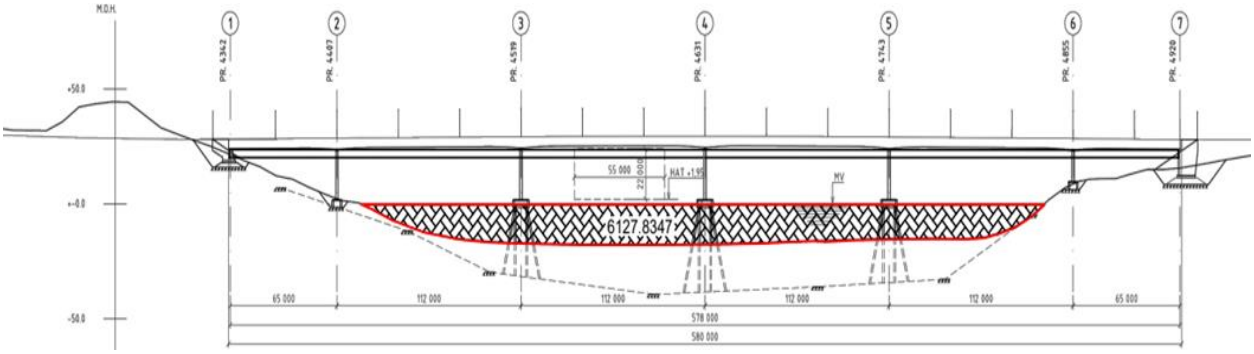

Figure 4-6 Cross section for the bridge (Nor consult, 2018)

4.3 River impact on tidal flow

Three rivers are falling in the fjord near the bridge location as shown in Figure 4-7. Their discharges are not that much high when compared to the volume of the fjord. The average water depth near the upstream location of the bridge is around 18 m based on the bathymetry, taken from the MIKE Zero, which is a software developed by the Danish Hydraulic Institute (DHI).

Figure 4-7 Three rivers falling in the fjord

As most of the current velocity will be due to the tidal current, which may change due to river discharge and density difference and mixing, previous studies suggest that changes in the amplitude and phase of a tidal constituent may be a function of multiple variables, as given the expression as under:

$$\Delta\, Amp_{tidal} = f\,(\Delta H, \Delta Qr, \Delta\rho, \Delta mx, \Delta r, \Delta\Psi\omega, \ldots)$$

Where:

H = the water depth,

ρ = water density,

r = friction,

mx = mixing,

Qr = river discharge, and

$\Psi\omega$ = frequency-dependent tidal response to astronomical tidal forcing.

The "…" in the expression above indicates other variables that are not listed here, such as wind. Since many of the variables which affect the sea level, such as river flow, density, and wind, can also affect tidal amplitudes, a correlated response is frequently observed. Identifying correlations between tidal range and mean sea level (MSL) is critical for making reliable predictions of water levels. (Devlin et.al, 2017).

The tidal theory indicates that tides and the river discharge interact through quadratic bed friction, which diminishes and distorts the tidal wave as the discharge increases in the river. The river discharge can affect water depth and flow velocity, which determine the friction factor. An increased river flow results in a deeper and wider channel, together with a higher convergence. The net effect results in lower values of the tidal velocity (Van den Berg, 2011). Therefore, this shows that the river inflow is one of the key drivers for the tidal current prediction and the morpho-dynamics and must be included in any long-term water level prediction. Hence, the catchment areas of the major rivers falling in the fjord are shown in Figure 4-8.

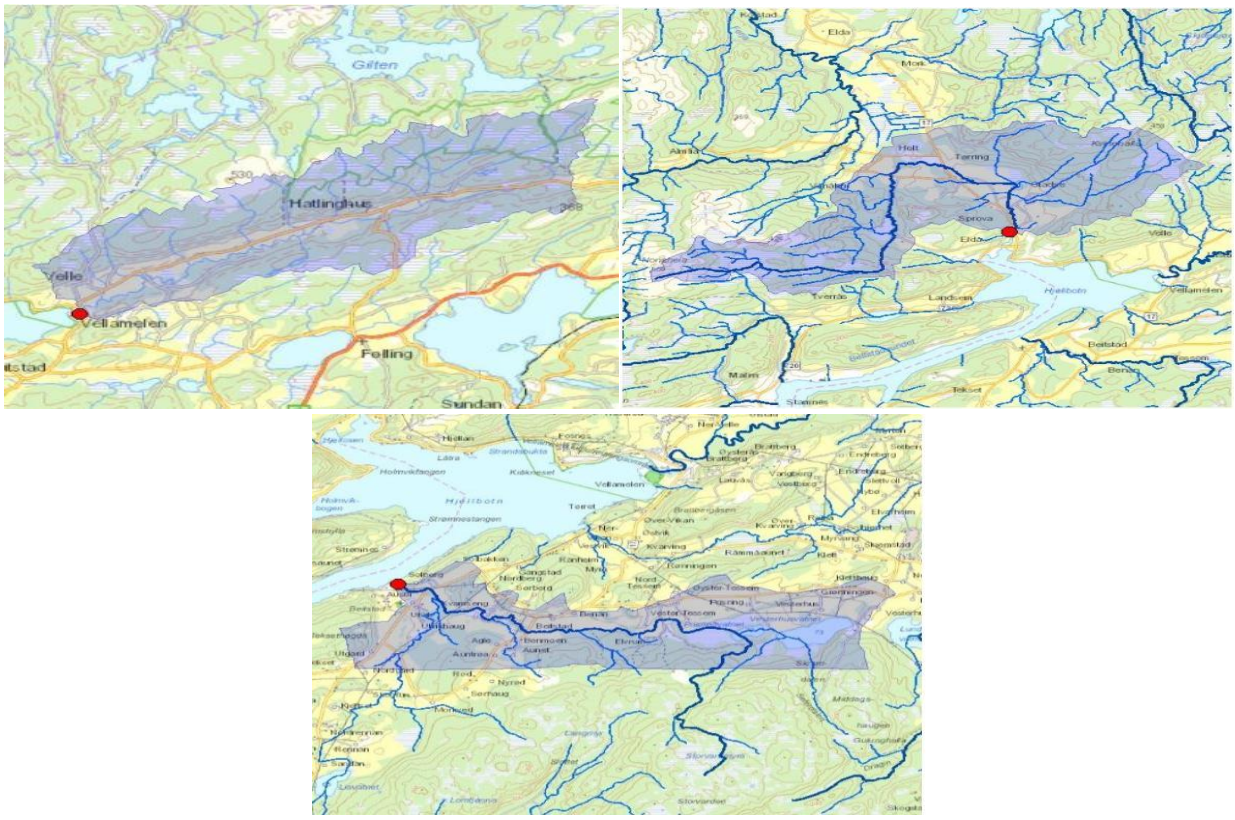

Figure 4-8 Catchment areas of the major rivers falling in the fjord (Reference: www.nve.no)

Moreover, the discharges of the rivers can affect the tidal current in the fjord. Therefore, it is vital to check how much the rivers discharges can impact the tidal volume of water in the fjord because the tidal current is the main driving force for the ice against the bridge piers. Discharges for different return periods for these rivers are shown in Table 4-1 to Table 4-3.

Table 4-1 Discharges of river 1 for different return periods

River 1	V $(s.km^2)$	Q^M (m^3/s)	Q 5 (m^3/s)	Q 10 (m^3/s)	Q 20 (m^3/s)	Q 50 (m^3/s)	Q 100 (m^3/s)	Q 200 (m^3/s)
95% upper limit (m^3/s)	1004.3	57.2	72.6	87.3	103.5	128.9	151.9	174.3
95% lower limit (m^3/s)	321	18.3	22.1	25.5	29	33.9	38	43.6

Table 4-2 Discharges of river 2 for different return periods

River 2	V $(s.km^2)$	Q^M (m^3/s)	Q 5 (m^3/s)	Q 10 (m^3/s)	Q 20 (m^3/s)	Q 50 (m^3/s)	Q 100 (m^3/s)	Q 200 (m^3/s)
95% upper limit (m^3/s)	31.5	1062.2	39.9	48	56.8	70.7	83.4	95.7
95% lower limit (m^3/s)	10.1	339	12.2	14	15.9	18.6	20.8	23.9

Table 4-3 Discharges of river 3 for different return periods

River 3	V $(s.km^2)$	Q^M (m^3/s)	Q 5 (m^3/s)	Q 10 (m^3/s)	Q 20 (m^3/s)	Q 50 (m^3/s)	Q 100 (m^3/s)	Q 200 (m^3/s)
95% upper limit (m^3/s)	6	744.5	7.6	9.3	11.1	14	16.6	19.2
95% lower limit (m^3/s)	1.9	238	2.3	2.7	3.1	3.7	4.2	4.8

To check the effect of the rivers on the tidal discharge, the tidal modeling was done in MATLAB. The cross-sectional area of the bridge (6127.84 m^2) and upstream surface area of the fjord (4072593 m^2) was calculated. Then, by knowing the tidal amplitude; the tidal prism was calculated and then the tidal discharge was calculated. The water level gets down as the rivers are discharging out of the fjord. Thus, they are contributing to the ebb tidal current in the fjord. The tide was simulated with(out) including discharges from the rivers, as shown in Figure 4-9 to 11.

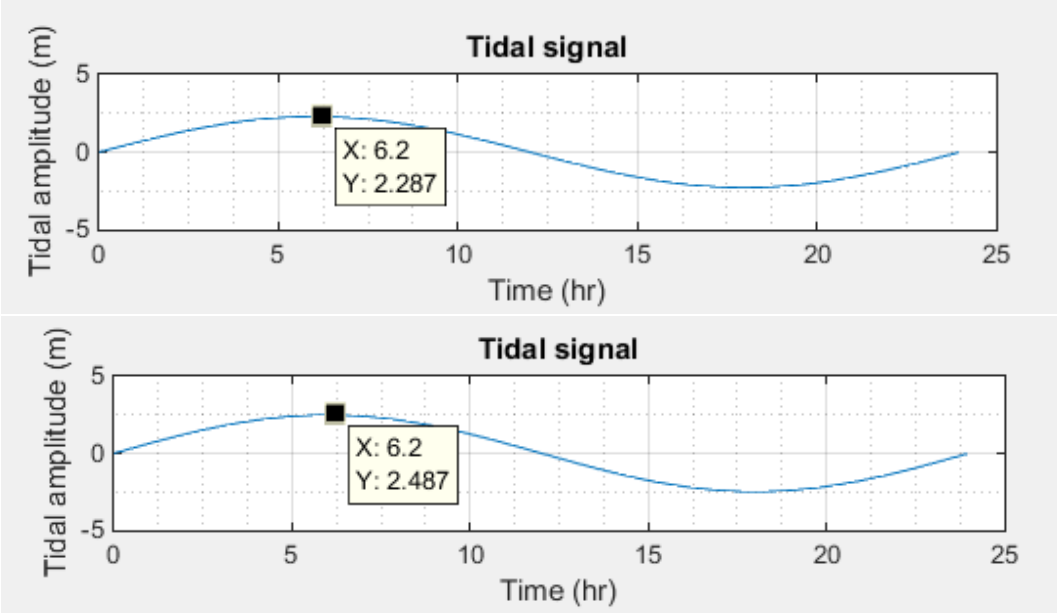

Figure 4-9 The tidal signal in the fjord over one whole day. The flood and ebb amplitudes are 2.29 and 2.49 m for 10-year and 100-year return periods, respectively

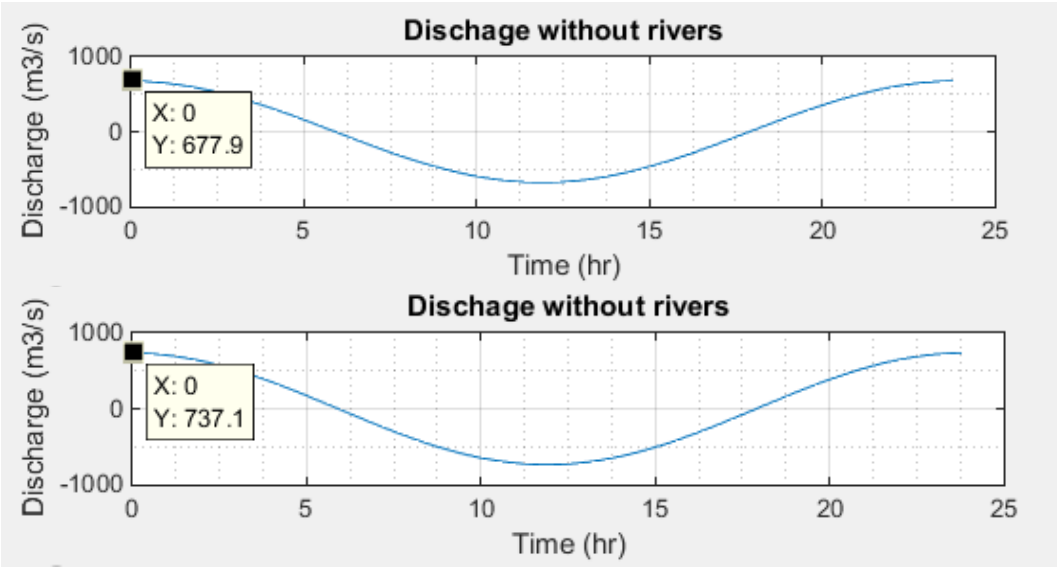

Figure 4-10 The discharge in the fjord - not including discharges from the rivers. Therefore, the tidal discharge is equal 677.9 m^3/s and 737.1 m^3/s for 10-year and 100-year return periods, respectively

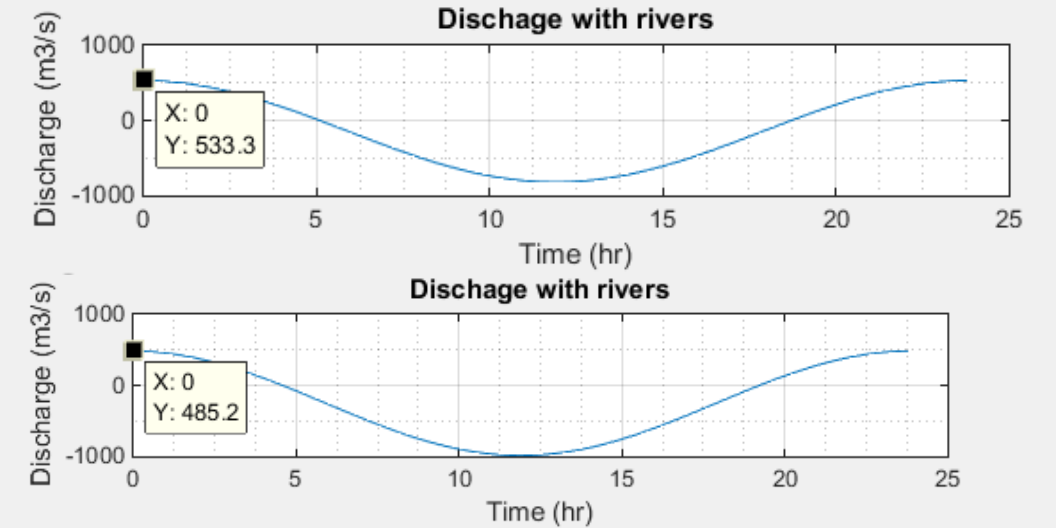

Figure 4-11 The discharge in the fjord - including discharges from the rivers with 95% upper limit. Therefore, the tidal discharge is equal 533.3 m^3/s and 485.2 m^3/s for 10-year and 100-year return periods, respectively

Based on the values for the discharge in the fjord with(out) including discharges from the rivers (that is, 677.9 m^3/s, 533.3 m^3/s, 737.1 m^3/s and 485.2 m^3/s, for 10-year and 100-year return periods, respectively), it is clear that the rivers are discharging towards the outside of the fjord and consequently the flood tidal discharge gets lower by a value of 252 m^3/s while the ebb tidal discharge gets higher. Since the flood tide drags the ice against the bridge pier, the flood tidal current is the main driving force of concern for the governing ice actions. Hence, it is shown that the discharges from the rivers are extremely lower than the discharge in the fjord, but they could affect the tidal discharge in the long-term prediction. Therefore, the effect of these rivers' discharges on the tidal current must be determined. This is done in the following section.

According to Marcel D. Steve et.al (2013), the transition between river-dominated flow and tide-dominated flow depends on the ratio of <Q>/Qr (that is, the ratio of the tidal flow to the river flow). The impact of the river on the tidal flow becomes minor when <Q>/Qr >= 20. In this case study, the combined river discharge for 100-year return period and 95% upper limit can be determined by adding up the values of 151.9 m^3/s, 83.4 m^3/s and 16.6 m^3/s. As a result, the combined river discharge is nearly 252 m^3/s which is the same value as the difference in the discharge in the fjord with(out) discharges from the rivers. Therefore, the ratio <Q>/Qr is nearly 4.7 which is less than 20. Thus, the combined river discharge has a significant impact on the tidal

flow in the fjord. Hereby, the impact of the river discharge on the tidal current must be checked and quantified for the consideration of the exact prediction of the tidal current during the design lifetime.

4.4 Water level impact on tidal current

Harker et al. (2018) showed that the tidal amplitudes are particularly sensitive to the sea level rise (SLR) with the consequences of increased tidal amplitudes as SLR is increasing. Therefore, the tidal amplitude for the 100-year return period must be used in the calculations of extreme value analysis for the highest astronomical tide (HAT); to include the effect of the sea level rise. A record of 20 years for the water levels was collected online from Kartverket. From Figure 4-12, the average value for the highest water levels is approximately 3.90 m, while the average value for the lowest water levels is -0.36 m. Figure 4-13 shows the SLR for the period from 2010 to 2100. The sea level is increasing with the rate of about 27 cm per 100 years.

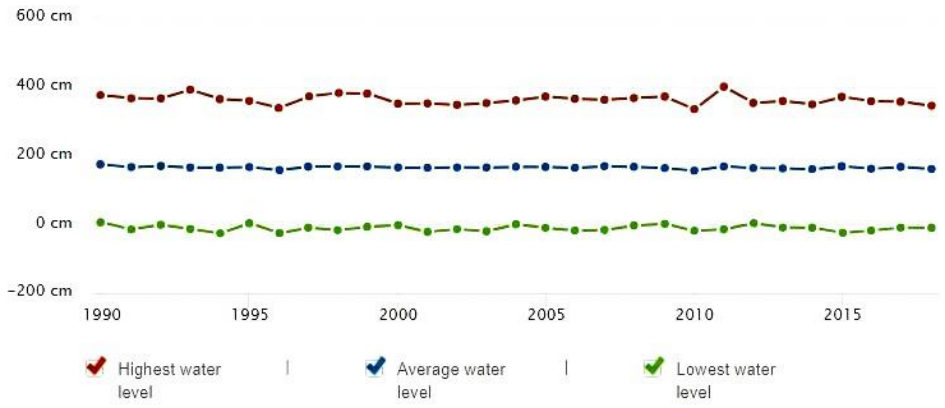

Figure 4-12 Water levels at Beitstadsund fjord over the past 25 years (Reference: www.kartverket.no)

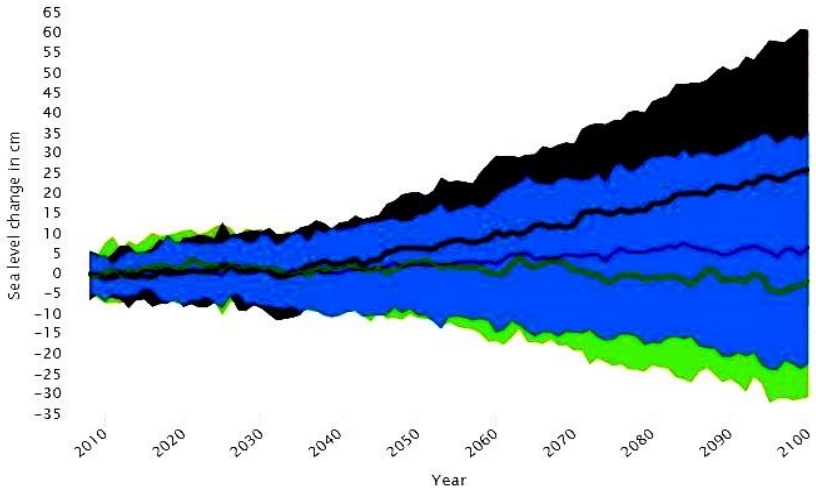

Figure 4-13 SLR at Beitstadsundet fjord from 2010 to 2100 in the Norwegian Sea (Reference: www.kartverket.no)

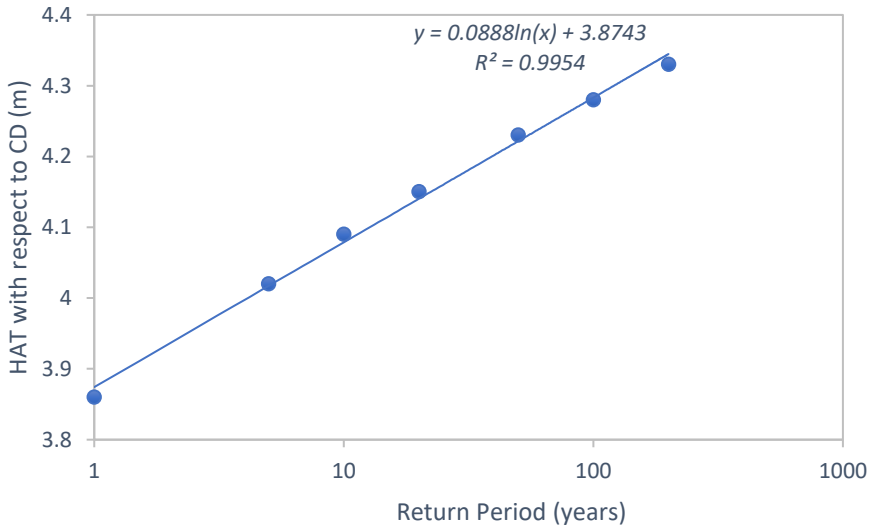

Figure 4-14 Extreme value analysis for HAT with respect to CD. HAT is about 4.094 m for a return period of 10 years, whereas it is 4.294 m for a return period of 100 years

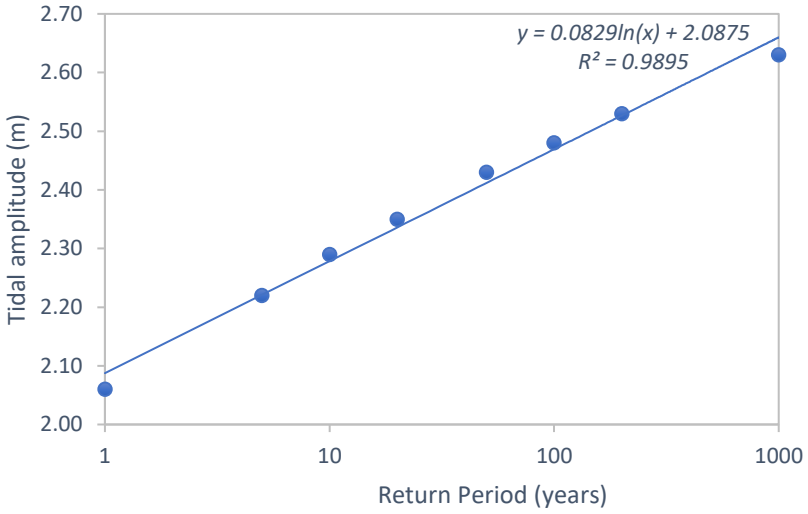

Figure 4-15 Extreme value analysis for the tidal amplitude. The tidal amplitude is about 2.29 m for a return period of 10 years, whereas it is 2.49 m for a return period of 100 years

Figure 4-15 shows the tidal amplitudes for return periods from 1 to 1000 years. For the case of the 10-year return period, the tidal amplitude is nearly 2.29 m, while it is nearly 2.49 m for the case of a 100-year return period. Figure 4-16 to 18 show the tidal amplitude and current for the 10-year return period, whereas Figure 4-19 to 21 show the same parameters for the 100-year return period. For the case of the 10-year return period, the tidal amplitude is nearly 2.29 m, while it is nearly 2.49 m for the case of a 100-year return period. In terms of the tidal current with(out) including discharges from the rivers, there is almost no difference between the values of the tidal current for both the 10-year and the 100-year return periods (0.09, 0.11, 0.08 and 0.12, respectively). Consequently, it can be said that the rivers' discharges have no impact on the tidal current, and therefore the effects from the rivers can be neglected in this project; to calculate the ice limit force that is required to find the governing ice actions against the bridge pier.

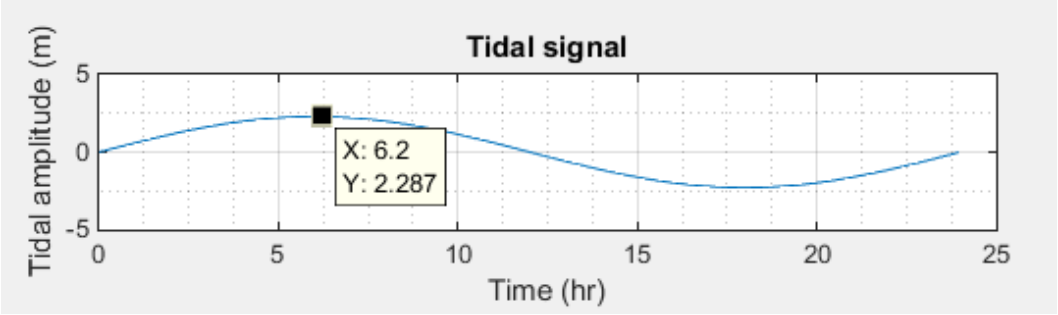

Figure 4-16 The tidal signal in the fjord over one whole day including SLR for the 10-year return period. The flood and ebb amplitudes are assumed symmetric and equal to 2.29m

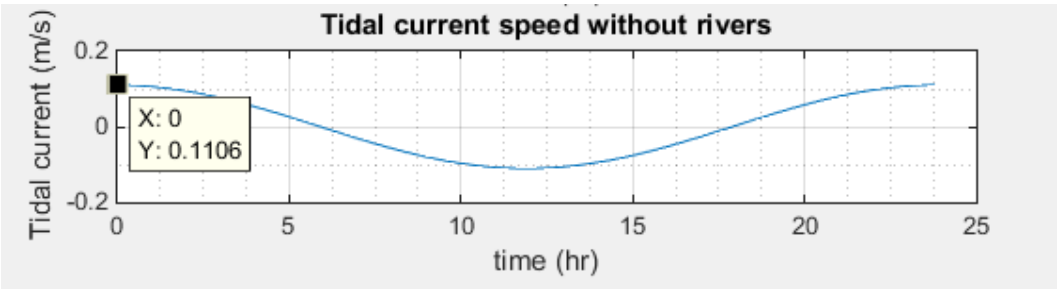

Figure 4-17 The tidal current in the fjord - not including the rivers, including SLR for a 10-year return period. Therefore, the flood tidal current is equal to 0.11 m/s

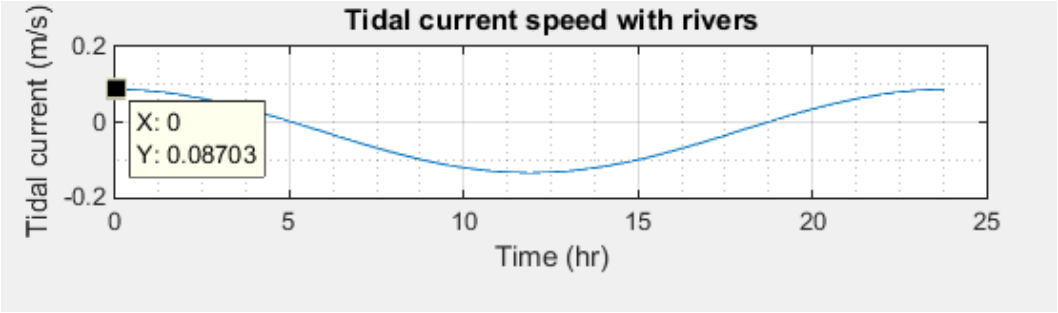

Figure 4-18 The tidal current in the fjord - including the rivers with 95% upper limit, including SLR for the 10-year return period. Therefore, the flood tidal current is equal to 0.09 m/s

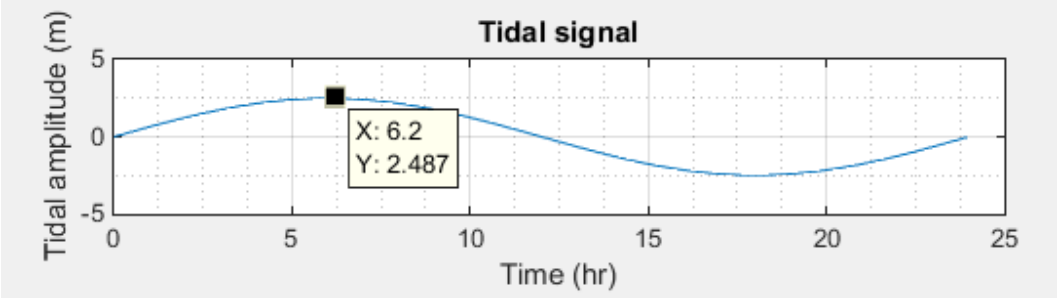

Figure 4-19 The tidal signal in the fjord over one whole day including SLR for the 100-year return period. The flood and ebb amplitudes are assumed symmetric and equal to 2.49 m

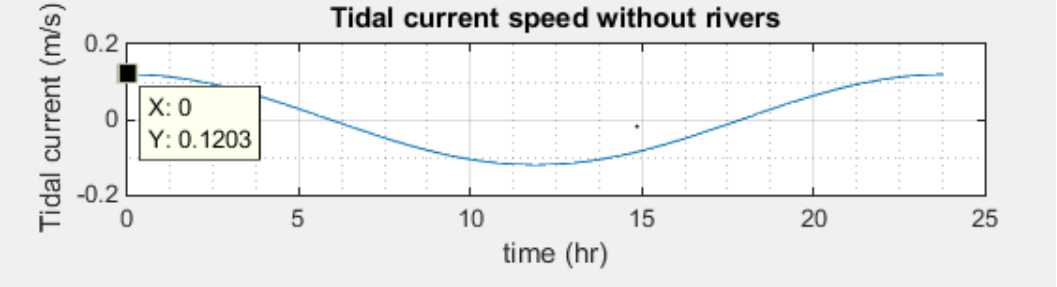

Figure 4-20 The tidal current in the fjord - not including the rivers, including SLR for the 100-year return period. Therefore, the flood tidal current is equal to 0.12 m/s

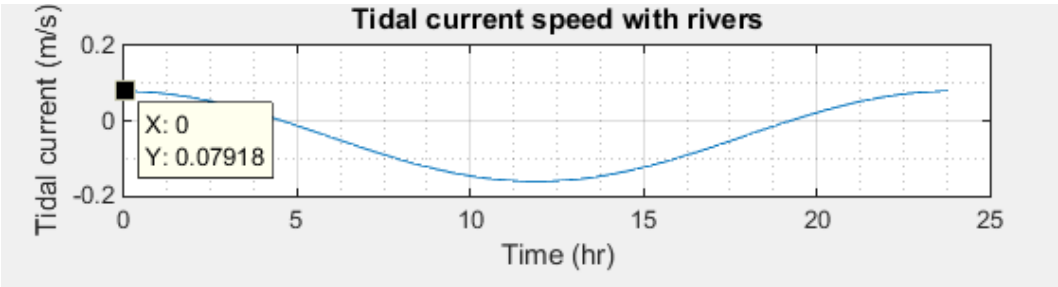

Figure 4-21 The tidal current in the fjord - including the rivers with 95% upper limit, including SLR for the 100-year return period. Therefore, the flood tidal current is equal to 0.08 m/s

The effect of rivers on the tidal currents is minimal and thus the variations in the tidal current computed for the past 50 years is very low, as shown in Figure 4-22, derived from the tidal modeling in MATLAB. The figure was computed by employing the formula for the tidal prism which is basically the multiplication of the fjord surface area and tidal range. Then the volume is divided over the tidal period to get the tidal current velocity.

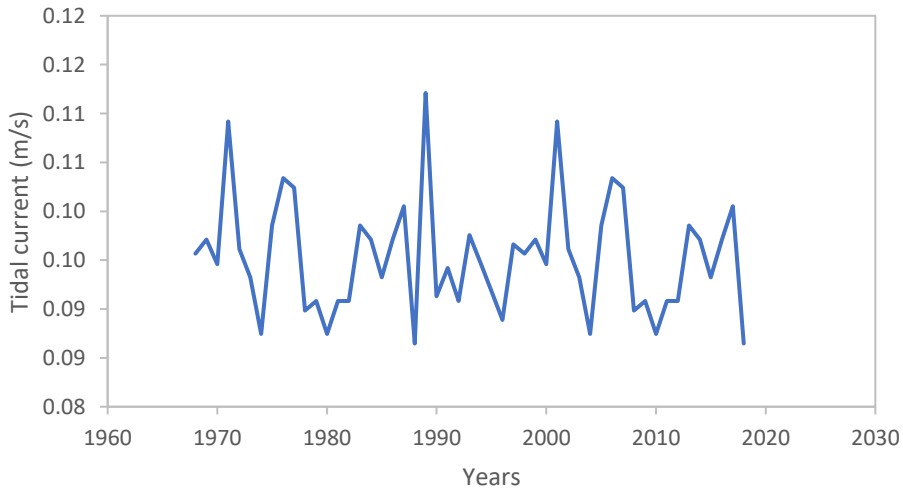

Figure 4-22 The tidal current velocity over the past 50 years

4.5 Waves impact

The location of the Beitstadsundet fjord is in a sheltered area from the waves in the Norwegian Sea, as shown in Figure 4-23, and therefore it is assumed that the effect of waves is not significant and can be neglected for this study.

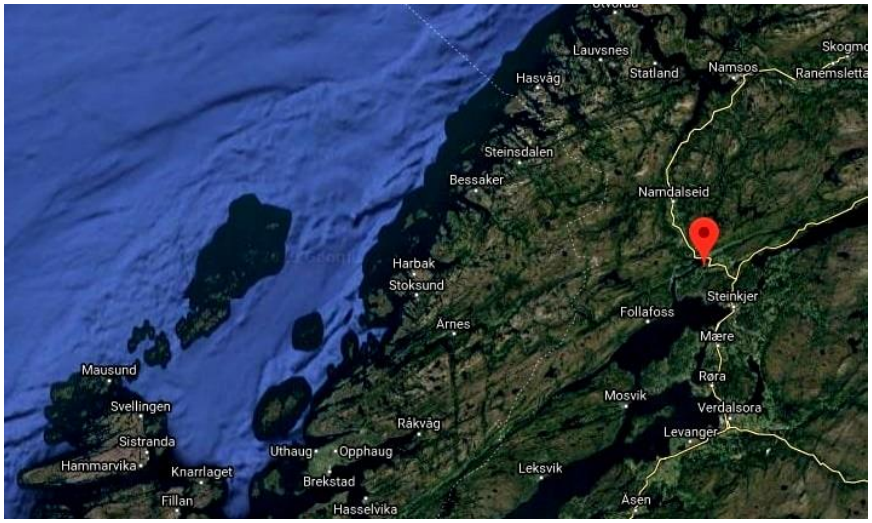

Figure 4-23 Location of the Beitstadsund fjord at a sheltered area from the Norwegian Sea (Reference: Google earth maps)

4.6 Wind speed and direction

In order to calculate the design wind speed, wind data for the past 50 years (i.e., from 1968 to 2018) was downloaded from eklima, and then Lognormal, Weibull and Gumble distributions were fitted by taking the annual maximum values; to eventually calculate the design wind speed at the 100-year return period by performing the extreme value analysis for the annual maximal wind speeds for the past 50 years.

Therefore, Figure 4-24 shows the maximal wind speed for the year 2018 (20 m/s), whereas Figure 4-25 shows the maximum wind speeds for all the years from 1968 to 2018, and the maximum wind speed was 35 m/s in the year 1971. Figure 4-26 shows the three different probabilistic distributions, and it can be clearly stated that Gumble distribution fits the best. Then, the extreme value analysis was done as shown in Figure 4-27. It is obvious that the design wind speed is 38

m/s for the 100-year return period, and the corresponding probability of exceedance is approximately 2%.

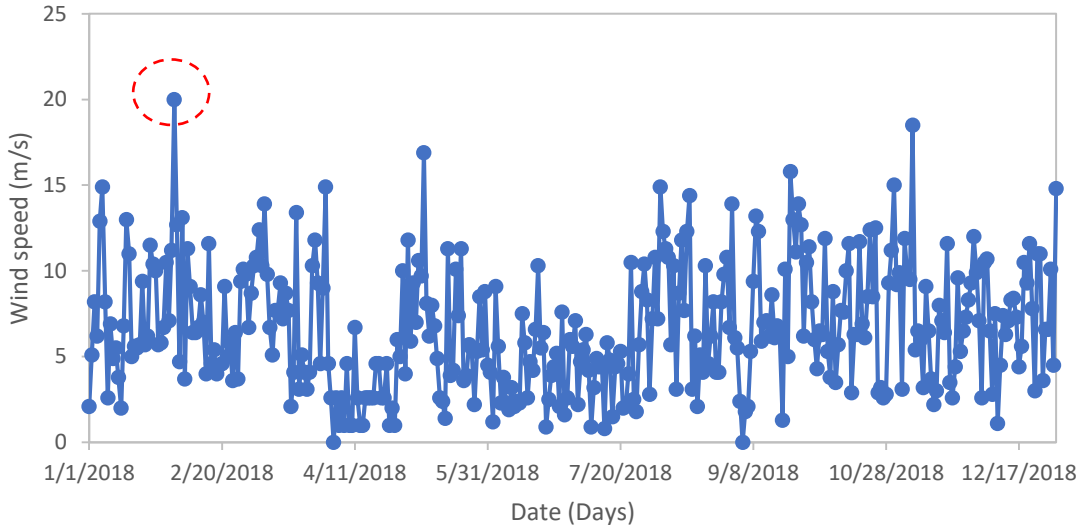

Figure 4-24 The maximal wind speed for the year 2018. The wind speed makes the top on 2/2/2018 for a value of 20 m/s

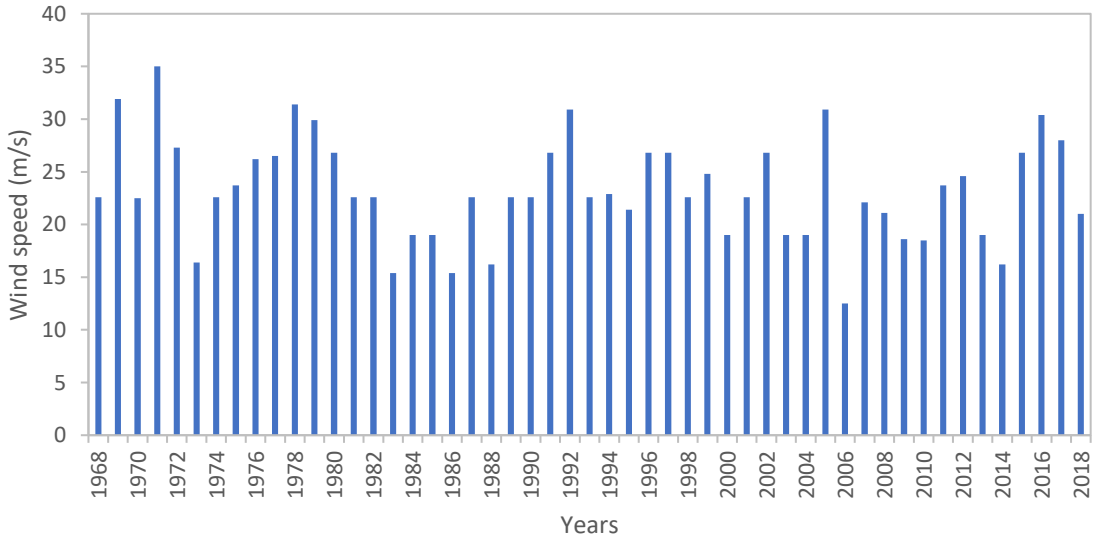

Figure 4-25 The maximal wind speeds for each of the 50 years. The wind speed makes the top in the year 1971 for a value of 35 m/s

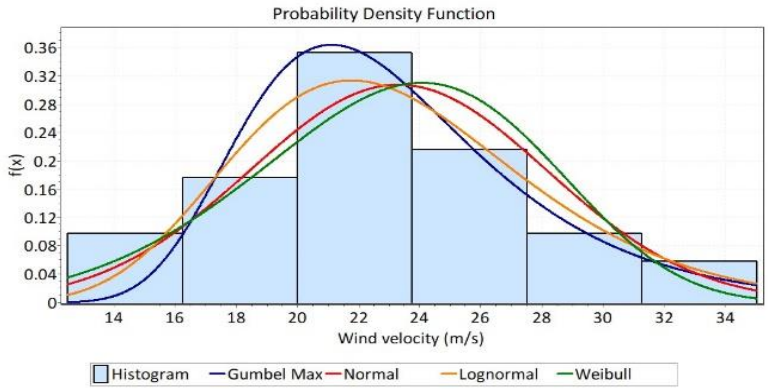

Figure 4-26 Gumble distribution of the annual maximal wind speed data

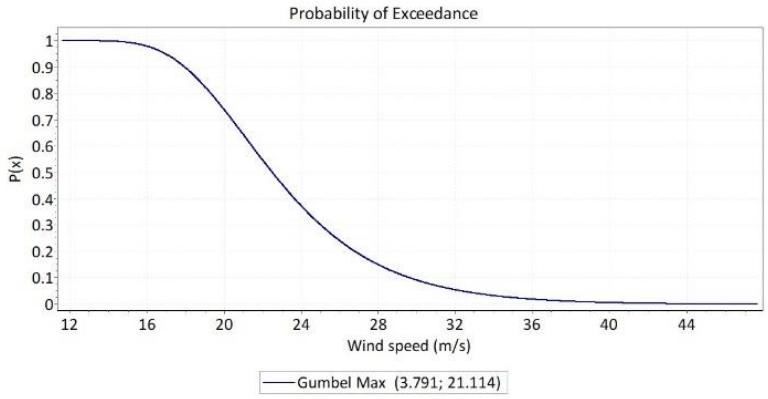

Figure 4-27 Extreme value analysis of the annual maximal wind speed data

The direction of wind contributes to the driving drag force due to the wind; it tells about the joint probability of wind and current, and so gives information on the worst scenario – when the wind and the current are aligned, the drag force becomes bigger. Therefore, Figure 4-28 shows the wind direction at Beitstadsundet. It is obvious that the extreme wind direction (i.e., greater than 61 km/hr. or 17 m/s) is mostly blowing from WSW and WNW towards ENE and ESE for 44 and 8 hours per year, respectively.

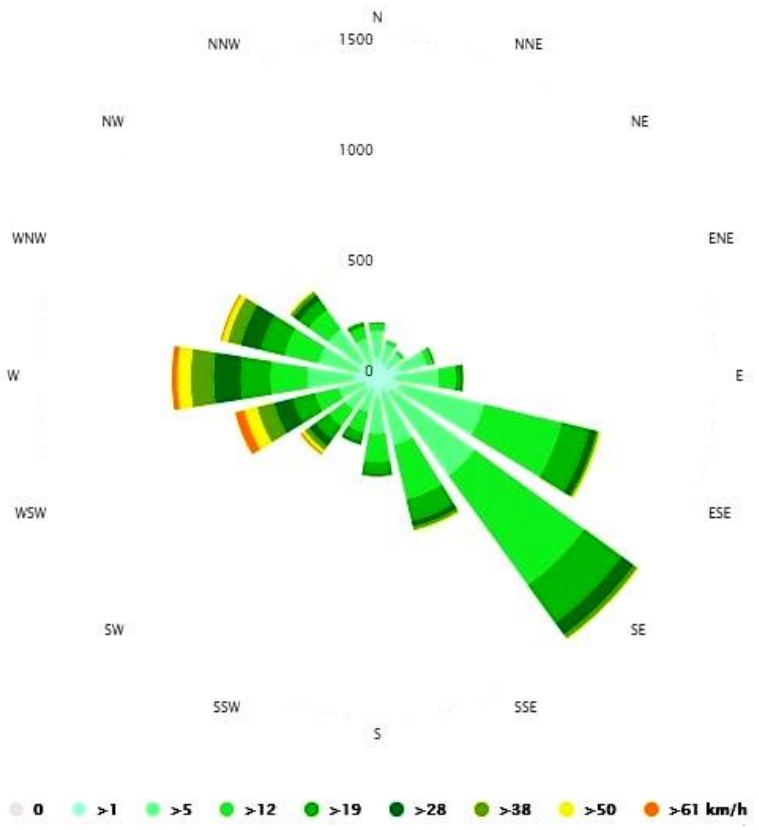

Figure 4-28 The wind rose for Beitstad shows how many hours per year the wind blows from the indicated direction (Reference: www.weatherspark.com)

4.7 Temperature and precipitation

The average daily air temperatures were taken from eklima and yr.no; to calculate the cumulated freezing degree days (C_{FDD}) to calculate the ice thickness and other ice parameters. Winterly average temperature values for the past 50 years at Beitstadsund are given in Figure 4-29 from November to April.

From Figure 4-29, it can be concluded that the winterly average temperature rose from -3.81 (1950) to -2.76 (2018) degrees Celsius (25.147 to 27.032° F) between 1968 and 2018. Temperatures are certain to go up further. Furthermore, the trend of the winterly average temperatures is increasing from -6.3 to -5.15 degrees Celsius (20.66 to 22.73° F) over the 50 years between 1968 and 2018.

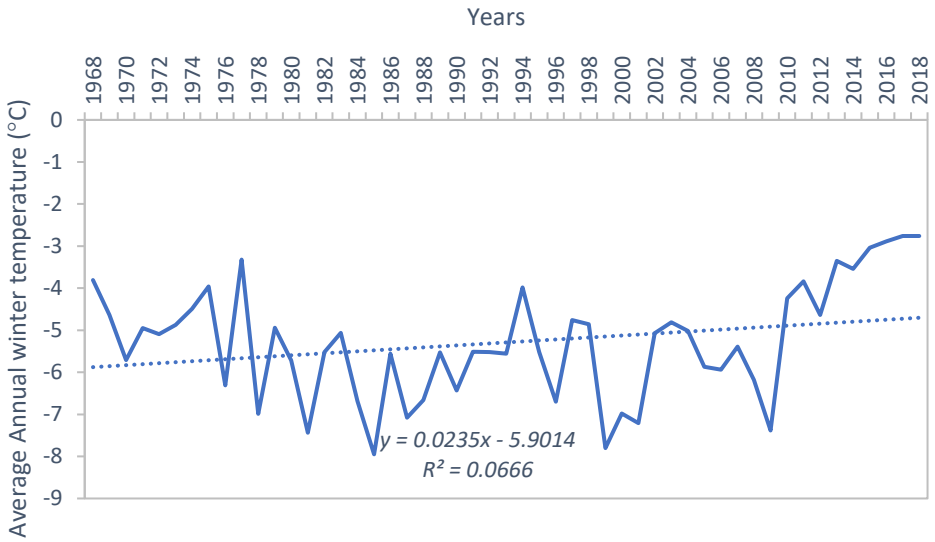

Figure 4-29 Average temperature from November to April.

Figure 4-30 shows how many days per month a certain amount of precipitation is reached at Beitstadsund. This is necessary to calculate the discharges for the rivers and for input into the process-based and empirical models; to calculate the accurate ice thickness, which is an important parameter to find the ice actions against the bridge pier. From the figure, there are, on average, 11 and 12.2 snow days in December and January, respectively, whereas there is almost no snow from the end of May to mid-September. In addition, the precipitation is less than 2 mm in most days.

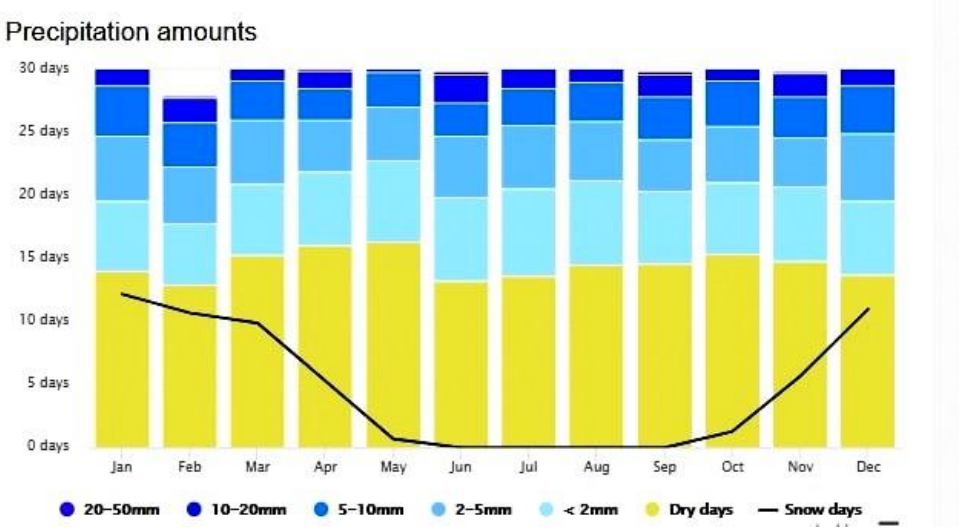

Figure 4-30 The precipitation diagram for Beitstad shows on how many days per month, certain precipitation amounts are reached. This diagram is based on 30 years of hourly weather model simulations. Monthly precipitations above 150 mm are mostly wet, below 30 mm mostly dry (Reference: www.weatherspark.com)

4.8 Snow depth

Snow depth is required to calculate accurate ice thickness values in both empirically and process-based model. Snow has an insulating impact on ice growth; it reduces ice thickness growth. From Figure 4-31, the snow depth starts growing from December until it makes its maximum in March.

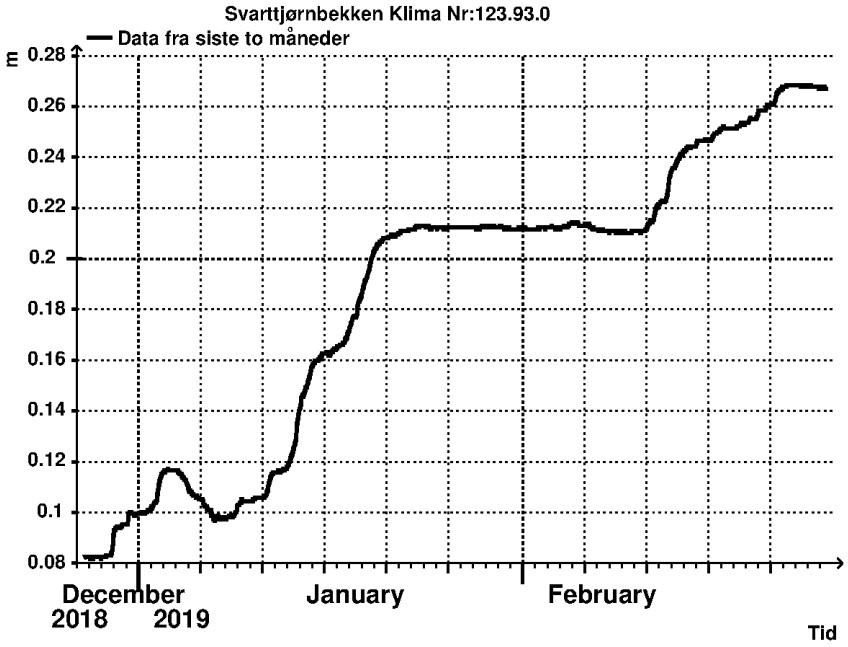

Figure 4-31 Snow depth at Beitstadsund (Reference: www.yr.no)

4.9 Cloudiness

Cloudiness is a very important parameter that is required to calculate the ice thickness and growth in the process-based model, Delft3D-FLOW (Ice module). Average values of the cloudiness in Malm, that is near to Beitstadsund, are shown in Figure 4-32. The average percentage of the sky covered by clouds experiences significant seasonal variation over the year.

The clearer part of the year in Malm begins around April 7 and ends around September 19, lasting for 5.4 months. On May 15, the clearest day of the year, the sky is clear, mostly clear, or partly cloudy 46% of the time, whereas, on January 26, the cloudiest day of the year, the sky is overcast or mostly cloudy 76% of the time. The cloudier part of the year begins around September 19 and ends around April 7.

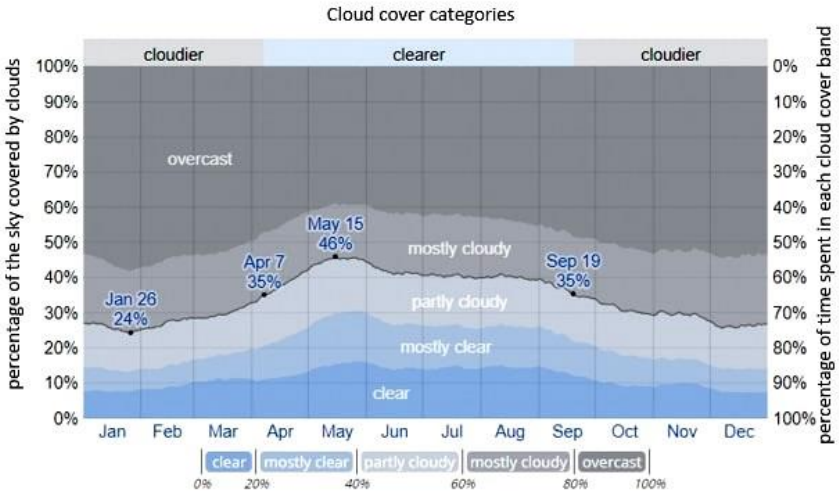

Figure 4-32 The percentage of time spent in each cloud cover band, categorized by the percentage of the sky covered by clouds (Reference: www.weatherspark.com)

4.10 Relative humidity

The relative humidity is also an important parameter that is required to calculate the ice thickness and growth in the process-based model, Delft3D-FLOW (Ice module). Since the average value for the relative humidity in Beitstadsund was not available, the average values of the relative humidity for the county Trøndelag were used for the ice growth analysis, as shown in Figure 4-33.

Figure 4-33 Relative humidity for each month of a year, averaged over the past 30 years (Reference: www.weatherspark.com)

Chapter 5

Ice conditions

5.1 Ice features

The characteristics of any interaction between moving ice and a bridge pier depend on the type of the ice feature, the shape, and stiffness of the pier, the motion of the ice feature and atmospheric conditions. For this case study, Ice floes having a diameter of between 50 to 580 m with uniform distribution is considered to calculate the ice actions. Figure 5-1 shows the conceptual drawing of the ice floe having a width equal to the length of the bridge.

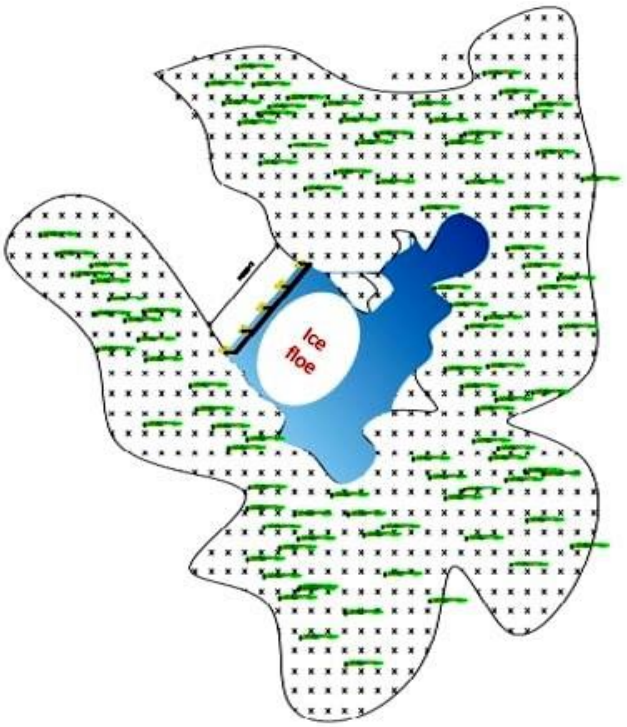

Figure 5-1 Ice floe moving towards the bridge

5.2 Salinity of ice

Salinity together with the temperature determines the brine volume. An increase of salinity a large brine volume and thus higher porosity, making the ice weaker. Figure 5-2 shows the variations in the salinity at Beitstad over the past 50 years. From the figure, it can be observed that the ice salinity is ranging from 7.1 to 9.6 ppt during the past 50 years.

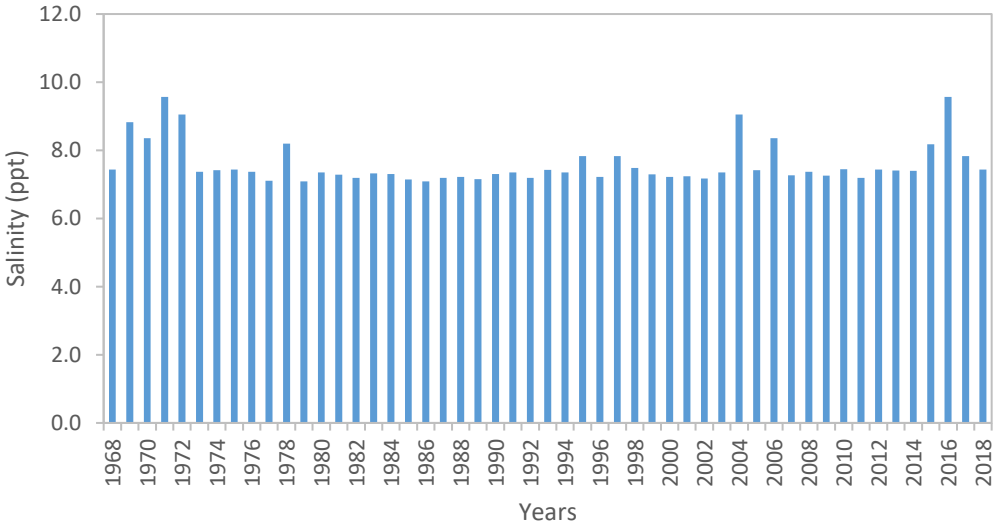

Figure 5-2 Salinity variations at Beitstad over the past 50 years

5.3 Ice porosity

An increase of porosity directly yields the ice to be weaker. Figure 5-3 shows the variations in the porosity at Beitstad over the past 50 years. From the figure, it can be observed that the ice porosity is ranging from 0.12 to 0.33 during the past 50 years. It is worthy to mention that the ice temperature considered equal to the average of the air temperature and freezing tempetarure of ice in the calculation of brine volume which is required to calculate the ice porosity.

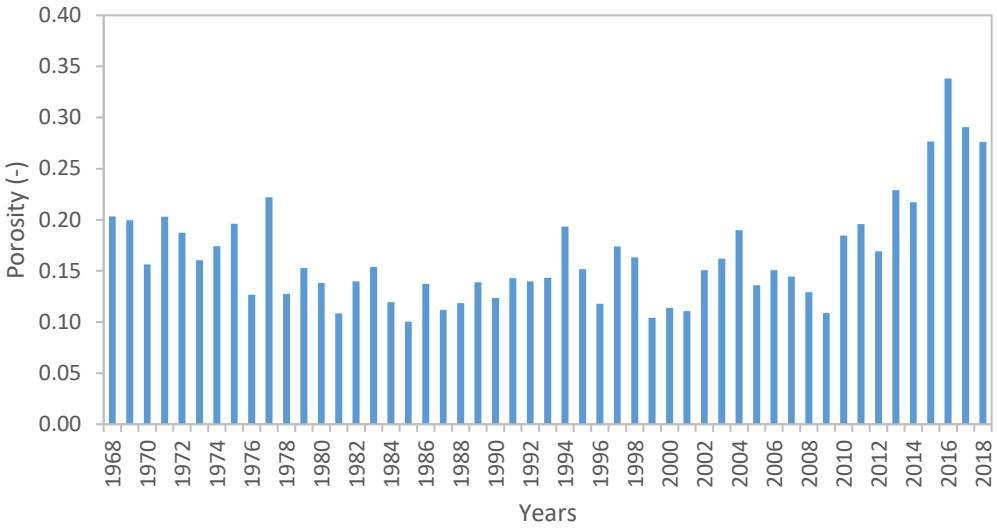

Figure 5-3 porosity variations at Beitstad over the past 50 years

5.4 Flexural strength

Figure 5-4 shows the variations in the flexural strength of the ice at Beitstad over the past 50 years. It is worthy to mention that the ice temperature considered equal to the average of the air temperature and freezing tempetarure of ice in the calculation of brine volume which is required to calculate the flexural strength. From the figure, it can be observed that the ice flexural strength is ranging from 0.1 to 0.3 MPa during the past 50 years.

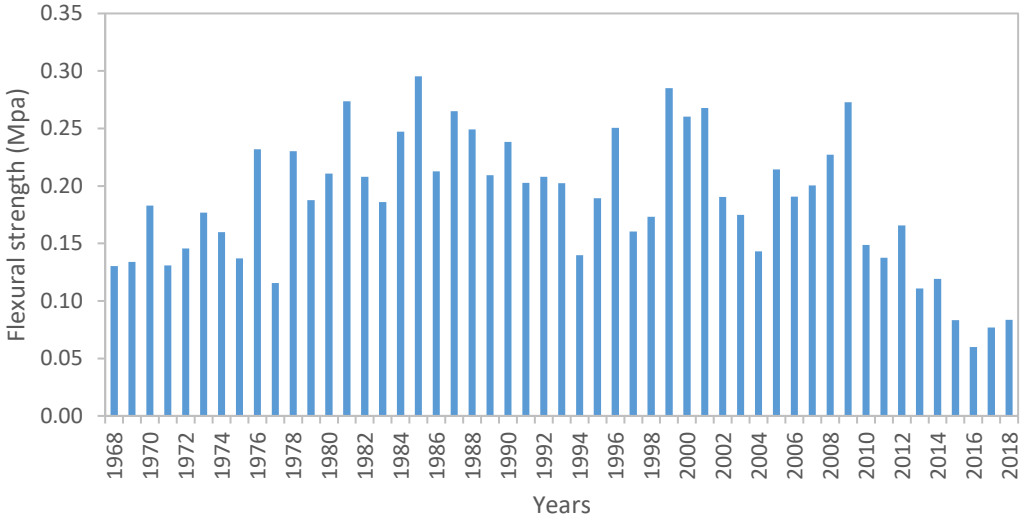

Figure 5-4 Flexural strength variations at Beitstad over the past 50 years

5.5 Ice floe thickness

Ice thickness is a very critical parameter irrespective of the failure mode and it is also a very important parameter for all the practical issues of the ice. It is very difficult to determine the accurate ice thickness in a given return period with limited data. Numerous methodologies are accessible, and every one of these methodologies has its very own properties and impediments. These prediction techniques for the ice thickness change from statistical-based analysis on ice thickness data to a wide range of numerical ice thickness predictors. (Comfort & Abdelnour, 2013).

Comfort & Abdelnour, (2013) concluded that the best way to deal with the estimation of thicknesses of ice relies on numerous factors, including the application and the accuracy requirements alongside the amount and quality of accessible ice thickness data and, contingent upon the technique utilized and the accessible environmental data. It is realized that the ice growth process is very composite and fluctuating. It is uncommon that the ice growth in winter happens totally by the thermal growth, however, the ice crystallography fluctuates significantly with the depth in the ice sheet. The development of a snow cover considerably hinders the ice growth process. A snow cover on an ice surface acts as an insulating layer as its thermal conductivity has the lower value than the thermal conductivity of the ice; and this impact is developed in the empirical model, made based on Stefan's law.

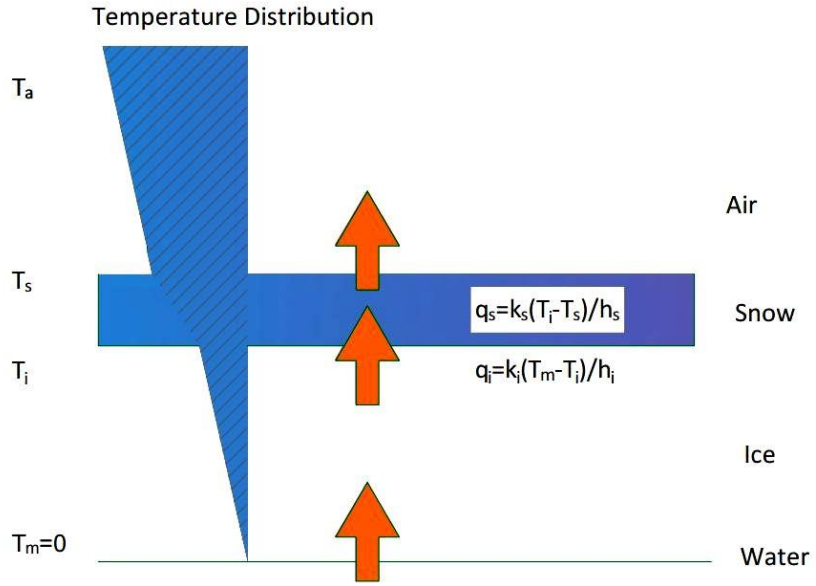

Figure 5-5 Heat flux through an ice cover (Comfort et.al, 2013; modified)

Stefan's formula is used to calculate the ice cover thickness. The ice thickness, produced by static ice formation, is commonly predicted based on the C_{FDD}, as given in Stefan's equation below. This equation is derived by solving the differential equation for the thermal growth rate, and by making several assumptions of simplifications (USACE, 2002). Figure 5-5 shows the heat flux through an ice cover. For this case study, the empirical models by Zubov (1943), Lebedev (1938), detailed Stefan's empirical model and simplified Stefan's empirical model based on freezing degree day factor (site specific) are employed which are used to calculate the maximum undisturbed ice thickness which is following respectively:

1. $h_i^2 + 50h_i = 8C_{FDD}$ (Zubov's empirical model)
2. $h_i = 1.33{C_{FDD}}^{0.58}$ (Lebedev's empirical model)
3. $h_i^2 - h_{i,0}^2 + \frac{2h_s k_i}{k_s} h_i - \frac{2h_s k_i}{k_s} h_{i,0} = \frac{2k_i}{\rho_i l_i} C_{FDD}.\alpha$ (Detailed Stefan's empirical model)
4. $h_{ice} = a\sqrt{C_{FDD}}$ (Simplified Stefan's empirical model)

Where:

h_0 = initial ice thickness,

h_{ice} = ice thickness,

C_{FDD} = cumulated freezing degree days and $C_{FDD} = \int (T_s - T_{fr}) dt$

T_s = Temperature at the ice surface in °C; which is taken equal to air temperature T_a

l = latent heat of diffusion, J/kg

k_{ice} = thermal conductivity of ice in $W/m°C$

ρ_{ice} = The density of ice, $kg/m3$

a = empirical freezing degree day factor (site-specific) having units of [m °C-1/2 day-1/2], and that varies from site to site depending on local conditions such as the snow cover, winds, and solar radiation. Table 5-1 lists common values for the freezing degree day factor.

α = 86400 seconds/day gives the correct units in the expression.

Table 5-1 Values for the Stefan Equation Coefficient 'a' (USACE, 2002; modified)

Ice Cover Condition	a^*	a†
Windy lake w/no snow	2.7	0.8
Average lake with snow	1.7-2.4	0.5-0.7
Average river with snow	1.4-1.7	0.4-0.5
Sheltered small river	0.7-1.4	0.2-0.4
* C_{FDD} calculated using degrees Celsius. The ice thickness is in centimeters.		
† C_{FDD} calculated using degrees Fahrenheit. The ice thickness is in inches.		

The degree-day factor is decided based on the study did by (Alferdesen, 2013) on the small Norwegian streams specifically Søkna, which in the same county, Trondelag, as the Beitstad. Alferdesen, (2013) decided this factor from (Brooks, 2010) who did a lot of research on Hydro-climatic counties for the northern hemisphere to find the degree-day factors.

According to (Ashton, 1989) The Stefan's formula basically overestimates the ice growth in the formation period and for the ice thicknesses less than about 0.1 m it is observed that the method results into too large ice thicknesses. The difference between stefan's detailed and simplified model used here is that in simplified stefan's model this source of error attempted to exclude by use of a lower degree-day factor in the formation period which has been taken until the first week of December, but in the detailed stefan's model constant values of all ice parameters i.e latent heat of fusion, thermal conductivity of both snow and ice, and ice density are used irrespective of the formation period. Here, the freezing degree day factor of 0.6 cm $°C^{-1/2}$ $day^{-1/2}$ in the formation period and 2.75 cm $°C^{-1/2}$ $day^{-1/2}$ is used in case of full ice cover in the simplified stefan's empirical model.

It is also worthy to mention that in this study a linear temperature method based on the thermal resistance in ice and snow is used. Firstly, the temperature at top of the ice cover is estimated and replaces the air temperature in the equation of the freezing degree days when snow is present. The conductivity of ice and snow for this study are taken as constants within normal ranges, 2.03 and 0.25-0.35 W m^{-1} $°C^{-1}$ respectively for the ice thickness calculation. (Sturm, Perovich, & Holmgren, 2002; Jasek, 2006; Byggforsk, 2007; Lundberg & Feiccabrino, 2009). According to the Norwegian Ice Service (NIS) daily ice charts, the first appearance of ice at near the areas of Beitstadsundet in past 50 years season was on mid of November and the last ice was noted on end

of April. Figure 5-6 shows the ice thickness at the bridge location in Beitstad for the past year. The figure was made based on the empirical Stefan's law of ice growth.

From the figure, the ice is noticeably growing from the end of November until the end of January. Then, ice cover is nearly plateaued from the start of February to the end of March after which ice thickness starts decreasing considerably. Moreover, the first snow was observed at the beginning of December, and the depth of snow increases until mid-March after which it starts decreasing until mid-April as shown in Figure 5-6.

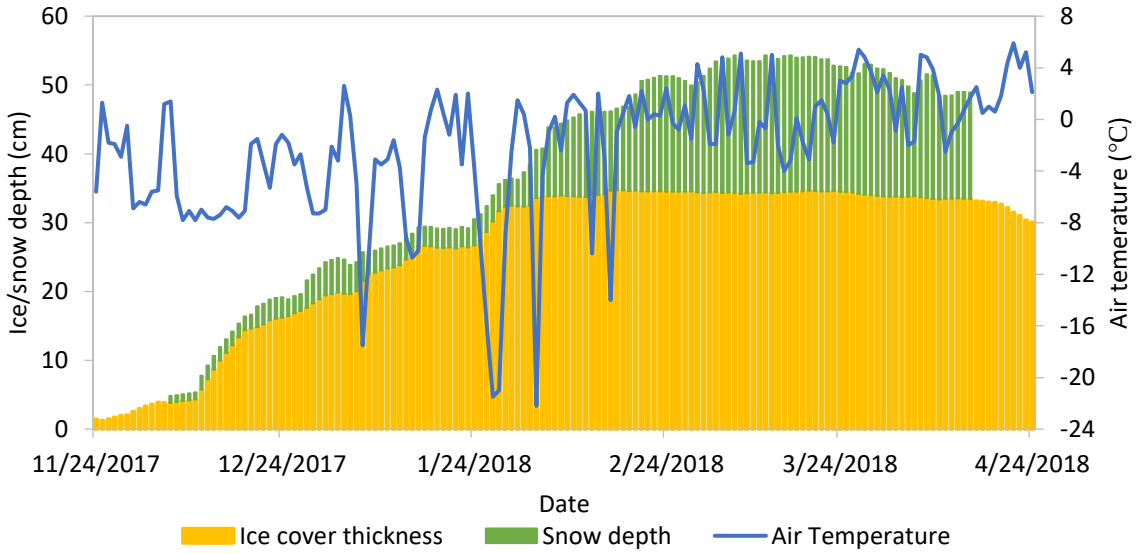

Figure 5-6 Ice cover thickness, snow depth and air temperature at Beitstad during winter 2017-2018 based on Stefan's empirical model

Figure 5-7 shows the ice thickness variations over the past 50 years at Beitstad. The ice cover thickness was calculated based on Stefan's law of ice growth. From the figure, the maximum ice cover thickness during the past 50 years was 0.56 m in the year 1986, whereas the minimum ice thickness was 0.22 m in the year 1971. It can also be observed that the trend of the ice cover is slightly falling. The reason behind this decrease might be global warming, while the reason behind the variations in the ice cover might be the climate change.

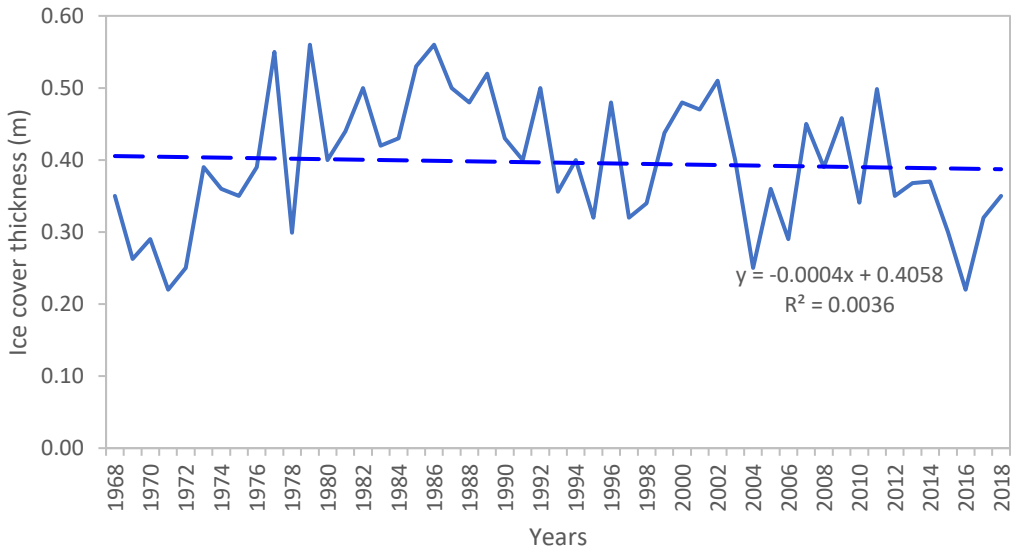

Figure 5-7 Winterly maximum ice thickness variations at Beitstad over the past 50 years

5.5.1 Effects of climate change on the ice cover

According to the Intergovernmental Panel on Climate Change (IPCC), human activities i.e. emission of greenhouse gases and other climate forcing substances, such as black carbon, into the atmosphere; have caused an increase in global temperatures of 1.0 °C over the past 150 years also global warming is expected to reach 1.5 °C between 2030 and 2052. Climate change occurs at two different timescales influencing both short-term extreme weather events, as well as causing gradual, long-term changes, including the sea level rise, melting of the glaciers and ice sheets, etc. Substantial changes in sea ice cover, snow cover, lake, and river ice cover, permafrost temperatures, glacier and ice sheet mass have been detected over the last few decades. Global and regional variations in temperature and precipitation largely influence the long-term changes in snow and ice, also it appears that these changes are occurring at an accelerating pace.

From the satellite data and sea ice modeling, it can be clearly observed that there is rapid loss in the sea ice which is one of the most prominent indicators of global climate change. Figure 5-8 shows that over the past few decades the area covered by sea ice in the Arctic has decreased, the ice has thinned, and less ice survives the summer melt. Sea ice volume and extent in the Arctic has shortened by almost forty percent since 1979, having the lowest amounts of observed ice in the last three summers: 2007, 2008, and 2009. It can also be observed that there is less multi-year sea

ice and sea ice is thinning in some regions. According to the different ice models forecast arctic summer almost without sea ice may be anticipated before the mid-century also the winter sea ice extent in the Antarctic region is also expected to become shorter.

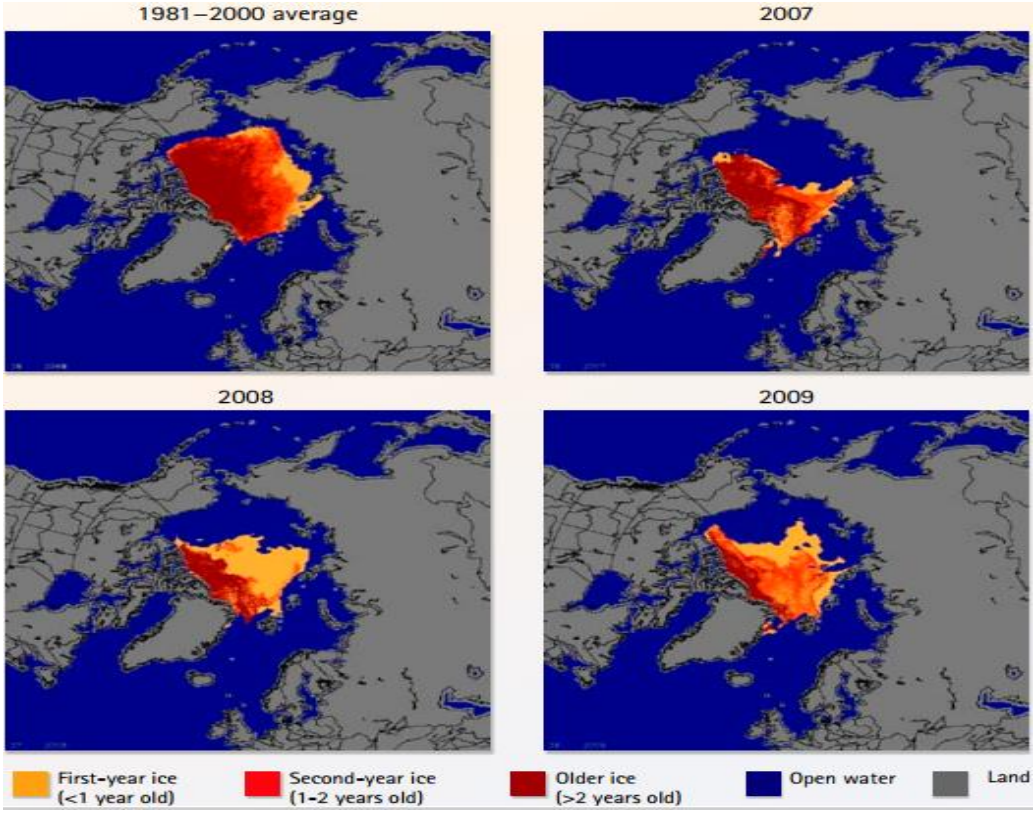

Figure 5-8 Thinning Arctic ice sheet (Reference: National Snow and Ice Data Center, USA)

According to National snow and ice data center, the University of Colorado at Boulder, USA; nearly sea ice-free Arctic summer may be anticipated before mid-century, and a relatively large decline in Antarctic winter sea ice extent is expected by the end of the century. Figure 5-9 shows the Northern Hemisphere sea ice extent in September as modeled by the 15 climate models used by the 2007 IPCC assessments (dotted lines). The mean values of these models are shown in the black line, while observations from the different satellites are shown in the red color. It is clear from the figure that the ice is melting at the rate of 11.2% per decade which is a noticeably faster rate than the predicted by any of the IPCC ice models.

Thus, in the late summer of 2009, more ice remained in the Arctic this year than during the previous record-setting low years of 2007 and 2008.

Though the recovery of the sea ice is not up to the previous levels and the shortening of the summer ice is approximately 30 years ahead of the climate model predictions. The climate model that was run recently by the IPCC shows that a nearly ice-free summer can be expected before mid-century.

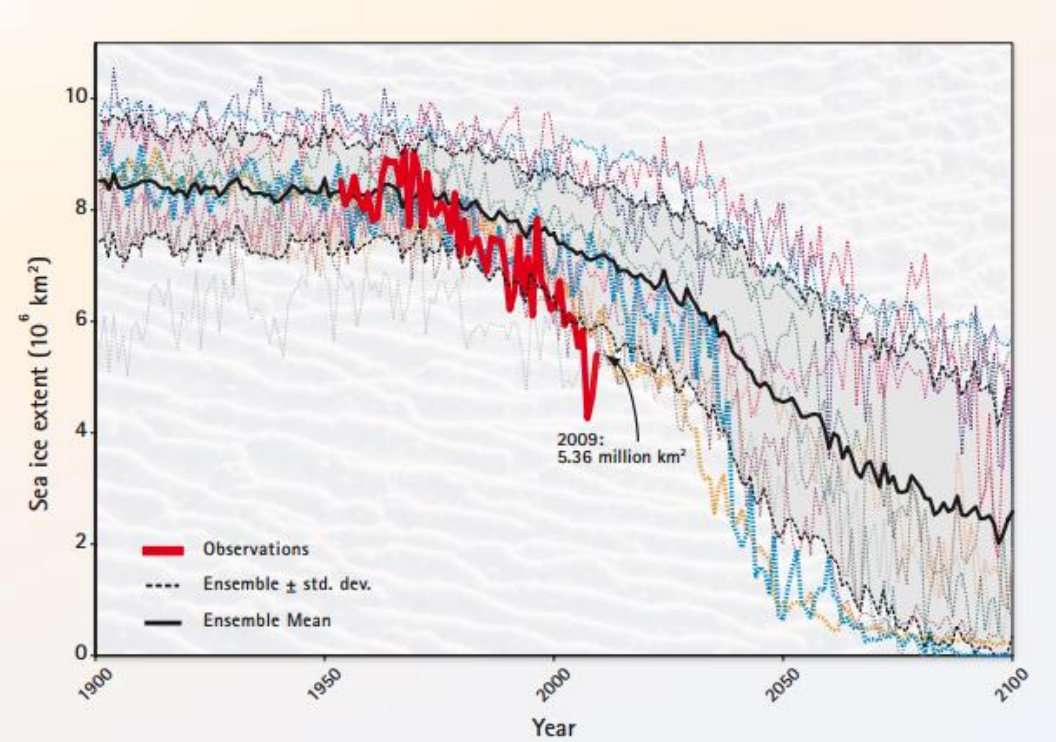

Figure 5-9 Arctic ocean sea ice loss (Reference: National Snow and Ice Data Center, USA)

In this case study, the effect of global warming has not been considered. As per the trend of the ice thickness, there will be no ice after the next 100 years. But again, there are some variations in the climate. So, to be on the conservative side extreme value analysis for the ice cover thickness is performed and after calculating the design ice cover thickness the design ice loads at Beitstadsundet bridge piers are computed.

5.6 Application into Delft3D-FLOW (Ice module)

5.6.1 Introduction

Numerical modeling of ice growth and transport in lakes, fjords, rivers or coastal seas can provide critical input for the safe and efficient design of coastal and hydraulic infrastructure in the Arctic, sub-arctic regions (de Goede et al. 2014; de Graaff et al. 2015). The modeling of ice growth and melt and related complex coastal and meteorological processes on these regional scales is however still rather unfolded (de Graaff et al. 2015). In these regions, the ice action on infrastructures such as platforms, lighthouses, sub-sea pipelines, or wind turbines may exceed the total forces of waves and currents and may, therefore, determine the design. Thus, the interaction of ice with planned structures might be important, and models of ice dynamics would be very helpful to engineering in these regions. (de Goede et al. 2014).

Delft3D-FLOW is a flexible integrated numerical modelling tool, which enables simulation of two-dimensional (2D, depth-averaged) or three-dimensional (3D) unsteady flow, sediment transport, morphology, waves, spills, water quality and ecology, including the effect of density differences due to a non-uniform temperature and salinity distribution (density-driven flow), and is capable of handling the interactions between these processes, and to cover all the relevant physical processes that determine the temporal and spatial characteristics of the ice and the thermal discharge, under influence of fresh river discharges, hydrodynamic, meteorological and atmospheric forcing, in combination with a recently developed ice module (de Goede et al. 2014; de Graaff et al. 2015). By coupling an ice module with these existing modules of Delft-3D, it becomes possible to not only predict the thickness and velocity of open-water ice and associated hydrodynamics, but also to study the interaction of ice with, for example, river banks, the seabed, water quality or spills of fine sediments or oil (de Goede et al. 2014).

As the ice cover concentration and extent in the polar regions are decreasing so, there is an increase in the human activities in both arctic and sub-arctic regions and thus there is an increasing demand for accurate ice modeling capabilities. (Thomas and Dieckmann 2010; Palmer and Croasdale 2012). Accurate predictions of ice thicknesses, ice loads, ice movement and other ice characteristics are vital for (de Goede et al. 2014; de Graaff et al. 2015):

- design of safe and sustainable structures in arctic and sub-arctic regions such as offshore wind farms, subsea pipelines, platforms.
- impact assessments (IA's), and
- planning of the safe marine operations.

5.6.2 Model description

5.6.2.1 General overview of Conceptual model

The ice module in Delft3D-FLOW has a thermodynamic model grounded on a single ice cover layer concept with snow on top (Semtner, 1976), and a dynamic model based on the elastic-viscous-plastic (EVP) sea-ice rheology (Hunke and Dukowicz, 1997). The hydrodynamic equations in Delft3D-FLOW are expressed in the spherical coordinates on the globe (de Goede et al. 2014; de Graaff et al. 2015). The transport equation, which for handiness is given in Cartesian rectangular coordinates in the horizontal and so-called σ-coordinates in the vertical, is described by (de Goede et al. 2014):

$$\frac{\partial [HC]}{\partial t} + \frac{\partial [HuC]}{\partial x} + \frac{\partial [HvC]}{\partial y} + \frac{\partial (\omega C)}{\partial \sigma} = \left[\frac{\partial}{\partial x}\left(D_h\, H \frac{\partial C}{\partial x}\right) + \frac{\partial}{\partial y}\left(D_h\, H \frac{\partial C}{\partial y}\right)\right] + \frac{1}{H}\frac{\partial}{\partial \sigma}\left[D_v \frac{\partial C}{\partial \sigma}\right] \pm \lambda_d (d + \zeta)\, C + S$$

Where:

λ_d = first-order decay process,

$C(x, y, \sigma, t)$ = concentration,

$H(x, y)$ = total water depth,

$D(h, v)$ = horizontal diffusion,

t = time, and

$u(x, y, \sigma, t), v(x, y, \sigma, t)$ and $\omega(x, y, \sigma, t)$ = velocity components in the horizontal x, y, and vertical σ-directions, respectively.

S represents the source and sink terms per unit area due to the discharge in q or withdrawal out q of water and the exchange of heat through the free surface Q_{tot}, which describes as following (de Goede et al. 2014):

$$S = (d + \zeta)(q_{in}\, C_{in} - q_{out}\, C_{out}) + Q_{tot}$$

The ice growth model comprises of three quantities, i.e. the ice thickness $h_i(x, y, t)$, the snow thickness $h_s(x, y, t)$ and the ice concentration $A(x, y, t)$. The equations for the conservation of the mass of ice and snow are given as (de Goede et al. 2014):

$$\frac{\partial(Ah_i)}{\partial t} + \frac{\partial(u_i Ah_i)}{\partial x} + \frac{\partial(v_i Ah_i)}{\partial y} = S_{ice} + D_{ice}$$

$$\frac{\partial(Ah_s)}{\partial t} + \frac{\partial(u_i Ah_i)}{\partial x} + \frac{\partial(v_i Ah_i)}{\partial y} = S_{snow} + D_{snow} + Q_{snow}$$

Where:

$u_i(x, y, t)$, $v_i(x, y, t)$ = ice velocity components in the horizontal, and

Q_{snow} = snowfall.

The expression for ice concentration A is given as (de Goede et al. 2014):

$$\frac{\partial(A)}{\partial t} + \frac{\partial(u_i A)}{\partial x} + \frac{\partial(v_i A)}{\partial y} = S_A + D_A$$

Where:

$0 \leq A \leq 1$.

Here, the ice concentration denotes the segment of a computational cell that is covered by the ice. Due to horizontal transport i.e. for a big ice sheet, it is probable that only a part of a computational cell is filled with ice (and snow). The ice velocities u_i and v_i are computed via the momentum equations are given as (de Goede et al. 2014):

$$M\left\{\frac{\partial u_i}{\partial t} + \frac{\partial(u_i u_i)}{\partial x} + \frac{\partial(v_i u_i)}{\partial y} - f v_i\right\} = Mg\frac{\partial \zeta}{\partial x} + \tau_a^x + \tau_w^x + F^x$$

$$M\left\{\frac{\partial v_i}{\partial t} + \frac{\partial(u_i v_i)}{\partial x} + \frac{\partial(v_i u_i)}{\partial y} - f u_i\right\} = Mg\frac{\partial \zeta}{\partial y} + \tau_a^y + \tau_w^y + F^y$$

Where:

λ_d = water elevation,

f = Coriolis force,

M = ice mass,

g = acceleration due to gravity,

F = internal stresses according to (Hibler, 1979), and

τ_a, τ_w = air and water stresses, respectively.

5.6.2.2 Numerical thermodynamic ice model

The decay or melt of ice is determined by the ice thermodynamics. The heat fluxes through the ice sheet are grounded on a simple one-layer ice model with snow on top, according to (Semtner, 1976). The right part in Figure 5-10 represents the standard temperature model in Delft3D-FLOW (Ice module) when ice is absent (de Goede et al. 2014; de Graaff et al. 2015).

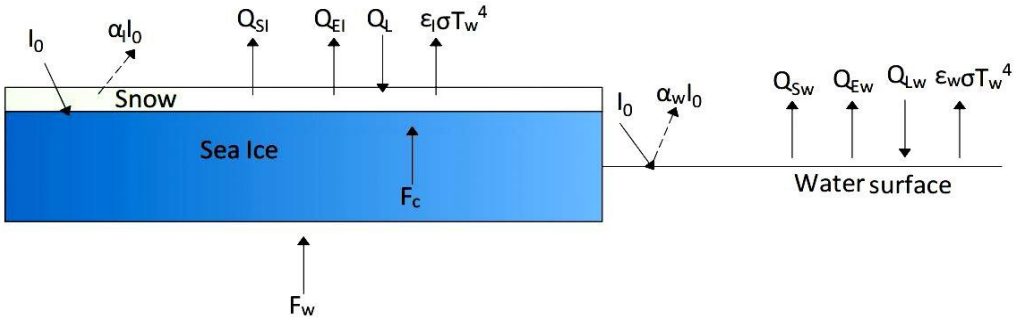

Figure 5-10 Conceptual diagram of the ice-growth (left) and temperature (right) model (Reference: de Goede et al. 2014; modified)

The total heat flux on the ice surface is given as following (de Goede et al. 2014; de Graaff et al. 2015):

$$Q_{tot} = I_0 + Q_{ai} - Q_{br} - Q_{ei} - Q_{si}$$

Where:

I_0 = net incident solar radiation (short wave),

Q_{ai} = net incident atmospheric radiation (long wave),

Q_{br} = back radiation (long wave),

Q_{ei} = evaporative heat flux (latent heat), and

Q_{si} = convective heat flux (sensible heat).

All of the heat fluxes expressions are described in the Delft3D-FLOW user manual (Deltares, 2013). The net atmospheric radiation Q_{ai} is given as (de Goede et al. 2014):

$$Q_{ai} = (1 - r)\varepsilon\sigma T_a^4 g(F_c)$$

Where:

T_a = air temperature (in K), and

r = reflection coefficient, and

ε = emissivity factor of ice.

In this numerical ice growth model, the temperature is supposed to be linear between the top and bottom of the ice sheet layer. Furthermore, it is assumed that the thermal conductive coefficient k_i for ice is constant and the heat conduction through the ice is given by (de Goede et al. 2014):

$$Q_{tot} = -k_i \left(T_a - T_f\right)/h_i$$

Where:

T_f = The freezing temperature of seawater.

In the grid cells in which ice is present, the heat flux between the ice and the water is given as (de Goede et al. 2014):

$$Q_{ice_water} = -C_{Tz} \left(T_f - T_s\right)$$

Where:

T_s = water temperature at the uppermost grid layer near the surface.

The heat transfer coefficient C_{Tz} is given by (de Goede et al. 2014):

$$C_{Tz} = \frac{u_*}{B_T + P_{rt} \ln(-z/z_0)/k}$$

Where:

$B_T = P_{rt}\, 3(z_0 u_*/v)^{1/2} P_t^{2/3}$,

u_* = friction velocity,

P_{rt} = a turbulent Prandtl number,

z = vertical coordinate corresponding to the temperature T,

z_0 = roughness length,

k = Von Karman constant,

B_T = molecular sublayer correction,

P_t = molecular Prantl number, and

v = the kinematic viscosity of water.

5.6.3 Previous case studies on ice growth

Delft3D-FLOW was applied for the implementation of an ice module in two case studies – modeling of ice growth and transport on a regional scale, with application to fountain lake, Minnesota, USA, and modeling of thermal discharge in an ice-covered estuary in Finland. In the first case study, the main goal of the research was to develop an ice module in Delft3D-FLOW and to conduct a validation with respect to the ice growth and melt and ice dynamic transport. The validation against Dutch ice growth and for the Fountain Lake was successful, within reasonable error associated with lack of data on snow cover. In this case study also the validation of the Delft3D-FLOW (Ice module) is done based on the empirical equations.

5.6.4 Data input for ice growth in Delft3D-FLOW (Ice module)

For the computation of the ice growth in Delft3D-FLOW, the following meteorological input parameters are required (de Goede et al. 2014):

- Wind speed [m/s],
- Air temperature [°C],
- Relative humidity [%],
- Fraction cloud coverage [%], and
- Snow thickness [m]
- Bathymetry

In this case study, schematized and simplified square basin also, detailed curvilinear grid basin, with constant values for the cloudiness and the relative humidity was considered.

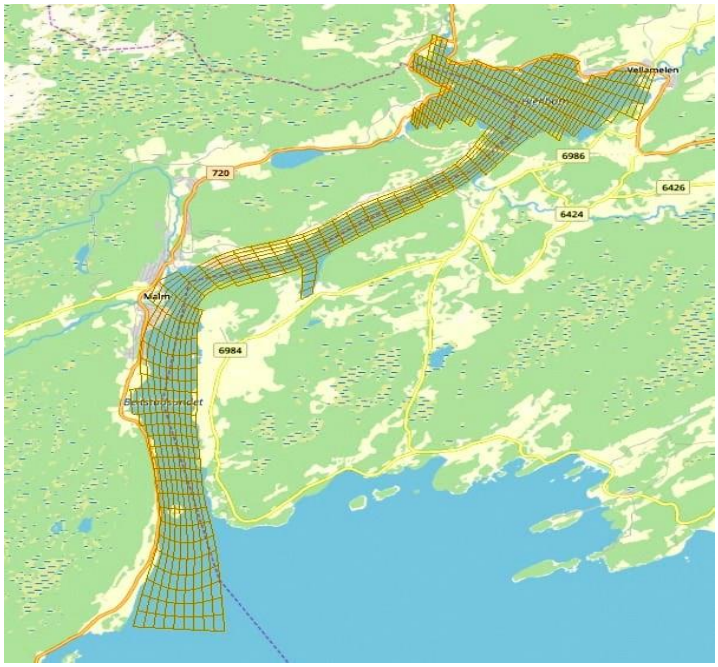

Figure 5-11 Computational grid of the land boundary at Beitstadsundet fjord

5.6.5 Results and discussion

The main aim of the ice growth modeling in Delft3D-FLOW (Ice module) was to conduct a validation with respect to the ice growth. Figure 5-12 & 13 shows the results of the ice growth simulation for the winter of 1950 – 2018 at only one grid point computed by the Delft3D-FLOW (Ice module) with and without snow at Beitstad. Firstly, a simplified swimming pool model is considered which shows the same ice thickness at the whole concerned boundary. Figure 5-14 shows the detailed simulation of ice thickness in the year 1968-69; at the inflow boundary in the south, the fjord is deeper, and the temperatures are warmer and ice thickness is thinner here. It is clear from the simulation figures that the ice starts growing from the mid of November to the end of March and then decreases. It is recognized that snow cover significantly hinders the ice formation. Because of its low thermal conductivity, the snow cover acts as an insulating blanket that slows down the conduction of heat from the ice to the surface, thus also slowing ice growth. To demonstrate this, simulations with and without snow cover are done as shown in Figure 5-12 & 13 respectively.

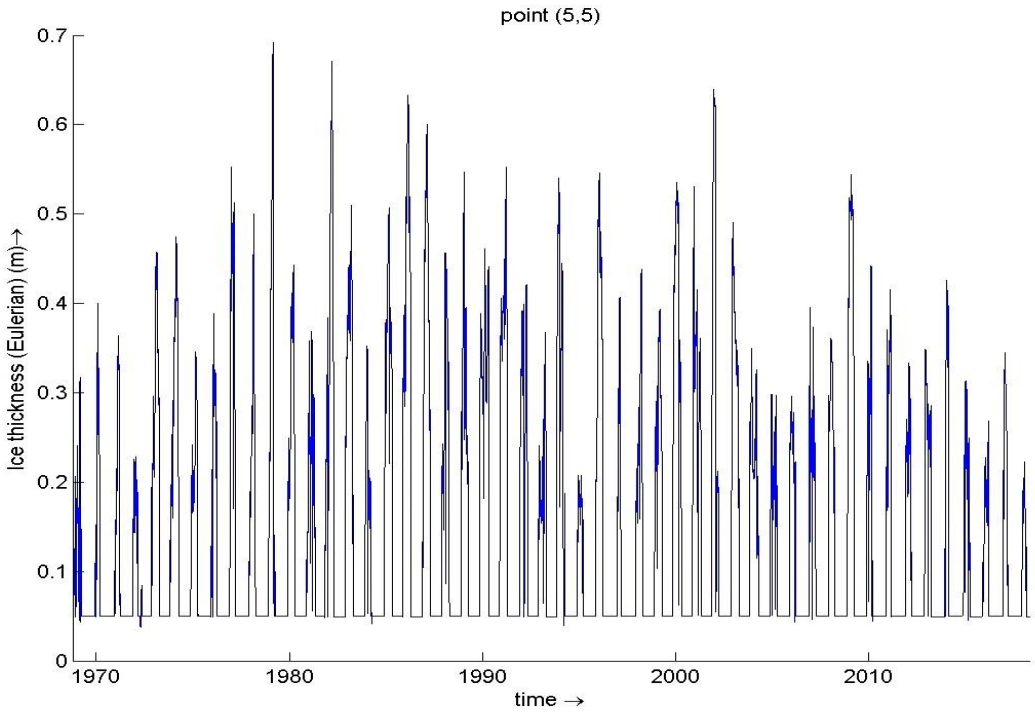

Figure 5-12 Ice thickness values (with snow cover) over the past 50 years computed from the Delft3D-FLOW (Ice module)

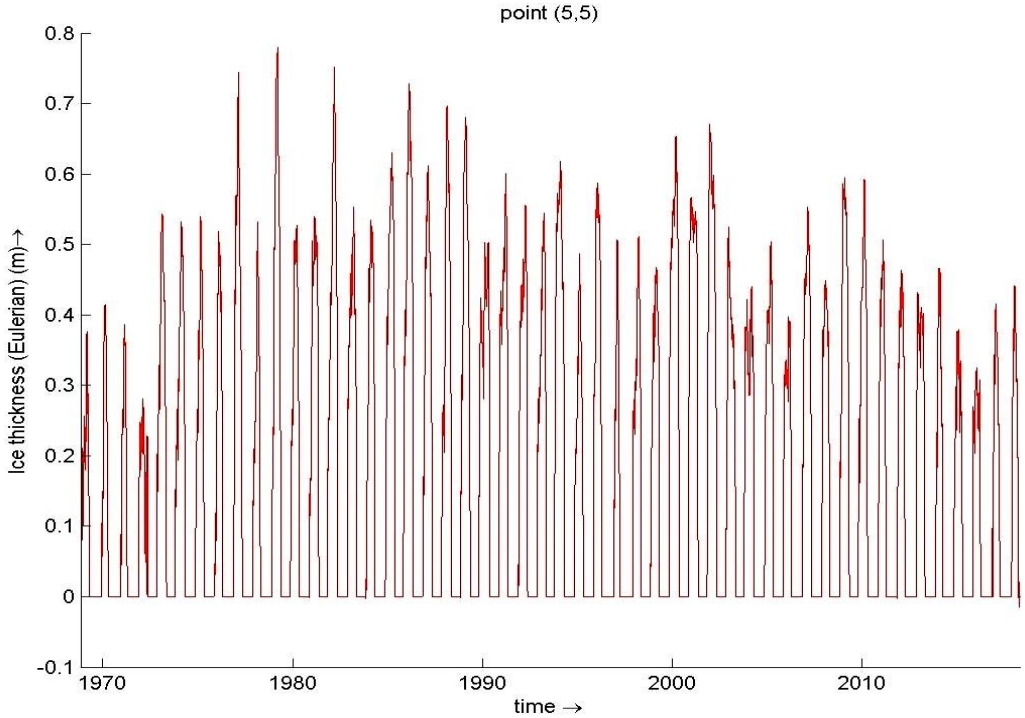

Figure 5-13 Ice thickness values (without snow cover) over the past 50 years computed from the Delft3D-FLOW (Ice module)

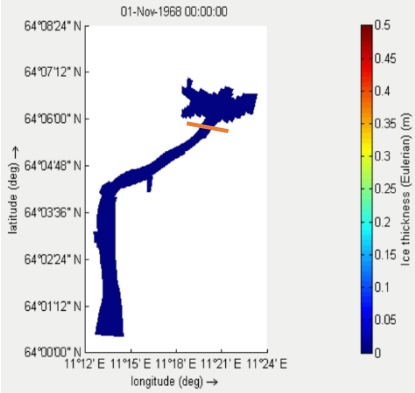
01-Nov-1968 00:00:00
64°08'24" N
64°07'12" N
64°06'00" N
64°04'48" N
64°03'36" N
64°02'24" N
64°01'12" N
64°00'00" N
11°12' E 11°15' E 11°18' E 11°21' E 11°24' E
latitude (deg) →
longitude (deg) →
Ice thickness (Eulerian) (m)
0.5
0.45
0.4
0.35
0.3
0.25
0.2
0.15
0.1
0.05
0

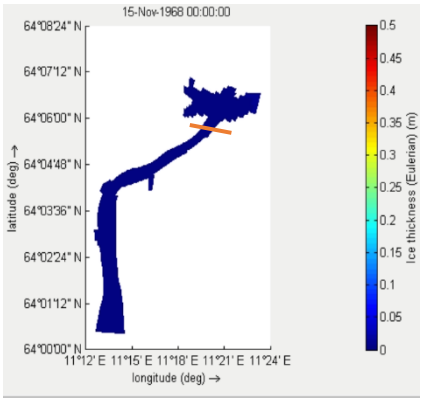
15-Nov-1968 00:00:00
64°08'24" N
64°07'12" N
64°06'00" N
64°04'48" N
64°03'36" N
64°02'24" N
64°01'12" N
64°00'00" N
11°12' E 11°15' E 11°18' E 11°21' E 11°24' E
latitude (deg) →
longitude (deg) →
Ice thickness (Eulerian) (m)
0.5
0.45
0.4
0.35
0.3
0.25
0.2
0.15
0.1
0.05
0

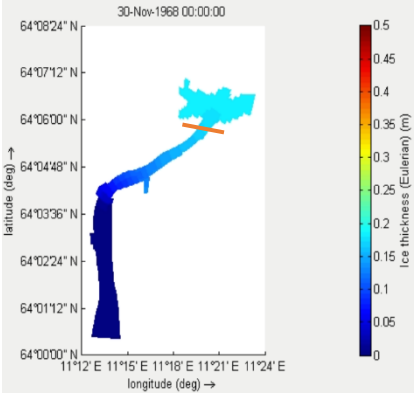
30-Nov-1968 00:00:00
64°08'24" N
64°07'12" N
64°06'00" N
64°04'48" N
64°03'36" N
64°02'24" N
64°01'12" N
64°00'00" N
11°12' E 11°15' E 11°18' E 11°21' E 11°24' E
latitude (deg) →
longitude (deg) →
Ice thickness (Eulerian) (m)
0.5
0.45
0.4
0.35
0.3
0.25
0.2
0.15
0.1
0.05
0

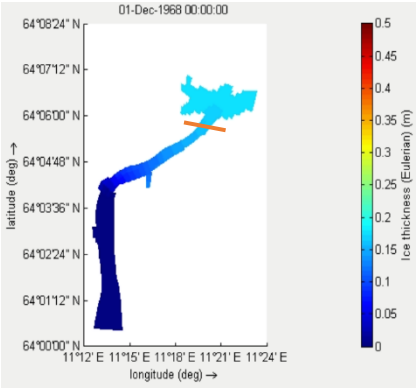
01-Dec-1968 00:00:00
64°08'24" N
64°07'12" N
64°06'00" N
64°04'48" N
64°03'36" N
64°02'24" N
64°01'12" N
64°00'00" N
11°12' E 11°15' E 11°18' E 11°21' E 11°24' E
latitude (deg) →
longitude (deg) →
Ice thickness (Eulerian) (m)
0.5
0.45
0.4
0.35
0.3
0.25
0.2
0.15
0.1
0.05
0

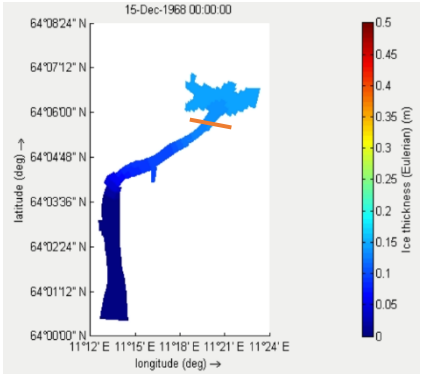
15-Dec-1968 00:00:00
64°08'24" N
64°07'12" N
64°06'00" N
64°04'48" N
64°03'36" N
64°02'24" N
64°01'12" N
64°00'00" N
11°12' E 11°15' E 11°18' E 11°21' E 11°24' E
latitude (deg) →
longitude (deg) →
Ice thickness (Eulerian) (m)
0.5
0.45
0.4
0.35
0.3
0.25
0.2
0.15
0.1
0.05
0

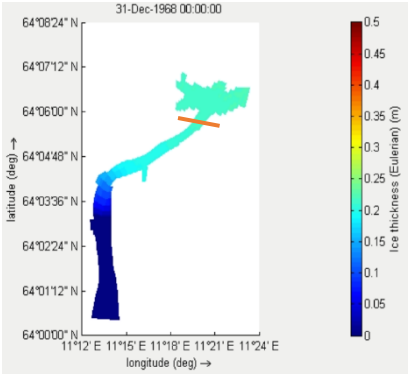
31-Dec-1968 00:00:00
64°08'24" N
64°07'12" N
64°06'00" N
64°04'48" N
64°03'36" N
64°02'24" N
64°01'12" N
64°00'00" N
11°12' E 11°15' E 11°18' E 11°21' E 11°24' E
latitude (deg) →
longitude (deg) →
Ice thickness (Eulerian) (m)
0.5
0.45
0.4
0.35
0.3
0.25
0.2
0.15
0.1
0.05
0

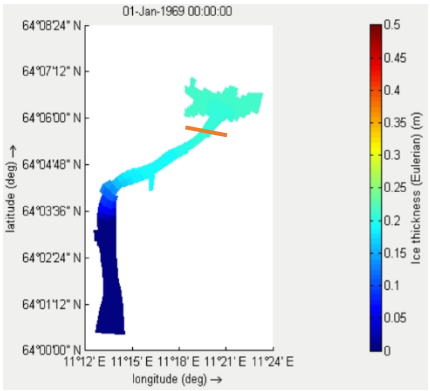
01-Jan-1969 00:00:00
64°08'24" N
64°07'12" N
64°06'00" N
64°04'48" N
64°03'36" N
64°02'24" N
64°01'12" N
64°00'00" N
11°12' E 11°15' E 11°18' E 11°21' E 11°24' E
latitude (deg) →
longitude (deg) →
Ice thickness (Eulerian) (m)
0.5
0.45
0.4
0.35
0.3
0.25
0.2
0.15
0.1
0.05
0

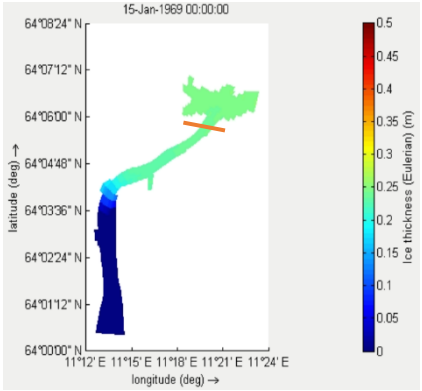
15-Jan-1969 00:00:00
64°08'24" N
64°07'12" N
64°06'00" N
64°04'48" N
64°03'36" N
64°02'24" N
64°01'12" N
64°00'00" N
11°12' E 11°15' E 11°18' E 11°21' E 11°24' E
latitude (deg) →
longitude (deg) →
Ice thickness (Eulerian) (m)
0.5
0.45
0.4
0.35
0.3
0.25
0.2
0.15
0.1
0.05
0

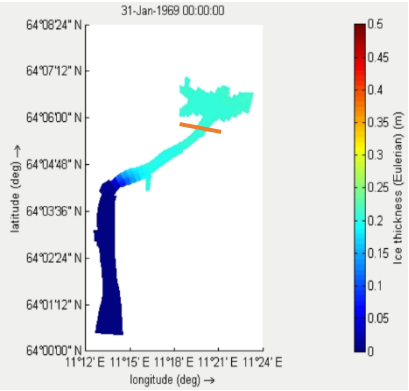
31-Jan-1969 00:00:00
64°08'24" N
64°07'12" N
64°06'00" N
64°04'48" N
64°03'36" N
64°02'24" N
64°01'12" N
64°00'00" N
11°12' E 11°15' E 11°18' E 11°21' E 11°24' E
latitude (deg) →
longitude (deg) →
Ice thickness (Eulerian) (m)
0.5
0.45
0.4
0.35
0.3
0.25
0.2
0.15
0.1
0.05
0

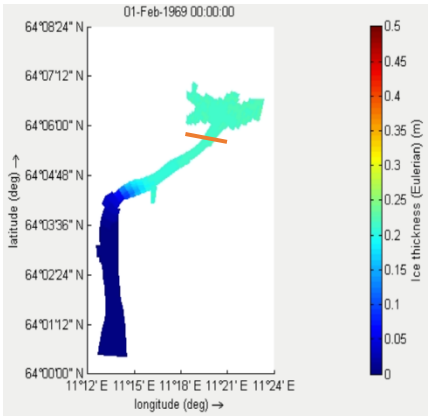
01-Feb-1969 00:00:00
64°08'24" N
64°07'12" N
64°06'00" N
64°04'48" N
64°03'36" N
64°02'24" N
64°01'12" N
64°00'00" N
11°12' E 11°15' E 11°18' E 11°21' E 11°24' E
latitude (deg) →
longitude (deg) →
Ice thickness (Eulerian) (m)
0.5
0.45
0.4
0.35
0.3
0.25
0.2
0.15
0.1
0.05
0

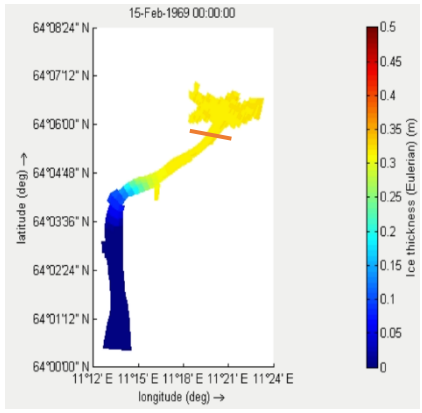
15-Feb-1969 00:00:00
64°08'24" N
64°07'12" N
64°06'00" N
64°04'48" N
64°03'36" N
64°02'24" N
64°01'12" N
64°00'00" N
11°12' E 11°15' E 11°18' E 11°21' E 11°24' E
latitude (deg) →
longitude (deg) →
Ice thickness (Eulerian) (m)
0.5
0.45
0.4
0.35
0.3
0.25
0.2
0.15
0.1
0.05
0

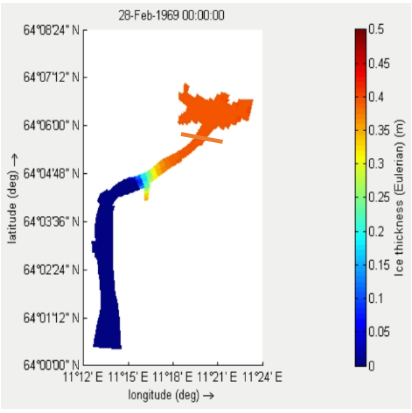
28-Feb-1969 00:00:00
64°08'24" N
64°07'12" N
64°06'00" N
64°04'48" N
64°03'36" N
64°02'24" N
64°01'12" N
64°00'00" N
11°12' E 11°15' E 11°18' E 11°21' E 11°24' E
latitude (deg) →
longitude (deg) →
Ice thickness (Eulerian) (m)
0.5
0.45
0.4
0.35
0.3
0.25
0.2
0.15
0.1
0.05
0

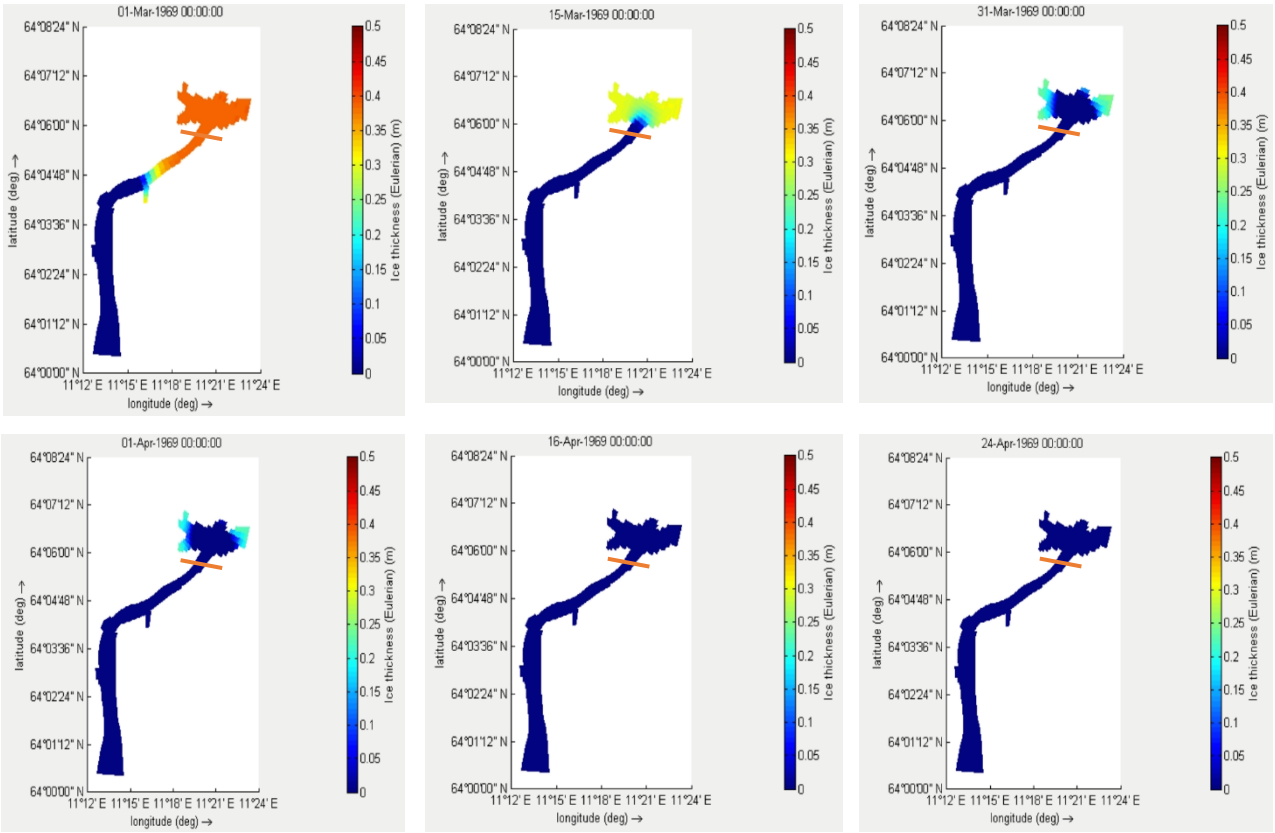

Figure 5-14 Ice thickness at the Beitstadsundet fjord started from the 1st November to end of April(1968-69); each row shows the ice thickness (with snow cover) in the beginning, middle and end of the month & orange line shows the bridge location in each figure.

5.6.6 Comparison between Delft3-FLOW (ice module) and empirical models for validation of the Process-based model

The main goal of the research presented for t ofhis case study to conduct a validation of the Delft3D-FLOW (Ice module) with respect to the ice cove thickness calculation. The validation against the Beitstadsundet is successful, within reasonable error associated with lack of data on snow cover, cloudiness and relative humidity as, monthly constant values for these variables are used.

Figure 5-15 shows the comparison between the ice thicknesses computed by Delft3D-FLOW (Ice module) and empirical models. From a global point of view, the process-based model results are in reasonable agreement with the empirical models, although differences up to 15-20 cm can be observed. The range of ice thickness computed from Delft3D-FLOW (Ice module) is 0.23 to 0.65

(with snow cover), 0.28 to 0.77 (without snow cover) and range of the discussed empirical models (Zubov,Lebedev,Stefan's detailed & simplified) is 0.17 to 0.38 (without snow cover), 0.24 to 0.44 (without snow cover), 0.16 to 0.36 (with snow cover), 0.22 to 0.56 (with snow cover) respectively. The average values of the ice thickness (with snow cover) computed by process-based and empirical models in the past 50 years are 0.42 & 0.35 m respectively. The differences between the ice thicknesses might be due to uncertainties produced by using the constant snow cover, cloudiness, and relative humidity data. In addition to this, the freezing degree day factor used in the equation based on the simplified Stefan's law which is site-specific and its constant value for the start of formation and then growth was used also in detailed Stefan's empirical equation the values of thermal conductivity of ice and snow and latent heat of fusion were assumed . This can also cause uncertainty in the ice cover thickness calculation.

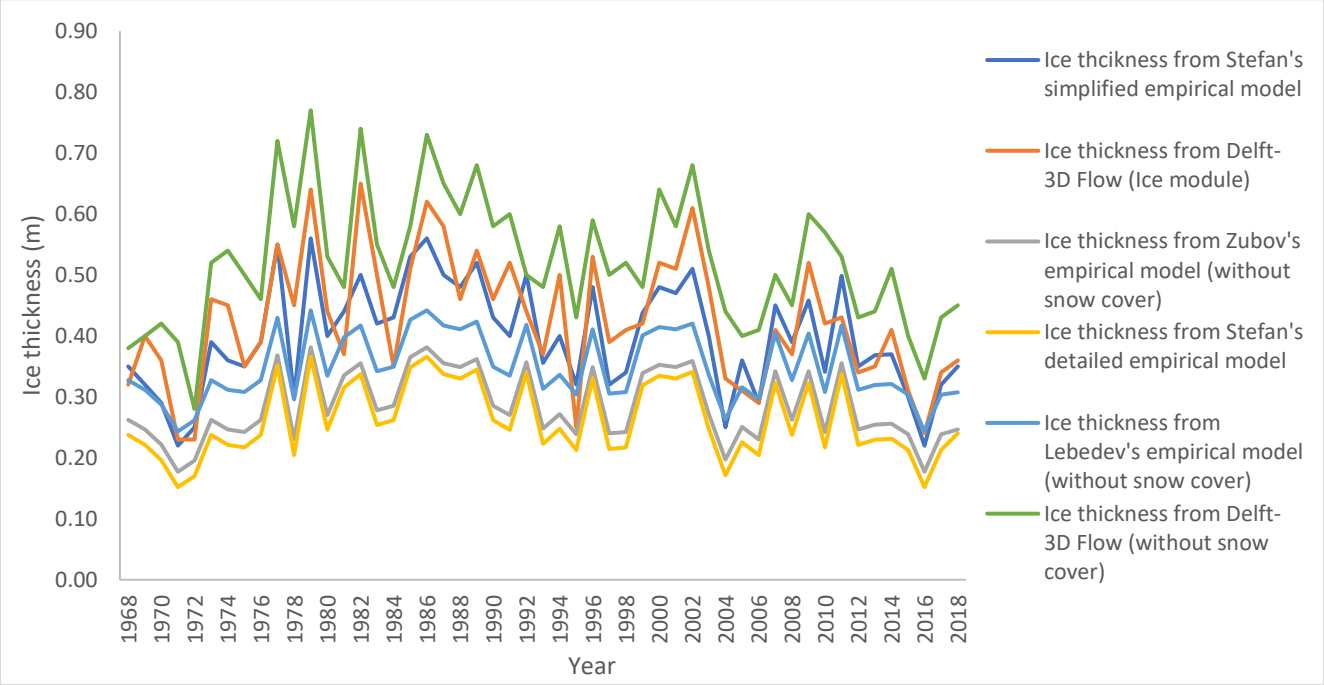

Figure 5-15 Winterly maximum ice floe thickness comparison between different empirical models and Delft3D-FLOW (Ice module) with and without snow cover

Chapter 6

Deterministic calculations of the ice actions

6.1 Standards for ice actions

6.1.1 International Organization of Standardization (ISO19906)

The ISO19906 standard (2010) gives information and methodology to compute the ice actions on offshore structures and based on the limit states approach determined Extreme-Level Ice Event (ELIE) and Abnormal-Level Ice Event (ALIE) ice actions which can be applied in the design of the proposed offshore structures. This standard based on the several methods for determining the governing ice actions depending on the specific site and ice conditions and type of the structure. Based on the three-limiting mechanism (Momentum, force, and stress) as shown in Figure 6-1 ISO19906 provides the guidance to calculate the governing ice action during the lifetime of the proposed structure.

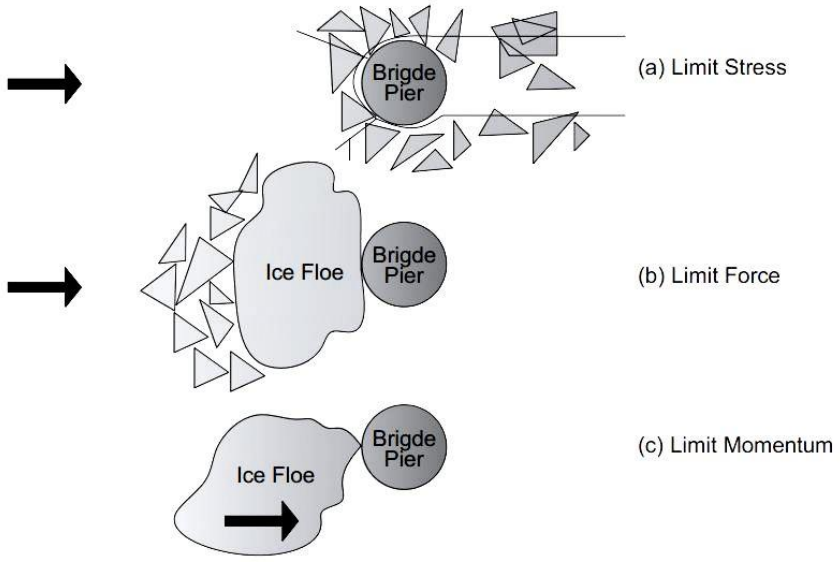

Figure 6-1 Design scenarios (Palmer and Croasdale, 2012; modified)

6.1.1.1 Limit force: driving forces

The ice forces on a structure for limit force follows directly from the action with which the ice feature is being driven against the structure. As shown in Figure 6-2, the driving forces on an ice feature may be due to the following:

- Direct ice actions (i.e., ice-ice interaction),
- Current drag,
- Wind drag, and
- Thermal expansion.

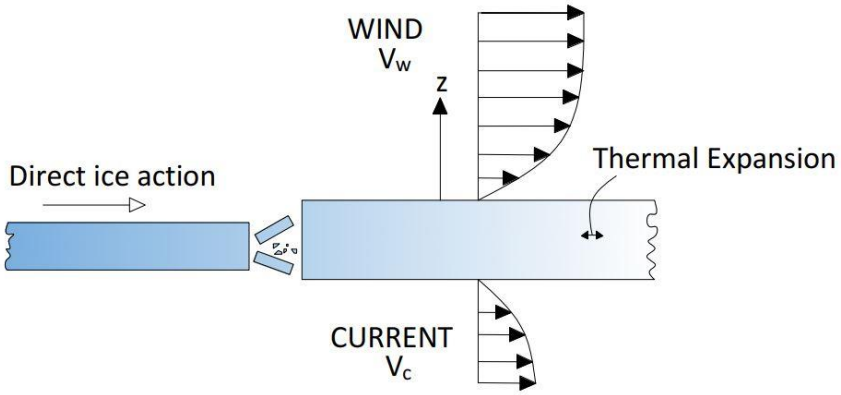

Figure 6-2 Environmental forces: wind and current drag forces and thermal expansion (Reference: Compendium OE44115 by Hoving, 2018; modified)

The total ice action for limit force is given as:

$$F_{LF} = F_{direct} + F_{wind} + F_{current} + F_{thermal}$$

In the thesis, it is considered that an isolated ice floe has no interaction with other floes and therefore: F_{direct} = 0. The drag action against the bridge pier then follows from the drag equation:

$$F_d = \frac{1}{2} C_d \rho A_{floe} V^2$$

To calculate the ice forces due to the wind and current drag, generally ice floes described as equivalent circular floes with a diameter D_{floe}, as shown in Figure 6-3. Consequently, the total limit force ice action for an isolated ice floe is then found as:

$$F_{LF,Floe} = \frac{\pi}{8} C_{d,a}\, \rho_a V_w^2 D_{floe}^2 + \frac{\pi}{8} C_{d,w}\, \rho_w V_c^2 D_{floe}^2$$

Where:

$C_{d,a}$ = Drag coefficient of air,

$C_{d,w}$ = Drag coefficient of water,

D_{floe} = Diameter of ice floe,

V_c = Current velocity,

V_w = Wind velocity,

ρ_a = Density of air, and

ρ_w = Density of water.

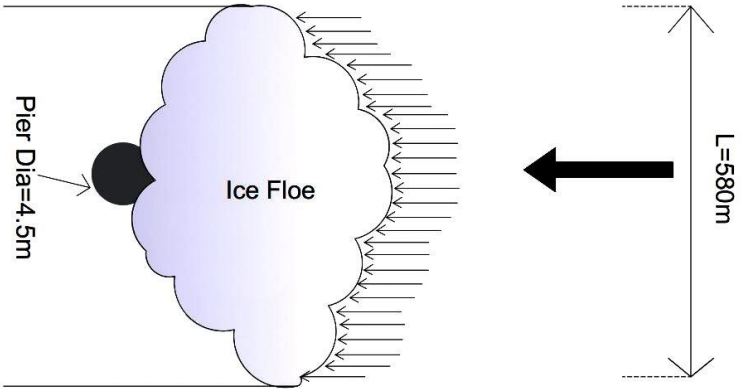

Figure 6-3 Ice floe diameter

As per Article A.8.2.4.11 in ISO19906, ice forces can also develop due to rising temperatures when ice expansion is restricted by structures or other obstructions in the sheltered areas. Based on full-scale model testing measurements made in Russian and Canadian sea areas, sea ice does not expand appreciably for ice temperatures above -10 °C for salinities greater than 3 or above -7 °C for salinities greater than 1%. The thermal action depends mainly on the initial ice surface temperature and the rate of temperature increase. This is shown in Figure 6-4 for freshwater ice sheets with complete lateral restraint. For an initial assessment of thermal forces, suggestive values in the range of 150 to 300 kN/m can be used regardless of the ice thickness. Thermal actions in freshwater ice are larger in magnitude than those in sea ice.

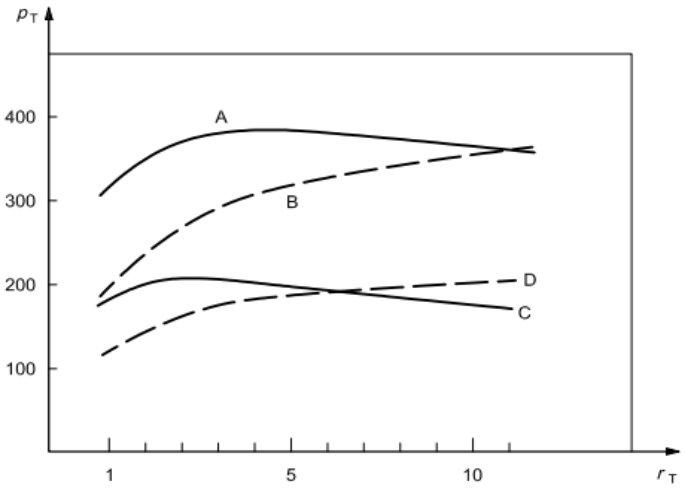

Key

A	T = –30 °C and h = 1,0 m	p_T	thermal ice pressure, expressed in kilonewtons per metre
B	T = –30 °C and h = 0,5 m	r_T	rate of temperature increase, expressed in degrees Celsius per hour
C	T = –20 °C and h = 1,0 m	h	ice thickness
D	T = –20 °C and h = 0,5 m		

Figure 6-4 Thermal ice load vs the rate of temperature increases of the ice surface (ISO19906 A-8-35)

6.1.1.2 Limit stress: ice crushing failure

According to ISO19906, Limit stress will only occur when the driving forces are large enough to cause the interacting ice feature to fail. Ice actions for limit stress largely depend on:

- The geometry of the ice-structure interaction, and
- The occurring failure mode such as crushing, bending, splitting, spalling or buckling.

For this case study, crushing failure has been considered the limiting stress mechanism for the vertical structure, and bending failure has been considered the limiting stress mechanism for sloping structures and ice floe interaction.

6.1.1.3 Ice crushing failure

As per ISO19906, when ice crushing occurs against a structure, the global ice action in the direction of the ice motion, denoted as F_G, is found regardless of the limiting mechanism as:

$$F_G = P_G A$$

Where:

P_G = Global average crushing pressure $[Pa]$, and

A = Nominal contact area $[m^2]$.

The nominal contact area is the projected interaction area between the ice and the structure normal to the direction of the ice motion. Irrespective of whether the ice is level ice, rafted ice or an ice ridge, the nominal contact area is found as the product of structure width w at the ice-structure interface and the ice thickness h, so that $A = wh$. The global ice action due to ice crushing is found using the following modified equation:

$$P_G = C_R\left(\left(\frac{h}{h^*}\right)^n\left(\frac{w}{h}\right)^m + e^{-\frac{w}{3h}}\sqrt{1+5\frac{h}{w}}\right)$$

Where:

P_G = effective ice pressure $[MPa]$,

w = structure width under ice action $[m]$,

h = ice thickness $[m]$,

h^* = reference thickness = 1.0 $[m]$,

m = experimental constant = -0.16,

n = experimental constant = -0.50 + h/5 while h < 1.0 m = -0.30 while h ≥ 1,0 m

C_R = ice reference strength for subarctic climate, which is taken as 1.8 MPa for circular cross-section and 2.0 MPa for a straight wall.

6.1.1.4 Ice bending failure

Figure 6-5 shows the ice forces on sloping structures in both horizontal and vertical directions. The total horizontal design load for bending failure is found according to the equation as given in ISO19906 as under:

$$F_H = \frac{H_B + H_P + H_R + H_L + H_T}{1 - \frac{H_B}{\sigma_f l_c h}}$$

Where:

H_B = load required to break the ice blocks against the slope,

H_R = load required to push the ice blocks up the slope,

H_T = load required to turn the ice block at the top of the slope,

H_P = load required to push the sheet ice through the rubble, and

H_L = load required to lift the ice rubble with the unbroken ice floe.

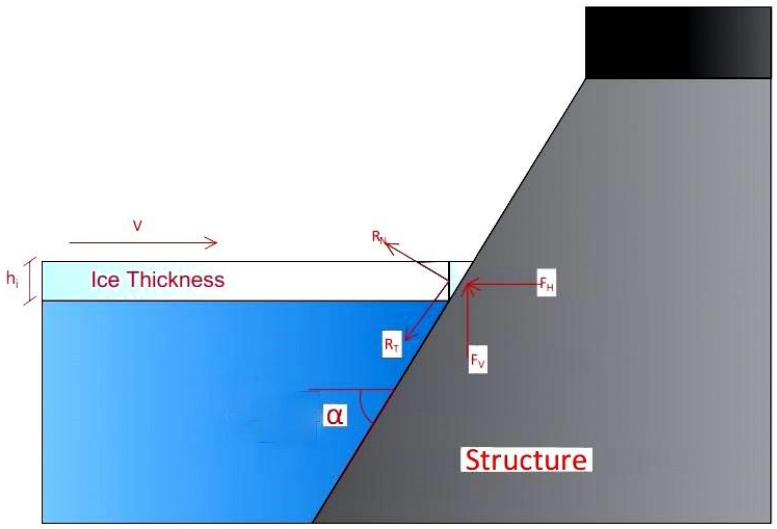

Figure 6-5 Ice forces on sloping structures: horizontal and vertical forces (Reference: Compendium OE44115 by Hoving, 2018; modified)

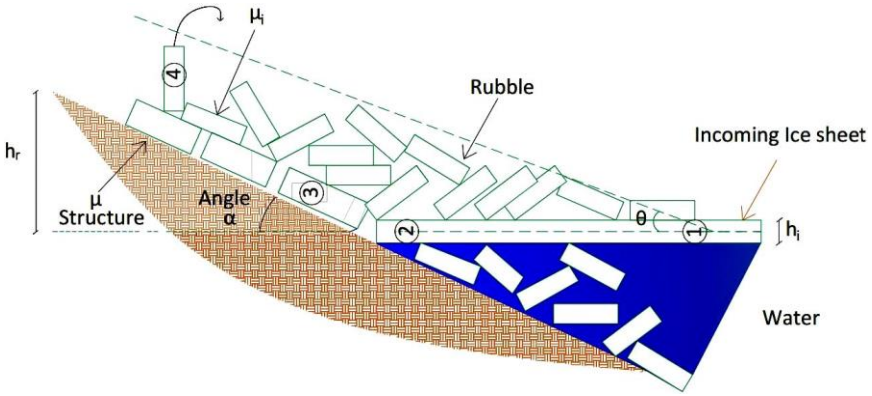

Figure 6-6 Level ice against 2D sloping structure and rubble ice – 1) incoming level of ice sheet; 2) level ice in contact with the structure; 3) ice moving along the structure and 4) ice failing back on rubble pile (Reference: Compendium TBA4265 by Høyland, 2017; modified)

These all forces can be calculated from the following formulas as per ISO19906 as follows:

i. The breaking component H_B is the main component, which is found as:

$$H_B = 0.68\rho\xi\sigma_f \left(\frac{\rho_w g h^5}{E}\right)^{0.25} l_c$$

$$\xi = \frac{\sin\alpha + \mu\cos\alpha}{\cos\alpha - \mu\sin\alpha}$$

$$l_c = w + \frac{\pi^2}{4} L_C$$

$$L_C = \left(\frac{Eh^3}{12\rho_w g(1-\nu^2)}\right)^{0.25}$$

Where:

ξ = ratio of horizontal and vertical forces,

σ_f = ice flexural strength,

ρ_w = water density,

g = the gravity,

E = elastic modulus of the ice,

w = structure width, and

l_c = length of circumferential bending crack.

ii. The force needed to push the ice through the rubble H_P, which is found as:

$$H_P = wh_\gamma^2 \mu_i \rho_i g(1-e)\left(1 - \frac{\tan\theta}{\tan\alpha}\right)^2 \frac{1}{2\tan\theta}$$

Where:

μ_i is the ice-ice coefficient of friction.

iii. The (horizontal) force needed to push to ice block up the slope H_R is given as:

$$H_R = \frac{w\rho_i g h_\gamma}{\cos\alpha - \mu\sin\alpha}\left(0.5(\mu_i + \mu)(1-e)h_\gamma\left(\mu_i\left(\frac{\sin\alpha}{\tan\theta} - \cos\alpha\right) + \frac{\cos\alpha}{\tan\alpha}\right)\left(1 - \frac{\tan\theta}{\tan\alpha}\right) + h\frac{\sin\alpha + \mu\cos\alpha}{\sin\alpha}\right)$$

iv. The force required to lift the ice rubble on top of the advancing ice sheet prior to breaking it, H_L can be calculated as:

$$H_L = wh_\gamma \xi \left(1 - \frac{\tan\theta}{\tan\alpha}\right)\left(0.5h_\gamma \rho_l g(1-e)\left(\frac{1}{\tan\theta} - \frac{1}{\tan\alpha} + \tan\phi\left(1 - \frac{\tan\theta}{\tan\alpha}\right)\right) + c\right)$$

v. The force to turn the ice block at the top of the slope H_T is given as:

$$H_T = 1.5wh^2\rho_i g \frac{\cos\alpha}{\sin\alpha - \mu\cos\alpha}$$

6.1.2 American Association of State Highways and Transportation Officials (AASHTO)

The AASHTO standard (2002) gives the procedure for evaluating the ice actions depends on the results of the theoretical and experimental research in ice mechanics and estimations of the ice actions in the field. Recently, understanding of the active ice processes during ice failure at different indentation speeds has been increased. Information on estimated ice forces on large structures has been published recently. AASHTO (2013) code considers dynamic and static ice loads on bridge piers, situated in rivers, lakes and coastal waters. The dynamic actions develop while floating ice is failing against a structure during the spring break up of the ice, or when currents and wind move ice floe past bridge piers at different times of the year. The static ice actions are developed by the thermal expansion of ice and by the variation in the water levels.

6.1.2.1 Environmental forces

6.1.2.1.1 Wind and current drag forces

According to the AASHTO (2013), the drag forces, caused by wind and water shear stresses on the top and the bottom surfaces of an ice cover, can be calculated from the following equation:

$$F_d = C_d \rho A v^2$$

Where:

C_d = drag coefficient,

ρ = density of air or water,

A = fetch area, and

v = velocity of air or water measured at a certain distance above or below an ice cover.

The value for C_d is 0.002 for a smooth ice cover, and 0.005 for a rough ice cover (Banke and Smith 1973). When enough data are available on wind and current speeds and the fetch area, it can be conceivable to calculate the wind and current drag forces on structures. In most conditions, the estimates of wind and current drag forces are larger than the force required to fail an ice sheet against the bridge pier, and the ice failure process limits the force to what is necessary to fail the ice against the structure. If wind and current drag forces can be estimated to be less than the force required to fail the ice sheet, the design force on a structure is taken to be equal to the estimate of wind and current drag forces (AASHTO, 2013).

6.1.2.1.2 Thermal ice forces

Ice expands like other structures with the increase of temperature. The temperature of ice changes due to conduction, radiation, convection, heat exchange, the presence or absence of snow and the environmental conditions. (Michel 1970, 1978; Sanderson 1988). The important factors affecting thermally generated ice forces are the magnitude and the rate of temperature increase, heat transfer at the top surface and in the ice sheet, boundaries resisting the expansion of an ice cover, and dry and wet cracks. Many researchers have been proposed different methods to calculate the thermally induced ice force, and thermally induced ice pressures have been also reviewed by several authors (Michel 1970, Kjeldgaard and Carstens 1980, Sanderson 1984).

AASHTO (2013) describes a procedure to calculate the temperature change with depth taking into consideration heat transfer by conduction, radiation, and convection which require site measurements to calculate the ice loads due to thermal expansion. For the starting point, this standard suggests some typical values of the thermal ice force in the range of 200–400 kNm^{-1} (1.5×10^5 to 2.95×10^5 $Ibft^{-1}$).

6.1.2.2 Loads due to ice failure

6.1.2.2.1 Ice crushing failure

To estimate dynamic ice actions due to ice crushing F_c on bridge piers resulting from moving ice, the following formula is used (AASHTO 2013):

$$F = F_c \text{ for } D/h > 6$$

Where:

$F_c = C_a PDh$ = horizontal force in which ice floes fail by crushing over the full width of a bridge pier,

$C_a = (5h/D + 1)^{0.5}$ = to account for the aspect ratio effect found in small-scale indentation tests,

P = effective ice crushing pressure.

D = pier diameter, and

h = ice thickness.

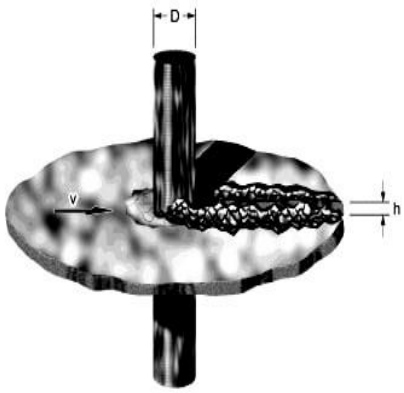

Figure 6-7 Total ice force F on a structure of width D attributable to the failure of an ice sheet of thickness h (Reference: AASHTO, 2013)

6.1.2.2.2 Ice bending failure

AASHTO (2013) gives a formula for the ice failure in bending based on API (1995) which gives equations for calculating the ice actions on sloping structures, where the broken ice pieces are assumed to ride up the sloping surface and fall into the water on the other side. Figure 6-8 shows forces during interaction of a floating ice sheet having thickness h being pushed against a wide sloping surface at an angle α with the horizontal axis. If the ice blocks are lifted a height z along

the sloping surface, the weight of the broken ice sheet on the sloping surface has a magnitude per unit width of $w = \rho_i ghz/\sin\alpha$, where $\rho_i g$ is the specific weight of ice, and h is the ice thickness. The normal force per unit width on the surface is $N = w\,cos\alpha$, and the tangential force along the surface is μN, where μ is the coefficient of friction between the surface and the ice. As shown in Figure 6-6, the force T acting between the broken ice on the sloping surface and the top of the floating ice sheet has a value per unit width of $T = w(\sin\alpha + \mu\cos\alpha)$.

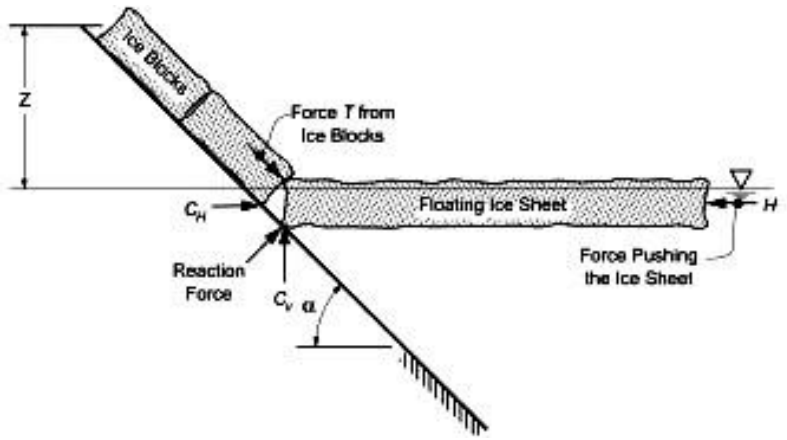

Figure 6-8 Forces during interaction of a floating ice sheet of thickness h being pushed against a wide sloping surface at an angle α with the horizontal (Reference: AASHTO, 2013)

By assuming that there is no moment acting on the floating ice sheet, the vertical force component C_v per unit width required to break the floating ice sheet and push it up is given by:

$$C_v = \frac{\sigma h^2 + 6le^{\frac{\pi}{4}} T\sin\alpha + Th\cos\alpha}{6le^{\frac{\pi}{4}} - h\tan(\alpha + \arctan\mu)}$$

Where:

σ = flexural strength of ice sheet,

h = ice thickness,

α = angle between the sloping surface and the horizontal,

$l = (Eh^3/12\rho_w g(1-\nu^2))^{0.25}$ = the characteristic length of floating ice sheet,

E = effective elastic modulus of ice,

ν = Poisson's ratio of ice, and

$\rho_i g$ = specific weight of ice.

For the typical ice bending rates, AASHTO suggests the effective elastic modulus of freshwater ice is in the range of 1-3 GPa and Poisson's ratio is about 1/3. The range of the coefficient of friction between ice and a structure is between 0.1 for freshly coated surfaces and 0.5 for rusty, rough surfaces. The horizontal force C_H per unit width on the ice sheet can be calculated as:

$$C_H = C_v \tan(\alpha + \arctan \mu)$$

The total force H per unit width generated during the ice structure interaction, to break the ice sheet at a distance away from the contact zone and to push the broken ice block along the sloping surface is given as:

$$H = C_H + T \cos \alpha$$

6.1.3 National Research Council of Canada (NRC-Canada)

The NRC-Canada standard (1967) gives instructions for determining ice loads on river structures. In this standard, guidelines are available to calculate the dynamic ice loads from impact of individual floating ice floes, dynamic ice loads resulting from ice jams, static ice loads due to thermal expansion of a continuous ice cover sheet, static ice load from an ice field due to the action of wind and current, static ice loads induced by ice frozen fast to the structure during fluctuations in water level, dynamic ice load resulting from the friction of floating ice against the surface of the structure. NRC-Canada recommends calculating only those ice actions that are most probably to occur during the lifetime of structure which depends on the type of structure and ice conditions.

6.1.3.1 The forces of drifting ice floes on piers

The load on a pier P_5 in tons. in a direction along its major axis resulting from a collision with a drifting ice floe is determined by the formula:

$$P_5 = j v_i h \sqrt{\Omega R_p m \tan \varepsilon}$$

Where:

P_5 = load on pie in a direction along its major axis resulting from a collision with a drifting ice floe [$tones$],

j = coefficient depends on the obstacle ice floe encounter [$sec.T/m^2$], for a pier, j = 0.43; for a wall, j = 0.7,

v_i = calculated velocity of a drifting ice floe, depending on wind velocity, v_i = 0.02 w to 0.6 [m/sec], and

w = wind velocity calculated based on metrological data [m/sec].

The calculated wind velocity w is based on meteorological data and when these are deficient it is determined from the area of the ice flow Ω using Table B-1 from Appendix B. Ω = calculated area of an ice floe in m^2, taken from the field observations; the calculated area of ice floe should not be less than the minimum area Ω_{min}, which is equal to 1.75 i^2; i = greatest span of the bridge between piers or the size of the ice discharge opening [m].

6.1.3.2 Thermal ice forces.

The ice load P_T, in T/m, per unit of length of contact between the ice and a structure resulting from thermal expansion of the ice cover is determined by the formula:

$$P_T = (R_0 h + 2\alpha h \vartheta \mu \varphi)s$$

Where:

P_T = static load per unit of length of contact between the ice and a structure resulting from thermal expansion of the ice cover [T/m],

R_0 = The elastic limit of ice = 5 T/m^2,

h = thickness of ice cover in meters which equals to the maximum ice thickness with a probability of 1% of being exceeded,

α = coefficient of linear expansion of ice = 5.5×10^{-5} 1/℃, and

ϑ = rate of increase in air temperature in degrees per hour during a time period of τ in hours.

During regular observations carried out four times a day, ϑ is equal to the highest value for any six-hour period of the day; μ = coefficient of ice viscosity [$T.\frac{h}{m^2}$], for $t \geq -20$ ℃; $\mu = (3.3 - 0.28t + 0.083t^2) \times 10^4$, for $t < -20$℃; $\mu = (3.3 - 1.85t) \times 10^4$; t = ice temperature in ℃, $t = \theta\eta_0 + {}^{\vartheta\tau}/_2\,\psi$; θ = initial air temperature from which the temperature begins to increase

[°C]; η_0 = The relative thickness of ice cover by considering the influence of snow; $\eta_0 = h/h_\pi = h/\left(h + h_c\sqrt{a/a_c} + \lambda/a_b\right)$; h_π = reduced thickness of ice cover; h_c = least thickness of ice cover corresponding to the period of calculation, determined by direct observations of ice cover for the given section of the river [m]; a = thermal diffusivity of ice, equal to 0.0041 m^2/hr; a_c = thermal diffusivity of snow, equal to 0.002 m^2/hr; λ = thermal conductivity of ice, equal to 2 $kcal/(m.hr.degree)$; a_b = coefficient of heat transfer from air to the snow-ice surface [$^{kcal}/_{(m^2.hr)}$], in the presence of snow; $a_b = 20\sqrt{w + 0.3}$, in the absence of snow; $a_b = 5\sqrt{w + 0.3}$; w = mean peak velocity of wind corresponding to the period of the largest calculated value of increase of air temperature ϑ [m/sec]; ψ, ϕ = coefficient of whose values are determined Figures C-1 and C-2 respectively from Appendix C, ψ, ϕ = depend on the value of $C = \alpha\tau/h_\pi^2$ and $\eta_0 = h/h_\pi$; and s = coefficient depending on the extent of ice cover, determined from Table B-2 in Appendix B.

The static load P_o in tons for the bridge piers can be determined using the following equation:

$$P_O = \left(1 + \frac{l}{3b}\right) bP_T$$

Where:

P_O = static load on a pier when an ice-free area is maintained in the spans between them [$tons$],

l = width of span [m].

b = width of support [m], and

P_T = static load (determined from the above equation).

6.1.3.3 Bridge piers with vertical leading edges

According to NRC-Canada (1973), the Ice force P_1 in tons on a pier in the direction of its longitudinal axis resulting from an ice field moving against the pier is determined by the following formula:

$$P_1 = mAR_p bh$$

Where:

P_1 = load in tons

m = coefficient for the shape of the pier; for a semi-circular leading edge, m = 0.9 for a triangular edge of a pier, m depends on the apex angle (2ε), refer to Table B-3 in Appendix B,

A = climatic coefficient is taken from Table B-4 in Appendix B,

R_p = crushing strength of ice; In the absence of experimental data, R_p = 75 T/m^2 at the time of the maximum water level at the breakup, R_p = 45 T/m^2,

b = width of the bridge pier at the water level occurring at breakup [m], and

h = calculated thickness of ice, 0.8 of the thickest ice during the winter with a probability of 1% of being exceeded [m].

6.1.3.4 Bridge piers with sloping leading edges

The horizontal component of the ice load P_2 in tons acting on a pier in the direction of its axis is calculated by the following formula:

$$P_{2H} = AR_i h^2 \tan\beta$$

Where:

P_{2H} = The horizontal component of the ice load acting on a pier in the direction of its axis [ton],

R_i = 0.5R_p = failure strength of ice in bending in [T/m^2], and

β = angle between the cutting edge of the pier and the horizontal [deg],

The vertical component P_{2V} in tons is determined by the following formula:

$$P_{2V} = \frac{P_{2H}}{\tan\beta}$$

Where:

P_{2V} = The vertical component of the ice load [$tons$].

6.2 Results of ice actions

6.2.1 Ice loads on vertical bridge piers

Figure 6-9 shows the ice actions on the Beitstadsundet bridge pier according to ISO19906. Even though there are many other failure mechanisms that could take place across vertical structural elements under ice actions, crushing failure mechanism is the most susceptible to occur. The bridge pier was considered vertical and the ice loads were calculated for the limit force and the limit stress mechanisms. The drag forces due to wind and current were calculated based on the annual maximal values for wind and current speeds over the past 50 years. The current speeds are very low that the drag forces are mainly due to wind speeds.

The ice loads due to the thermal expansion were calculated by assuming the values for the temperature and the ice cover thickness (-20 ℃ and 0.5 m, respectively). The rate of temperature increase was assumed 1 ℃/hour. From Figure 6-4, the thermal ice pressure was found 120 kN/m. Considering the width of the structure (4.5 m), the thermal force was calculated (0.54 MN). From Figure 6-9, it is obvious that the limit force is ranging from 0.622 to 1.012 MN, with an average value of 0.767 MN. Also, the limit stress is ranging from 2.195 to 4.466 MN, with an average value of 3.322 MN. Therefore, based on the calculated values for the limit force and the limit stress over the past 50 years, it can be concluded that the limit force is governing as the ice actions on the bridge pier.

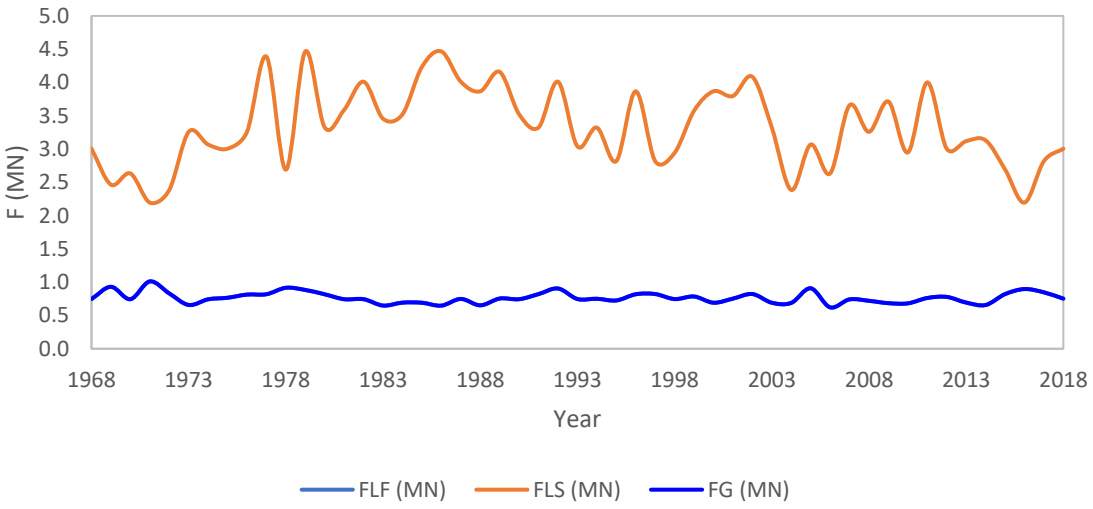

Figure 6-9 Annual maximum ice actions on vertical structures based on ISO19906

Figure 6-10 shows the ice actions on the Beitstadsundet bridge pier according to AASHTO. The ice loads were calculated for the limit force and the limit stress mechanisms. The drag forces due to the wind and current speeds over the past 50 years were calculated based on the fetch area which was considered the same as the ice floe area. Therefore, the values of the limit force are equal for both ISO19906 and AASHTO. The current speed is very low that the drag forces are mainly due to wind speed. Also, the ice loads due to the thermal expansion were calculated by using the same approach in ISO19906 (0.54 MN). From the figure, it can be observed that the limit force is ranging from 0.622 to 1.012 MN, with an average value of 0.767 MN, whereas the limit stress is ranging up to 9.094 MN, with an average value of 5.317 MN.

Therefore, based on the calculated values for the limit force and the limit stress over the past 50 years, it can be concluded that the limit force is governing as the ice actions on the bridge pier almost in all the years. Moreover, the limit stress has dropped to very low values is 2016. The reason behind this drop is that the average winterly temperature has been increasing due to global warming and the ice cover thickness is decreasing. Consequently, the compressive strength of ice is decreasing along with the ice actions due to the limit stress. It can also be observed that the expression given in the AASHTO is very sensitive to the ice thickness.

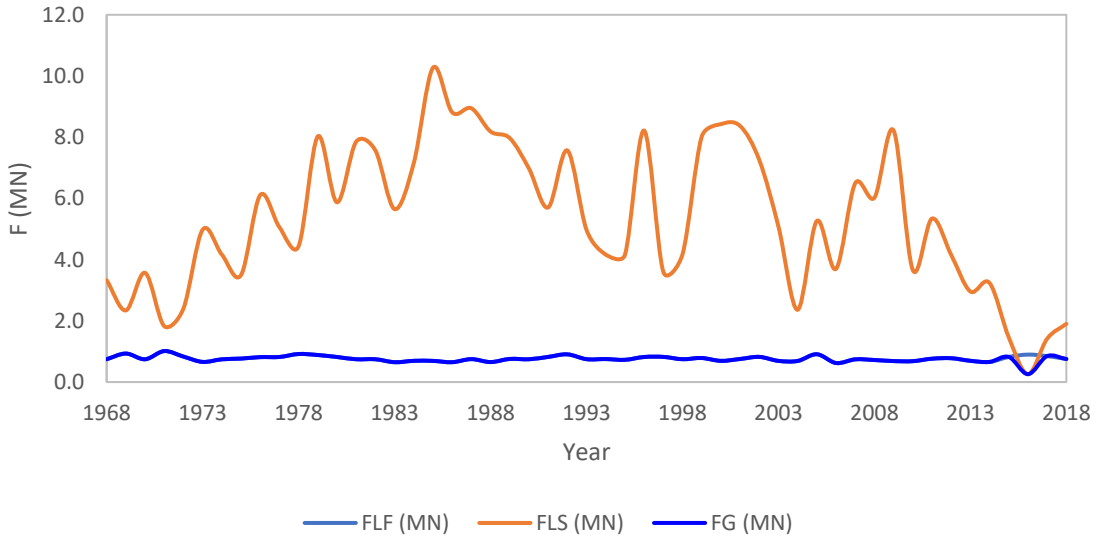

Figure 6-10 Annual maximum ice actions on vertical structures based on AASHTO

Figure 6-11 shows the ice actions on the Beitstadsundet bridge pier according to NRC. The ice loads were calculated for the limit force and the limit stress mechanisms. The limit force was

calculated as the summation of the load due to thermal expansion and the load on the bridge pier resulting from the collision with a drifting ice floe with a speed depending on the wind velocity. The maximum ice cover thickness with a probability of 1% of being exceeded was used in the calculation. The load due to thermal expansion of the ice cover is static per unit of length of contact with the bridge pier. From the figure, the limit force is ranging from 0.158 to 0.405 MN, with an average value of 0.286 MN.

It is found that the limit stress is ranging from 0.125 to 4.339 MN, with an average value of 2.364 MN. Therefore, based on the calculated values for the limit force and the limit stress over the past 50 years also it can be concluded that the limit force is governing as the ice actions on the bridge piers. Furthermore, it can be observed that there is a lot of variations in the ice forces on the bridge pier. This is due to the changes in metrological data and ice conditions which have come as a result of global warming and climate change.

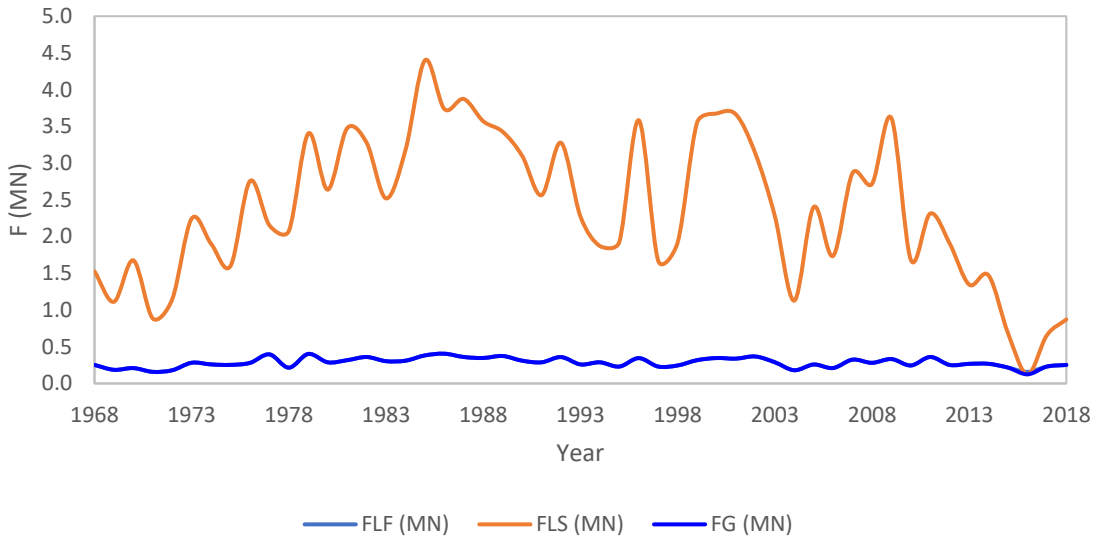

Figure 6-11 Annual maximum ice actions on vertical structures based on NRC

6.2.2 Ice loads on sloping bridge piers

Figure 6-12 shows the ice actions on the Beitstadsundet sloping bridge pier according to ISO19906. Even though there are many other failure mechanisms that could take place across

sloping structural elements under ice actions, bending failure mechanism is the most susceptible to occur. According to ISO19906, two types of bending were recognized in sloping structures – upward and downward bending. The weight of ice on an upward slope is replaced by its buoyancy for a downward slope, and an ice block will turn in water before the end of the downward slope and thus HT may be completely neglected. In this case study, ice has been assumed to fail in upward bending against the sloping structure. The ice loads were calculated in five different ice force components – breaking, pushing up the slope, turning, pushing through the rubble and lifting. These forces were calculated based on the maximum winterly ice cover thicknesses over the past 50 years. HB was found ranging from 0.019 to 0.329 MN, with an average value of 0.144 MN, whereas HT is ranging from 0.006 to 0.036 MN, with an average value of 0.019 MN. Also, HR was calculated and found ranging from 0.092 to 0.235 MN, with an average value of 0.167 MN, while HP and HT are zeros; because the ice rubble angle and the cone angle were assumed equal to 45°. Moreover, the influence of these two parameters on the total horizontal and vertical ice forces was checked in the sensitivity analysis (refer to section 6.4).

Consequently, the total horizontal ice force was found ranging from 0.125 to 0.534 MN, with an average value of 0.356 MN, whereas the total vertical ice force was ranging from 0.038 to 0.195 MN, with an average value of 0.109 MN. Therefore, based on the calculated values for the limit force and the total horizontal ice force over the past 50 years, it can be concluded that the limit stress due to bending failure is governing as the ice actions on the bridge pier.

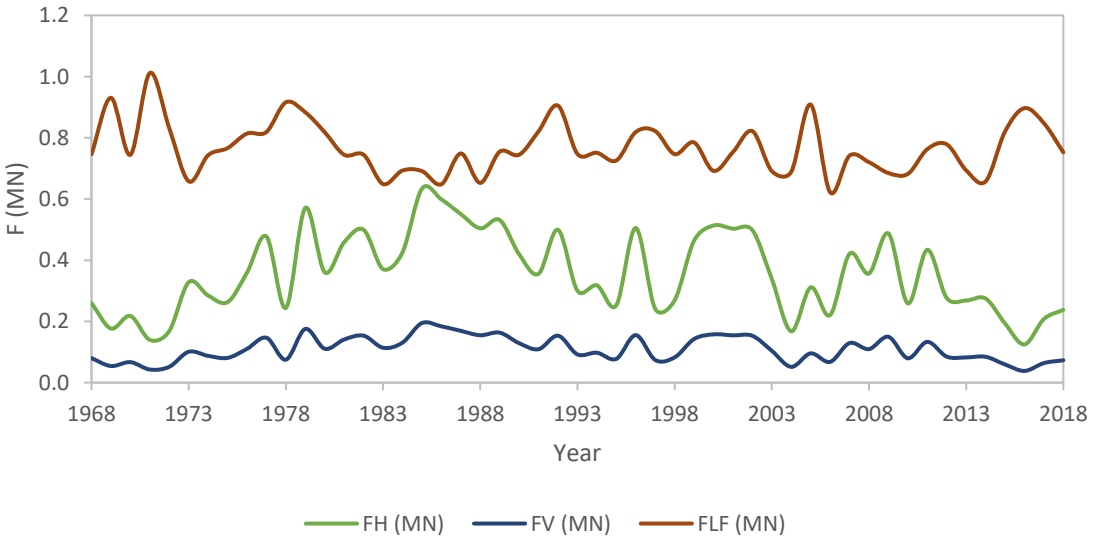

Figure 6-12 Annual maximum ice actions on sloping structures based on ISO19906

Figure 6-13 shows the ice actions on the Beitstadsundet sloping bridge pier according to AASHTO. The ice loads in the vertical direction have been calculated mainly based on the flexural strength of ice and the weight of the ice rubble accumulating on the slope of the structure. Then, the ice loads in the horizontal direction were calculated from the vertical ice loads, considering the cone angle, as described in section 6.1.2. Therefore, the ice loads were calculated in two different ice force components – horizontal and vertical directions. Consequently, the total horizontal ice force was found ranging from 0.131 to 0.682 MN, with an average value of 0.433 MN, whereas the total vertical ice force was ranging from 0.053 to 0.138 MN, with an average value of 0.097 MN.

Based on the calculated values for the limit force and the total horizontal ice force over the past 50 years, it can be concluded that in most of the years the limit stress due to bending failure is governing as the ice actions on the bridge pier. In the year 1986, the limit force was governing with a value less than the horizontal ice force (0.648 and 0.668 MN, respectively). The reason behind this is that ice cover thickness (i.e., 0.56 m) was maximum and the annual maximal wind speed at 10-m height was much lower than the average value over the past 50 years (i.e., 15.6 and 23.3 m/s, respectively).

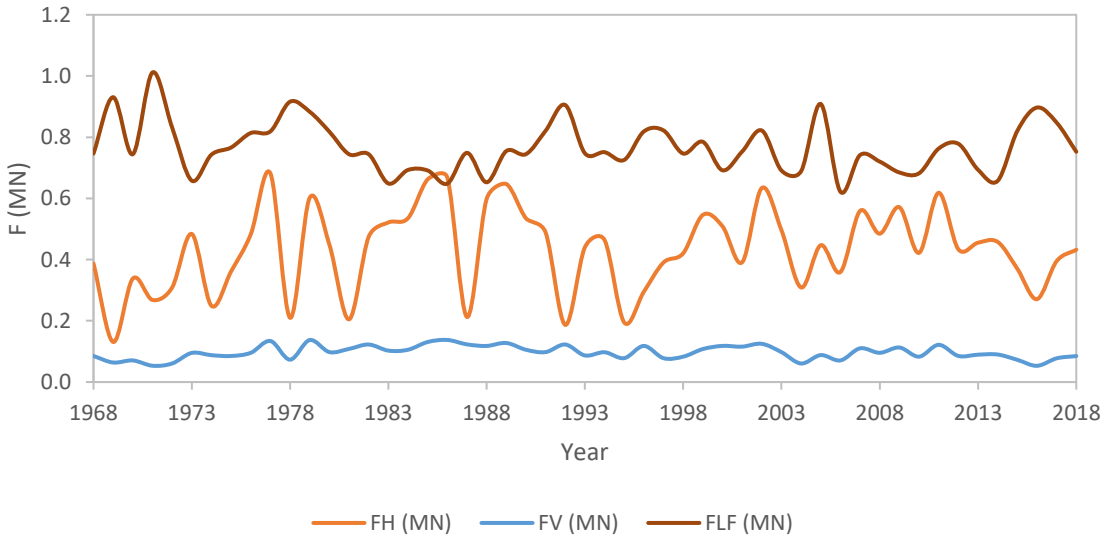

Figure 6-13 Annual maximum ice actions on sloping structures based on AASHTO

Figure 6-14 shows the ice actions on the Beitstadsundet sloping bridge pier according to NRC-Canada. The ice loads in the horizontal direction have been calculated mainly based on the ice

cover thickness and the flexural strength of ice. Then, the ice loads in the vertical direction were calculated from the horizontal ice loads, considering the cone angle, as described in section 6.1.3. Therefore, the ice loads were calculated in two different ice force components – horizontal and vertical directions. Consequently, the total ice force was found equal in both horizontal and vertical directions, because the cone angle has been assumed 45°. Hence, the total ice force is equal in both directions and ranging from 0.004 to 0.366 MN, with an average value of 0.159 MN. The limit force has been evaluated considering the compressive strength of the ice, the maximal annual ice cover thickness and the wind speed at 10-m height. Also, the ice loads due to thermal expansion were calculated mainly based on the ice thickness, the wind speed, hourly change in temperature and climatic coefficients.

Based on the calculated values for the limit force and the total horizontal ice force over the past 50 years, it can be concluded that the limit stress due to bending failure is governing; because the limit force was extremely higher than the limit stress since the Canadian standard includes a number of multipliers, e.g., empirical climatic and shape coefficients. From the figure, the limit force had increased in the year 1977 and then dropped after the year 2012. This reason behind this drop is the increased average winterly temperature and the decreased annual maximal ice thickness due to climate change and global warming.

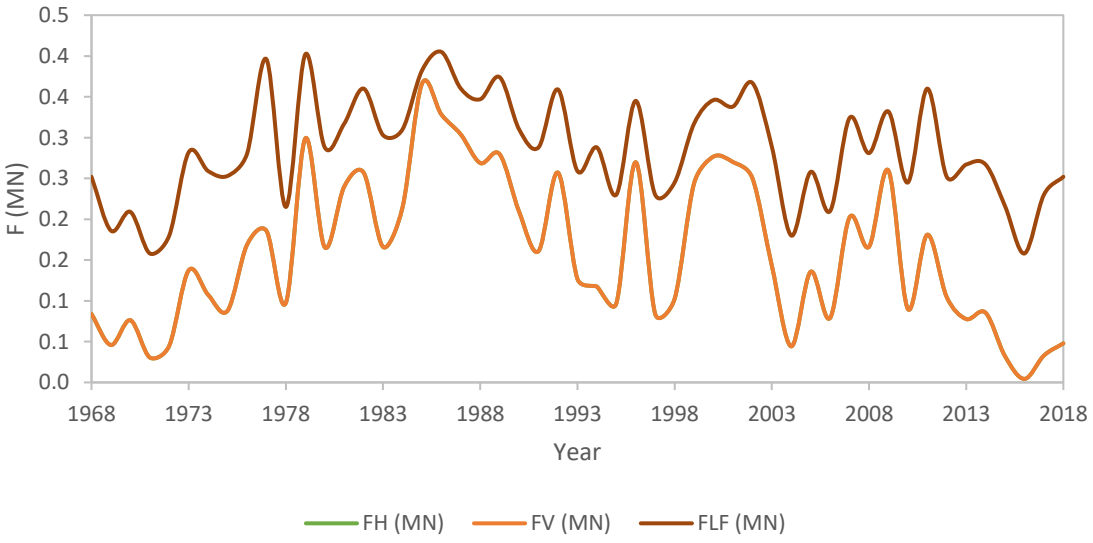

Figure 6-14 Annual maximum ice actions on sloping structures based on NRC-Canada – FH is equal to FV

6.2.3 Comparison of ice loads among different standards

6.2.3.1 Comparison of ice loads on vertical structures

Figure 6-15 shows the limit stress and the limit force for vertical structures according to ISO19906, AASHTO, and NRC-Canada. From the figure, it can be observed that AASHTO gives significantly higher values for the limit stress when compared to the other two standards, whereas NRC-Canada gives the lowest among the three standards; because the formula for the limit stress according to NRC-Canada includes empirical factors of reduction that are related to the climate and the shape of structure (25 and 10% reduction, respectively). In addition to that, AASHTO has mentioned that their formula gives conservative values for the limit stress and thus given reduction factors for small streams, but there is no guidance on the use of reduction factors for fjords. Therefore, no reduction factors have been used for AASHTO in this case study. After the year 2015, ice actions due to the limit stress dropped due to that fact that the ice cover thickness decreased below the average ice thickness over the past 50 years (0.22 and 0.4 m, respectively).

It can also be seen that NRC-Canada gives the lowest values for the limit force when compared to the other two standards, whereas AASHTO has given the same value for the limit force as ISO19906; because of the fact that the fetch area in AASHTO formula was taken equal to the ice floe area in ISO19906 formula. Hence, Figure 6-16 shows the governing ice forces on vertical structures for the three standards, and it is obvious that NRC-Canada gives the lowest estimation of the ice loads on vertical structures. One of the reasons is that the ice force due to thermal expansion was driven from the formula in NRC-Canada was found smaller than what has been driven from the graph in ISO19906 (0.286 and 0.540 MN, respectively for the average value over the past 50 years).

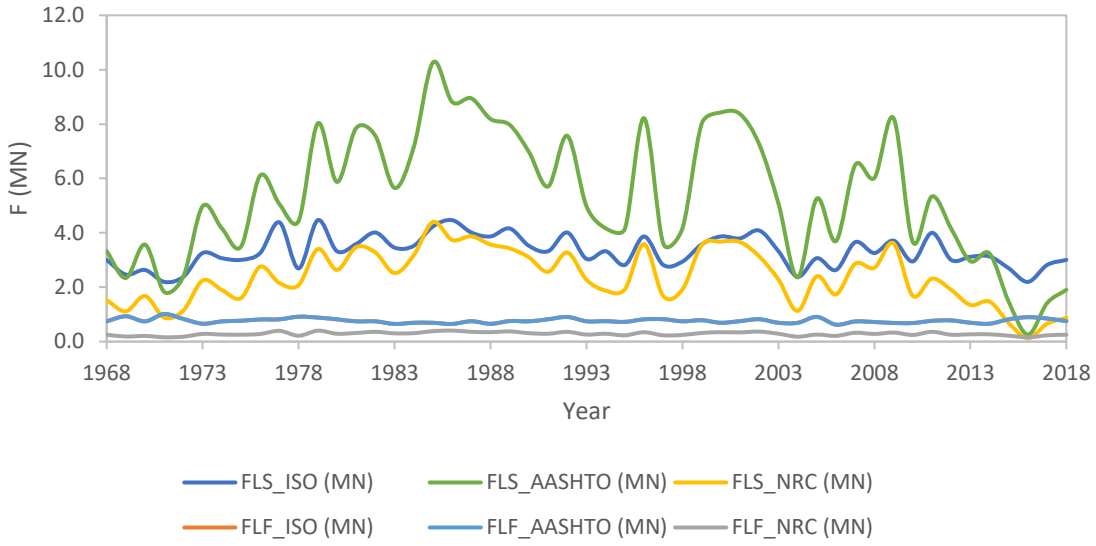

Figure 6-15 Comparison of annual maximum limit stress and limit force for vertical structures among different standards – ISO19906, AASHTO and NRC-Canada

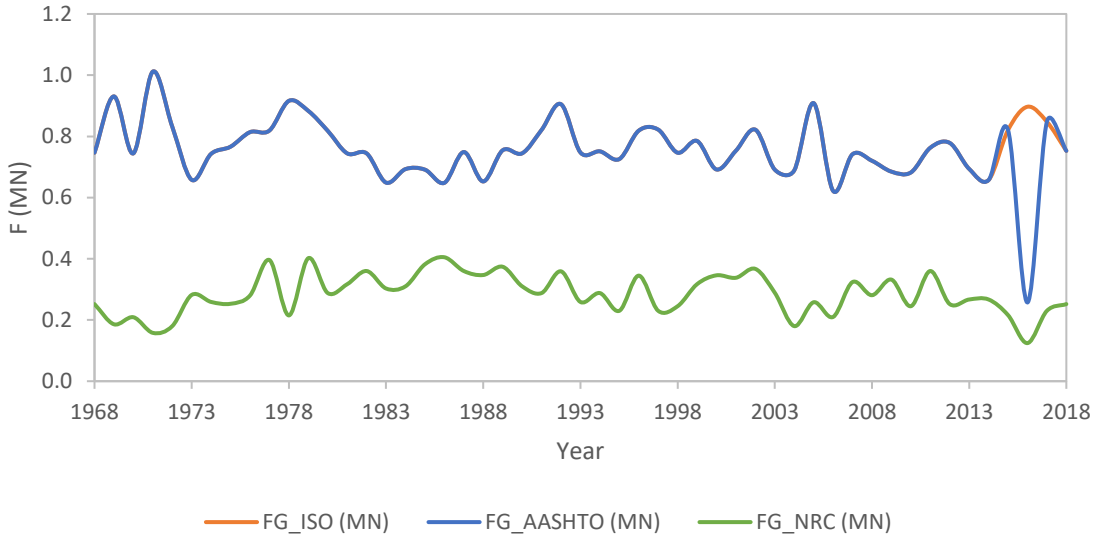

Figure 6-16 Comparison of ice loads on vertical structures among different standards – ISO19906, AASHTO, and NRC-Canada

6.2.3.2 Comparison of ice loads on sloping structures

The limit stress and the limit force for sloping structures have been calculated according to ISO19906, AASHTO, and NRC-Canada and drawn as shown in Figure 6-17. From the figure, it

can be observed that NRC-Canada gives the lowest estimation of the horizontal ice force (0.159 MN) when compared to the other two standards (0.360, 0.430 MN, respectively for ISO19906 and AASHTO); because of the formula for the horizontal ice force implies a climatic coefficient of 25% reduction effect to account for the climate of the region. Moreover, the ice forces calculated according to NRC-Canada are equal in both directions; because of the cone angle of 45°. Furthermore, AASHTO has given values for the ice forces close to that of ISO19906. The reason behind this might be that they both include the same ice and structural parameters even though the formulae are different.

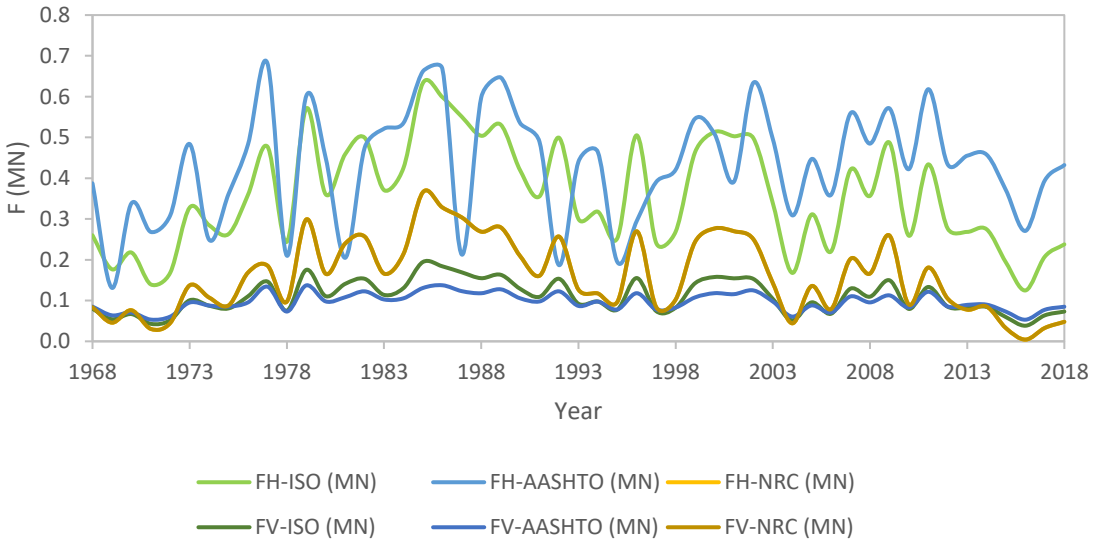

Figure 6-17 Comparison of annual maximum ice loads on sloping structures among different standards

6.3 Loads due to ice jams

Montgomery et al. (1984) studied ice forces due to jamming. A breakup ice jam is considered a cohesionless collection of ice floes that exchange ice loads to a bridge pier as a granular mass slightly confined by the buoyancy. For a wide bridge pier in respect to accumulating thickness, the action imposed on the bridge pier could be determined by the multiplication of the confining normal stress and the passive pressure coefficient, which strongly depends on the internal angle of friction of the ice rubble.

Ice jams can damage the bridge pier and the deck when the water level in the fjord is sufficiently high to get the ice rubble contact with the superstructure. After that Ice is broken and away by the ice and water. Well-known instances of superstructure damage are the Honeymoon bridge over the Niagara River (1936) and the Perth-Andover bridge over the Saint John River (1987). An indirect impact of ice jamming is the scour around bridge piers that can result from high current velocities that accompany ice-jam releases. Various bridges are known to have been damaged or demolished because of ice-jam related scour (Beltaos et al. 2003).

An inquiry that frequently emerges in bridge design is whether a bridge can initiate ice jamming due to the obstacle made by bridge piers and abutments. For example, Kawai et al. (1997) expressed that amid the breakup process, the ice sheet and bride pier interaction might lead to the ice jamming. This is a significant component of the design on the grounds that the formation of another ice-jamming site will have repercussions to adjacent communities and the local environments.

Ice-related issues were a significant thought in the design of the Confederation Bridge, which crosses the Northumberland Strait connecting the Provinces of New Brunswick and Prince Edward Island. As a part of the environmental impact assessment, a detailed modeling program was undertaken to find the effect of the bridge on the ice regime (Brown, 1997). This work concentrated on the potential for ice jamming against the bridge and potential for ice breakup in the Northumberland Strait to be postponed. Brown (1997) expressed that an ice jam could create from an individual ice floe that lodges against adjacent piers or by an accumulation of floes that arch between adjacent bridge piers. The probability of the main kind of ice jam relies on the size distribution of ice floes and the spacing between the piers.

6.3.1 Assessment of ice jamming caused by the bridge pier considering different standards

The initial phase in evaluating whether a bridge can cause ice jamming is to see how breakup ice jams form under the natural conditions. The pertinent processes have been depicted by Beltaos (1997), as follows: rising flows and water levels due to snowmelt, precipitation, or water discharged from storage, enlarge the forces applied on the underside of the ice cover. At first, hinge

cracks form along and close to the banks, permitting the main component of the ice sheet to rise with the water level. The gravity action and flow under the ice subjects the ice cover to bending moments and flexure in the horizontal plane, which inevitably leads to transverse splitting and development of a series of separate ice sheets. The main continued movement of the ice at a site is known as the beginning of ice breakup at that site. Now, when ice sheets are set in motion, they impact other ice sheets and break down into little fragments that are transported downstream. If the broken-ice floes interact with stationary ice sheet or a channel feature that delays the ice movement, at that point, an ice jam is started (Beltaos et al. 2003).

The bridge piers constructed over the fjord can locally impede the beginning of ice breakup by holding ice sheet that would have generally been set in motion. The restrained ice cover would thus act as a jam initiator. This idea can be visualized by contrasting ice-driving forces with bridge generated resistance forces (crushing, bending) at the time when the water level in the fjord is equal to that which would have initiated breakup under natural conditions, i.e. in the absence of the bridge. This concept would be able to express that ice jamming would happen if the total ice driving force, FD, were less than the total force resisting ice movement, FR.

$$FD \leq FR \Rightarrow ice\ jamming$$

However, the bridge piers will hold back the upstream ice beyond the naturally occurring breakup beginning stage, until the ice driving forces increase to the point that FD just surpasses FR. On the other hand, if FD is above FR, it may be presumed that the bridge piers won't impede the movement of the ice cover. The bridge won't cause ice jamming on the grounds that the ice cover will most likely to move once the required stage is reached, even with the bridge piers (Beltaos et al. 2003).

According to Dutch standard, ice jams can form near piers, bends, and constrictions in a river. The initiation and growth of ice jams is also determined by the Froude number F_r:

$$F_r = \frac{v}{\sqrt{gh}}$$

Where:

g = acceleration of gravity $[m/s^2]$

h = water depth $[m]$

v = flow velocity $[m/s]$

From Froude number, it can be determined the initiation and growth of ice jams where:

- $F_r < 0.07$: ice accumulates at the upstream end, growing in the horizontal plane.
- $0.07 < F_r < 0.09$: the ice cover has the tendency to become thicker, growing in the vertical direction.
- $F_r > 0.09$: incoming ice is carried under the surface ice and attaches itself the closest place at which the shear stress against the ice cover is below a critical value. When the accumulated ice has constricted the cross section the velocity increases and the ice will be carried further (CRESS Coastal and River Engineering Support System)

In ISO19906, the ice jamming is included in the form of a factor k_j in the global ice action on a multi-leg structure which is obtained by first determining the global ice action FG on one leg of the structure (for example using the equations for ice crushing) and then multiplying this load by a set of empirical factors for non-simultaneous failure, sheltering & jamming. According to ISO, the ice jamming factor will only be considered when $L/w < 4$; here, L is the clear distance between the legs or piers. In the case of the Beitstadsundet the bridge span length; $L = 112\ m$ and width or diameter of the pier; $w = 4.5\ m$ which gives $L/w = 24.89\ m$. It is clear from the calculations that the ice jamming will not have an effect.

6.3.2 Approach to find the occurrence of ice jamming at Beitstad

The potential of the bridge to initiate the ice jams can be examined by means of the approach as FD ≤ FR ⇒ ice jamming. In this whole process, the first step is to determine the relevant reach-average hydraulic parameters at a typical onset-of-breakup stage with the help of using the local bathymetric data. There are five piers in the fjord, each having a diameter of about 4.5 m at the breakup level. By using the Canadian bridge code (CSA, 1988) the driving and resisting forces can be determined. From the results of design ice action, the driving forces due to the wind and tidal current against the bridge are much lower than the resisting forces i.e. crushing so, there might be a chance of ice jamming at the Beitstadsundet. It must be kept in mind, however, that the above analysis is not complete and only given here as an illustration. The variation of the quantities i.e. the diameter of floe, current and wind velocity can be assessed using a more elaborate approach

that would consider changes in fjord's cross-sectional geometry, and slope. Moreover, additional calculations should be performed for the calculation of ice velocity, flow shear stress, and freeze-up levels, to examine their effects on the ratio FD/FR.

Secondly, Near the Beitstadsundet the flow of water is only due to tidal current which has a design value of $Vc{\sim}0.12\ m/s$ and average water depth near the upstream side of the bridge is approximately 20 m which gives Froud number 0.008 which comes in category 1 (as described above); which means ice accumulates at the upstream end, growing in the horizontal plane.

6.3.3 Loads resulting from the ice jamming

The Canadian and American standard contains the information about the ice jam load calculation, but ISO and Dutch standard do not have any information regarding the load exerted on the bridge due to an ice jam.

According to Canadian standard, the load Pz, in tons, against a structure during the accumulation of ice (perpendicular to the ice front) is determined by the formula;

$$P_z = \xi\ L_z(p_1 + p_2 + p_3 + p_4)$$

Where:

P_1 = the force caused by current drag on the lower surface of the ice field per unit area $[T/m^2]$,

P_2 = the force of hydrodynamic pressure on the edge of the ice field caused by flow, per unit edge surface area $[T/m^2]$,

P_3 = the horizontal component of the force of gravity on the ice field where there is a slope of the free flow surface, per unit surface area of the ice field $[T/m^2]$,

P_4 = the force resulting from the air drag against the upper surface of the ice field, per unit surface area $[T/m^2]$, and

L_z = the length of the ice jam from which pressure is transmitted against the structure, taken to be 1 time the width of the river at the structure $[m]$.

The values of P_1 P_2, P_3, P_4 in T/m^2 are taken to be:

$$P_1 = k_1 v^2$$

$$P_2 = k_2 h/L\ v^2$$

$$P_3 = k_3 hi$$

$$P_4 = k_4\ w^2$$

Where:

k_1 = a coefficient having the dimensions of $T.s^2/m^4$ and taken to be 5×10^{-4} for a continuous ice field and 20×10^{-4} for ice jams,

k_2 = coefficient having the dimension of $T.s^2/m^4$ and taken to be 5×10^{-2},

k_3 = coefficient having the dimension of T/m^3 taken to be 0.92,

k_4 = coefficient having the dimension of $T.s^2/m^4$ and taken to be 2×10^{-6},

v = flow rate of water under the ice in m/s during the periods of ice accumulation its design value is 0.12 m/s,

w = velocity of wind in m/sec during the period of breakup and design value is 38 m/s,

h = thickness of an ice field in meters, its design value is 0.63 m,

L = mean length of ice field in the direction of the flow taken from field observations but not to exceed three times the width, in meters which equal to 870 m,

i = water surface slope, which is very mild and taken to be 0.0002, and

ξ = coefficient of lateral pressure taken from Table B-5 in Appendix B.

The load exerted by an ice jam on a unit length of structure parallel to the direction of flow is equal to 0.081575 MN. The value is not that much high as compared to the other loads as current velocity is very low and the only considerable driving force is due to the wind speed.

According to ISO19906, the global action on a multi-leg structure can be found as:

$$F_s = k_s\ k_j\ k_n\ F_G$$

Where:

F_G = the global average pressure, for crushing.

k_s = interference and sheltering factor ranges from 3.0 to 3.5

k_n = The factor for the effect of non-simultaneous failure, in absence of test data generally assumed 0.9, and

k_j = ice jamming factor; for $L/w < 4$: $k_j = 1.0$ to 2.0 and $L/w \geq 4$: $k_j = 1$

As there will be no ice jamming the value of the jamming factor can be considered one. The design global action due to ice in this by putting global ice action due to crushing equal to 1.34 MN, and by taking k_s = 3.3, $k_n = 0.9$, and k_j = 1, the resulting load for the multi-leg structure equal to 3.9798 MN.

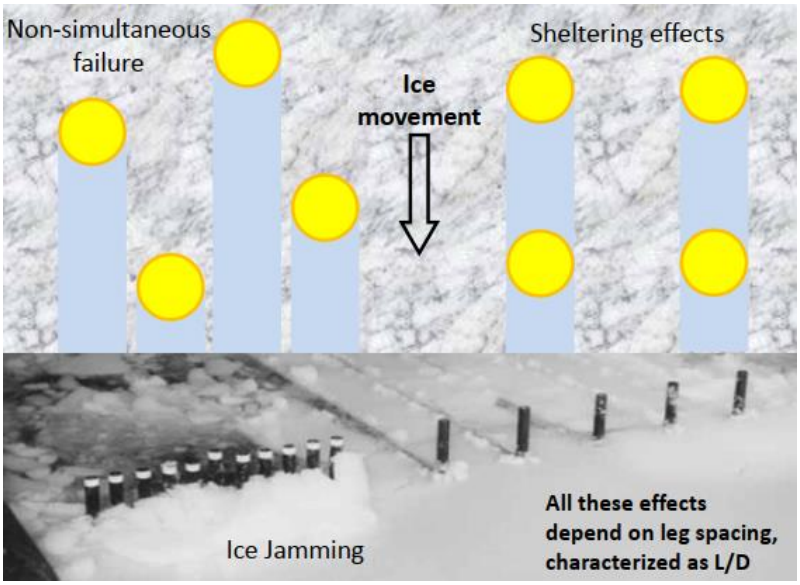

Figure 6-18 Ice jamming effects (Reference: Compendium OE44115 by Hoving, 2018)

6.3.4 Possibility of Modelling Ice jamming in HEC-RAS

HEC-RAS has the capability in modeling the ice-covered channels, with known ice properties, or to simulate wide-stream jams (Daly et. al, 1998). For ice modeling in HEC-RAS, there are two approaches the first is to model the ice cover thickness and roughness at each cross-section of the fjord and in the second case, the ice jam thickness is determined at each section by solving the ice-jam force balancing equation. The ice jam can be restricted to the main channel or can incorporate both the main channel and the right and left over banks. At Beitstad the flow is only due to the tidal current, but HEC-RAS does not have any tool to model the tidal discharge so that's why its application here is questionable. The reasonable approach to use this software is to run the model

by considering tidal flow as the uniform steady flow but it will give very conservative results regarding the ice jam thickness and volumes at each upstream and downstream cross-section.

6.4 Sensitivity analysis

Sensitivity analysis is a term used to describe the techniques for testing the model's reaction to the effects of changing a small number of model inputs, often independently of each other (Practical Financial Modelling Third Edition, 2016). The technique is used to determine how independent variable values will impact a dependent variable under a given set of assumptions is defined as a sensitivity analysis. Its usage will depend on one or more input variables within the specific boundaries. It is also known as what-if analysis. It can also be used for any system, including decisions at corporate levels can be done through sensitivity analysis. It helps in analyzing how sensitive the output is, by the changes in one input while keeping the other inputs constant. It works on the simple principle: change the model and observe the behavior (edupristine.com/blog/all-about-sensitivity-analysis).

The aims to measure changes in the system caused by variations in the probabilities of the events. The effects on the top event are evaluated when the probabilities of the basic events change. A sensitivity analysis can answer the following questions:

1) What are the weaknesses of the system of equations?
2) How do variations in the input parameters affect the ice actions?
3) What event is better to invest in to improve the ice actions?

The system of equations is assumed to be sensitive to an event when a variation in the probability of this event leads to the system to vary considerably.

Piecemeal sensitivity analysis shows how the results change when we vary the value of key parameters one-by-one, with central values of all parameters except the one under consideration (sciencedirect.com/topics/economics-econometrics-and-finance/sensitivity-analysis).
For the design of coastal structures in the arctic or subarctic region, the ISO19906 standard is commonly employed by the offshore industry (Sinsabvarodom,2018). The objective of this sensitivity analysis is to explore the stochasticity of the ice actions input parameters related to the ice actions that are acting on sloping and vertical structures based on the ISO19906 standard.

6.4.1 Piecemeal sensitivity analysis: vertical structures

From Figure 6-19, it can be seen that changing the ice thickness and/or the structure width affects only the limit stress, whereas changing the ice floe diameter affects only the limit force through the wind drag component as the current velocity is very low so it can be neglected. Any increase in the ice thickness and/or the structure width will increase the nominal contact area. Therefore, the limit stress due to the ice crushing will increase. The limit stress is governing up to ice thickness of 0.275 m at which both the limit stress and limit force are equal, with the further increase in the ice thickness the limit force will govern. Also, the limit stress is governing up to structure width of 3.60 m at which both the limit stress and limit force are equal, with the further increase in the structure width the limit force will govern.

On the other hand, any increase in the ice floe diameter will increase the ice floe area subject to the drag forces due to wind and current. Therefore, the limit force due to the drag action will increase. The limit force is governing up to ice floe diameter of 0.630 km at which both the limit force and limit stress are equal, with the further increase in the ice floe diameter the limit stress will govern. It is worthy to mention that the expected maximum ice floe diameter is equal to the distance between the left and right over banks of the fjord (that is, 0.580 km).

In further, increasing the air drag coefficient by three times will increase the drag force due to wind with almost the same rate, and thus the limit force will also increase with the same rate. Also, increasing the water drag coefficient by six times will increase the drag force due to current with almost the same rate. However, the limit force will be almost constant; because the current verbosities are very low that can be ignored in the calculation of the limit force.

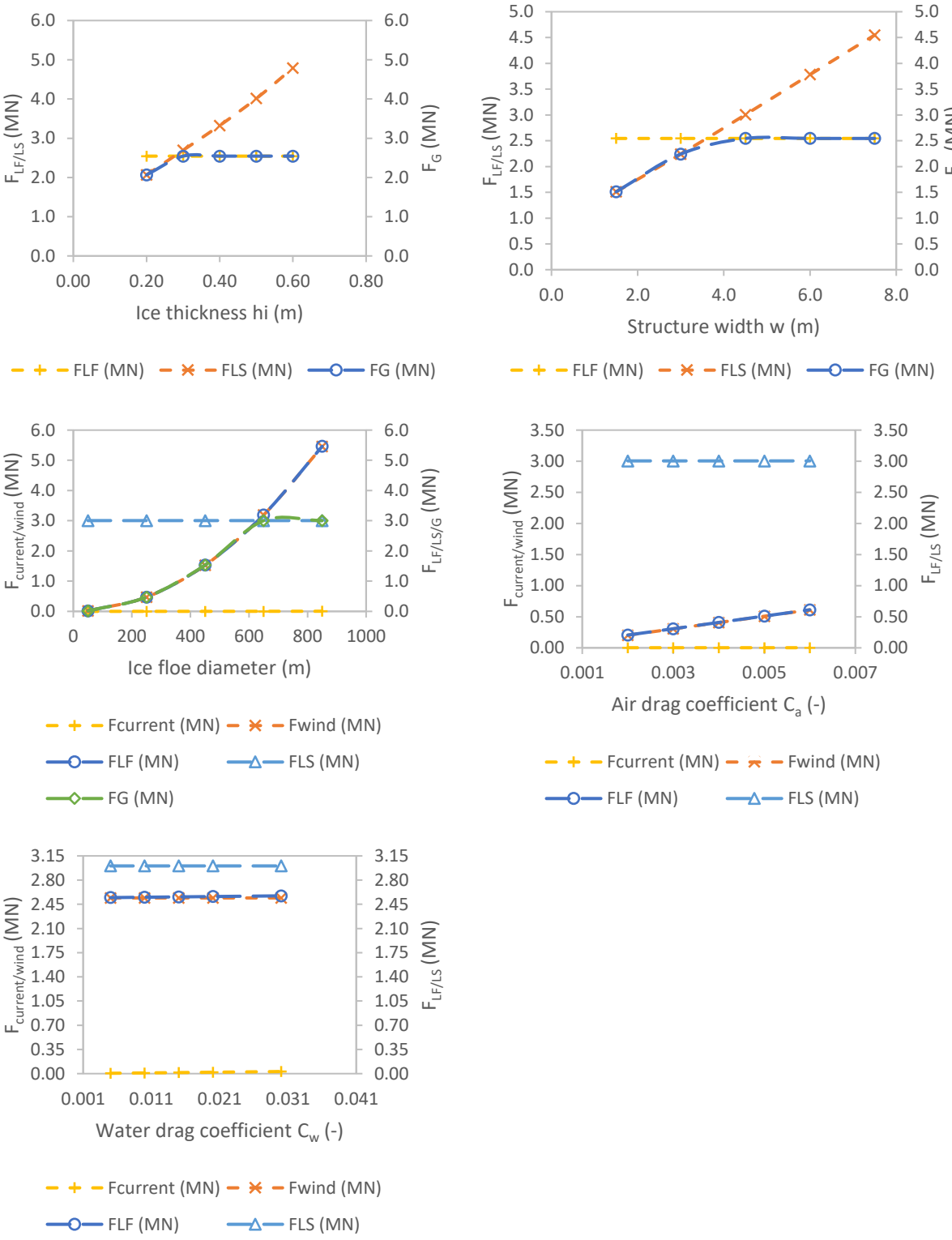

Figure 6-19 From top left to bottom right: (a) effects of changing the ice thickness on the ice actions on vertical structures; (b) effects of changing the structure width on the ice actions on vertical structures; (c) effects of changing the ice floe diameter on the ice actions on vertical

structures; (e) effects of changing air drag coefficient on the ice actions on vertical structures; and (d) effects of changing water drag coefficient on the ice actions on vertical structures

As the limit force scenario is governing in almost all the 50 years, from the graphs, it can be concluded that the wind and current speed, ice floe diameter, wind and water drag coefficients are the parameters most sensitive to the ice actions in case of the vertical bridge pier. It is worthy to mention that the magnitude of tidal current is very low it can also be taken as a constant value or even can be ignored for this case study but here for the deterministic extreme value analysis it is considered as a stochastic variable. These parameters depend on the ice and metreological conditions which are variable and stochastic in nature. Hence, these parameters will be considered as random variables in the probabilistic analysis of the ice loads on vertical structures and type of the distribution will be decided based on the best fit of the available and all the other variables will be considered as deterministic. The parameters that are considered as being deterministic and stochastic based on the sensitivity analysis are shown in Table 7-1.

6.4.2 Piecemeal sensitivity analysis: sloping structures

From Figure 6-20 (a), changing the ice thickness affects only H_B, H_T and H_R. Increasing the ice thickness by two times will increase H_B and H_T noticeably, whereas H_R will increase significantly. Also, the total ice actions on sloping structures will increase significantly in both horizontal and vertical directions.

From Figure 6-20 (b), changing poison's ratio affects only H_B. Increasing poison's ratio by four times will increase H_B exponentially. However, the total ice actions on sloping structures will be almost constant in both horizontal and vertical directions.

From Figure 6-20 (c), by changing the ice-structure friction coefficient affects only H_T and H_R. Increasing the ice-structure friction coefficient by five times will increase H_T slightly, whereas H_R will increase notably. Also, the total ice actions on sloping structures will increase significantly in the horizontal direction but will decrease in the vertical direction.

From Figure 6-20 (d), changing the ice rubble porosity affects only H_P, H_R and H_L. Increasing the ice rubble porosity by four times will cause almost no change in the three force components. Also,

the total ice actions on sloping structures will be almost constant in the horizontal and vertical directions.

From Figure 6-20 (e), changing the ice rubble angle of repose affects only H_P, H_R and H_L. Increasing the ice rubble angle of repose from 20 to 45 degrees will decrease H_L exponentially but the other two force components remain almost constant. Also, the total ice actions on sloping structures will decrease exponentially in the horizontal and vertical directions.

From Figure 6-20 (f), changing the cohesion of ice rubble affects only H_L. Increasing the cohesion of ice rubble four times will increase H_L slightly. Also, the total ice actions on sloping structures will slightly increase in the horizontal and vertical directions.

From Figure 6-20 (g), changing the internal friction angle of ice rubble affects only H_L. Increasing the internal friction angle of ice rubble by two times will cause almost no changes in H_L. Hence, the total ice actions on sloping structures will remain almost constant in the horizontal and vertical directions.

From Figure 6-20 (h), changing the cone angle affects only H_T, H_P H_R and H_L. Increasing the cone angle from 40 to 60 degrees will cause almost no change in H_P and H_T, whereas H_R will increase slightly and H_L increase exponentially. Also, the total ice actions on sloping structures will increase exponentially in the horizontal direction but slightly in the vertical direction.

From Figure 6-20 (i), changing the ice rubble height affects only H_P, H_R and H_L. Increasing the ice rubble height by 2.5 times will cause almost no change in H_P and H_L but a considerable increase in H_R. Also, the total ice actions on sloping structures will increase linearly in the horizontal and vertical directions.

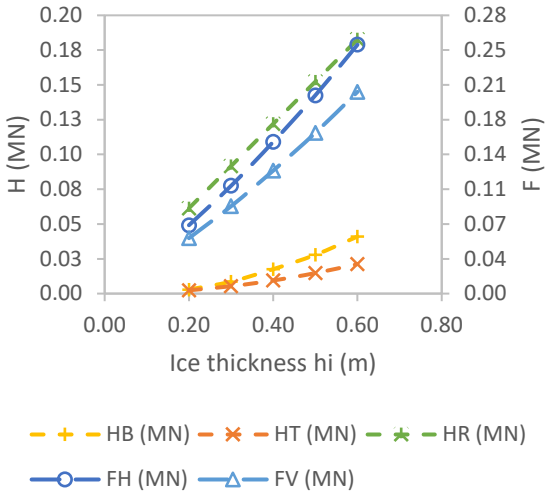
H (MN)
F (MN)
Ice thickness hi (m)
HB (MN)
HT (MN)
HR (MN)
FH (MN)
FV (MN)

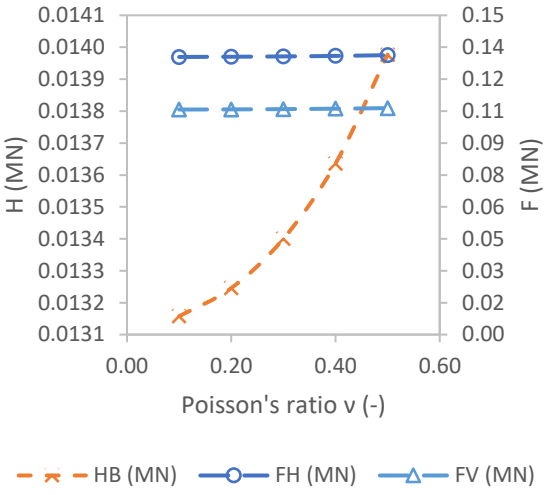
H (MN)
F (MN)
Poisson's ratio ν (-)
HB (MN)
FH (MN)
FV (MN)

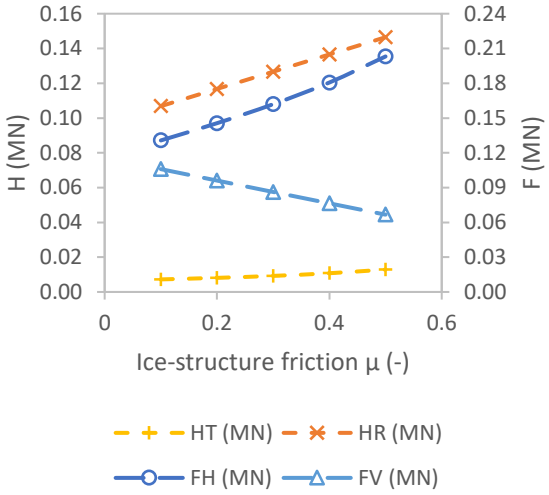
H (MN)
F (MN)
Ice-structure friction μ (-)
HT (MN)
HR (MN)
FH (MN)
FV (MN)

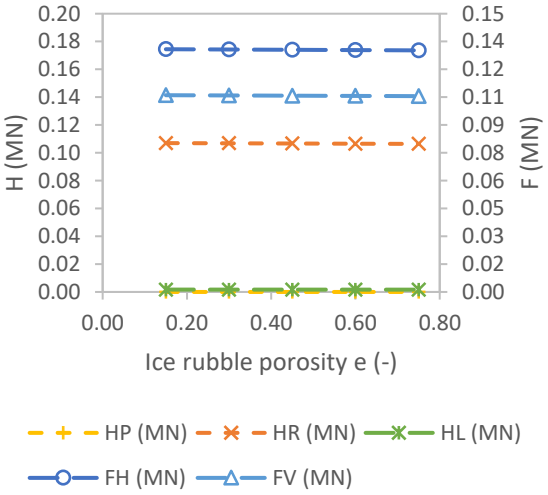
H (MN)
F (MN)
Ice rubble porosity e (-)
HP (MN)
HR (MN)
HL (MN)
FH (MN)
FV (MN)

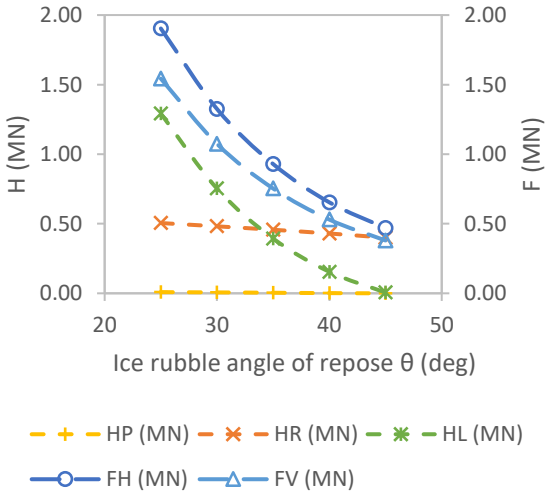
H (MN)
F (MN)
Ice rubble angle of repose θ (deg)
HP (MN)
HR (MN)
HL (MN)
FH (MN)
FV (MN)

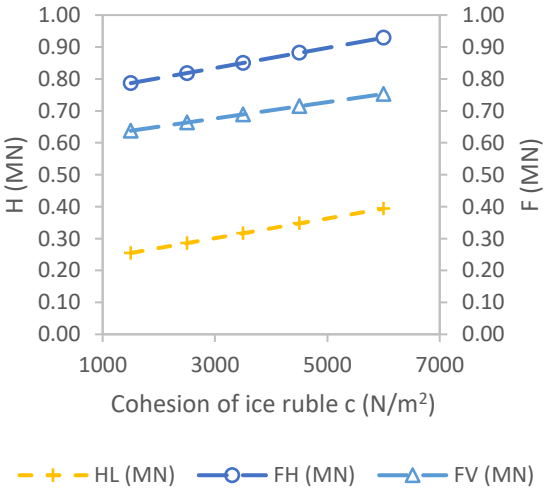
H (MN)
F (MN)
Cohesion of ice ruble c (N/m²)
HL (MN)
FH (MN)
FV (MN)

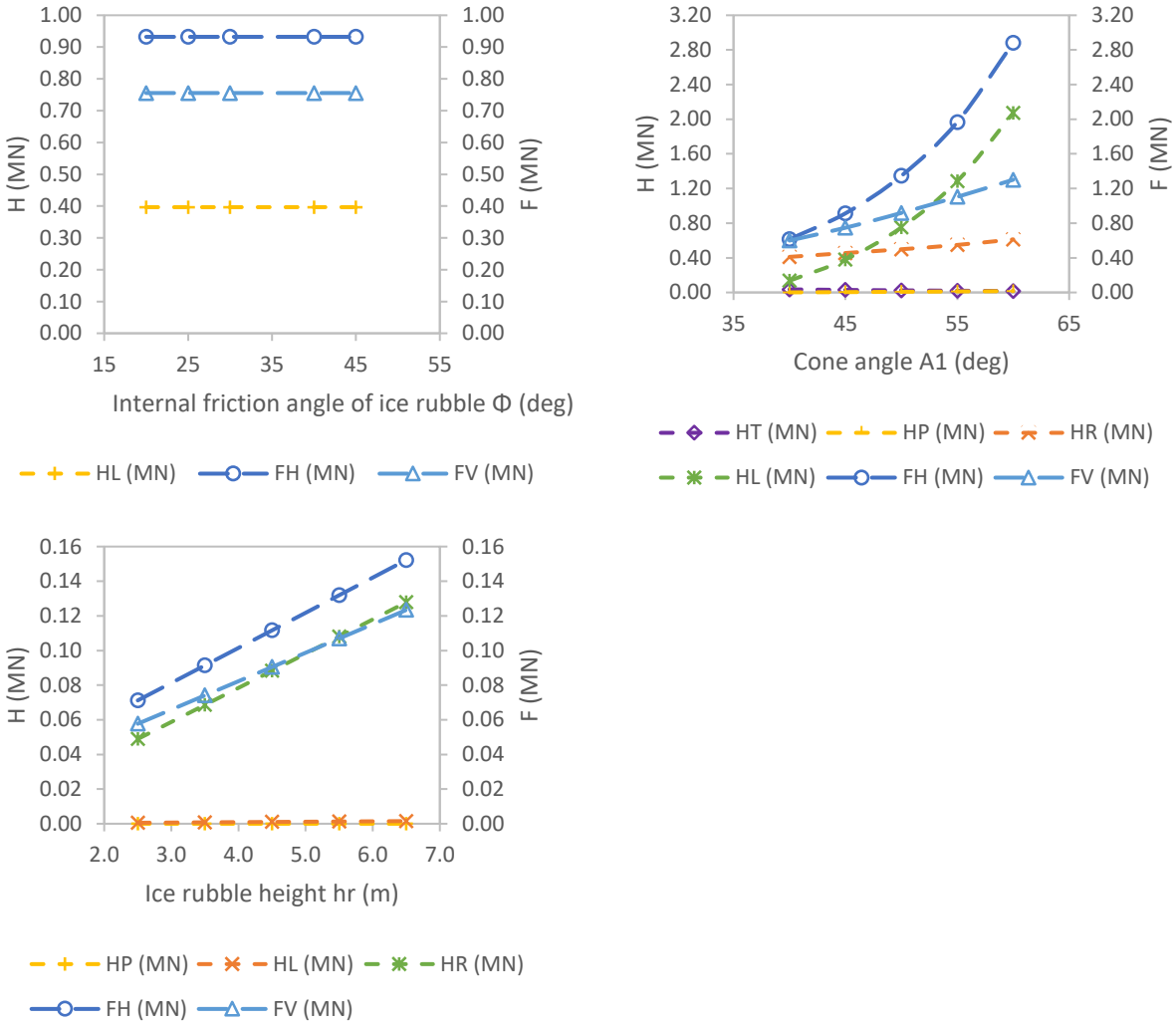

Figure 6-20 From top left to bottom right: (a) effects of changing the ice thickness on the ice actions on sloping structures; (b) effects of changing Poisson's ratio on the ice actions on sloping structures; (c) effects of changing the ice-structure friction coefficient on the ice actions on sloping structures; (d) effects of changing the ice rubble porosity on the ice actions on sloping structures; (e) effects of changing ice rubble angle of repose on the ice actions on sloping structures; (f) effects of changing the ice rubble cohesion on the ice actions on sloping structures; (g) effects of changing internal friction angle of ice rubble on the ice actions on sloping structures; (h) effects of changing the cone angle on the ice actions on sloping structures; and (i) effects of changing the ice rubble height on the ice actions on sloping structures

As the limit stress scenario is governing in almost all the 50 years, from the graphs, it can be concluded that the ice thickness, rubble height, ice-structure friction coefficient are the parameters most sensitive to the ice actions in case of the sloping bridge pier. It is worthy to mention that the cone angle can be taken as a random value but for the deterministic extreme value analysis it is considered as a deterministic variable, to be on the most realistic side. These parameters depend

on the ice and metreological conditions which are variable and stochastic in nature. Hence, these parameters will be considered as random variables in the probabilistic analysis of the ice loads on sloping structures and type of the distribution will be decided based on the best fit of the available and all the other variables will be considered as deterministic. The parameters that are considered as being deterministic and stochastic based on the sensitivity analysis are shown in Table 7-1.

6.5 Pressure-area relationship

In this case study, the bridge pillar has a structure width of 4.5 m, while the ice thickness is ranging from 0.25 m to 0.55 m over the past 50 years. Therefore, the nominal contact area can take any value from 1.125 to 2.475 m^2. Hence, global pressure decreases from 2.27 to 1.88 MPa, as shown in Figure 6-21. The ice forces, the structure width, and the ice thickness are the only consideration, and the results were as per Sanderson's curve (1988) as expected. This means that the pressure-area relationship is still valid in the range of the nominal contact area in this case study. About this concept, the limit stress might be governing at lower nominal contact areas, but this is not related to this case study; because the current velocity is close to zero and can be ignored.

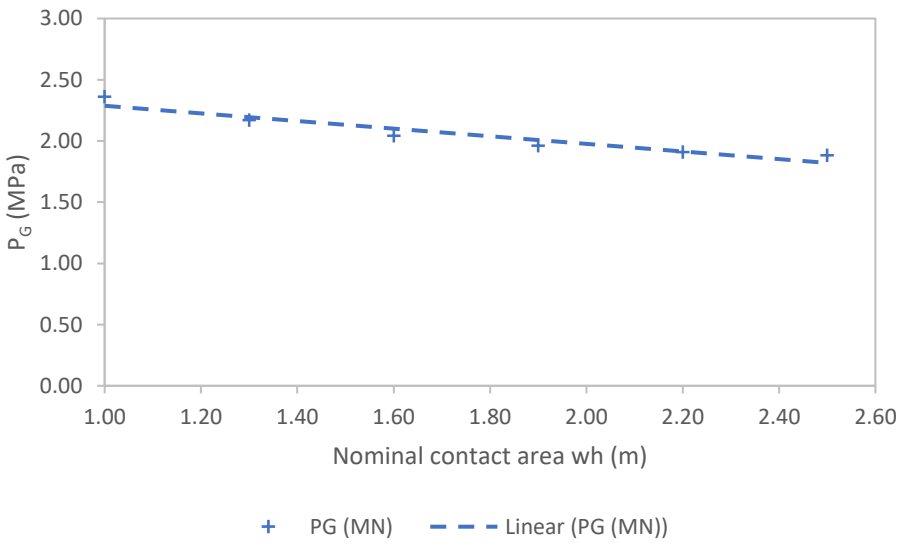

Figure 6-21 Sanderson's curve – the nominal pressure vs. the nominal contact area

Chapter 7

Deterministic Extreme value analysis & probabilistic assessment of Ice loads using Monte Carlo simulations

Probabilistic methods give more in-depth details to explore and a better understanding of the ice input parameters, including the effect of exposure to ice loads, the sensitivity of ice actions to different ice parameters and the assumptions to account for limit stress, driving force, and kinetic energy in a consistent manner (Thijssen, 2014). The properties of the ice parameters are linked with a high degree of uncertainty due to the formation of the ice under the different conditions within different areas. Probabilistic models are frequently introduced in the order to cope with this inherent variability of the sea ice and the associated ice loads. For the design of coastal structures in the arctic or subarctic region, the ISO19906 standard is commonly employed by the offshore industry (Sinsabvarodom,2018). The objective of this research is to explore the uncertainty related to the ice actions that are acting on sloping and vertical structures based on the ISO19906 standard. Moreover, the effect of correlation between the observed ice parameters on the ice forces was determined. Monte-Carlo simulation and Extreme value analysis are applied in order to assess the uncertainty associated with the governing ice action and to calculate the design ice actions during the lifetime of the bridge pier at Beitstadsundet.

7.1 Correlations between the observed parameters over the past 50 years

For the probabilistic assessment of the ice loads correlation between different ice and metrological parameters plays a very important role in the determination of design ice loads. Correlation gives information about the strength of the relationship between two variables that can affect the ice loads. The important correlations between important observed input parameters are given as follows.

7.1.1 Correlation between wind speed and tidal current

Figure 7-1 shows the location of the bridge pier including the global coordinate system projected over the whole bridge structure and the fjord area. From the figure, it can be clearly seen that the wind direction drives the ice floes against the bridge pier when it is blowing to SW. The same holds for the tidal current direction as well. Therefore, we need to know how frequently the wind is blowing to SW over the fjord? And how often the current is driving to SW in the fjord? To answer these two questions data records for each of the wind speeds and directions and the tidal current speed are needed.

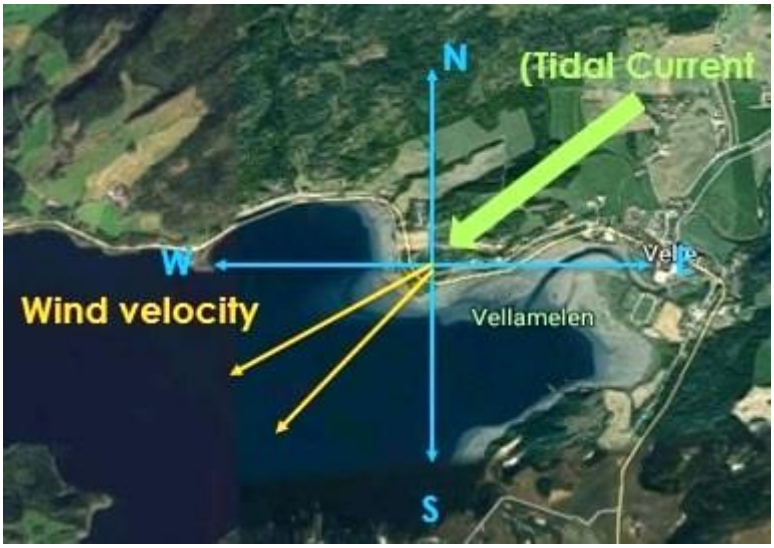

Figure 7-1 Global coordinate system of the bridge pier in the fjord

When the tidal current is flooding, it is driving to SW, moving the ice floes in the fjord against the pier structure. This happens for half the day which means that 50% of the time the current is driving to SW. In terms of the wind direction, it depends on whether considering an absolute wind direction approach or a range wind direction approach. 5% of the time the wind is blowing to SW only while 25% of the time the wind is blowing to any direction between 220 and 250 degrees (or in the direction that makes 225 degrees with the North). It is crucial to stress out the absolute wind direction was chosen depending on the wind rose provided from the internet (refer to Figure 4-28) whereas the range wind direction was chosen depending on the wind data collected online from eklima (refer to Figure 4-25).

The data records of the current speeds and the wind speeds, regardless of the wind directions, were correlated by performing the data analysis in Microsoft Excel. For the data records of the past 50 years, higher satisfaction current speeds were correlated with higher satisfaction wind speeds, $r = 0.11$ (r is referred to as the correlation coefficient) as shown in Figure 7-2, which can be considered a small effect that one can ignore when calculating the probability of having the current speeds and the winds speeds are taking place in the same direction.

If two events have been defined A and B where A is the event that wind is blowing to SW whereas B is the event that the tidal current is driving to SW, then A and B can be assumed independent events. Also, if the years have been assumed identical repetitive units of time, then 25% of the time the wind is blowing to SW. Therefore:

$$P(A|B) = \frac{P(A \cap B)}{P(B)} = \frac{P(A).P(B)}{P(B)}$$

But the correlation between the wind and the tidal current can be ignored; it is also known that the origins of generation for both wind and tidal current are different. Thus, there is no correlation between the two events A and B, and hence the previous formula can be applied as follows:

$$P(A|B) = \frac{P(A \cap B)}{P(B)} = \frac{P(A).P(B)}{P(B)} = \frac{0.25 \times 0.5}{0.5} = 25\%$$

$$P(A|B) = \frac{P(A \cap B)}{P(B)} = \frac{P(A).P(B)}{P(B)} = \frac{0.05 \times 0.5}{0.5} = 5\%$$

Note that the probability that the wind is blowing to SW while the current is driving towards SW is 25% and 5% depending on which base calculation is considered – either data from eklima or wind rose, respectively. Even though the wind and the tidal current could be aligned over 25% of the time, the tidal current velocity is too low that cannot impact the bridge pier that much that needs to be considered. Hence, the drag force due to the tidal current can be ignored in the calculation of the drag force component in the limit force method.

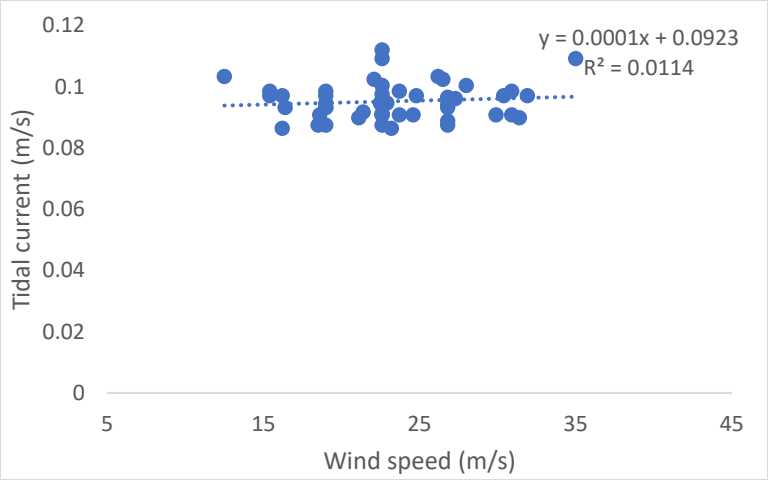

Figure 7-2 Correlation between tidal current and wind speed based on 50 years observed data

7.1.2 Correlation between salinity and tidal current

Figure 7-3 shows the correlation between the salinity and tidal current based on the measured data. It can be seen from the figure that there is a very weak dependency between these variables and correlation coefficient between these two parameters is 0.13 which indicates very weak positive dependency.

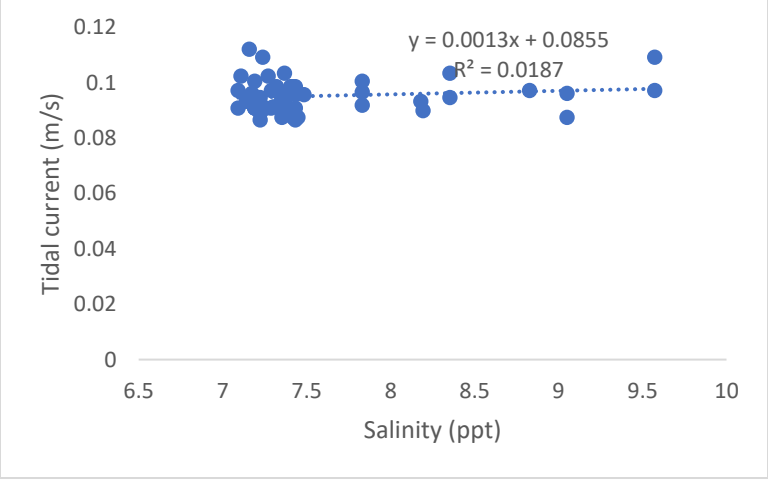

Figure 7-3 Correlation between tidal current and salinity based on 50 years observed data

7.1.3 Correlation between ice thickness and wind speed

Figure 7-4 shows the correlation between ice thickness and wind speed based on the measured data from eklima. It can be seen from the figure that there is a very weak dependency between these variables and correlation coefficient between these two parameters is -0.23 which indicates very weak negative dependency.

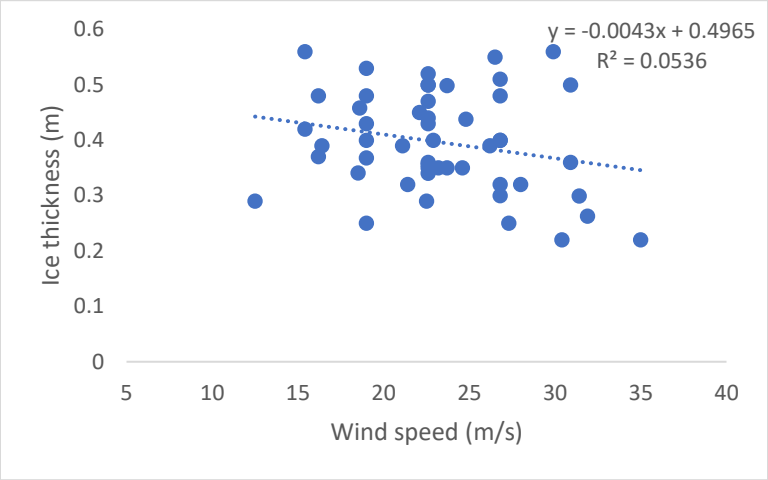

Figure 7-4 Correlation between ice thickness and wind speed based on 50 years observed data

7.1.4 Correlation between ice thickness and tidal current

Figure 7-5 shows the correlation between ice thickness and wind speed based on the measured data from eklima. It can be seen from the figure that there is a very weak dependency between these variables and correlation coefficient between these two parameters is -0.005 which indicates very weak negative dependency.

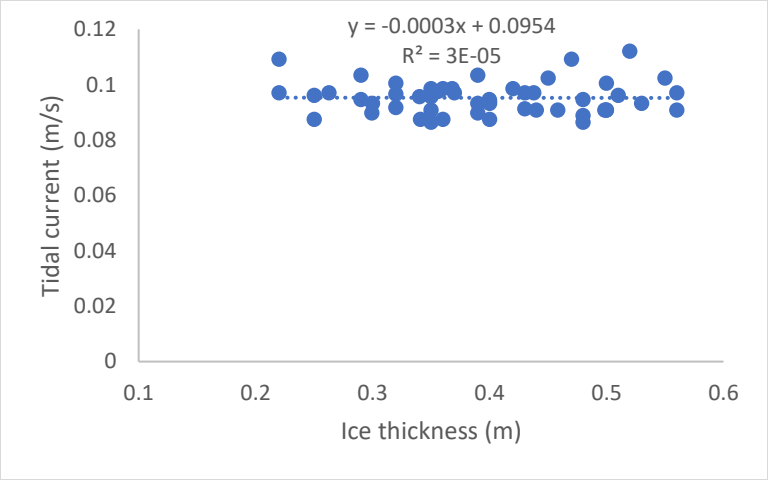

Figure 7-5 Correlation between tidal current and ice thickness based on 50 years observed data

7.1.5 Correlation between salinity and wind speed

Figure 7-6 shows the correlation between ice thickness and wind speed based on the measured data from eklima. It can be seen from the figure that there is a very weak dependency between these variables and correlation coefficient between these two parameters is 0.36 which indicates weak positive dependency.

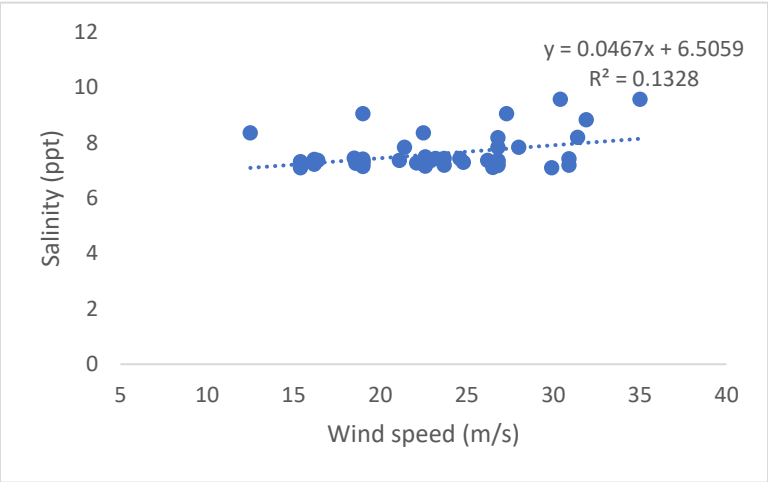

Figure 7-6 Correlation between salinity and wind speed based on 50 years observed data

According to the observed data almost very weak positive and negative dependencies between the ice and metrological parameters. In case of vertical structure, ice limit force scenario is governing

according to the all standard's ice force calculations, so, the correlation between tidal current and wind velocity is very important for the calculation of the ice actions on the vertical structure. For the sloping structure, limit stress is governing for almost all the past years, ice thickness and flexural strength (functions of brine volume and salinity) are very important parameters. For the probabilistic assessment, the effect of correlations between these observed variables is considered for the design ice load determination (refer 7.3).

7.2 Extreme value analysis for the ice actions

7.2.1 Scenarios for vertical structures

Figure 7-7 shows the five scenarios that were made for the deterministic extreme value analysis of the ice actions on vertical structures. In the first scenario (S1) distributions of each stochastic parameter are considered based on the past 50 years available data and after calculation of their design values for the 100 years from the best probabilistic distribution fitting, the design load was determined deterministically. In the second scenario (S2), distributions were fit on the ice actions due to limit force and limit stress which are calculated deterministically based on the past data of 50 years. In the third scenario (S3) distributions were fit on the governing ice actions calculated based on the minimum value of the limit stress and limit force and then its extreme value was calculated corresponding to the 100-year design life of the structure based on the best probabilistic fitting. In the fourth scenario (S4) a linear regression analysis or trendline was drawn which gives a mathematical expression to calculate the design value of ice loads in 2119. It is worthy to mention that in all the above four scenarios individual hitting of ice floe is considered. In the fifth scenario (S5) the effects of hitting rate per year (number of hits per year) which is a sort of deterministic uncertainty analysis of the ice loads; are considered and concluded that with the increase of hitting per year magnitude of ice actions increases.

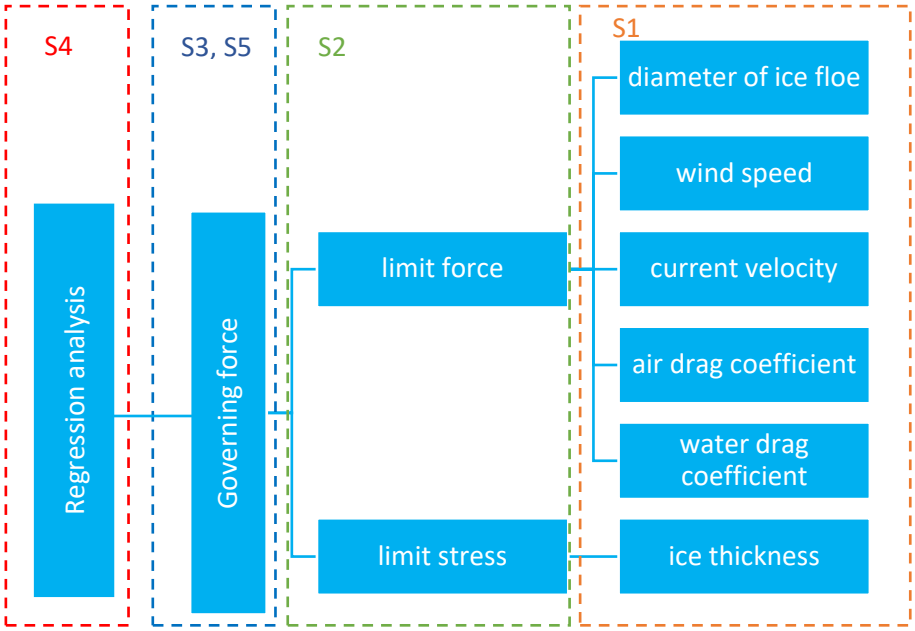

Figure 7-7 Simulation scenarios for ice actions on vertical structures

The design ice loads were determined using probabilistic scenarios. The quantities that were considered as being deterministic and stochastic based on the sensitivity analysis are shown in Table 7-1. In the simulation, freezing degree-days were calculated for the years under consideration based on the temperature data which were collected online from eklima.no. The environmental parameters (wind and current speeds) were collected online from eklima.no. and kartverket, respectively. The current speeds were calculated depending on the water level data available on kartverket.no. By knowing the water levels, the tidal prism can then be calculated as the volume of water accommodated between the highest and the lowest astronomical tides. Therefore, the value for the current speed can be obtained by dividing the tidal prism over the time of one whole day.

Table 7-1 Inputs for extreme value analysis

Parameters	Nature of variable	Distribution/values
Ice failure model for both crushing and bending		
Ice floe thickness	Random	Gamma, depending on freezing-degree days, modified for annual conditions
Flexural strength	Random	Normal, depending on brine volume
Young's modulus	Constant	3400 MPa
Ice density	Constant	8.92 kN/m^3
Ice-structure friction	Random	Uniform, 0.10-0.30
Rubble height	Random	Uniform, 0 to maximum, based on ice thickness
Rubble angle of repose	Constant	45°
Rubble porosity	Constant	0.3
Rubble internal friction angle	Constant	45°
Rubble cohesion	Constant	5 kPa
Ice-ice friction	Constant	0.1
Cone Angle	Constant	45°
Ice strength coefficient	Constant	1.8 MPa
The environmental driving force model		
Floe diameter	Random	Uniform, 50 to 580 m, based on ice conditions
Wind velocity	Random	Gumble Max
Current velocity	Random	Gumble Max
Air drag coefficient	Random	Uniform, 0.001-0.003
Water drag coefficient	Random	Uniform, 0.005-0.03
Density of air	Constant	0.0134 kN/m^3
Density of water	Constant	10.05 kN/m^3

7.2.1.1 Scenario No 1: distribution of the input variables for individual interaction (S1)

The distributions have been taken into consideration for each of the stochastic input variables as shown in Figure 7-8. Math-wave data analysis and simulation tool was used to fit the best distributions on the stochastic input variables. These variables are divided into the two ice force

components: ice limit force and ice limit stress. These variables are the ice floe diameter, the wind speed, the air drag coefficient, the tidal current speed, the water drag coefficient, and the ice thickness. The ice floe diameter was considered uniformly distributed with a design value of 580 m, whereas the ice floe thickness was found to follow Gamma distribution with a design value of 0.63 m. Even though the design value for the ice cover thickness has been expected to rise to 0.63 m and the trend of the ice cover thickness was assumed to increase over the lifetime of structure, it can be seen from Figure 5-7 that the trend of the ice cover thickness has slightly decreased over the past 50 years with a standard deviation of 9 cm due to climate change and global warming. This explains the Conservancy of the calculations in this case study.

On the other hand, the wind and current speeds were seen to fit Gumble Max distribution with design values of 38 and 0.112 m/s, while the air and water drag coefficients were regarded as uniformly distributed with design values of 0.00258 and 0.0308, respectively. Therefore, the ice limit force and the ice limit-stress force were calculated and found to be 1.345 and 5.044 MN, respectively. Hence, the governing ice force has been taken as 1.345 MN which is the extreme value in the 100 years. It can be noticed that the limit force is governing; because the current speed is very low, and hence the drag force component exerted by the tidal current can be neglected.

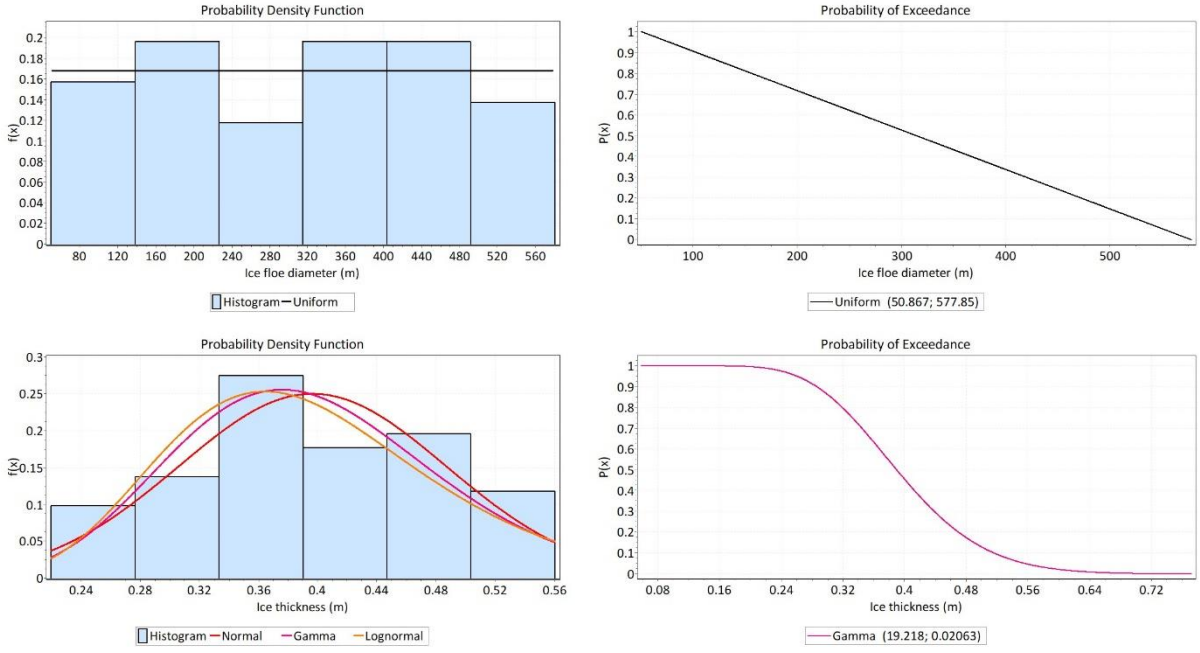

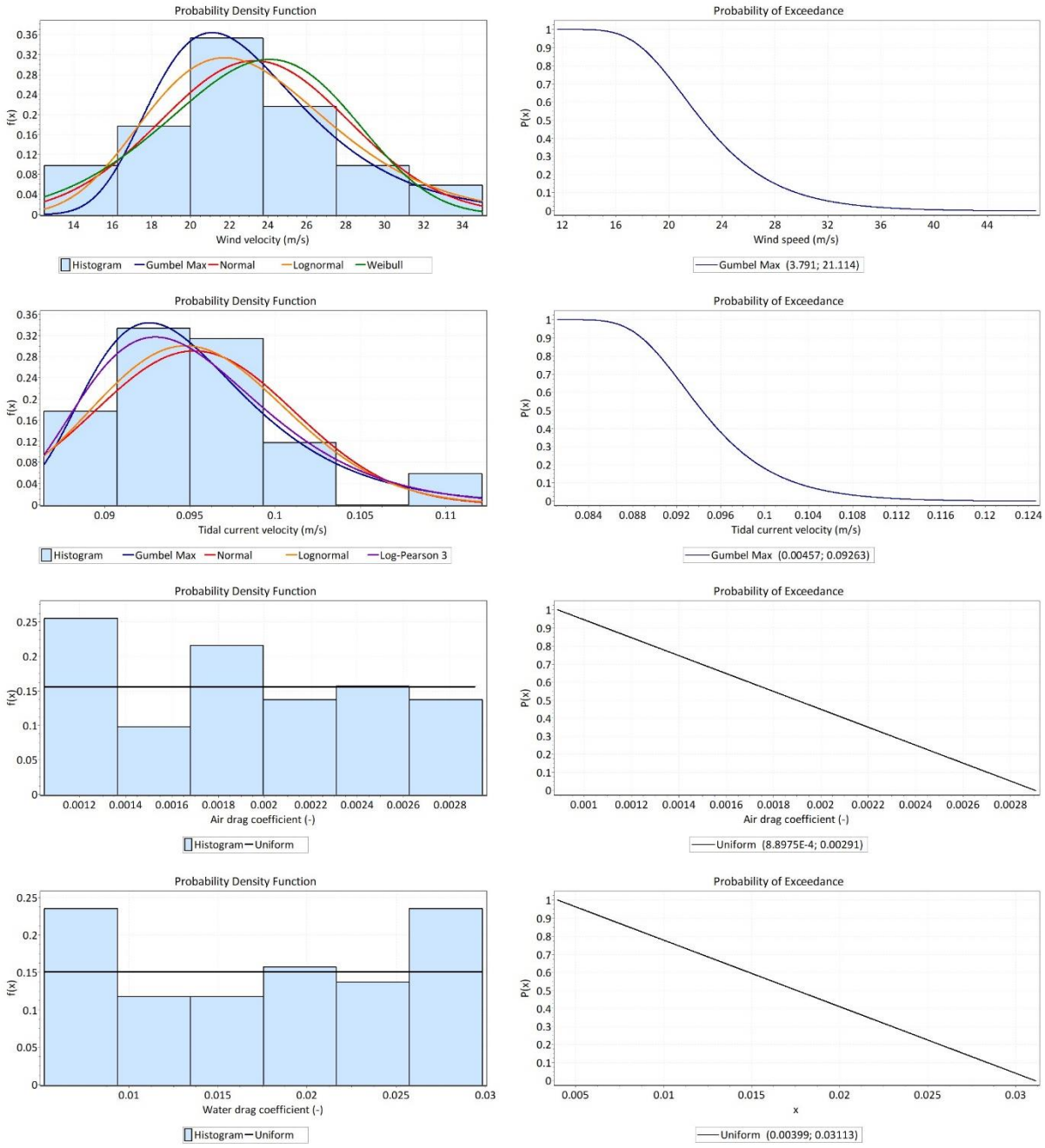

Figure 7-8 From up left to down right: (a) uniform distribution fit for the ice floe diameter; (b) exceedance probability for the ice floe diameter; (c) comparison of different fits for the ice floe thickness; (d) exceedance probability for the ice floe thickness; (e) comparison of different fits for the wind speed; (f) exceedance probability for the wind speed; (g) comparison of different fits for the current speed; (h) exceedance probability for the current speed; (i) uniform distribution fit for the air drag coefficient; (j) exceedance probability for the air drag coefficient; (k) uniform distribution fit for the water drag coefficient; and (l) exceedance probability for the water drag coefficient.

7.2.1.2 Scenario No 2: distribution of the limiting mechanisms for individual interaction (S2)

The distribution has been taken into consideration for each of the limiting mechanisms as shown in Figure 7-9. These variables are divided as the two ice force components: ice limit force and ice limit stress. The ice floe diameter was assumed maximum as 580 m, whereas the air and water drag coefficients were taken as mean values (0.0020 and 0.0175, respectively) of the range considered as shown in Table 7-1. Therefore, the ice limit force and the ice limit-stress force were calculated and found to fit Gumble Max distribution with design values of 1.26 and 5.198 MN, respectively. Hence, the extreme value for the 100-year design life of the governing ice force has been taken as 1.26 MN. It can be noticed that the limit force is governing and smaller than the limit force obtained in scenario S1; because the air and water drag coefficients were taken as mean values which are lesser than the design values that have been estimated in scenario S1.

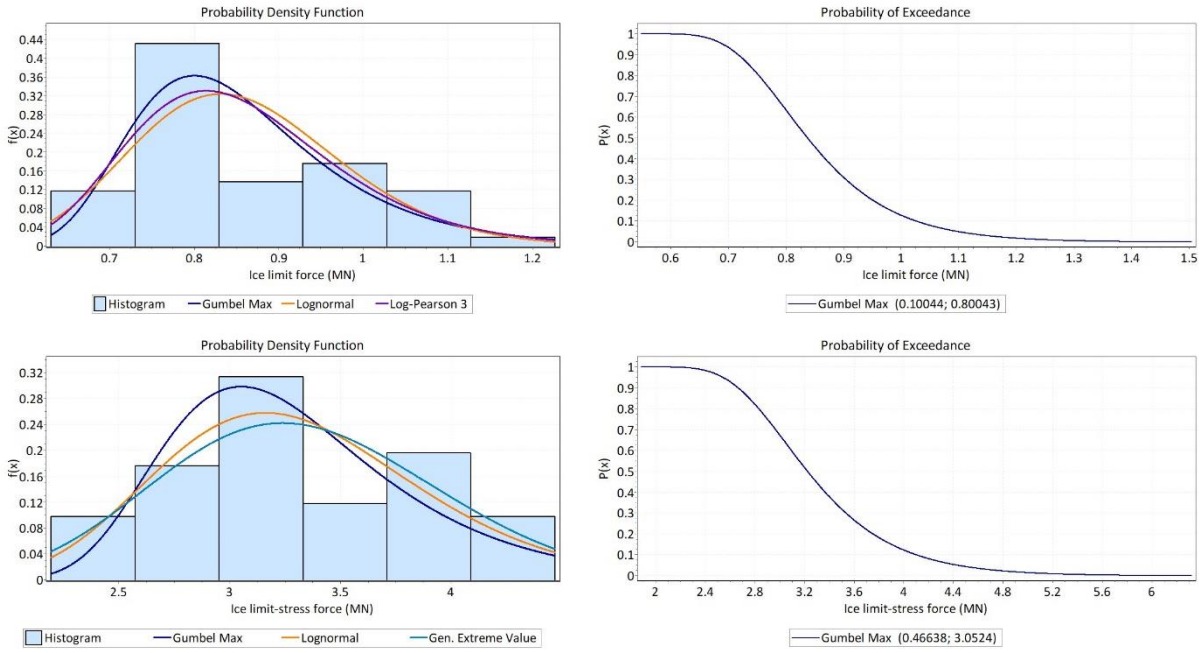

Figure 7-9 From up left to down right: (a) comparison of different fits for the limit force; (b) exceedance probability for the limit force; (c) comparison of different fits for the limit-stress force; and (d) exceedance probability for the limit-stress force

7.2.1.3 Scenario No 3: distribution of governing ice action for individual interaction (S3)

The distribution has been taken into consideration for each of the governing ice action as shown in Figure 7-10. These variables are only the governing ice force which is taken as the minimum force component amongst the two limiting force components. The ice floe diameter was assumed maximum as 580 m, whereas the air and water drag coefficients were taken as mean values (0.0020 and 0.0175, respectively) of the range considered as shown in Table 7-1. Therefore, the ice limit force and the ice limit-stress force have been evaluated, and the governing ice force was then calculated and found to fit Gumble Max with a design value at a 100-year return period of 1.262 MN. The limit force is governing and smaller than the limit force obtained in scenario S1; because the air and water drag coefficients were taken as mean values which are lesser than the design values that have been estimated in scenario S1.

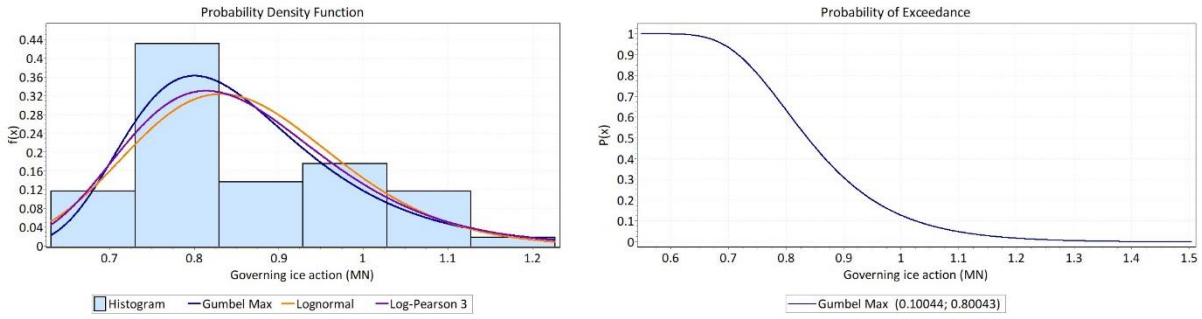

Figure 7-10 From up left to down right: (a) comparison of different fits for the governing ice action; and (b) exceedance probability for the governing ice action

7.2.1.4 Scenario No 4: trendline of the governing ice action for individual interaction (S4)

The ice limit force and the ice limit-stress force have been evaluated, and the governing ice force was calculated based on data for the past 50 years, and then fit and interpret as linear relationship in regression analysis (as shown in Figure 7-11) for the design lifetime of the vertical structure, which is 100 years. Hence, there will be no ice force according to the trend for the design year 2119, because the average annual ice thickness is decreasing, and the average annual temperature

is climbing up year after year. Thus, global warming might be a reason for the decreased ice actions in the future.

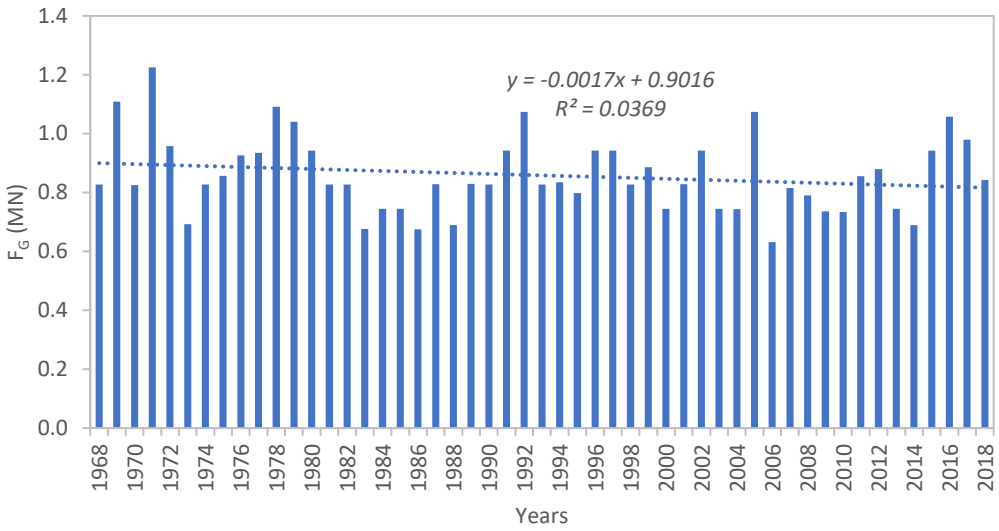

Figure 7-11 Linear regression for the governing ice action on vertical structures

7.2.1.5 Scenario No 5: distribution of the governing ice action for the life of the structure (S5)

The distribution has been taken into consideration for each of the governing ice action as shown in Figure 7-10. These variables are only the governing ice force which is taken as the minimum force among the two limiting force components. The ice floe diameter was assumed maximum as 580 m, whereas the air and water drag coefficients were taken as mean values (0.0020 and 0.0175, respectively) of the range considered as shown in Table 7-1. Therefore, the ice limit force and the ice limit-stress force have been evaluated, and the governing ice force was then calculated and found to fit Gumble Max. Thus, the probability of exceedance has been evaluated for each value of the governing ice force vector. In this scenario, the distribution of the governing ice load derived in scenario S3 was used to estimate maximum ice load statistics for the 100-year design life. If N is the number of impacts per year, based on the fundamental probability theory, the cumulative distribution function (CDF) of the maximum impact load can be calculated as:

$$F_{max}(X) = \mathrm{F_{single}(X)^N}$$

Where:

$F_{max}(X)$ = CDF of the maximum impact load considering individual events happens N times

$F_{\mathrm{single}}(X)$ = CDF of the individual event

If T is the lifetime of the structure and R is the average hitting rate of the ice floe per year, the probability of exceedance Pr at any given load level can be obtained as follows:

$$Pr = 1 - (1 - p)^{\mathrm{RT}}$$

Where:

Pr = probability of exceedance for life of the structure, and

p = probability of exceedance for a single year.

Further, it was also assumed that all the impact events are independent and represent samples from the same distribution. Based on the distribution of single impact events in scenario S3, distribution of the maximum impact load in a given time span has been derived. Figure 7-12 shows the exceedance probability of ice force when ice floes hit a vertical structure at an average rate of 0.05 per year (N = 20). The curves below have been generated using the Gumble-max parameters described earlier in scenario S3 for the single impact event (blue curve). The 25-, 50-, 75- and 100-year maximum event curves were generated using the above equation. Moreover, ISO19906 gives an approximation to calculate the encounter probability of the ice floe to hit the structure, which is based on the work done by Dunwoody (1983), Nessim et al. (1986), Jordaan (1987) and Sanderson (1987) on the Beaufort Sea. Therefore, the encounter probability is given as under:

$$Pr(I) = \rho\bar{V}(\bar{L} + d)$$

Where:

d = ice floe diameter,

$\bar{L}$ = mean ice floe diameter,

$\bar{V}$ = mean drifting velocity of an ice floe, and

ρ = Arial density of ice floe (number per unit area), also, $\rho = c/A$, c = concentration and A is the floe area.

In this case study, the hitting rate of 0.05 per year was assumed for the maximum lifetime probability distribution. An approximation method has been used to find the ice force corresponding to 1% exceedance probability. This was performed by extending the tail of the curve (5% of the data or last 103 values) with an error of only 1%. Therefore, the design values for the ice force were found as follows: 1.262, 1.264, 1.288, 1.298 and 1.303 MN for 1-, 25-, 50-, 75- and 100-year lifetimes of the proposed vertical structure. It is obvious that the design ice force increases with the extended lifetime of the structure.

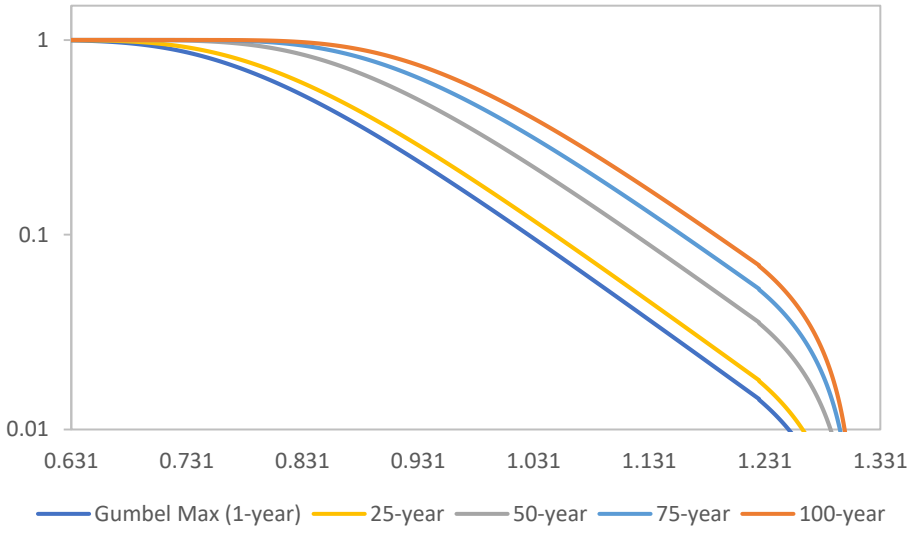

Figure 7-12 Exceedance probability of maximum ice force event for different lifetimes of vertical structures – from left to right: a) 1 year; b) 25 years; c) 50 years; d) 75 years and e) 100 years

Figure 7-13 shows the exceedance probability of the maximum event for different hitting rates (i.e., R = 0.05, 0.1, 0.15, 0.2, 0.25, 0.3 and 0.35) for 100-year lifetime of the proposed vertical structure. From the figure, it is obvious that the exceedance probability noticeably increases with the increased rate of hitting ice floe against vertical structures. Also, the design ice force noticeably increases with increased hitting rates.

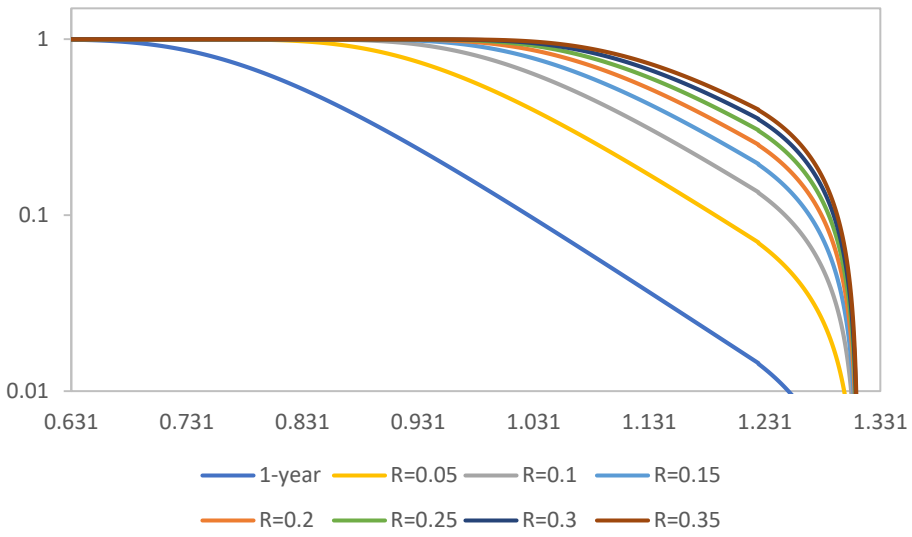

Figure 7-13 Exceedance probability of maximum ice force event for a different rate of hitting of ice floe against vertical structures during the 100-year lifetime of the structure.

7.2.2 Scenarios for sloping structures

Figure 7-14 shows the five scenarios that were made for the deterministic extreme value analysis of the ice actions on sloping structures. In the first scenario (S1) distributions of each stochastic parameter are considered based on the past 50 years available data and after calculation of their design values for the 100 years from the best probabilistic distribution fitting, the design load was determined deterministically. In the second scenario (S2), distributions were fit on the ice actions due to limit force and limit stress which are calculated deterministically based on the past data of 50 years. In the third scenario (S3) distributions were fit on the governing ice actions calculated based on the minimum value of the limit stress and limit force and then its extreme value was calculated corresponding to the 100-year design life of the structure based on the best probabilistic fitting. In the fourth scenario (S4) a linear regression analysis or trendline was drawn which gives a mathematical expression to calculate the design value of ice loads in 2119. It is worthy to mention that in all the above four scenarios individual hitting of ice floe is considered. In the fifth scenario (S5) the effects of hitting rate per year (number of hits per year) are considered and concluded that with the increase of hitting per year magnitude of ice actions increases.

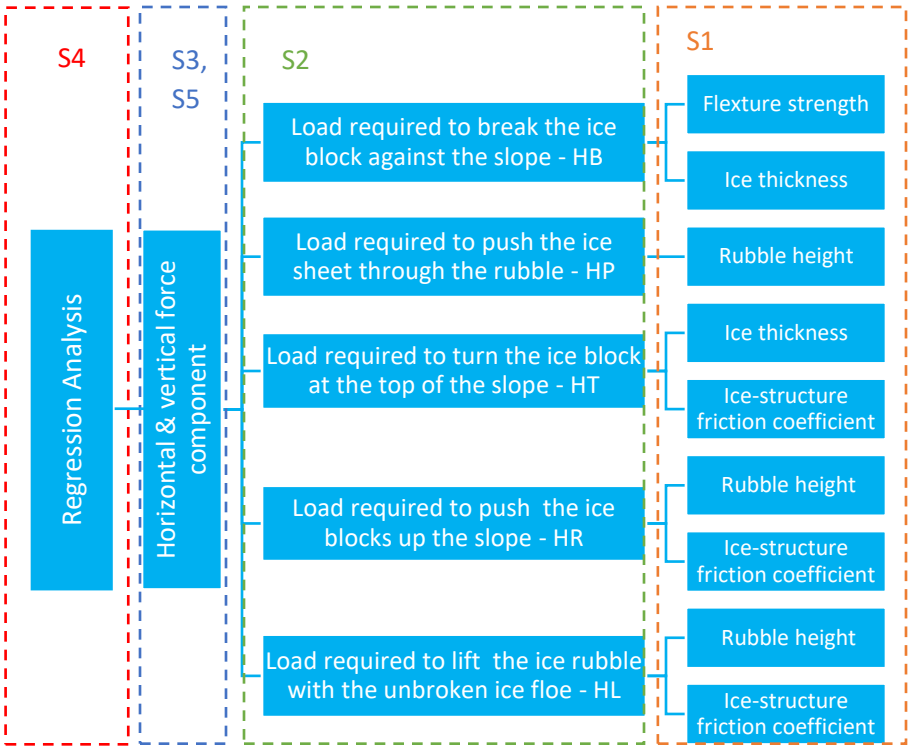

Figure 7-14 Simulation scenarios for ice actions on sloping structures

7.2.2.1 Scenario No 1: distribution of the input variables for individual interaction (S1)

The distribution has been taken into consideration for each of the stochastic input as shown in Figure 7-15. These variables are divided into five ice force components: the load required to break the ice block against the slope (HB), the load required to push the ice sheet through the rubble (HP), the load required to turn the ice block at the top of the slope (HT), the load required to push the ice blocks up the slope (HR), and the load required to lift the ice rubble with the unbroken ice floe (HL). These variables are the ice thickness, the ice rubble height, ice-structure friction coefficient, and the ice flexural strength. The ice thickness was found to fit Gamma distribution with a design value of 0.63 m, whereas the ice rubble height was considered uniformly distributed with a design value of 5.44 m.

On the other hand, the ice flexural strength and ice-structure friction coefficient were seen to fit Normal and Uniform distributions with design values of 0.335 MPa and 0.314, respectively. Any

other variables are assumed constants as shown in Table 7-1. Therefore, HB, HP, HT, HR, and HL were calculated and found to be 0.276, 0.00, 0.031, 0.227, and 0.00 MN, respectively. HP and HL are zero because the rubble angle of repose and cone angle is assumed to be equal. Furthermore, the sensitivity of both these ice force components has been described in article 6.4.1. Hence, the design ice action for the 100-year design lifetime has been evaluated for 0.561 and 0.293 MN in the horizontal and vertical directions, respectively. It can be noticed that the horizontal ice action is approximately two times as the vertical ice action. Also, the design ice action due to limit force is 1.345 for scenario S1 and 1.26 MN for scenario S2.

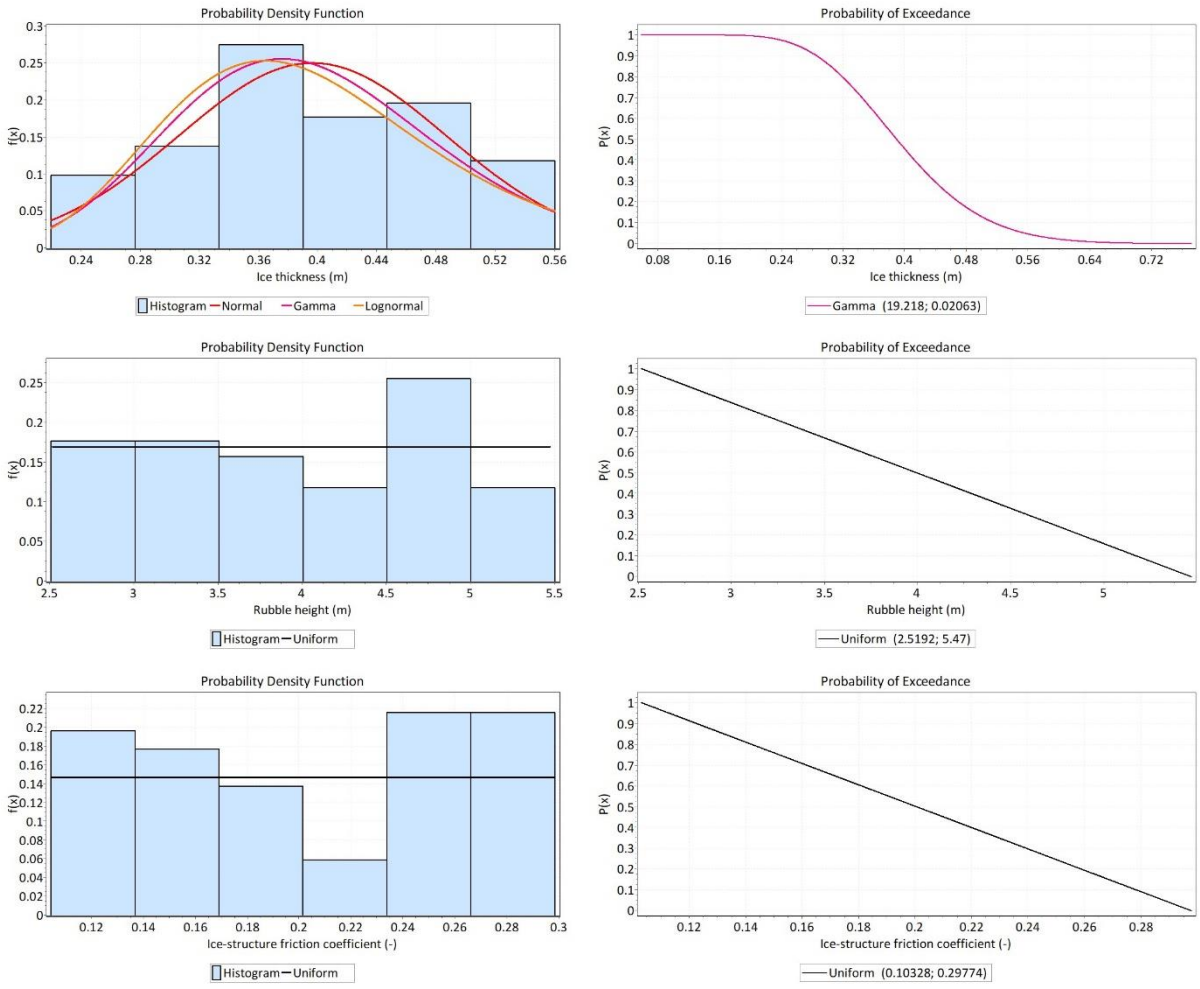

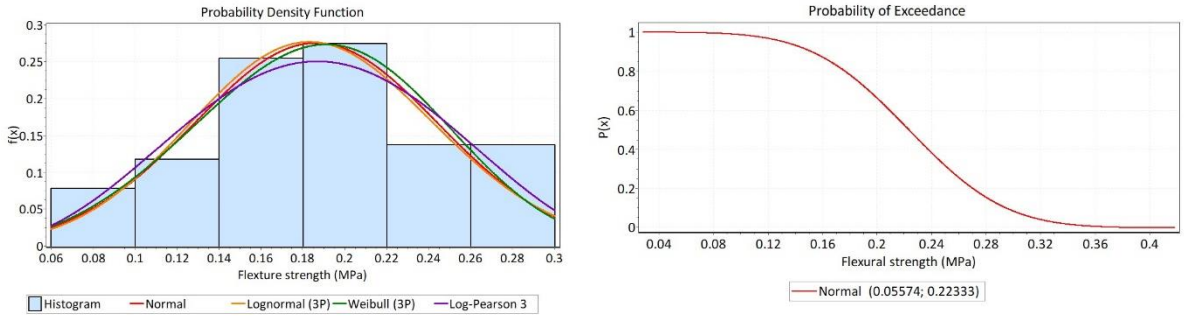

Figure 7-15 From up left to down right: (a) comparison of different fits for the ice floe thickness; (b) exceedance probability for the ice floe thickness; (c) comparison of different fits for the ice rubble height; (d) exceedance probability for the ice rubble height; (e) comparison of different fits for the ice-structure friction coefficient; (f) exceedance probability for the ice-structure friction coefficient; (g) comparison of different fits for the ice flexural strength; and (h) exceedance probability for the ice flexural strength

7.2.2.2 Scenario No 2: distribution of the limiting mechanisms for individual interaction (S2)

The distribution has been taken into consideration for each of the limiting mechanisms as shown in Figure 7-16. These variables are divided into the five ice force components: the load required to break the ice block against the slope (HB), the load required to push the ice sheet through the rubble (HP), the load required to turn the ice block at the top of the slope (HT), the load required to push the ice blocks up the slope (HR), and the load required to lift the ice rubble with the unbroken ice floe (HL). HB and HT were found to fit Log Pierson 3 distribution with a design value of 0.394 MN and 0.043 MN respectively. Also, HR was found to fit the Generalized Extreme Value distribution with a design value of 0.252 MN.

On the other hand, the ice rubble height and the ice-structure friction coefficient were taken as mean values (that is, 5.44 m and 0.321, respectively). Any other variables are assumed constants as shown in Table 7-1. Therefore, the 100-year extreme value of the ice action has been evaluated for 0.740 and 0.386 MN in the horizontal and vertical directions, respectively. It can be noticed that the horizontal ice action is approximately two times as the vertical ice action. It is also obvious that there is an increase of nearly 25% in the ice action when compared to scenario S1.

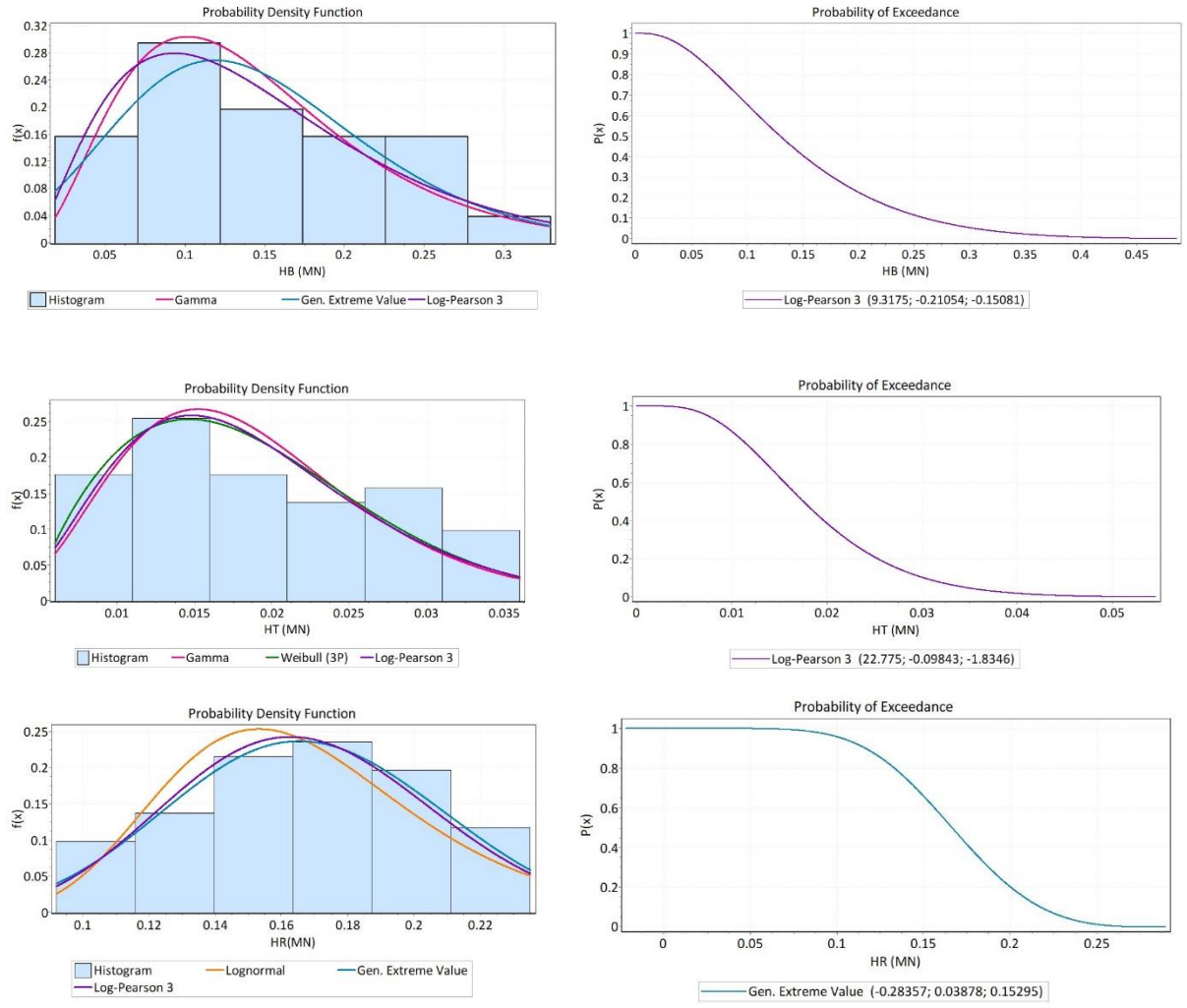

Figure 7-16 From up left to down right: (a) comparison of different fits for HB; (b) exceedance probability for HB; (c) comparison of different fits for HT; (d) exceedance probability for HT; (e) comparison of different fits for HR; and (f) exceedance probability for HR

7.2.2.3 Scenario No 3: distribution of the governing ice action for individual interaction (S3)

The distribution has been taken into consideration for each of the governing ice action as shown in Figure 7-17. These variables are only the resultant ice action which is calculated using a formula that includes the summation of the five ice force components: the load required to break the ice block against the slope (HB), the load required to push the ice sheet through the rubble (HP), the load required to turn the ice block at the top of the slope (HT), the load required to push the ice

blocks up the slope (HR), and the load required to lift the ice rubble with the unbroken ice floe (HL).

On the other hand, the ice rubble height and the ice-structure friction coefficient were taken as mean values (that is, 5.44 m and 0.321, respectively) of the range considered. Any other variables are assumed constants as shown in Table 7-1. Therefore, the horizontal ice action has been evaluated and found to fit Generalized extreme value distribution with a 100-year design value of 0.686 MN. Consequently, the vertical component of the ice action for the design lifetime has been evaluated for 0.228 MN by fitting Log Pierson 3 distribution. The horizontal ice action is three times as the vertical ice action. It can also be concluded that there is an increase of nearly 20% in the ice action when compared to scenario S1.

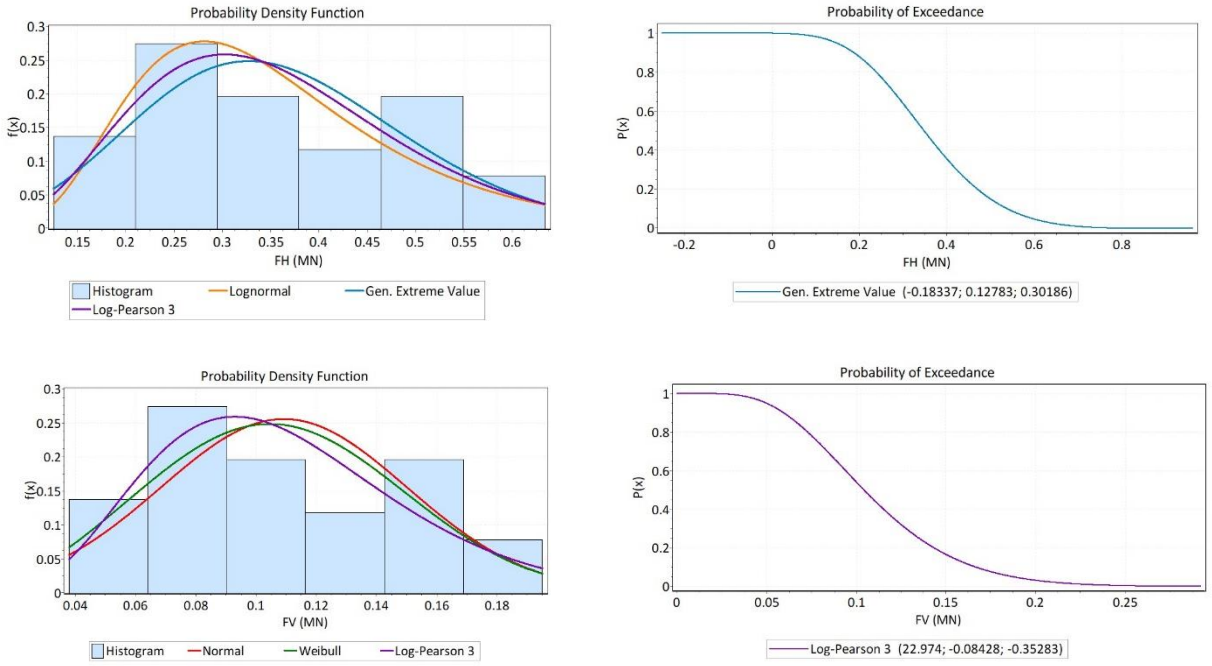

Figure 7-17 From up left to down right: (a) comparison of different fits for the horizontal ice action; and (b) exceedance probability for the horizontal ice action

7.2.2.4 Scenario No 4: trendline of the governing ice action for individual interaction (S4)

The ice action for the previous 50 years has been evaluated, and then fit and interpret as a linear relationship in regression analysis for the design lifetime of the vertical structure, which is 100 years as shown in Figure 7-18. Hence, according to the graph, there will not be any ice actions in 2119. Because the average annual ice thickness is decreasing, and the average annual winterly temperature is climbing up year after year. Thus, climate change and global warming might be the reasons behind the decreased ice actions in the future.

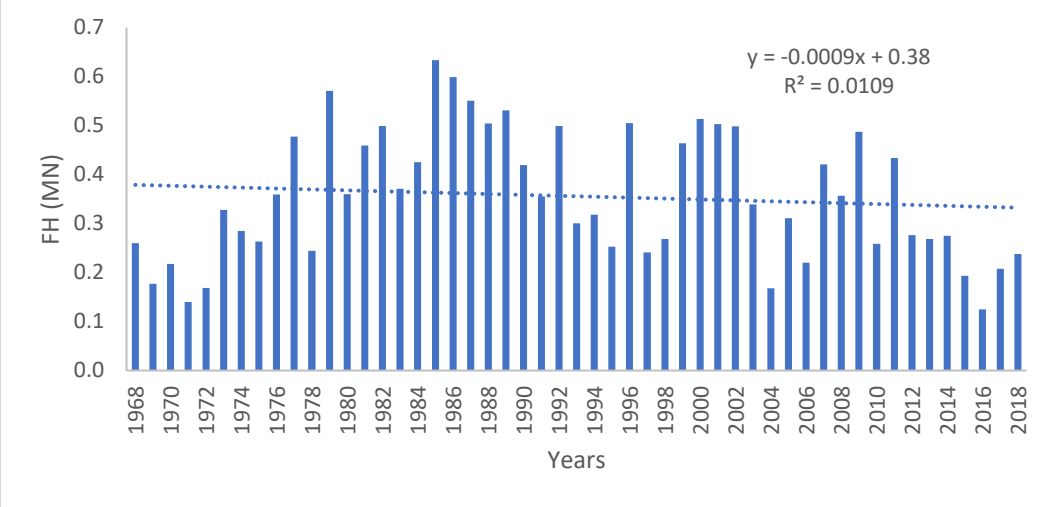

Figure 7-18 Linear regression for the horizontal ice action on sloping structures

7.2.2.5 Scenario No 5: distribution of the governing ice action for the life of the structure (S5)

The distribution has been taken into consideration for each of the governing ice action as shown in Figure 7-17. These variables are only the governing ice force which is taken as the minimum force among the two limiting force components. The ice floe diameter was assumed maximum as 580 m, whereas the air and water drag coefficients were taken as mean values (0.0020 and 0.0175, respectively) of the range considered as shown in Table 7-1. Therefore, the ice limit force and the ice limit-stress force have been evaluated, and the governing ice force was then calculated and

found to fit Gumble Max. Thus, the probability of exceedance has been evaluated for each value of the governing ice force vector.

Figure 7-19 shows the exceedance probability of ice force when ice floes hit a sloping structure at an average rate of 0.05 per year (N = 20). The curves below have been generated using Gumble Max parameters described earlier in scenario 3 for the single impact event (blue curve). The 25-, 50-, 75- and 100-year maximum event curves were generated using the equation described earlier in section 7.2.1.5. In this case study, the hitting rate of 0.05 per year was assumed for the maximum lifetime probability distribution. An approximation method has been used to find the ice force corresponding to 1% exceedance probability. This was performed by extending the tail of the curve (5% of the data or last 103 data points) with an error of only 1%. Therefore, the design values for the ice force were found as follows: 0.765, 0.771, 0.785, 0.791 and 0.797 MN for 1-, 25-, 50-, 75- and 100-year lifetimes of the proposed sloping structures. It is obvious that the design ice force increases with the extended lifetime of the sloping structure.

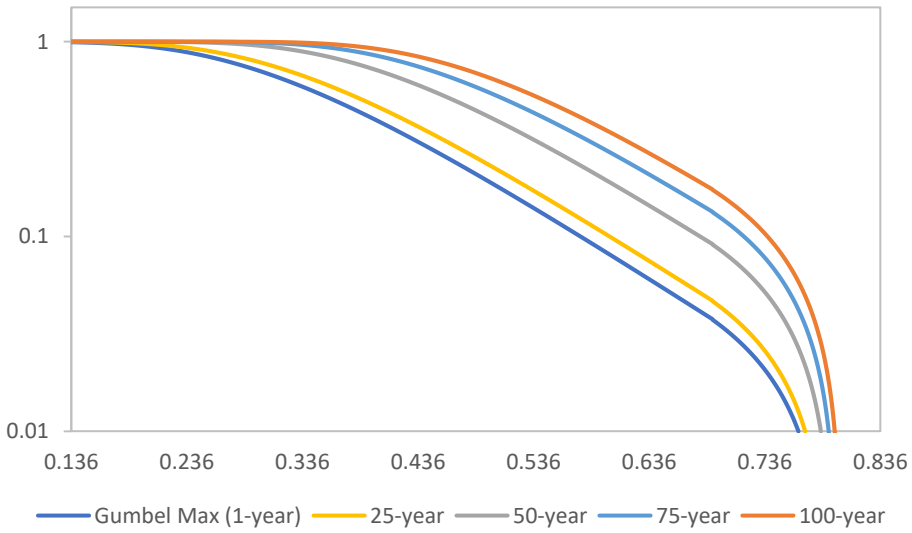

Figure 7-19 Exceedance probability of maximum ice force event for different lifetimes of sloping structures – a) 1 year; b) 25 years; c) 50 years; d) 75 years and e) 100 years

Figure 7-20 shows the exceedance probability of the maximum event for different hitting rates (i.e., R = 0.05, 0.1, 0.15, 0.2, 0.25, 0.3 and 0.35) for 100-year lifetime of the proposed sloping structure. From the figure, it is obvious that the exceedance probability significantly increases with

the increased rate of hitting ice floe against sloping structures. Also, the design ice force significantly increases with the increased hitting rates.

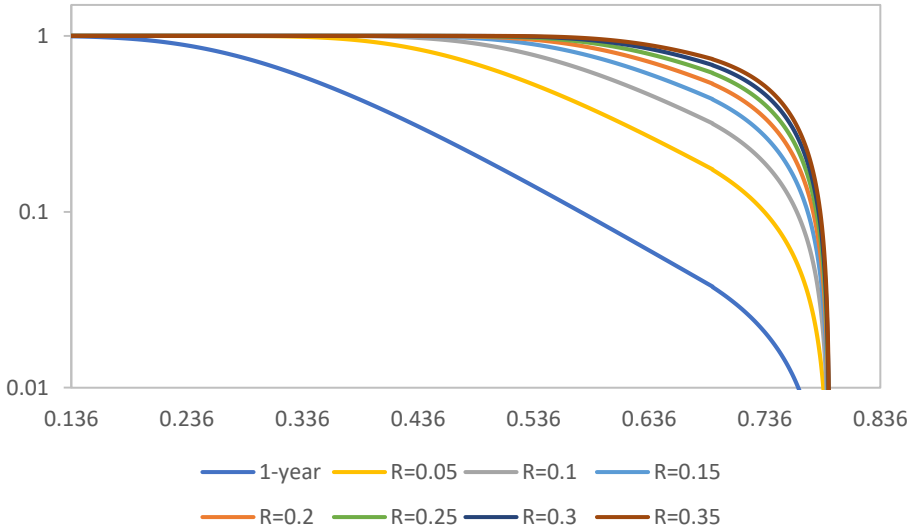

Figure 7-20 Exceedance probability of maximum ice force event for a different rate of hitting of ice floe against sloping structures for the 100-year lifetime of the structure

7.3 Probabilistic analysis and uncertainty quantification by using Monte-Carlo simulations for the ice actions

The Monte-Carlo method is a robust simulation technique in which probability distributions are used for different model inputs based on available data and judgment. Ice loads are simulated for large numbers of ice-structure interactions by generating random values from the input distributions for each interaction and running appropriate load models. The output from the Monte -Carlo simulation is a probability distribution for simulated ice loads on the structure from which the extreme ice loads in 100-year design period are determined. The probabilistic framework is illustrated in Figure 7-21.

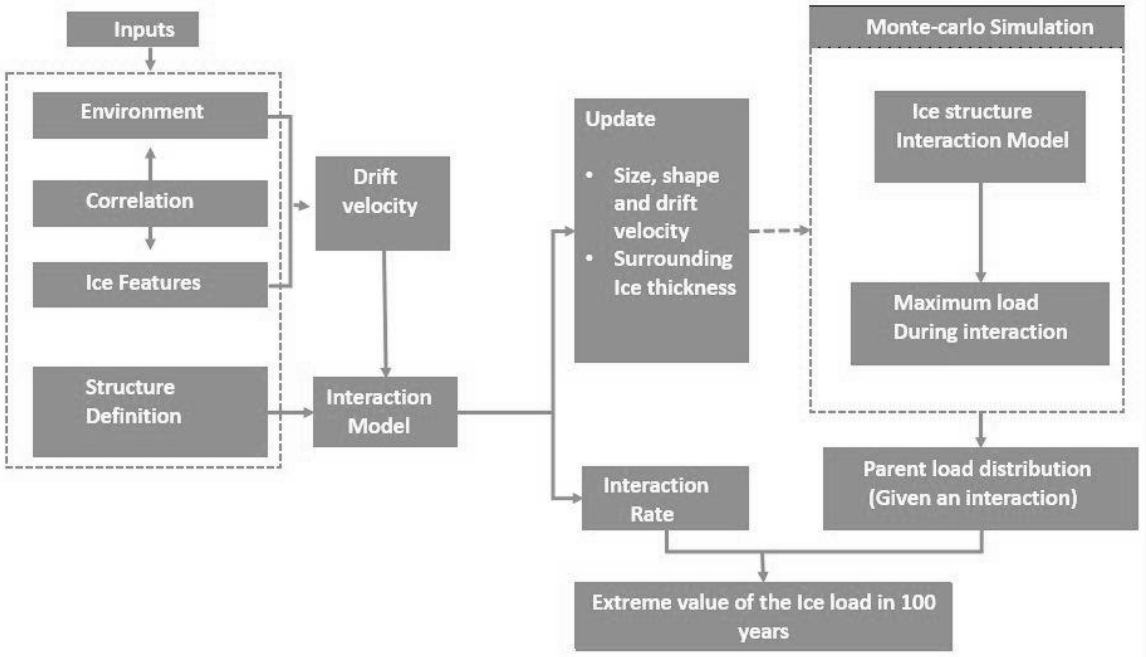

Figure 7-21 Probabilistic framework for determining design loads (Jan Thijssen, 2014; modified)

For the probabilistic analysis, Monte-Carlo simulation has been performed. By simulating the ISO19906 equations for limit force and limit stress (crushing and bending failure mechanisms for vertical and sloping structures, respectively) in MATLAB, based on the sensitivity analysis, the most sensitive ice parameters are taken as random while other kept constant as did in the extreme value analysis. In this probabilistic analysis, the same variables are taken as stochastic as given in the extreme value analysis. Based on the best fit of the probability distribution 10,000 random samples for each stochastic variable were generated. Along with this effect of different correlations between the most important input paraments was included to embrace the uncertainty in the calculation of the design ice actions. After that, the Monte-Carlo simulation was performed. Monte Carlo simulation is a computerized mathematical technique to generate random samples data based on the known input parameter distributions for numerical experiments. This method is applied to risk quantitative analysis and decision-making problems. Following are the three significant features of Monte-Carlo simulation:

- Its output i.e. governing ice action must generate the random samples,
- Its input distribution i.e. stochastic ice parameters must be known, and
- Its result must be known while performing an experiment.

(https://www.tutorialspoint.com/modelling_and_simulation/modelling_and_simulation_monte_carlo_simulation.htm). The following figure shows a generalized flowchart of the Monte-Carlo simulation.

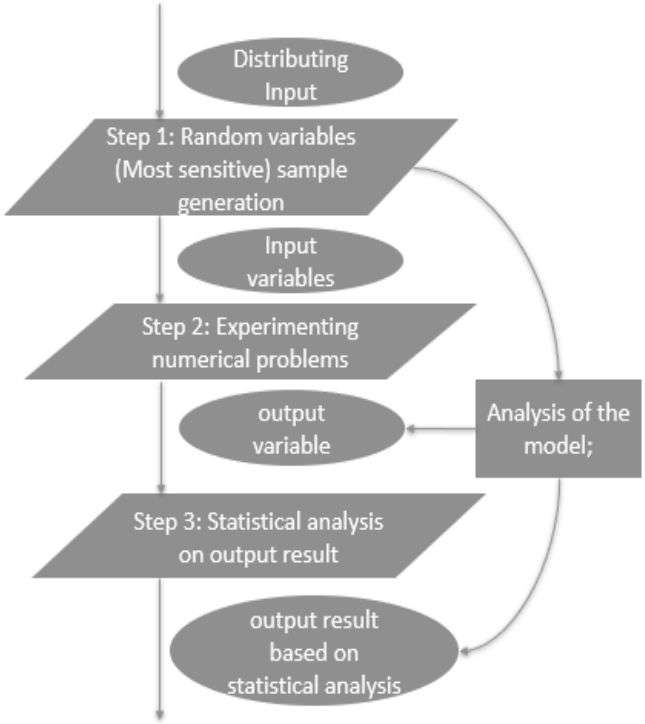

Figure 7-22 Generalized flowchart of Monte-Carlo simulation

For both the vertical and sloping bridge piers this simulation was performed. Probability distributions which fit the best on stochastic parameters are the same as given in Table 7-1. As all the variables have different distributions and the distribution of output variable in unknown. Based on the results of the Monte Carlo simulation for both vertical and sloping structures, the probability distribution of the governing ice action is determined from which the extreme value of the ice load in the 100-year design life is determined by considering the effect of different correlation coefficient values of the most important input parameters.

7.3.1 Ice action on vertical structures

The distribution has been taken into consideration for each of the stochastic input variables as shown in Figure 7-23 and these variables are divided into the two ice force components: ice limit force and ice limit stress. These variables are the ice floe diameter, the wind speed, the air drag

coefficient, the tidal current speed, the water drag coefficient, and the ice thickness. The ice floe diameter was considered uniformly distributed with a design value of 580 m, whereas the ice floe thickness was found to follow Gamma distribution with a design value of 0.63 m.

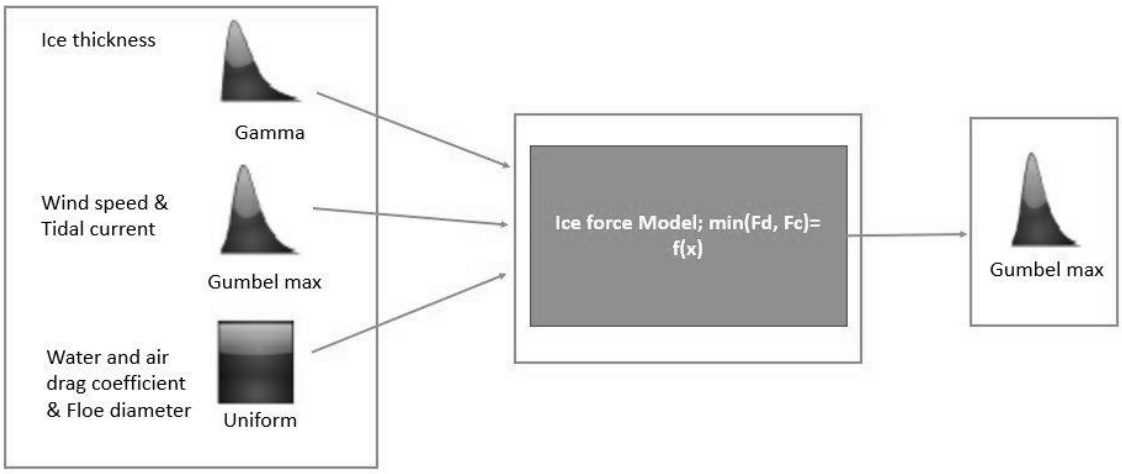

Figure 7-23 Probabilistic framework for determining design loads for the vertical structure

On the other hand, the wind and current speeds were seen to fit Gumble Max distribution with design values of 38 and 0.112 m/s, while the air and water drag coefficients were regarded as uniformly distributed with design values of 0.00258 and 0.0308, respectively. Any other variables are assumed constants as shown in Table 7-1. As the limit force interaction scenario is governing so, the correlation between the current and wind velocity is considered to check how the ice forces change with the independence, positive and negative correlations between the tidal current and wind speed. The Nataf model or Gaussian copula is applied to generate the correlated variables of both wind speed and tidal current (both have Gumble distributions). In the present analysis, the sample size is equal to n = 10,000. The effect of introducing the correlation between wind velocity and tidal current is also investigated as shown in Figure 7-24. In the first case, independence between the basic variables is assumed. Accordingly, the correlation coefficient between the variables is taken as $\rho = 0$, which is given as input to the MCS and then for the other cases (ρ = -0.8,-0.5,0.8,0.5) were assumed and checked the correlation effect on the governing ice action.

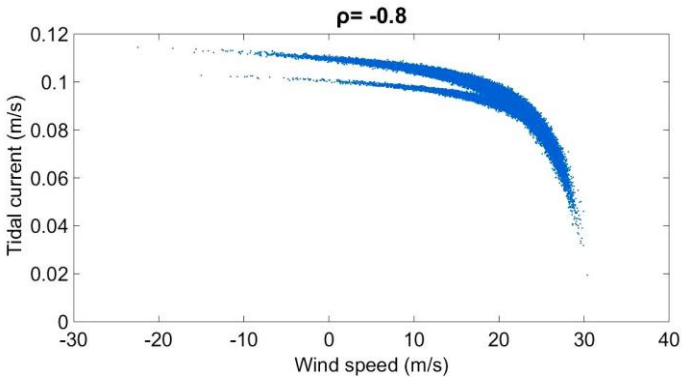
ρ= -0.8
Tidal current (m/s)
Wind speed (m/s)
0.12
0.1
0.08
0.06
0.04
0.02
0
-30
-20
-10
0
10
20
30
40

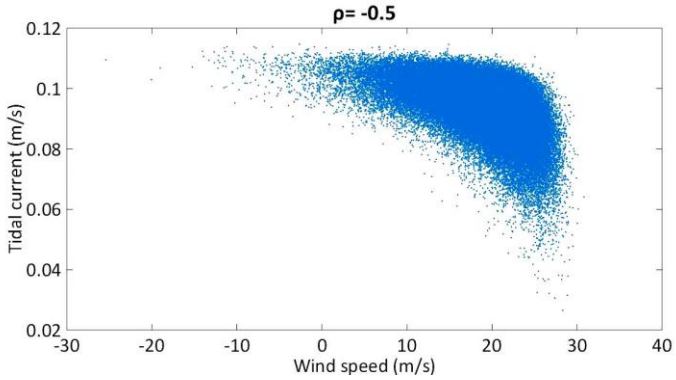
ρ= -0.5
Tidal current (m/s)
Wind speed (m/s)
0.12
0.1
0.08
0.06
0.04
0.02
-30
-20
-10
0
10
20
30
40

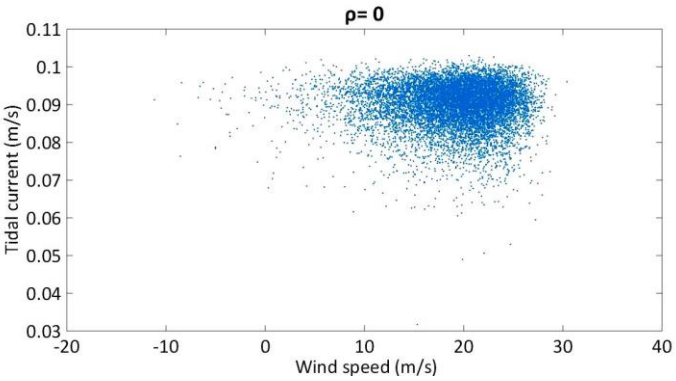
ρ= 0
Tidal current (m/s)
Wind speed (m/s)
0.11
0.1
0.09
0.08
0.07
0.06
0.05
0.04
0.03
-20
-10
0
10
20
30
40

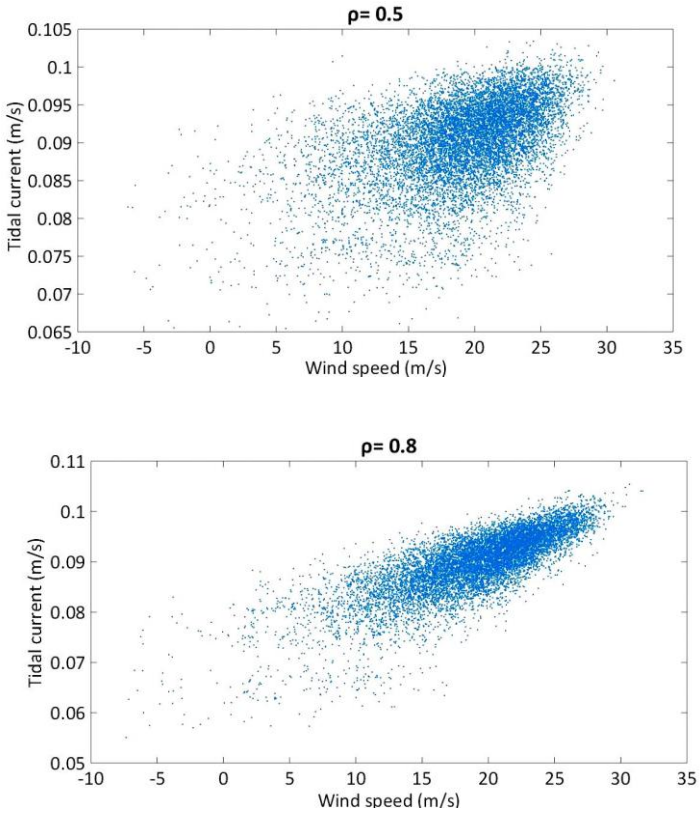

Figure 7-24 Correlations between wind speed and tidal current by using Gaussian Copula

The governing ice action was found to fit Gumble distribution and thus the exceedance probability distribution for the ice actions on the vertical structure is determined as shown in Figure 7-25.

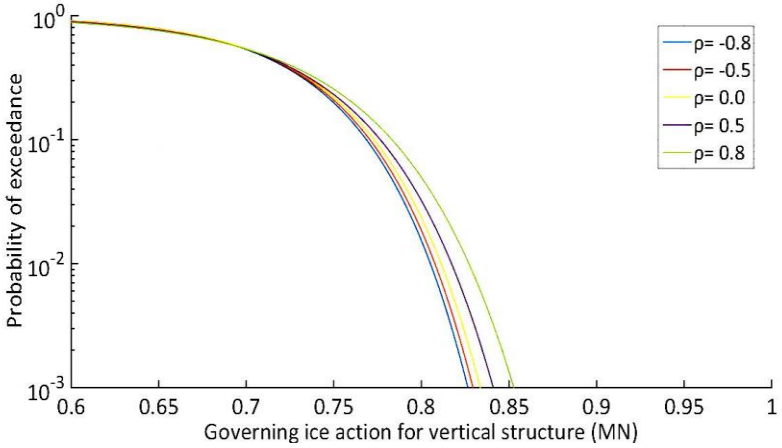

Figure 7-25 Exceedance probability for the governing ice action on vertical structures by fitting Gumble distribution

It is clear from the figure that the effects of the correlation between these two stochastic parameters are not that much big on the governing ice actions, but a little increase has been observed by increasing the correlation between the wind speed and current velocity. The extreme values of governing ice actions including the correlation between the wind velocity ad tidal current in 100-year design lifetime of the structure are 0.8053,0.8076,0.8114,0.8173,0.8267 MN for the correlation coefficient of (-0.8,-0.5,0,0.5,0.8) respectively.

7.3.2 Ice action on sloping structures

The distribution has been taken into consideration for each of the stochastic input as shown in Figure 7-26. These variables are divided into five ice force components: the load required to break the ice block against the slope (HB), the load required to push the ice sheet through the rubble (HP), the load required to turn the ice block at the top of the slope (HT), the load required to push the ice blocks up the slope (HR), and the load required to lift the ice rubble with the unbroken ice floe (HL). These variables are the ice thickness, the ice rubble height, ice-structure friction coefficient, and the ice flexural strength. The ice thickness was found to fit Gamma distribution with a design value of 0.63 m, whereas the ice rubble height was considered uniformly distributed with a design value of 5.44 m.

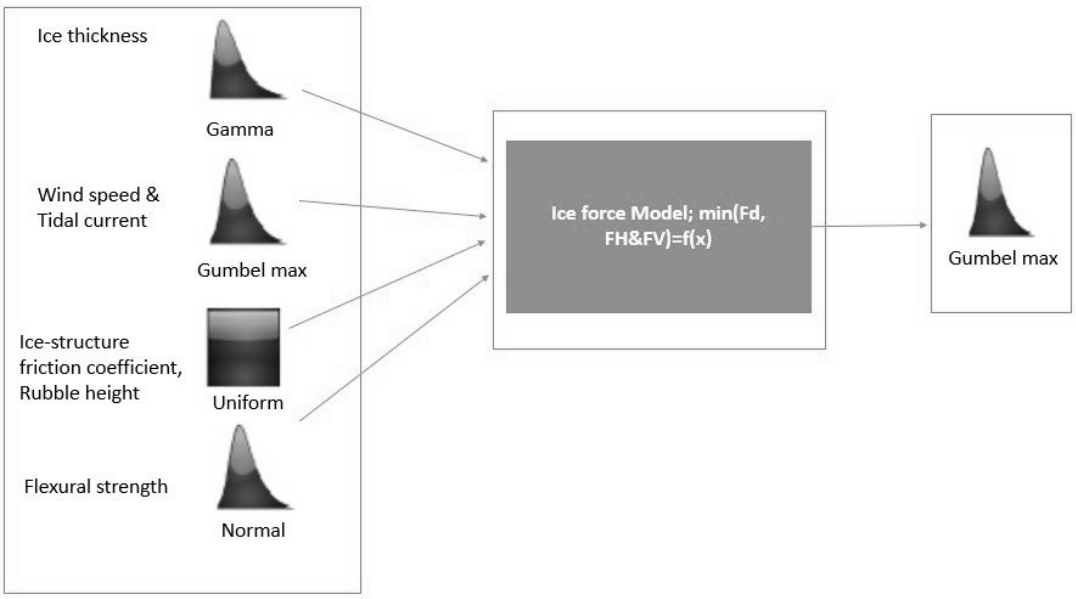

Figure 7-26 Probabilistic framework for determining design loads for the sloping structure

On the other hand, the ice flexural strength and ice-structure friction coefficient were seen to fit Normal and Uniform distributions with design values of 0.335 MN and 0.314, respectively. Any other variables are assumed constants as shown in Table 7-1. In the present analysis, the sample size is equal to n = 10,000. The effect of introducing a correlation between the ice thickness and flexural strength is also investigated as shown in Figure 7-27. The Nataf model or Gaussian copula is applied to generate the correlated variables of both ice thickness and flexural strength (have Gamma and Normal distributions respectively). In the first case, independence between the basic variables is assumed. Accordingly, the correlation coefficient between the variables is taken as ρ = 0, which is given as input to the MCS and then for the other cases (ρ = -0.8,-0.5,0.8,0.5) were assumed and checked the correlation effect on the governing ice action.

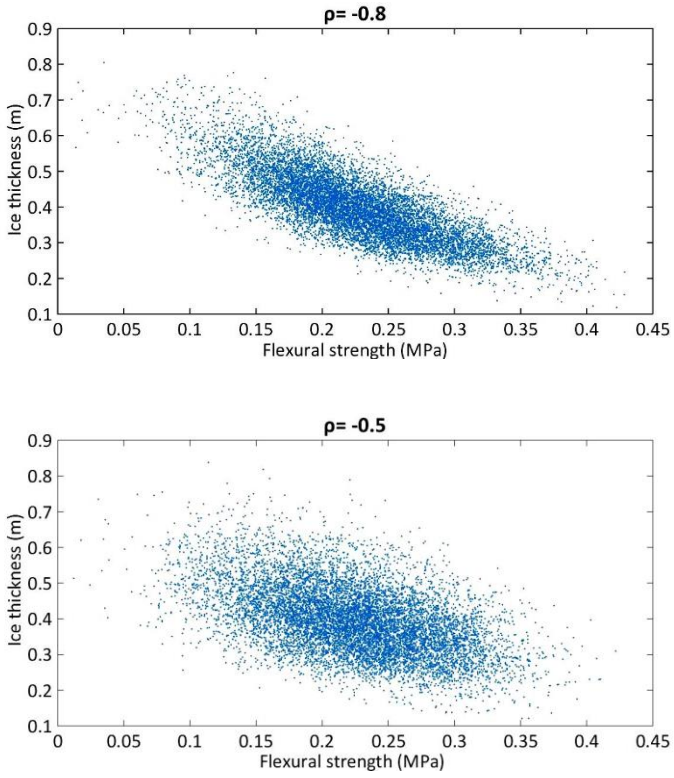

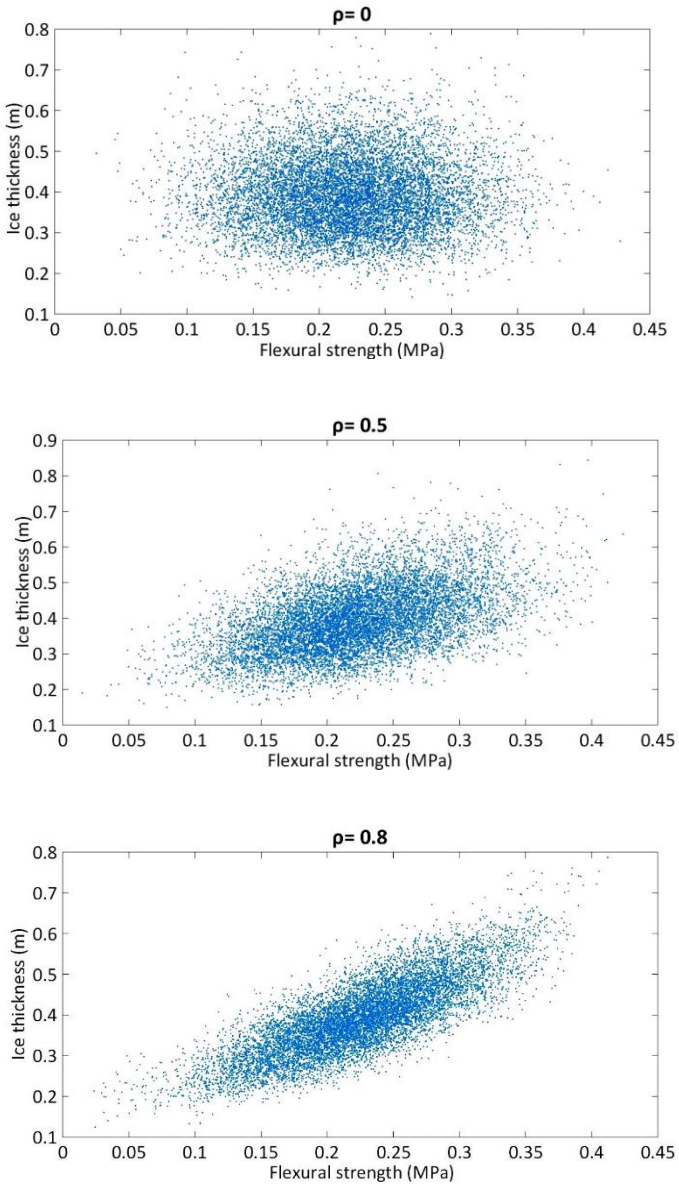

Figure 7-27 Correlation between flexural strength and ice thickness by using Gaussian Copula

The horizontal ice action was found to fit Gumble distribution and thus the exceedance probability for the horizontal ice action on the sloping structure is determined and as shown in Figure 7-28.

It is clear from the figure that the effects of the correlation between these two stochastic parameters i.e. ice thickness and flexural strength are noticeable on the horizontal ice actions. The governing ice action increase is increasing with an increase or positive correlation between the ice thickness and flexural strength. The extreme values of governing ice actions including the correlation

between the ice thickness and flexural strength in 100-year design lifetime of the bridge pier are 0.3019,0.3540,0.4124,0.5081,0.5190 MN for the correlations of (-0.8,-0.5,0,0.5,0.8) respectively.

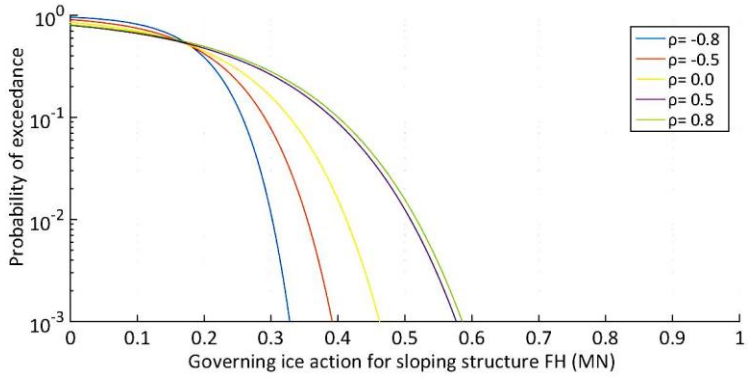

Figure 7-28 Exceedance probability for the governing ice actions on sloping structures by fitting Gumble distribution

Chapter 8

Conclusions and recommendations

8.1 Conclusions

In this thesis, ice action expected in the design lifetime of the Beitstadsundet bridge was determined. Firstly, the required environmental and met-ocean data (i.e. temperature, wind speed, water levels, bathymetry, cloudiness, relative humidity, snow thickness, precipitation, etc.) for developing the relationship between the ice conditions and metrological parameters, is downloaded from different relevant websites (Yr.no, Nve.no, Kartverket.no, Eklima.no) and the interpolation and extrapolation of the missing data is done based on this available data. The data for the bridge characteristics and alignment is extracted from the feasibility study report by the Norconsult in Norway. All the main conclusions are summarized as following;

- Three rivers are falling in the fjord near the bridge location. As most of the current velocity is due to the tidal current, which may change due to change in the tidal amplitude and tidal constituent. The effect of the river discharges is checked on the tidal current which is found very minimal and can be ignored for this study.
- From the metrological data the expected ice conditions (salinity, porosity, flexural strength, ice thickness) which are very important in determining the ice action, are determined. From the different formulas given in AASHTO and ISO19906 and UNESCO handbook; salinity is ranging from 7.1 to 9.6 ppt, ice porosity is ranging from 0.12 to 0.33, the flexural strength of ice is ranging from 0.1 to 0.3 MPa over the past 50 years.
- For this case study, the empirical models by Zubov (1943) and Lebedev (1938), detailed Stefan's empirical model and simplified Stefan's empirical model based on freezing degree day factor (site specific) are employed which are used to calculate the maximum undisturbed ice thickness and to validate the Delft3D-FLOW (Ice module). Table 8-1 shows the ranges of the computed ice thickness from each of the models. The differences

between the ice thicknesses might be due to uncertainties produced by using the constant snow cover, cloudiness, and relative humidity data. In addition to this, the freezing degree day factor used in the equation based on the simplified Stefan's law which is site-specific and it's a constant value; also in detailed Stefan's empirical equation the values of thermal conductivity of ice and snow and latent heat of fusion were assumed. This can also cause uncertainty in the ice cover thickness calculation. It is worthy to mention that, the process-based model needs a lot of input variables and there is a lot of uncertainty in the available data, Stefan's empirical model is preferred to use for the computation of ice floe thickness.

Table 8-1 Winterly annual maximum Ice floe thickness

Ice floe thickness					
Delft3D-FLOW (Ice module)		**Stefan's simplified model**	**Stefan's detailed empirical model**	**Zubov's model**	**Lebedev's model**
with snow cover	without snow cover	with snow cover	with snow cover	without snow cover	without snow cover
Range (m)	Range (m)	Range (m)	Range (m)	Range(m)	Range (m)
0.23 to 0.65	0.28 to 0.77	0.22 to 0.56	0.16 to 0.36	0.17 to 0.38	0.24 to 0.44

- As per the drawings of the Norconsult report, the bridge piers are vertical at the Beitstadsundet but in this case study, the effect of change in the shape of the pier i.e. both sloping and vertical are checked. Table 8-2 shows the range and mean values of the annual maximum ice loads computed from the different standards.

Table 8-2 Annual maximum ice actions on Beitstadsundet bridge pier by using different standards

Forces on the vertical pier						
Standard	**Limit force (MN)**		**Limit stress (MN)**		**Governing Ice action (MN)**	
	Range	Mean	Range	Mean	Range	Mean
ISO	0.622 to 1.012	0.767	2.195 to 4.466	3.322	0.622 to 1.012	0.767
AASHTO	0.622 to 1.012	0.767	0.257 to 9.094	5.317	0.257 to 1.012	0.754
NRC	0.158 to 0.405	0.286	0.125 to 4.339	2.364	0.125 to 0.405	0.285

Forces on the sloping pier (Horizontal direction)						
Standard	**Limit force (MN)**		**Limit stress (MN)**		**Governing Ice action (MN)**	
	Range	Mean	Range	Mean	Range	Mean
ISO	0.622 to 1.012	0.767	0.125 to 0.534	0.356	0.125 to 0.534	0.356
AASHTO	0.622 to 1.012	0.767	0.131 to 0.682	0.433	0.131 to 0.681	0.432
NRC	0.158 to 0.405	0.286	0.004 to 0.366	0.159	0.004 to 0.366	0.159
Forces on the sloping pier (Vertical direction)						
Standard	**Limit force (MN)**		**Limit stress (MN)**		**Governing Ice action (MN)**	
	Range	Mean	Range	Mean	Range	Mean
ISO	0.622 to 1.012	0.767	0.038 to 0.195	0.109	0.038 to 0.195	0.109
AASHTO	0.622 to 1.012	0.767	0.053 to 0.138	0.097	0.053 to 0.138	0.097
NRC	0.158 to 0.405	0.286	0.004 to 0.366	0.159	0.004 to 0.366	0.159

- Ice jamming can also enhance the ice forces against the bridge piers. According to the American and Canadian standards ice jamming can occur at Beitstadsundet but the probability of occurence is very low; in case of ice jamming the load exerted by an ice jam on a unit length of structure parallel to the direction of flow is equal to 0.081575 MN which is very low as compared to the other loads.
- For the computation of the design ice loads, the results from the ISO19906 equations have been used because ISO19906 equations are more detailed in nature and contain many variables. The sensitivity analysis of ISO19906 equations was carried out to check which input parameters can be the most sensitive in the computation of the governing ice actions. Sensitivity analysis of the ice load parameters gives information about the parameters that should be considered as stochastic variables and which parameters should be taken as deterministic values. From the sensitivity analysis it is concluded that the wind speed and and ice floe diameter are more important parameters in case of vertical structure as limit force is governing in almost all the standards; flexural strength and ice thickness are more sensitive in case of the sloping structure as limit stress is governing in this case almost in all the standards.
- The correlation analysis between the most sensitive observed or measured parameters was made which can be very critical to find out the design ice actions since it can increase the

probability of exceedance and governing ice actions. Then, the deterministic extreme value analysis for the computation of the design ice load is done, where different scenarios are considered to find the governing ice action. The deterministic extreme value in the design life of the structure for the governing ice force in the vertical structures is ranging from 1.15 to 1.35 MN depending up the number of hitting of ice floes per year as the hitting rate per year increases the ice actions also increases. In case of the sloping bridge pier, the deterministic extreme value in the design life of the structure for the governing ice force is ranging from 0.56 to 0.79 MN depending up the number of hits per year and the ice force in the horizontal direction is more important than the vertical because of high magnitudes.

- In the case of the probabilistic assessment and uncertainty analysis by using the Montecarlo simulation, the extreme values of governing ice actions in case of the vertical pier, including the effect of correlation between the wind speed and tidal current are given in Table 8-3:

Table 8-3 Governing ice action in case of the vertical pier by using Monte-Carlo simulation

100-year design values of the governing ice action in case of vertical pier	
Correlation coefficient between V_c and V_w	**Governing Ice action (MN)**
ρ= -0.8	0.8053
ρ= -0.5	0.8076
ρ = 0	0.8114
ρ= 0.5	0.8173
ρ= 0.8	0.8267

- Probabilistic assessment and uncertainty analysis by using the Montecarlo simulation, the extreme values of governing ice actions in case of sloping bridge pier, including the effect of correlation between the ice thickness and flexural strength are given in Table 8-4:

Table 8-4 Governing ice action in case of the sloping pier by using Monte-Carlo simulation

100-year design values of the governing ice action in case of the sloping pier (F_H)	
Correlation coefficient between h_i and σ_f	**Governing Ice action (MN)**
ρ= -0.8	0.3019
ρ= -0.5	0.3540
ρ = 0	0.4124
ρ= 0.5	0.5081
ρ= 0.8	0.5190

The main aim of the deterministic extreme value is to calculate the extreme values of ice loads in the 100-year design lifetime and Monte-Carlo simulation is to know about the uncertainty associated with the governing ice actions. It is worthy to mention that for this probabilistic analysis sample size of 10,000 was taken, also by taking a greater number of samples accuracy will improve and the convergence between the results will occur. In the end, it is concluded that by increasing the correlation between these two variables i.e. tidal current and wind speed in case of vertical structure (limit force is governing); flexural strength and ice thickness in case of sloping structure (limit stress is governing); the magnitude of ice actions will increase.

In the conclusion of all the above discussion, the ice force magnitude may vary between the 0.805 MN to 1.350 MN in case of the vertical pier and 0.302 MN to 0.790MN for the sloping pier in the horizontal direction and these values depend on the correlation coefficient between the most sensitive observed ice input parameters and also encounter probability of ice floe.

8.2 Recommendations

- More refined results can be obtained if the data scatter is reduced by considering an extent more focused on the study area location. However, it was not possible for this study as the available met-ocean collection data points are at some substantial distance from the site and there is no other alternative except to use those data points.
- In order to determine the ice feature, a site visit should have conducted. This visit may have unfolded some scenarios which are yet not considered while working without a visit.
- If ice concentration and encounter probability of the ice floes are exactly known from the site, the results would be better. As this was not available, therefore encounter probability is assumed in this study.
- Snow cover, relative humidity, and cloudiness are assumed constant for the calculations; however, the exact situation is quite contrary and if we had used them differently, then the ice thickness would be different which will eventually change ice action.
- After the construction of the bridge, strain gauges and load panels can be installed on the pier to measure the ice loads at the site and then a comparison can be drawn between values recommended in this study and actual ice action.
- A physical model study can reveal the situations which are not yet known and calculated by numerical models; therefore, it is recommended to carry out the physical model study.
- Reliability analysis by using level 2 (FORM) and 3 (Monte-Carlo) probabilistic approaches is also recommended to find the probability of failure of the bridge pier by considering the different failure mechanisms i.e bucking, shear and bending failures, etc under the ice actions which may give an idea about how much the ice loads are contributing in the total loads on the bridge pier.

References

AASHTO (1994) American Association of State Highway and Transportation Officials (1994).

AASHTO LFRD Bridge Design Specifications, 444 North Capitol Street, N.W., Suite 249, Washington, D. C. 20001.

Ahmed, D, 1994, Ice loads on conical piers: A finite element investigation, International Journal of Offshore and Polar Engineering, 4(1), pg: 53-61

API (1995) American Petroleum Institute (1995) Recommended Practice for Planning, Designing, and Constructing Structures and Pipelines for Arctic Conditions, 2nd Edition, API Publications, 1220 L Street N.W., Washington, DC 20005

Applying HEC-RAS to simulate river ice jams: snags and practical hints Spyros Beltaos and Patrick Tang, Watershed Hydrology and Ecology Research Division, National Water Research Institute, Environment Canada, 867 Lakeshore Rd., Burlington, ON L7R 4A6

Ashton, G., 1986, River and Lake Ice Engineering, Water Resources Publications, Littleton, Col.

Brooks, R. N. (2010). Quantifying Peak Freshwater Ice across the Northern Hemisphere using a Regionally Defined Degree-day Ice-growth model. Department of Geography. University of Victoria

Brown, T. G., Tibbo, J. S., Tripathi, D., Obert, K., and Shrestha, N. (2009). “Extreme Ice Load Events on the Confederation Bridge.” Cold Regions Science and Technology, Cold Regions Science and Technology 60, 1-14.

Brown, T.G et al. (2010). Extreme Ice Load Events on the Confederation Bridge, Cold Regions Science, and Technology, 60, pg: 1-14.

Brown, T.G. 1997. The Confederation Bridge: analysis of environmental impacts related to ice. Canadian Journal of Civil Engineering, 24: 908–914.

Cammaert, A.B., Jordaan, I.J., Bruneau, S.E, Crocker, G.B., McKenna, R.F., and Williams, S.A. "Probabilistic Analysis of Ice Loads on Conical Bridge Piers for the Northumberland Strait Crossing Project". Contract report for Stanley Atlantic Inc., C-CORE Contract Number 93-C2

Canadian standard (NRC) to compute the ice forces on bridge piers (https://nrc publications.canada.ca/eng/export/ris/?id=c85068e5-22eb-43d9-a501-11a7a8edd62a)

Comfort, G., Gong, Y., Singh, S., and Abdelnour, R., 2003a, Static Ice Loads on Dams, CSCE Special Journal on River Ice, Canadian Journal of Civil Engineering, 30:42-68(2003).

Croasdale et al (1977) Croasdale, K.R., N.R. Morgenstern, and J.B. Nuttall (1977) Indentation tests to investigate ice pressures on vertical piers, Journal of Glaciology, 81:301–312.

Croasdale, K., Jordaan, I., Verlaan, P. (2011): Offshore platforms and deterministic ice actions. Kashagan phase 2 Development: North Caspian Sea. Proceedings of the 21st International Conference on Port and Ocean Engineering under Arctic Conditions, July 10-14, 2011, Montréal, Canada, POAC11-117

CSA (2000) Canadian Standards Association (2000) Design of Highway Bridges, A National Standard of Canada, CAN/CSA-S6-88, Rexdale, Ontario, Canada.

Development concepts for the northern Caspian Sea by Arkhat E. Sultabayev (2015).

Danabasoglu, G. et al. (2013). North Atlantic simulations in Coordinated Ocean-ice Reference. Experiments phase II (CORE-II). Part I: Mean states Ocean Dynamics. To appear.

Deltares (2013). Delft3D-FLOW User Manual. Simulation of multi-dimensional hydrodynamic flows and transport phenomena, including sediments. Version: 3.15.30059. 6 September 2013.

Frederking, R., Barker, A., (2002): Friction of sea ice on various construction materials. Proceedings of the 16th IAHR International Symposium on Ice, Dunedin, New Zealand, vol. 1, pp. 442–449.

Frederking, R.M.W., Timco, G.W., (1986): Field measurements of the shear strength of columnar-grained sea ice. Proceedings 8th International Association for Hydraulic Research Symposium on Ice, vol. I, pp. 279–292. Iowa City, U.S.A.

Frederking, RMW, Sayed, M., and Penney, G. 1992, Ice forces on light piers in the St. Lawrence Seaway, International Journal of Offshore and Polar Engineering, 2(1), pg: 67-72

Gürtner, A. (2009): Experimental and Numerical Investigations of Ice-Structure Interaction. Doctoral theses at NTNU, Trondheim, January 2009.

Gerritsen, H., E.D. de Goede, F.W. Platzek, M. Genseberger, J.A.Th.M. van Kester and R.E. Uittenbogaard (2007). Validation Document Delft3D-FLOW; a software system for 3D flow simulations. Version 1.0. 31 December 2007. WL | Delft Hydraulics report X0256, M3470

Hydraulic Interaction Between Ice and Bridges by Spyros Beltaos (2003); Research Scientist, Climate Impacts on Hydrology and Aquatic Ecosystems Project, Aquatic Ecosystems Impacts Research Branch, National Water Research Institute, Environment Canada, Burlington, Ontario, Canada.

Handbook of Computable General Equilibrium Modeling SET, Vols. 1A and 1B by David G. Tarr (2013)

Hibler, W. D., III (1979). A dynamic thermodynamic sea ice model. J. Phys. Oceanogr., 9, 815–846.

The Los Alamos sea ice model documentation and software user's manual. Technical report LA-CC-06-012. 8 August 2008. Los Alamos National Laboratory

Ice Breakup in Small Norwegian Streams; Siv Heggen1 and Knut Alferdesen Department of Hydraulic and Environmental Engineering Norwegian University of Science and Technology S.P. Andersens Vei 5, 7491 Trondheim, Norway.

ICE LOADS ON STRUCTURES by Robert Frederking; National Research Council of Canada, Ottawa, Canada & Karl Shkhinek; Saint Petersburg State Polytechnical University (SPbSPU), Russia.

Ice Thickness Prediction: A Comparison of Various Practical Approaches George Comfort1, and Razek Abdelnour, G. Comfort, Ice Engineering Ltd., 2 Conacher Gate, Kanata, Ont. K2K 3H1

International Standards Office, 2010. ISO/FDIS 19906:2010(E) Petroleum and natural gas industries — Arctic offshore structures, Geneva: ISO.

Logical Decision Tree Analysis by Alberto Pliego Marugán, Fausto Pedro García Márquez .

Lietaer, O., T. Fichefet and V. Legat (2008). The effects of resolving the Canadian Arctic Archipelago in a finite element sea ice model, Ocean Modelling, 24, 140-152.

Løset and Sayed (1993) Løset, S. and M. Sayed (1993) Proportional strain tests of freshwater ice rubble, Journal of Cold Regions Engineering, 7(2): 44–61.

Løset, S. (2014a): Arctic Offshore Structures/Fields. Lecture 1, the course AT-327 “Arctic offshore engineering”, UNIS, 2014

Løset, S. (2014b): Ice Physic. Structure and Formation of Ice Part I. Lecture 3, the course AT-327 “Arctic offshore engineering”, UNIS, 2014

Løset, S. (2014c): Global and Local Ice Loads. Lecture 7, the course AT-327 “The Arctic offshore engineering”, UNIS, 2014

Løset, S., Shkhinek, K., and Høyland. K.V. (1998): Ice physics and mechanics. Trondheim, NTNU, pp. 73-87

Løset, S., Shkhinek, K.N., Gudmestad, O.T., and Høyland. K.V. (2006): Action from Ice on Arctic Offshore and Coastal Structures. Student's Book for Institutes of Higher Education. St.-Petersburg: Publisher "Lan", p.9

Michel (1970) Michel, B. (1970) Ice Pressures on Engineering Structures. Monograph III-B1b, U.S. Army Cold Regions Research and Engineering Laboratory, Hanover, NH.

Michel (1978) Michel, B. (1978) Ice Mechanics. Laval University Press, Quebec, PQ, Canada.

Montgomery et al. (1984) Montgomery, C.J., R. Gerard, W.J. Huiskamp, R.W. Kornelson (1984) Application of ice engineering to bridge design standards, Proceedings, Cold Regions Engineering Specialty Conference, 4–6 April, 1984, Canadian Society for Civil Engineering, Montreal, Canada, pp. 795–810

Montgomery, C. J., Gerard, R., Huiskamp, W. J., and Kornelsen, R. W. (1984). "Application of Ice Engineering to Bridge Design Standards." Canadian Society for Civil Engineering, 795-810. Niehus, C. A. (2002). "Estimation of Ice Thickness and Strength for Determination of Lateral Ice Loads on Bridge Substructures in South Dakota." South Dakota Department of Transportation Office of Research, SD98-04-F, 1-64.

National Oceanic and Atmospheric Administration, 2001, Climatic extremes and record events: accessed August 27, 2001, at URL http://www.crh.noaa.gov/fsd/archive2.htm

National Research Council Canada, "Response of Confederation Bridge to ice forces: Winter 2008-2010", CHC-TR-075, 2010

Palmer, A. and K. Croasdale (2012). Arctic offshore engineering. Singapore, World Scientific Publishing Co. p. 129-136

Palmer, A. and K.R. Croasdale (2012). Arctic Offshore Engineering. World Scientific Publishing Co. Ptr. Ltd. ISBN 978-981- 4368-77-3.

Prather, M.J. (1986). Numerical advection by conservation of second order moments. J. Geophys. Res. 91, 6671–6681

Review of empirical relationships between inlet cross-section and a tidal prism by Marcel J.F. Stive and R.D. Rakhorst.

Sand, B. (2008): Nonlinear finete element simulations of ice forces on offshore structures. Doctoral Thesis at Luleå university of technology, Luleå, Sweden, June 2008

Sinsabvarodom, C., Chai, W., Leira, B.J., Høyland, K.V., Naess, A., 2018. Probabilistic Analysis of Ice and Sloping Structure Interaction Based on ISO Standard by using Monte-Carlo Simulation.

Sodhi and Nevel (1980) Sodhi, D.S. and Nevel, D.S. (1980) A review of buckling analyses of ice sheets, IAHR Working Group on Ice Forces on Structures (Ed. T. Carstens), Special Report 80-26, U.S. Army Cold Regions Research and Engineering Laboratory, Hanover, NH, pp. 131−146.

Thomas G. Brown, J. Susan Tibbo, Dhruba Tripathi, Keely Obert, Noorma Shrestha. 2010. Extreme ice load events on the Confederation Bridge. Cold Regions Science and Technology 60:1, 1-14.

Timco GW., Nwogu OG., and Christensen FT., 1995, Compliant model tests with the Great Belt West Bridge piers in ice Part I: Test methods and key results, Cold Region Science and Technology, 23, pg: 149-164.

Timco, G.W. and Weeks, W.F. (2010): A review of the engineering properties of sea ice. Cold Regions Science and Technology 60 (2010) p.107–129

U.S. Geological Survey, 2002, Estimation of Ice Thickness and Strength for Determination of Lateral Ice Loads on Bridge Substructures in South Dakota, Technical Report SD98-04-F, September 2002.

USACE, 2002, Engineering and Design Manual: Ice Engineering, Engineer Manual EM-1110-2-1612, United States Army Corps of Engineers.

Wang, J., Q. Liu, M. Jin, M. Ikeda, F.J. Saucier (2005). A coupled ice-ocean model in the Pan-Arctic and North Atlantic ocean: simulation of seasonal cycles. J. Oceanogr., 61, 213–233.

Yuan Z., Yu T., and Zhang H., 2009, Research on percussive force of river ice and bridge, Proceedings of 2nd International Conference on Modeling and Simulation, Manchester, UK.

Appendices

Appendix A: MATLAB codes

Appendix B: Tables for NRC-Canada

Appendix C: Graphs for NRC-Canada

Appendix D: Winterly ice thickness graphs

Appendix E: Detailed AutoCAD drawing of the bridge pier

Appendix A: MATLAB codes

Required inputs

The script for the Montecarlo analysis reads from the CSV file. The file must be in the same directory to run the code. Note that some lines of the scripts are 'commented out'. All the units are in meter-kg-N format.

```
   1. **Effect of river discharge on tidal discharge and current**

t=0:0.2:24; %time in hour
h=sin(t/24*2*pi)*2.49; % tidal amplitude (m)
A_f=6128; % cross section of fjord (m^2)
L_b=580; % Length of the bridge cross-section (m^2)
A_p=4072593; %surface area of fjord (m^2)
R1=151.9; % River 1 Discharge (m^3/s)
R2=83s.40; %River 2 Discharge (m^3/s)
R3=16.6; %River 3 Discharge (m^3/s)
%%
for i=1:1:120
input_vol(i)=(h(i+1)-h(i))*A_p; %Volume of the water(m^3)
    input_d_wr(i)=input_vol(i)/((t(i+1)-t(i))*3600);% converting volume to
discharge without river (m^3/s)
    input_d(i)=input_d_wr(i)-R1-R2-R3; % converting volume to discharge
    (m^3/s)
end
u_t1=input_d/A_f;
u_t2=input_d_wr/A_f;
%%
figure
subplot(4,2,1)
plot(t,h)
xlabel('Time (hr)')
ylabel('Tidal amplitude (m)')
grid on;
grid minor;
```

```
title('Tidal signal')

subplot(4,2,2)
plot(t(1:120),input_d_wr);
xlabel('Time (hr)')
ylabel('Discharge (m^3/s)')
grid on;
grid minor;
title('Discharge without rivers')
subplot(4,2,3)
plot(t(1:120),input_d);
xlabel('Time (hr)')
ylabel('Discharge (m^3/s)')
grid on;
grid minor;
title('Discharge with rivers')

subplot(4,2,4)
plot(t(1:120),u_t1);
xlabel('Time (hr)')
ylabel('Tidal current (m/s)')
grid on;
grid minor;
title('Tidal current speed with rivers')

subplot(4,2,5)
plot(t(1:120),u_t2);
xlabel('time (hr)')
ylabel('Tidal current (m/s)')
grid on;
grid minor;
title('Tidal current speed without rivers')
```

2. **Monte Carlo simulations code for probabilistic analysis**

```
% % Vertical structure (1SO19906) %%
```

```
function [Fg]=vertical_structure(Df)
dA = 1.37; % Density of Air (Kg/m3).
dW = 1025; % Density of Water (Kg/m3).
dI = 910; %Ice density (Kg/m3)
Va = 25; % Wind velocity (m/s).
Vc = 0.011;     % Current velocity (m/s).
Df = 0.580;     % Equivalent Diameter of Ice floe (m).
Ca= 0.002; % Drag coefficient for wind.
Cw = 0.0175; % Drag coefficient for water.
Af = (pi/8)*(Df)^2; % Area of Ice floe.
h = 0.5;     % Ice thickness. (m)
g = 9.81; %gravitational acceleration (m/s2)
w = 4.5;      %width of ice-structure interaction (m)
hr = 1; %Reference thickness (m)
m = -0.16; %Experimental constant
n = -0.30; %Experimental constant
CR = 1.8; %Ice reference strength (Mpa)
pc = CR*((h/hr)^(-0.5+n))*(w/h)^(m)+(exp(-w/3*h)*sqrt(1+(5*h/w))); %Effective
Ice pressure (Crushing) (Mpa)

                                %***Output***

Fwind = Af*Ca* dA*(Va)^2; %Drag force due to wind (MN)
Fcurrent = Af*Cw* dW*(Vc)^2; %Drag force due to Tidal current (MN)
Fthermal = 0.50; %Force due to thermal expansion (MN)
Fc = pc*h*w; %Limit stress scenario due to crushing (MN)
Flf = Fwind + Fcurrent + Fthermal; %Limit force scenario (MN)
Fg = min(Flf,Fc);

                        % % Sloping structure (ISO19906) %%

Ym= 3400*10^6; %Youngs modulus(Pa)
PR= 0.3; %Poisson's ratio
RH = 5.44; %Rubble height (m)
If= 0.1; %Ice to-ice friction coefficient
P= 0.3; %Porosity of the ice rubble
AR= 0.79; %Rubble angle of repose (radians)
```

```
CR= 5000; %Cohesion of ice ruble (Pa)
RA= 0.79; %Internal friction angle ice rubble (radians)
Isf= 0.53; %ice structure friction coefficient
CA =0.79; %Cone Angle (radians)
Wd= 4; %waterline diameter (m)
FS= 0.2; %flexural strength (Mpa)
zeta = (sin(CA)+Isf*cos(CA))/(cos(CA)-Isf*sin(CA));
Lc = ((Ym*h^3)/(12*dW*g*(1-PR^2)))^0.25;
lc = Wd+(((3.1415)^2/4)*Lc);% Length of circumferential bending crack (m)

                                %***Output***

HB = 0.68*zeta*FS*(((dW*9.81*h^5)/Ym)^0.25)*lc; % Load required to break the
ice blocks against the slope (MN)
HP = (Wd*RH^2*If*dI*g*(1-P)*((1-(tan(AR)/tan(CA)))^2)*(1/2*tan(AR)))/10^6;
%Load required to push the sheet ice through the rubble
HT = 1.5*Wd*(h^2)*dI*g*(cos(CA)/(sin(CA)-Isf*cos(CA)))/10^6; %Load required to
turn the ice block at the top of the slope (MN)
HR =(((Wd*dI*g*h/cos(CA)-Isf*sin(CA))*(0.5*(If+Isf)*(1-
P)*RH*(If*((sin(CA)/tan(RA))-cos(CA))+cos(CA)/tan(CA))*(1-
tan(RA)/tan(CA))+(h*(sin(CA)+Isf*cos(CA))/sin(CA))))/10^6);%Load required to
push the ice blocks up the slope (MN)
HL = Wd*RH*zeta*(1-tan(RA)/tan(CA))*(0.5*RH*dI*g*(1-P)*((1/tan(RA))-
1/tan(CA))+tan(AR)*(1-tan(RA)/tan(CA))+CR)/10^6; %Load required to lift the
ice rubble with the unbroken ice floe (MN)
FH =(HB+HP+HT+HR+HL)/(1-HB/(FS*lc*h)); % The total horizontal design load for
bending failure is found according to ISO19906 (MN)
FV = FH/zeta; % The total horizontal design load (MN)
end

                            %% Monte Carlo simulations

n=10000;

%% Random variables for both vertical and sloping structures (considering
independence)
h=gamrnd(2,1,n,1); %ice thickness gamma distributed
```

```
Df=50+530*rand(n,1); % Ice floe diameter uniform distributed
Ca=0.001+0.002*rand(n,1); % Drag coefficient for wind uniform distribution.
Cw =0.005+0.025*rand(n,1); % Drag coefficient for water uniform distribution.
Va = evrnd(3.791,21.114);     % Gumble max distributed Wind velocity (m/s).
Vc = evrnd(0.00457,0.09263);     % Gumble max distributed Current velocity
(m/s)
FS=(randn(n,1) * 0.05793) + 0.18627; %Normal distributed flexural strength
Isf=0.1+0.2*rand(n,1); %ice structure friction coefficient uniform
distributed
RH=2.5+3*rand(n,1); %uniform distributed Rubble height
for i=1:1:n
    [Fg(i)]=vertical_structure(Df(i));
end
normpdf(Fg)

        ##%% Correlating random variables by using Gaussian copula %%##

%% Variables

clear all;
hi_rand=random('Gamma',19.218,0.02063,1000,1);%Ice thickness random variables
fs_rand=random('Normal',0.2234,0.05574,1000,1);%Flexural strength random
variables
vw_rand=random('ExtremeValue',21.114,3.791,1000,1);%wind velocity random
variables
vc_rand=random('ExtremeValue',0.09263,0.00457,1000,1); %Tidal current random
variables
 % variables in which correlation has to generate
a=vw_rand;
b=vc_rand;
 % Correlation coefficient value
Rho=0.8;
 % Random variables from  Gaussian copula
r = copularnd('Gaussian',Rho,10000);
u1 = r(:,1);
v1 = r(:,2);
 % Sample data from copula
x1 = ksdensity(a,u1,'function','icdf');
```

```
y1 = ksdensity(b,v1,'function','icdf');
 % Uncorrealted
figure;
 scatter(a,b,'.')
 % Correalated
 scatter(x1,y1,'.')

%% Recalling correlated variables stored in the text file for plotting
n=10000;
                  %% Random variables for sloping structure

 Sequence = [1 2 1 3 4]
 for sheeti = 1:5
 if(sheeti == 1)
 fileIDFx = fopen('FxN0.8.txt','r');
 formatSpec = '%f';
 FS = fscanf(fileIDFx,formatSpec);
 fileIDTh = fopen('ThN0.8.txt','r');
 formatSpec = '%f';
 h = fscanf(fileIDTh,formatSpec);
 figure
 plot(FS,h,'.')
 elseif(sheeti == 2)
 fileIDFx = fopen('FxN0.5.txt','r');
 formatSpec = '%f';
 FS = fscanf(fileIDFx,formatSpec);
 fileIDTh = fopen('ThN0.5.txt','r');
 formatSpec = '%f';
 h = fscanf(fileIDTh,formatSpec);
 figure
 plot(FS,h,'.')
 elseif(sheeti == 3)
 h=gamrnd(19.218,0.02063,n,1); %ice thickness gamma distributed
 FS=normrnd(0.223,0.054439,n,1) ; %Normal distributed flexural strength
 figure
 plot(FS,h,'.')
 elseif(sheeti == 4)
 fileIDFx = fopen('Fx0.5.txt','r');
```

```
formatSpec = '%f';
FS = fscanf(fileIDFx,formatSpec);
fileIDTh = fopen('Th0.5.txt','r');
formatSpec = '%f';
h = fscanf(fileIDTh,formatSpec);
figure
plot(FS,h,'.')
elseif(sheeti == 5)
fileIDFx = fopen('Fx0.8 .txt','r');
formatSpec = '%f';
FS = fscanf(fileIDFx,formatSpec);
fileIDTh = fopen('Th0.8.txt','r');
formatSpec = '%f';
h = fscanf(fileIDTh,formatSpec);
figure
plot(FS,h,'.')
end


%%Plotting of monte carlo simulation pdf considering both independency and
dependency between variables for sloping structure

for i=1:1:n
[FH(i)]=Sloping_structure(h(i),FS(i));
End
x1 = -0.2:0.0001:0.8;
pd_FH = fitdist(FH','Extreme value');
FH_x =1-cdf(pd_FH,x1); %1-cdf for probability
figure(100)
hold on
plot(x1,FH_x)
hold off
ylim([0 10^10-3])
xlim([0 1.3])
grid on
set(gca, 'YScale', 'log')
end
```

```
%%Plotting of Monte Carlo simulation pdf considering both independence and
dependency between variables for the vertical structure

                %% Random variables for vertical structure %%

 n=10000;

%% Correlated random variables for vertical structure recalling from the
stored text file

Sequence = [1 2 1 3 4]
for sheeti = 1:5
if(sheeti == 1)
fileIDVa = fopen('VaN0.8.txt','r');
formatSpec = '%f';
Va = fscanf(fileIDVa,formatSpec);
fileIDVc = fopen('VcN0.8.txt','r');
formatSpec = '%f';
Vc = fscanf(fileIDVc,formatSpec);
figure
plot(Va,Vc,'.')

elseif(sheeti == 2)
fileIDVa = fopen('VaN0.5.txt','r');
formatSpec = '%f';
Va = fscanf(fileIDVa,formatSpec);
fileIDVc = fopen('VcN0.5.txt','r');
formatSpec = '%f';
Vc = fscanf(fileIDVc,formatSpec);
figure
plot(Va,Vc,'.')
elseif(sheeti == 3)
Va = evrnd(21.114,3.791,n,1);     % Gumble max distributed Wind velocity
(m/s).
Vc = evrnd(0.09263,0.00457,n,1);     % Gumble max distributed Current
velocity (m/s)
figure
plot(Va,Vc,'.')
```

```
elseif(sheeti == 4)
fileIDVa = fopen('Va0.5.txt','r');
formatSpec = '%f';
Va = fscanf(fileIDVa,formatSpec);
fileIDVc = fopen('Vc0.5.txt','r');
formatSpec = '%f';
Vc = fscanf(fileIDVc,formatSpec);
figure
plot(Va,Vc,'.')
elseif(sheeti == 5)
fileIDVa = fopen('Va0.8.txt','r');
formatSpec = '%f';
Va = fscanf(fileIDVa,formatSpec);
fileIDVc = fopen('Vc0.8.txt','r');
formatSpec = '%f';
c = fscanf(fileIDVc,formatSpec);
figure
plot(Va,Vc,'.')
end

Df=0.050+0.530;%*rand(n,1); % Ice floe diameter uniform distributed
Ca=0.001+0.002;%*rand(n,1);  % Drag coefficient for wind uniform
distribution.
Cw =0.005+0.025;%*rand(n,1); % Drag coefficient for water uniform
distribution.
  %% monte carlo simulation
 for i=1:1:n
[Fg(i)]=vertical_structure(Va(i),Vc(i));
 End
x1 = 0:0.0001:1;
pd_Fg = fitdist(Fg','Extreme value');
Fg_x =1-cdf(pd_Fg,x1);
figure(100)
hold on
plot(x1,Fg_x)
hold off
ylim([0 10^10-3])
xlim([0.5 1.2])
```

```
grid on
set(gca, 'YScale', 'log')
end

%Code for plotting correlated probability distributions of variables,
recalling these variables stored in the excel sheet

clc, clear all, close all
fileIDFx = fopen('Flexural strength_Normal.txt','r');
formatSpec = '%f';
Data_FS = fscanf(fileIDFx,formatSpec);
fileIDTh = fopen('Ice thickness_Gamma.txt','r');
formatSpec = '%f';
Data_h = fscanf(fileIDTh,formatSpec);
x1 = 0.001:0.001:1;
mean1 = mean(Data_Fx);
std1 = std(Data_Fx);
pd_Fx = makedist('normal','mu',mean1,'sigma',std1);
sigma_Fx = pdf(pd_Fx,x1);
mean2 = mean(Data_Th);
std2 = std(Data_Th);
%pd_hi = fitdist(Data_hi,'gamma');
 pd_Th = makedist('Gamma','a',19.218,'b',0.02063);
 Th = pdf(pd_Th,x1);
 figure
 hold on
 plot(x1,sigma_Fx)
 plot(x1,hi)
 hold off
 N = 10000
 RhoLoop = [-0.8 -0.5 0.5 0.8];
 filename = 'Sloping_Structure.xlsx';
 A = {'Flexural Strength','Ice Thickness','','Correlation Coefficient ='};
```

Appendix B: Tables for NRC-Canada

Table B-1 Calculated wind velocity

$\Omega*10^{-3}$ (m^2)	w (m/s)
10	34
40	31
250	27
1000	24

Table B-2 Value of coefficient S

L (m)	S
≤ 50	1
51 – 75	0.9
76 – 100	0.8
101 – 150	0.7
> 150	0.6

Table B-3 Value of coefficient m

2 ε	M
45	0.54
60	0.59
75	0.64
90	0.69
120	0.77
180	1

Table B-4 Value of climatic coefficient A

Region No.	Boundaries of region	Climatic coefficient (A)	Notes
1	*South of the line* Talin - Minsk - Khar'kov - Astrakhan - Nukus - Alma-Ata	0.75	1) For regions No. 2-5 the lower boundary is also the boundary of the foregoing region. 2) The climatic coefficient can be based on field observations of conditions at spring breakup, but for a breakup with negative air temperatures < 0°C) it must not be less than 2.
2	*South of the line* Vyborg - Smolensk – Kamyshin - Aktyubinsk – Balkhash	1	
3	*South of the line* Arkhangel'sk - Kirov - Ufa - Kustanai - Karaganda - Ust' – Kamenogorsk	1.25	
4	*South of the line* Vorkuta - Khanty - Mansiisk - Krasnoyarsk - Ulan - Ude - Nikolaevsk-na-Amure	1.75	
5	*South of the line* Dikson - Noril'sk - Vodaibo - Okhotsk	2	
6	*North of the line* Dikson - Noril'sk Vodaibo – Okhotsk	2.25	

Table B-5 Value of coefficient ξ

Computation cases	ξ
Compression when there is a trend towards a limiting stress state for gently sloping sandy shores	0.7
The same for rocky shores and vertical walls of structures	0.9

Appendix C: Graphs for NRC-Canada

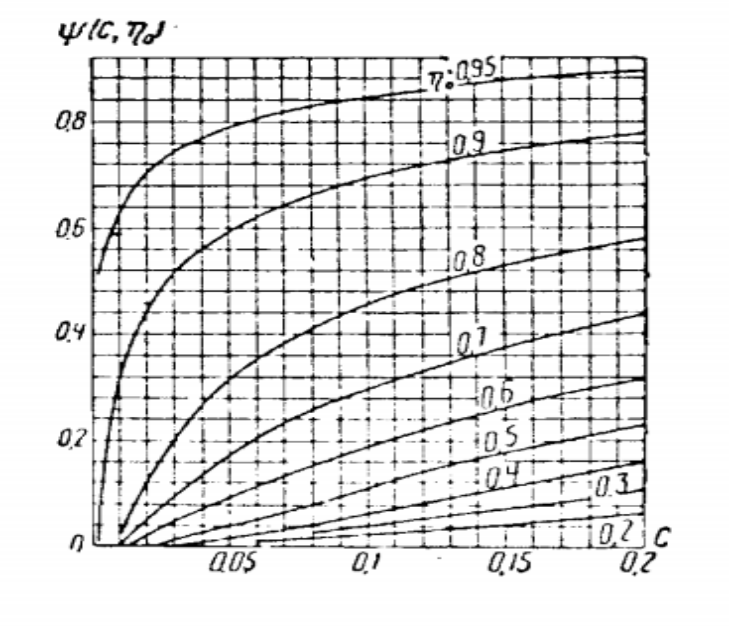

Figure C-1 Graph for determining ψ

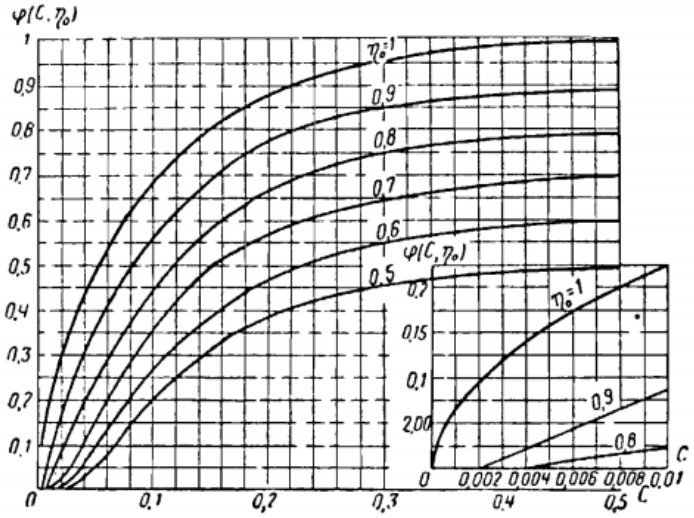

Figure C-2 Graph for determining Φ

Appendix D: Winterly ice thicknesses graphs

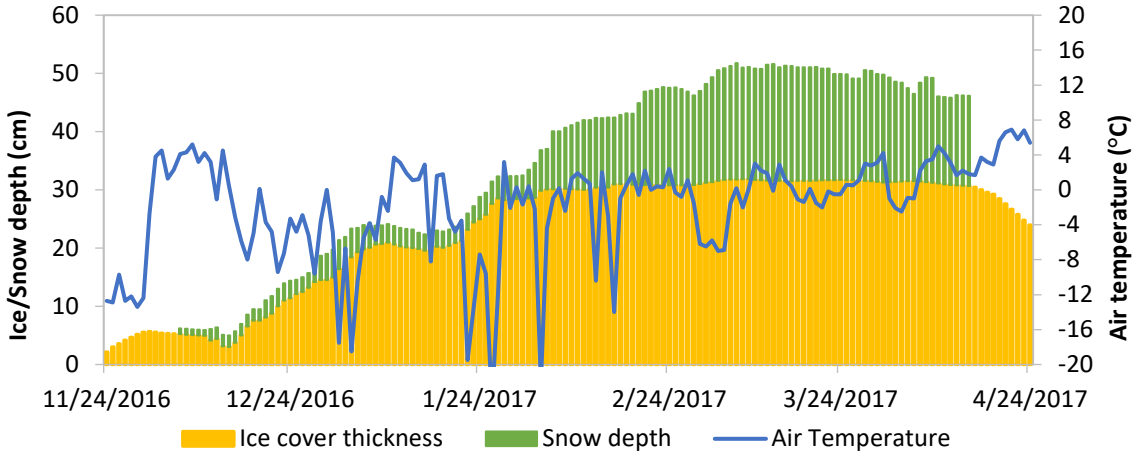

Figure D-1 Winterly ice thickness and air temperature at Beitstad in 2016-2017

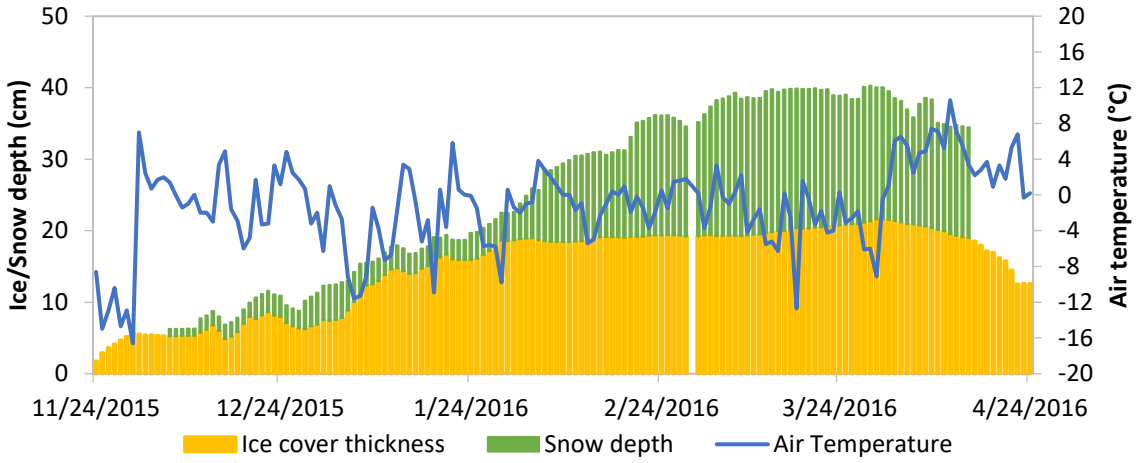

Figure D-2 Winterly ice thickness and air temperature at Beitstad in 2015-2016

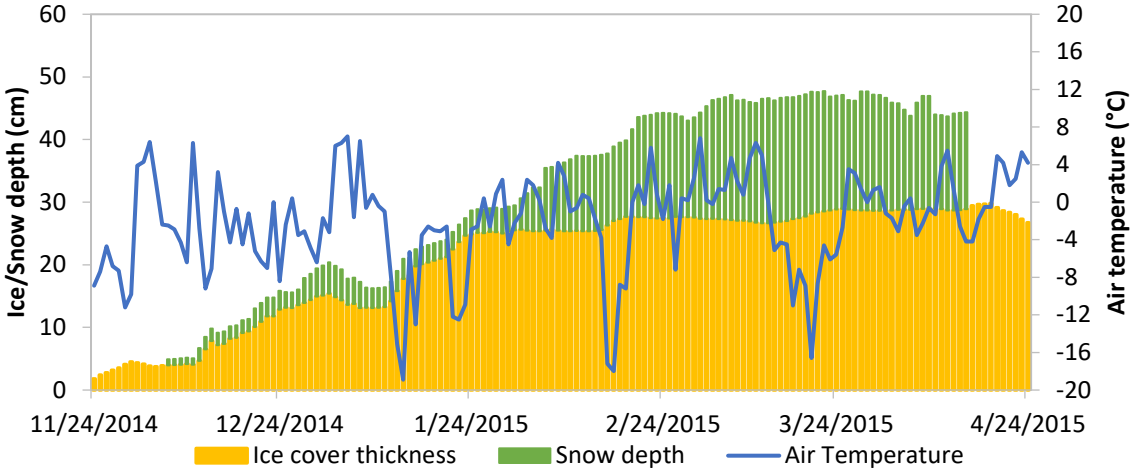

Figure D-3 Winterly ice thickness and air temperature at Beitstad in 2014-2015

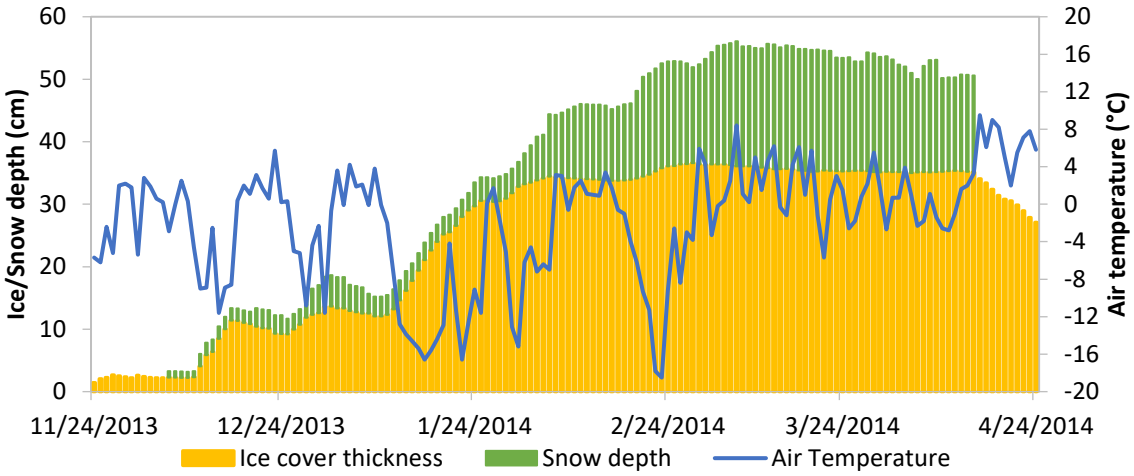

Figure D-4 Winterly ice thickness and air temperature at Beitstad in 2013-2014

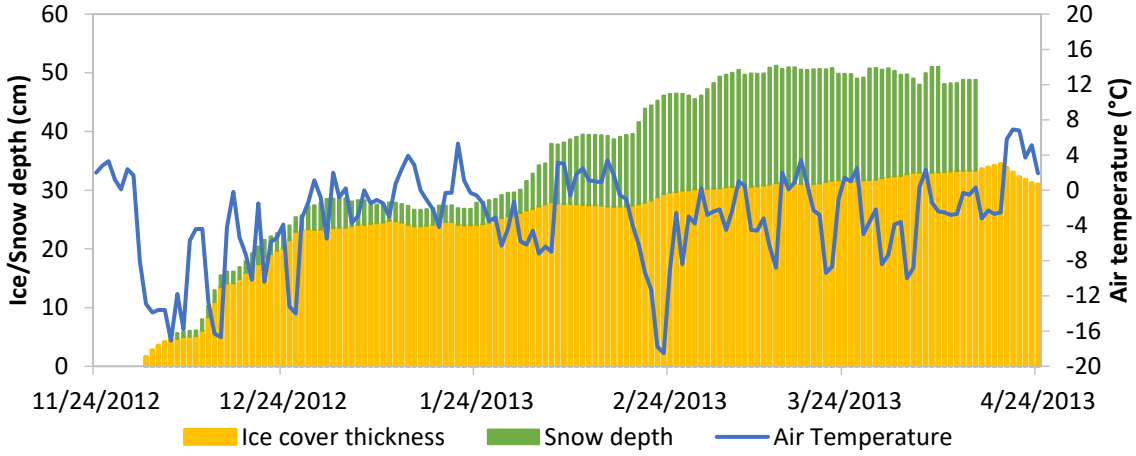

Figure D-5 Winterly ice thickness and air temperature at Beitstad in 2012-2013

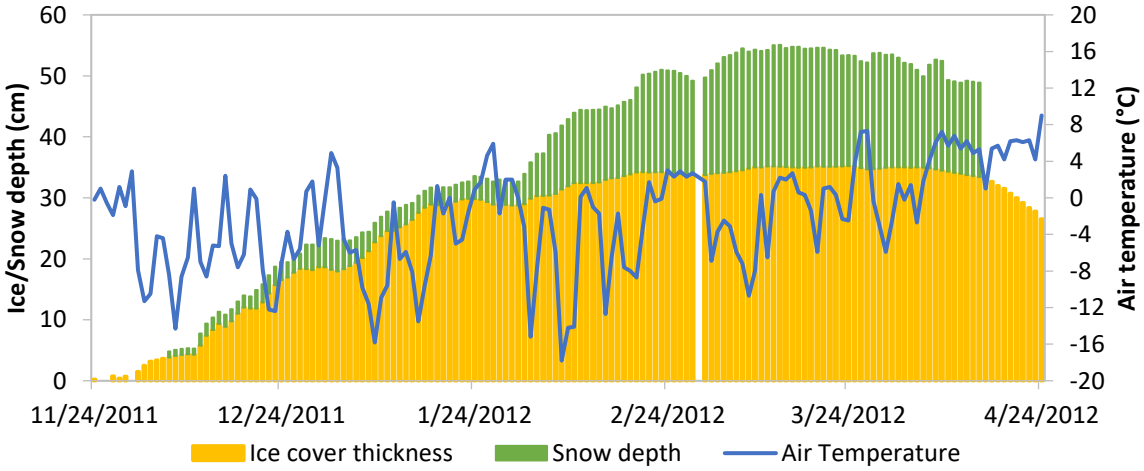

Figure D-6 Winterly ice thickness and air temperature at Beitstad in 2011-2012

Appendix E: Detailed AutoCAD drawing of the bridge pier (Norconsult)

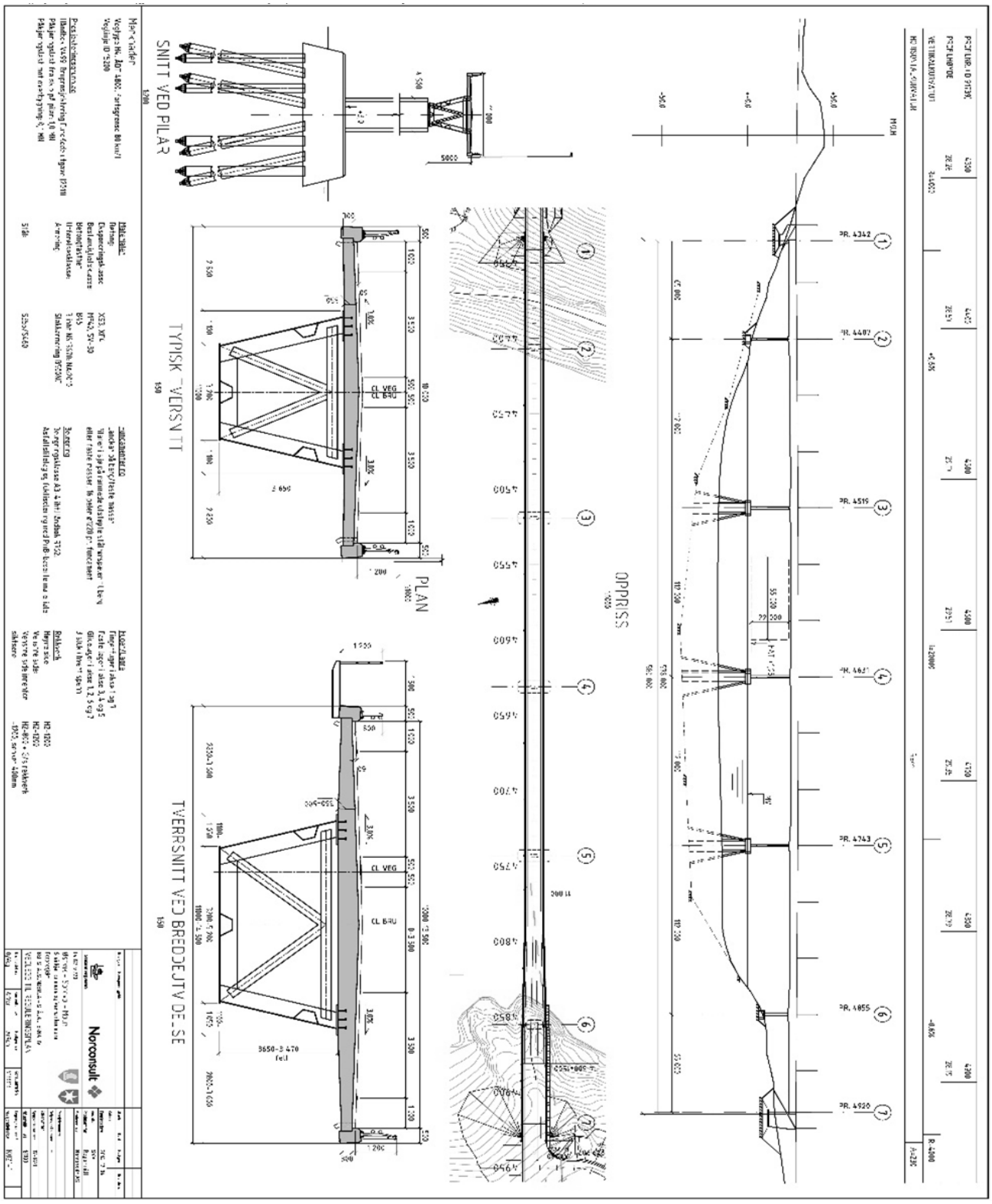

Fahad Pervaiz

Ice actions on bridges

NTNU
Norwegian University of
Science and Technology